CRANFIELD UNIVERSITY

School of Engineering

Department of Engineering Mechanics and Structures

Ph.D. Thesis

Academic Year 2001-02

Moutaz Mohamed Ebrahim HEGAZE

FINITE ELEMENT ANALYSIS OF FATIGUE DAMAGE OF COMPOSITE LAMINATED STRUCTURES

Supervisor: Dr. A. El-Zafrany

Dr. D. Mba

February 2002

This thesis is submitted in partial fulfilment of the requirements for the degree of

Doctorate of Philosophy

ABSTRACT

Composite materials are increasingly believed to be the materials of the future with potential for application in high performance structures. One of the reasons for that is the indication that composite materials have a rather good rating with regard to life time in fatigue. Fatigue of composite materials is a quite complex phenomenon, and the fatigue behaviour of these heterogeneous materials is fundamentally different from the behaviour of metals. Finite element method is a powerful numerical technique for the solution of such complex problems. The present work comprises theoretical and experimental research into the implementation of composite materials in structure applications. A new finite element derivation was carried out based on a high-order shear deformation theory, which is accurate for a wide range of thickness. The geometric nonlinearity effect was considered in the derivation of the element. The force increment method was also introduced to improve the accuracy of nonlinear analysis. Experimental measurements were carried out with two different types of composite materials, carbon/epoxy and glass/epoxy, in order to obtain fatigue life diagrams (S/N diagrams) to be used for the fatigue damage assessment. Fatigue damage assessments were developed to predict the fatigue behaviour of laminated plates and shells based on two aspects; damage by initiation and damage by crack growth. A computer package was built based on the proposed finite element theory to carry out the previous analyses. Several finite element solvers and eigenproblem solvers are available to users of the package to choose the suitable one for their applications. The validation of the developed package for some analyses such as stress analysis, natural frequency analysis, stability analysis and fatigue analysis was successfully achieved using a number of composite case studies. A parametric study was also carried out to illustrate the potential of the package to be used as a good optimization tool. Fatigue life assessment by damage growth has been achieved by a single run of the package, thus saving enormous user effort and computer resources, compared with the use of commercial finite element packages.

ACKNOWLEDGEMENTS

First of all, I thank Alla (God) almighty, for giving me the ability, health and knowledge, which enabled me to complete this work.

I would like to express my sincere appreciation and thanks to my supervisor Dr. A. El-Zafrany for his invaluable help, guidance, genuine friendship and encouragement throughout the course of this research.

I would like also to thank my second supervisor Dr. D. Mba for his suggestions and efforts regarding the experimental work.

I would like also to thank Mr. H. Jim from the School of Industrial and Manufacturing Science (SIMS) at Cranfield University for his help and support during the manufacturing of the experimental specimens.

I would like to thank the Egyptian government, which gave me the opportunity to complete my study in U.K.

Words are not enough to express my gratitude and indebtedness to my wife for her patience, care and generosity during the period of study at Cranfield, and my lovely son Mohamed who always cheer me up. Thanks also to all members of my family in Egypt for moral support and encouragement during the course of this study, especially my brother Mostafa, my sister, my mother-in-law and my father-in-law.

I would like to dedicate this manuscript to the souls of my parents, who were interested in my education and inspired me with their love.

LIST OF CONTENTS

LIST OF FIGURES

LIST OF TABLES

1

INTRODUCTION

1.1 BACKGROUNG TO THE RESEARCH

Composite materials have a long history of usage. The ancient Egyptians were the first users of composite materials. They used plywood when they realized the wood could be rearranged to achieve superior strength and resistance to thermal expansion. A composite is a material system made up of two or more material components. This type of materials is ideal for structural applications where high strength-to-weight and stiffness-to-weight ratios are required such as, aircraft and spacecraft applications, which are typical weight-sensitive structures in which composite materials are cost-effective. Also, in civil and sport industries, composite materials may be a better alternative than steel and aluminium alloys. Useful properties of these new materials are high tensile strength, high damping, and low density (one-fourth compared with steels, two-thirds compared with aluminium alloys).

Composite materials are increasingly believed to be the materials of the future with potential for application in high performance structures. As a result of their high specific stiffness and strength, composite materials are often selected for weight-critical structural applications. One of the reasons for believing this is the indication that composite materials have a rather good rating with regard to life time in fatigue (Talreja, 1987).

In the field of engineering we may come across complex problems, the solution of which is extremely tedious and usually not possible by analytical methods. In such cases we have to resort to the use of numerical techniques. Finite element method is an extremely powerful numerical technique for the solution of such complex problems. The method has a wide range of applications, such as stress analysis, heat transfer, fluid flow, ... etc.

The development of digital computers and the increasing complexity in many areas of modern technology have ensured that the finite element method now enjoys a unique position as a powerful and adaptable solution technique for a large range of advanced engineering problems. Due to the popularity of the finite element method, there are hundreds of finite element computer packages, available on mainframe computers, workstations, and PC's, and they can deal with a huge range of applications. Nevertheless, most of these packages are mysterious black boxes to the majority of their users. Some of the basic problems associated with the finite element method are element selection, type of analysis, finite element mesh, and limitation of accuracy.

From the engineering point of view, the most attractive and yet possibly the most dangerous feature of the finite element method is the fact that it approximates. In the hands of an experienced and careful analyst it is a very useful means of obtaining insight into certain problems for which no analytical tool is appropriate.

The oldest finite element plate theory which still enjoys considerable status is the so-called classical plate theory. That theory based on Kirchhoff's assumption which neglects the effect of transverse shear. To improve the accuracy of the results obtained by that theory, Reissner and Mindlin plate theories, where the transverse shear effects are considered could be implemented. In Mindlin theory, the reduced integration scheme is recommended with thin plates due to the shear locking phenomenon. To have a plate bending finite element theory which considers transverse shear effect and to deal easily with thin and thick plates some researchers have introduced high-order deformation theories where the transverse shear stresses are accurately modelled over the thickness.

1.2 RESEARCH PROBLEM AND HYPOTHESES

Fatigue of composite materials is a quite complex phenomenon, and the fatigue behaviour of these heterogeneous materials is fundamentally different from the behaviour exposed by metals. Due to the degradation of the stiffness properties during fatigue life, stresses are continuously redistributed across the composite construction, which has more complex mechanisms than metals. Composite materials are inhomogeneous and anisotropic, and their behaviour is more difficult to predict than that of homogeneous and isotropic materials such as metals.

There are indeed a number of significant differences between the fatigue behaviour of metals and that of composites. In metals, the stage of gradual and invisible deterioration spans nearly the complete life time. In a composite, damage is initiated during the first few cycles and the extent of the damage zones will grow during fatigue life. The gradual deterioration of a composite - with a loss of stiffness in the damaged zones - leads to a continuous redistribution of stress and a reduction of stress concentrations inside a structural component.

As a consequence, an appraisal of the actual state or a prediction of the final state (when and where final failure is to be expected) requires the simulation of the complete path of successive

damage states. Today deficiencies in existing life prediction methodologies for these materials often require large factors to be adopted, such as experimental data.

The use of finite element method to analyse the composite material structures has been the subject of many investigations. A large amount of researches has been devoted to the development of old finite element theories and to the study of their effect with laminated structures.

It is advantageous to have finite elements based on high-order plate theory which considers transverse shear effects in order to correctly predict the damage and residual stiffness of laminated structures after a certain number of fatigue loading cycles. These elements can deal easily with the geometrical nonlinear effects due to large deformation of the structure.

1.3 RESEARCH OBJECTIVES

The present work comprises theoretical and experimental research into the implementation of composite materials in structure applications. The research objectives are summarized in the following points:

(i) A new finite element derivation was to be carried out based on a high-order shear deformation theory to be accurate for a wide range of thickness.

(ii) The geometric nonlinearity effect would be considered in the derivation of the element. The force increment method was also to be introduced to improve the result accuracy.

(iii) Experimental measurements were to be carried out with two different types of composite materials, carbon/epoxy and glass/epoxy, in order to obtain fatigue life diagrams (S-N diagrams) to be used for the fatigue damage assessment.

(iv) Fatigue damage assessments would be developed to predict the fatigue behaviour of laminated plates and shells based two aspects; damage by initiation and damage by crack growth.

(v) A computer package would be built based on the proposed finite element to carry out the previous analyses. Several finite element solvers and eigenproblem solvers should be available to the user in the package to choose the suitable one for his application.

(vi) The validation of the proposed package with some analyses such as stress analysis, natural frequency analysis, stability analysis and fatigue analysis was to be considered.

(vii) A parametric study was to be carried out to illustrate the potential of the package to be a good optimization tool.

1.4 JUSTIFICATION FOR THE RESEARCH

The research objectives have been justified through the following points:

(i) The finite element method is the most popular numerical technique, and it has been applied successfully with many engineering disciplines.

(ii) Composite materials are increasingly believed to be the materials of the future with potential for application in high performance structures.

(iii) The higher-order theory for the analysis of laminated plates has received increased attention in the last decade.

(iv) Relative omission of the geometric nonlinearity effect by previous researchers casts some doubt on the accuracy of their fatigue results, and there is also a need for more accurate theory than the classical one to account for the transverse shear and rotary inertia effects and to deal easily with thin and thick plates.

(v) The need for further development of efficient numerical tools for buckling and free vibration studies.

(vi) Most of fatigue assessments of composites have been based on finite element commercial packages, which lead to a lot of restrictions on the user. Hence, there is a need for an accurate tool in order to correctly predict the fatigue damage behaviour of laminated structures under cyclic load.

1.5 METHODOLOGY

The research methodology has been subdivided into the following set of stages.

- Literature review

  To critically review the international literature in the areas of laminated structures, finite element theories and fatigue damage growth of laminated structures.

- Theoretical investigations

  To study finite element theory, the development of appropriate algorithms for the stress/vibration analyses of laminated structures.

- Software development/implementation

  Development of a suite of computer programs for the modelling, analysis and design assessment and optimization of laminated structures.

- Experimental investigations

  To carry out experimental measurements and mechanical characterizations of failure in selected composites to provide information for the verification of the developed theory and algorithms.

1.6 OUTLINE OF THE THESIS

A summary of the contents of each chapter is given as follows:

Chapter 1 gives background information to the project, introduces the research, gives the justification of the research and general methodology.

Chapter 2 reviews the current status in the literature of laminated structures, finite element theories and fatigue damage growth phenomena. A summary of the conclusions from the review is presented at the end of this chapter.

Chapter 3 reviews the basic theories of composite materials and its constitutive equations which govern the stress-strain relations of the laminated composite materials. A quick review on the manufacturing process of the composite specimens used in this work is also described in this chapter with an explanation of the experimental setup.

Chapter 4 describes the deformation theory of the high-order shear element through the displacement formulation, nodal parameters and strain displacement relations.

Chapter 5 gives the details of proposed high-order finite element theory to analyse laminated structures. The element is proposed to deal easily with the fatigue damage phenomena of laminated structures.

Chapter 6 introduces the governing equations of the fatigue damage phenomena in composites. The fatigue damage is introduced through two types; fatigue damage by initiation and fatigue damage by crack growth. Full descriptions of these two phenomena are presented.

Chapter 7 gives a brief description of the finite element programming package with flowcharts demonstrating each analysis part within the package.

Chapter 8 demonstrates the validation procedures of the finite element package for different types of analyses using different case studies. It provides detailed results and discussions with different case studies to investigate some effective parameters through detailed parametric studies.

Chapter 9 gives the final conclusions and some recommendations for future work.

2

LITERATURE REVIEW

2.1 INTRODUCTION

A literature review has been carried out based on different keywords; finite element analysis, high order theory, composite materials and fatigue damage. The main objective of this chapter is to review and update the information on the fields of the previous keywords.

Recent publications on the use of composite materials have been reviewed including the mathematical models used in their analyses. Also, the advantages of using the finite element method as a mathematical tool with the composite material analyses have been discussed.

The fatigue behaviour of composite materials is considered one of the difficult problems with this type of materials, as it is more complex than metals. That problem seems to be an important topic for several researchers as illustrated later in this chapter.

2.2 FINITE ELEMENT HIGH-ORDER SHEAR THEORY

The finite element method can be considered the most popular numerical technique ever known to man. It has been applied successfully to many engineering disciplines, such as structural mechanics, computational fluid dynamics, ... etc. A large number of finite element books have been published since the appearance of the finite element method, see for example Zienkiewiez, (1977), Hinton and Owen (1979), Rao (1982), and many others.

Plate and shell elements are employed for plate and shell structures. Stress analysis parameters defined within plate or shell domains are usually modelled in the finite element theory by a two-dimensional piecewise interpolation in items of midplane parameters, together with analytical expressions in the thickness direction.

The plate bending problem is one of basic stress analysis problems of plates and shells, and it is still an active research subject up till now. The available literature related to this issue is classified into three groups, classical plate theory, first-order shear deformation theories and refined theories.

The first plate theory to appear in the literature is the so-called classical plate theory (CPT). In that theory, a normal to the midplane before deformation remains normal after deformation

(Kirchhoff's hypothesis). The effect of transverse stresses is ignored in this hypothesis. Due to the limitation of the (CPT), some analyses based on (CPT) give inaccurate results especially for application with high shear deformation effects. Various textbooks have described that theory and its application to the analysis of laminated composite structures such as, Lekhnitskii (1963), Ashton and Whitney (1970), and others.

Several conforming and non-conforming elements have been reviewed in the literature by Zienkiewicz (1977). These elements are based upon Kirchhoff's theory, which ignores the effect of transverse stresses. Also, several elements appeared to study the behaviour of the plates in bending case (linear and geometrically nonlinear).

Reissner, (1945) developed a plate theory with parabolic distributions for transverse shear stresses over the plate thickness. A first order plate theory (FOPT) was introduced by Mindlin, (1951), where normals to midplanes before deformation remain straight but not necessarily normal after deformation. Most of the recent work in the development of efficient plate finite elements has been based on those theories. The first element to employ Mindlin's theory was introduced by Hinton et al. (1975).

A comparison of the performance of linear, serendipity, Lagrangian and Heterosis elements was given through the study of Pica et al. (1980) on the geometrically non-linear behaviour of square, skew, circular and elliptical plates using Mindlin finite elements.

A finite element based on a shear deformable theory and von Karman theory of layered composite plates was presented by Reddy (1982). Numerical results for static bending and free vibrations were given for isotropic, orthotropic and layered composite plates of rectangular geometry where the effect of geometrical nonlinearity was taken into consideration.

The demand for more accurate theory to represent structures with high thickness to span ratio has encouraged the researchers to investigate in this field. Several proposed theories represented a realistic parabolic variation of transverse shear stresses through the element thickness and did not require the use of assumed shear correction coefficients as in the (FOPT) of Mindlin.

Reddy (1984) presented a higher order shear deformation theory of plates accounting for the Von Karman strains. The theory contained the same dependent unknowns as in the (FOPT) while a

parabolic distribution of the transverse shear strains through the thickness of the plate was assumed.

In (1985), Phan and Reddy used the proposed theory of Reddy (1984) for some stability and vibration analyses and to make a comparison with the classical plate theory and the three-dimensional elasticity theory.

Shape functions are considered the most important part in the derivation of a new finite element and theory. El-Zafrany and Cookson (1986a), (1986b) introduced a general theory for the derivation of shape functions for the triangular and quadrilateral family of finite elements, respectively.

Noor and Butron (1989) introduced a review of the different approaches used for modelling multilayered composite plates. Their discussion was focused on different approaches for developing two-dimensional shear deformation theories; classification of two –dimensional theories based on introducing plausible displacement, strain and/or stress assumptions in the thickness direction; and first-order shear deformation theories based on linear displacement assumption in the thickness co-ordinate.

A series of elements based on Reissner and Mindlin assumptions has been introduced. These elements have proved to be very effective; however their relation to straightforward mixed approximations has not been clear. Zienkiewicz et al. (1990) discussed this relationship and explained the reasons for their success. This allowed new and effective triangular elements to be developed.

Madhujit and Abhijit (1990) presented an isoparametric stiffened plate-bending element for the buckling analysis of stiffened plate. The proposed finite element is based on Mindlin's hypothesis to evaluate the fundamental equations. An eight-noded isoparametric plate element had been chosen for this study.

Tasneem and Zabaras (1992) presented a refined model for the linear transient dynamic and damping analysis of laminated anisotropy composite plates. The specific damping capacity of laminated plates was discussed using an experimental measurement of specific damping capacity of laminated beams.

A new two-dimensional laminate plate theory was developed for linear elastostatic analysis of thick composite plates by Tessler (1993). That theory employed equivalent single-layer assumptions for displacements, transverse shear strains and transverse normal stresses. The inplane and transverse displacements were respectively linear and quadratic expansions through the thickness. The transverse shear strains and transverse normal stress were assumed to be quadratic and cubic, respectively through the thickness.

Verijenko et al. (1995) presented a finite element formulation for the analysis of laminated composite plates based on a higher order theory. Transverse shear and normal deformation effects have been taken into consideration. The degree of freedom of the nodal points of those elements was independent of the number of layers.

A rectangular four node finite element based on a simple higher-order shear deformation theory was developed by Sheela et al. (1996). That element was introduced during the investigation of the stability characteristics of laminated plates subjected to various types of in-plane loadings.

Attia (1996) introduced a new conforming and non-conforming finite elements for the static and dynamic analysis of rotating composite layered plates and shells. The elements consider parabolic distribution of transverse shear stresses and were based on Lagrangian and Hermitian shape functions.

Meek and Ristic (1997) introduced large displacement analysis of flat facetted element. Six nodes with three degrees of freedom and six Loof nodes with one degree of freedom represent the element.

A family of high-order facetted shell elements for linear and non-linear stress and vibration analysis of composite layered plates and shell structures was introduced by Attia and El-Zafrany (1999). Engineering slope angles were employed in element equations, and transverse stresses were expanded over the thickness.

A single layer higher order shear deformation theory was used by Moita et al. (1999) to deal with buckling and free vibrations of multilaminated structures. That model is based on an eight-node serendipity finite element with 10 degrees of freedom per node.

A recent paper was published by Matsunaga (2000), who analysed the natural frequency and buckling stress of cross-ply laminated composite plates by taking into consideration the effects of shear deformation, thickness change and rotary inertia. Two-dimensional high-order theory for thick plates was derived through Hamilton's principle.

2.3 COMPOSITE MATERIALS

Composite materials are widely used in many structural applications due to their strength to weight ratio. The study of the review articles and other recent publications reveals that geometrically nonlinear, natural vibration, and stability problems for laminated composite plates (stiffened and unstiffened) even now have attracted the attention of many researchers and investigators. Stiffened plates are often used at the present day engineering especially in aerospace and military applications.

Transverse shear deformation plays an important role even in thin laminated structures and therefore must be included in the analysis. Buckling phenomenon is considered one of the major problems of structures that are designed to withstand inplane forces. The study of the buckling phenomenon of such structures helps in the understanding of their behaviour under inplane forces.

With the increased applications of composite materials in various fields, research on their behaviour in different structural forms has also increased. Most commonly used structural forms are beams, plates and shells, which are employed in aircraft, ships and other applications. Many textbooks on the stress analysis of composite materials have been published, such as Stephen and Hahn (1980), Daniel and Ishai (1994), Staab (1999), and many others.

Crawley (1979) experimentally determined the natural frequencies and mode shapes of a number of graphite/epoxy and graphite/epoxy-aluminium plates and shells. The samples tested include 8-plies graphite/epoxy plates, cylindrical shell sections and graphite/epoxy-aluminium hybrid plates of various laminates and aspect ratios.

Stroud et al. (1984) introduced a very useful NASA report for buckling analysis of stiffened panels. The analysis, which was based upon computer packages, can be considered as accurate benchmark calculations for evaluating similar analysis procedures.

Mei and Prasad (1987) studied the influence of large deflection on random response of rectangular symmetric composite laminates to acoustic loads. The effect of transverse shear was included in the formulation but the rotary inertia effect was neglected. The study gave us an accurate analysis on the effect of transverse shear for thick and thin plates.

An "exact" mathematical tool to analyse the free vibration and buckling of symmetric cross-ply laminated plates was developed by Khdeir (1988). The procedure, which was based on a generalised Levy type solution, considered in conjunction with the state space concept, enables one to solve exactly the equations governing the laminated anisotropy plate theory as considered by Reddy (1984).

Narita and Leissa (1990) presented extensive and accurate numerical results for the critical buckling loads of simply supported, rectangular, laminated composite plates subjected to five types of loading conditions. The Ritz method was used to solve the problems.

A degenerated shell element with a degenerated beam element as a stiffener was developed for the geometric nonlinear analysis of laminated stiffened shells by Chung and Reddy (1990). Lagrangian description is used to formulate the incremental equation of motion based on the principle of virtual work.

Narita and Leissa (1992) presented an analytical approach and accurate numerical results for the free vibration of cantilevered, symmetrically laminated rectangular plates. The problem was solved by the Ritz method, and the natural frequencies were calculated for a wide range of parameters: e.g. composite material constants, fibre angles and stacking sequences.

Most structures are subjected to different types of loads during their operation. Thus, theories that can predict the complete behaviour become necessary for good understanding of the complex phenomenon of multi-layer composite structures.

Mallikarjuna and Kant (1993) classified a critical review of available literature under two broad heading: free vibrations and transient dynamics. Each of these groups described the various theoretical developments in fibre reinforced laminated composite and sandwich plates. This literature review was limited to linear free vibration and transient dynamic analysis, and geometric non-linear transient response of multilayer sandwich/fibre-reinforced composite plates.

Large deflection analysis gives more accurate response, especially at higher loads where the transverse deflection of the plate is large compared to its thickness. Chattopadhhyay et al. (1995) analysed composite stiffened plates for large deflection using the finite element method. An eight-nodded isoparametric plate element has been used where it has the capability of including transverse shear deformation. The finite element analysis has been made using Mindlin's formulation with the assumption of small rotation.

A finite element procedure was established and plate models were derived by Gaudenzi et al. (1995) for the stress analysis of laminated plates. To take into account the transverse shear distribution effect, the out-of-plane displacements were not assumed to be constant along the thickness.

Buckling analysis of laminated plates and shells under axial compression was carried out by Kim (1996) using the finite element method. The formulation of a geometrically non-linear composite shell element based on the updated Lagrangian method was presented to study the buckling behaviour. The element is capable of small strain and large displacement analysis with finite rotations. It has eight nodes with six degrees of freedom per node. Transverse shear deformation effects were included using a 1st order theory.

Rakesh and Andrew (1996) developed a method applicable to the study of generally laminated thick, skew, trapezoidal plates. The 1st order shear deformation theory was utilised to account for the transverse shear effects. All appropriate inertia terms were retained. The higher-order shear deformation theory of plates introduced by Reddy (1984) was employed in an exact analysis of laminated composite plates.

Leung and Zhou (1996) presented an analysis for the vibration and stability problem of composite laminated plates by using the dynamic stiffness matrix method. A dynamic stiffness matrix was formed by frequency dependent shape functions which are exact solutions of the governing differential equations.

Kreja et al. (1997) used the 1st order shear deformation moderate rotation shell theory of Schmidt and Reddy (1988) as a basis for the development of finite element models for the analysis of the static, geometrically non-linear response of anisotropy and laminated structures.

A finite element analysis was carried out by Jiang et al. (1997) for the bending and buckling of unstiffened, sandwich and hat-stiffened orthotropic, rectangular plates.

In the previous publications, systematic calculation were performed for deflection, stress and critical buckling load of the plate using 1st order shell elements, and 1st and 2nd order 3D solid elements.

In the analysis of composite beams and plates, higher-order shear deformation theory can lead to finite elements having the same number of nodal variables but giving solutions with improved accuracy. Shi et al. (1998) discussed an efficient finite element modelling of composite beams and plates based on higher-order shear deformation theories, i.e. how to choose the proper strain expressions to formulate accurate elements under the same number of nodal degrees of freedom.

Khdeir and Reddy (1999) obtained composite sets of linear equations with a 2nd order theory for laminated composite plates. The proposed derivations were based on the earlier theories of Reddy (1984), Schmidt and Reddy (1988). A free vibration behaviour of cross-ply and anti-symmetric angle-ply laminated plates was discussed and compared with the analytical solution.

Ferreira and Barbosa (2000) using a finite element model presented a geometric non-linear analysis of composite shell structures. The material was assumed to have an orthotropic behaviour and the performance of the model has been tested in some buckling examples. In the same field of buckling analysis, Istvan and Laszlo (2001) introduced formulas for the calculation of the buckling load of rectangular orthotropic plates with clamped and/or simply supported edges.

Parhi et al. (2000) developed a simple multiple delamination model for the dynamic analysis of multi-layered laminated composite plates having arbitrarily located multiple delamination. The displacements of any sub-laminate were expressed with respect to the mid-plane of the original laminate. The first order shear deformation theory was applied to derive the finite element equations.

2.4 FATIGUE DAMAGE OF COMPOSITE MATERIALS

Recently, composite laminates have been used extensively in the mechanical and aerospace industries, especially for the fabrication of high performance structures. To ensure high reliability of the structures, the actual behaviour of the laminated composite parts in service must be accurately predicted and carefully monitored.

A lot of research has been dedicated to the fatigue behaviour of laminated composite materials due to their increasing use in all sorts of applications. These materials have a quite good rating with regard to lifetime in fatigue and their behaviour is more complex than that of metals.

The strength and stiffness are very important design parameters of the material, but the life of the material is also an important factor. In general, fatigue is concerned with the loss of properties and performance caused by internal processes driven by the continued application and variation of external influence such as mechanical loading, thermal loading and chemical environments.

A large number of fatigue and fracture textbooks have been published since the appearance of this phenomenon, such as those by Fuchs and Stephens (1980), Carol (1982), Ewalds and Wanhill (1986) and many others. In the design of structures made from composite materials, fatigue damage is an important parameter that has been the subject of many authors, such as, Talreja (1987), Reifsnider (1991), and others.

Experimental investigations can improve our understanding of fatigue damage phenomena. An experimental program that investigated the effect of imbedded delamination on the compression fatigue behaviour of quasi-isotropic T300/5208 graphite/epoxy laminate was discussed by Ramkumar (1982). Three different stacking sequences of 64-ply layup were tested.

The effect of stacking sequence on damage growth and failure modes in composite laminates was discussed by Ratwani and Kan (1982). Tests were conducted on AS/3501-6 graphite/epoxy coupons with four different stacking sequences. The specimens were periodically taken out of the testing machine and subjected to non-destructive inspection using X-ray radiography. The results of non-destructive inspection indicate that the direction of damage propagation depends on the stacking sequence in the composite laminate.

Badaliance and Dill (1982) described observations of fatigue damage mechanism in composites subjected to compression dominated fatigue loading, formulation of a damage indicating parameter based on the intralaminar microcracking of the resin, and its application in conjunction with a linear fatigue damage model to predict spectrum life of graphite/epoxy composite laminates.

Most of the researchers concentrate on the analyses of [0°/90°] laminates as cracks propagate faster in the 90° plies. Hashin (1985) used the variational method to analyse cracked cross-ply laminates $[0^\circ/90^\circ]_s$ under tension and shear loading. Typical stress variations were presented for glass/epoxy and for graphite/epoxy laminates and their implications for the progressive damage and failure process of laminates were discussed.

Ogin et al. (1985) developed a model for the stiffness reduction due to transverse ply crack growth during the fatigue of a $[0^\circ/90^\circ]_s$ glass-fibre reinforced plastic laminate. An approximate formula for the stress intensity factor was derived for a transverse ply crack and related to the stiffness reduction rate by Paris law.

Talreja (1987) presented a simple procedure for measuring the changes in stiffness properties of a unidirectional fibrous composite caused by fatigue damage. Cracks in composite laminates were characterised by a set of vectors.

The study of matrix cracking and the associated stiffness reduction during the static and fatigue loading of cross-ply laminates has generated many publications over the years. Ogin and Smith (1987) described a model for transverse ply crack growth during the static and fatigue loading of laminates containing 90° plies.

The influence of the stress ratio on near-threshold growth of delamination fatigue cracks was investigated by Hojo et al. (1987). Tests of delamination fatigue crack propagation were carried out under mode I opening loading. The growth rates were expressed as a power function of fracture mechanics parameters.

Chang and Chang (1987a, b) introduced two researches about the progressive damage in laminated composites. The first one is the post-failure analysis of bolted composite joints in tension or shear-out mode failure. The second research concentrates on the progressive damage

model for laminated composites containing stress concentrations. The two models are capable of assessing damage accumulated in laminates with arbitrary ply orientations during mechanical loading and of predicting the ultimate strength of the joints which failed in tension or shear-out mode and of the notched laminates.

Norman and George (1988) provided a well-defined model for transverse cracking in cross-ply composite laminates based on statistical fracture mechanics. This model is well defined in the sense that no adjustable parameters are available to fit a particular set of experiments. Amongst other things, the model delivers explicit formula for the loss of stiffness as a function of crack density, and for crack density as a function of applied load.

Nairn (1989) calculated the energy release rate due to formulation of a new microcrack. A new microcracking stress analysis was discussed based on variational principles. That analysis was carried out on two types of cross-ply laminates $[0^o/90^o]_s$ and $[90^o/0^o]_s$.

An investigation was conducted by Chang et al. (1991) to study tensile failure of laminated composites containing open hole. This investigation was especially concerned with determining the response, type and extent of damage in composites as a function of applied load. A progressive damage analysis was developed to study the problem.

In case of cyclic loading, it is necessary first to derive a damage growth law and then relate the residual properties to accumulated damage. Mark et al. (1991) presented a modelling approach that recognised that the residual properties of composite laminates after any form of loading depend on the damage state. The propagation of fatigue damage in notched laminates was investigated. A power law relationship between damage growth and the strain energy release rate was developed. The strain energy release rates were calculated using a simple finite element representation of the damaged specimen.

Reddy and Reddy (1992) used the 1st order shear deformation laminate theory and the finite element method to compute the linear and non-linear first-ply failure loads for three different types of loads on the plates and four different types of boundary conditions. The first-ply failure analysis is based on the assumption that a given ply would fail if the failure index at any point within the ply reaches a value of unity.

Liu and Nairn (1992) described a series of experimental results on a wide variety of composite material systems and of cross-ply lay-ups of generic type $[0^{o}/90^{o}]_{s}$. The variational mechanics energy release rate analysis was used to predict all features of the experimental results and to draw some new conclusions about the progression of damage in cross-ply laminates.

Non-linear finite element method, which is based on the von Karman-Mindlin plate theory and the principle of minimum total potential energy, was used by Kam et al. (1996) to study the deflection and first-ply failure of thin laminated composite plates. A hypothetical stiffness reduction model was adopted to improve the prediction of load-displacement curves of damaged laminated composite plates.

Howard et al. (1996) presented a method to predict fatigue life, which explicitly accounts for specimen specific damage histories and the statistical distribution of quasi-static tensile strengths. In that case, a critical element was identified as that of the composite that controls failure and the stress on that element was monitored. Then a cumulative damage model based on the remaining strength of the critical element was used to extract an intrinsic S-N curve for the critical element fatigue response from the fatigue data and the stress history.

The finite element analysis (using ABAQUS commercial package) of the component of interest was run to capture a three-dimensional state of stress by Eason and Ochoa (1996). The motivation of that work was to enable designers to model composite structures with plate/shell elements that capture a three-dimensional state of stress for damage progression.

Gilchrist et al. (1996a, b) discussed the mechanical performance of carbon-fibre and glass fibre reinforced epoxy I-beams through a series of papers. The first one introduced the mechanical response of unnotched carbon-fibre/epoxy and glass-fibre/epoxy I-beams, as well as the behaviour of identical beams which contains a series of holes in the web and flange region. In the second part, fractographic observations associated with the mechanical behaviour under static load of both unnotched and web- and flange-notched continuously reinforced carbon-fibre and glass-fibre/epoxy I-beams were discussed. Ultrasonic scanning X-radiography and both optical and scanning electron microscopy were used to elucidate the presence of different damage mechanisms.

A recently developed technique for predicting the fatigue damage growth in fibre-reinforced plastic-composite materials due to matrix cracking was presented by Feng et al. (1997) using the ABAQUS commercial package. A fracture-mechanics approach was used to obtain experimentally the relationship between the maximum strain-energy release rate and the rate of growth of the damage area.

Interesting work was introduced by Mahmood and Lessard (1997a, b) to examine the fatigue behaviour of a unidirectional composite lamina from theoretical and experimental viewpoints. A technique to use experimental data from a unidirectional ply under uinaxial fatigue to simulate the behaviour of that ply in multiaxial fatigue loading was established in the first part. The second part of that work introduced an experimental validation of the generalized residual material property degradation model in the first one.

Sciuva et al. (1998) presented the results of the application of a procedure, developed by Reddy and Reddy (1992), for the evaluation of the first-ply failure load in multilayered composite plates. The study referred to the failure analysis of thin and thick plates under a uniformly distributed transverse load. Furthermore, a comparison of the failure criteria when the shear stresses were evaluated by means of the constitutive equations and by means of the local equilibrium equation was carried out. A very simple degradation model of the mechanical properties to account for the stiffness decrease consequent to the failure was adapted.

Gilchrist et al. (1999) introduced the third part of the series which described in details the static and fatigue mechanical behaviour and fractographic observations of the failure of composite I-beams. Experimental investigation into the fatigue response of both unnotched and web- and flange-notched continuously reinforced carbon-fibre/epoxy and glass-fibre/epoxy I-beams were discussed.

Huang et al. (2000) investigated the matrix cracking behaviour of a new high-performance composite material. Depending on the stacking sequence of the laminates and the type of loading, various matrix cracking behaviour were found, under static loading, the matrix cracks were mainly close to the specimen edges. A few cracks were found to penetrate the specimen width, even when the load was large enough to break the specimen. Combined with the fatigue Paris Rule and considering the ply thickness and stacking sequence, the energy release rate method was

applied to predict the relations between the loading strain amplitude and fatigue cycles for matrix cracking failure.

A modelling technique for simulating the fatigue behaviour of laminated composite materials, with or without stress concentrations was established by Mahmood and Lessard (2000a). The model is capable of simulating the residual stiffness, residual strength and fatigue life of composite laminates with arbitrary geometry and stacking sequence under complicated fatigue loading conditions. That model is an integration of three major components: stress analysis, failure analysis and materials property degradation rules. To validate that model, Mahmood and Lessard (2000b) carried out an experimental work using graphite/epoxy AS4/3501-6 material.

Recently, Attia, et al. (2001) proposed a methodology for predicting the fatigue life of fibre-composites and structures which combines relatively short-term fracture mechanics data, obtained from experimental measurements, with a finite-element analysis (FEA) of the component or structure. The approach was used to study the growth of damage and the fatigue life of I-beams, manufactured using carbon-fibre-reinforced-plastic. The 'ABAQUS' FEA package was employed and each ply of different orientation of the laminate was modelled individually. Hence, an automatic 'search-store-modify' technique was implemented whereby a 'UNIX' operating system and a 'FORTRAN' subprogram were used, which ran the 'ABAQUS' FEA software.

2.5 CONCLUSION

The following conclusion points can be drawn from the literature review:

(i) The finite element method (FEM) is the most popular numerical technique, and it has been applied successfully with many engineering disciplines.

(ii) Composite materials are increasingly believed to be the materials of the future with potential for application in high performance structures.

(iii) The higher-order theory for the analysis of laminated plates has received increased attention in the last decade. The main reasons are that:

- Composite materials have been increasingly used for structural purpose in many engineering applications.

- The need for more accurate theory than the classical one to account for the transverse shear and rotary inertia effects.

(iv) There is a need for further developments of efficient numerical tools for buckling and free vibration studies.

(v) Although, there is very little published work on the use of the finite element method for fatigue damage analysis of composite materials, most of that work is based on the current versions of commercial packages, which means that the methodology followed has to be changed corresponding to any new version. Furthermore, it is restricted to a certain accuracy of results, while in the fatigue damage analysis one may need results of six or more digits. From the point of view of time and effort required, that work has the limitations of needing a huge amount of computer memory for creating input and output files during every run, and requiring a great amount of CPU time. Hence, the analysis with commercial finite element packages may require an expensive workstation dedicated to only one user during the long time of the analysis to use it.

(vi) There is a need for an element, which can be used in assessing the composite fatigue damage accurately and efficiently.

3

COMPOSITE THEORY AND EXPERIMENTAL SETUP

3.1 INTRODUCTION

A material is called composite when it is formed from two or more materials. Depending on the number of these constituent materials and their properties, the material properties of the composite are defined.

From the different types of composite materials, fibre reinforced composites have a wide range of applications, because it is the most efficient type from the point of view of stiffness and strength. Fibre reinforced composites can be classified into three broad categories according to the matrix used: polymer matrix, metal matrix and ceramic matrix.

In this chapter, the basic concepts and theories of the composite materials are discussed. From these concepts, the material coordinate system and the constitutive equations which govern the stress-strain relations of the laminated composite materials are defined. The transformation of the constitutive equations from the material coordinate system to the local coordinate system is discussed as the finite element equations are derived with respect to the local coordinate system. Damage development and the fatigue damage growth of composite materials are introduced.

The manufacturing process is one of the most important stages in the application of composite materials. A quick review on the manufacturing process and the methods used with it will be introduced in this chapter. The experimental setup (natural frequency test, buckling test and fatigue test) and the instruments used with these tests are explained.

3.2 BASIC CONCEPTS OF COMPOSITE MATERIALS

Some basic concepts of composite materials, which are used later in the derivation of the finite element equations, are defined.

3.2.1 Constituents of composite materials

A composite material is formed when two or more materials are combined so that the properties of the composite are different (and usually better) from those of the individual

constituents. Composites are made up of continuous and discontinuous mediums. The continuous medium is called "matrix". The main functions of the matrix are to support and protect the fibres and provide a means of distributing load among and transmitting load between the fibres. The discontinuous medium, which is usually the harder and the stronger one, is called "reinforcement or fibre".

From the types of matrix materials, epoxy resins are the most commonly used matrices in advanced composite materials. The most widely used fibres are the glass fibres and carbon fibres, which are the most popular fibres in high-performance composite structures.

3.2.2 Unidirectional composite material

From the conclusions of the literature review, it is clear that the unidirectional composite materials are the most efficient types of composite materials from the point of view of stiffness and strength. Fig (3.1) shows a basic unit of composite material in which unidirectional fibres are embedded in a matrix.

3.2.3 Lamina and laminate

A lamina is the basic building block in a laminated fibre reinforced composite. A lamina is a flat (sometimes curved as in a shell) arrangement of unidirectional fibres in a matrix as shown in Fig. (3.1).

A laminate is a stack of laminas with various orientations of principal material directions in the lamina. The laminate's layers are usually bound together by the same matrix material that is used in the lamina. A major purpose of lamination is to tailor the directional dependence of strength and stiffness of a material to match the loading environment of the structural element. Laminates are uniquely suited to this objective since the principal material directions of each layer can be oriented according to need.

For many composite laminates, there are cases for which the stiffness takes on simplified values. These special laminates are particularly popular in practice. The following special

cases are recognised as shown in Figure (3.2): symmetric laminates $[\theta/-\theta/-\theta/\theta] \equiv [\pm\theta]_s$, asymmetric laminate $[\theta/-\theta/\theta/-\theta] \equiv [\pm\theta]_2$, cross-ply laminates [0/90] and others.

3.2.4 Coordinate systems

Figure (3.3) shows the coordinate system x'-y'-z' so that, the x axis lies along the fibre direction and axes y' and z' are directed perpendicular to it. This coordinate system is called the material coordinate system. It differs from layer to layer depending upon the orientation of the fibres, which is defined by the angle of orientation θ. When multiple plies are present, as for a composite laminate, a second coordinate system is chosen with respect to which all material transformation and homogenisation procedures are performed. This coordinate system is labelled x-y-z, and called the local coordinate system.

3.2.5 Macromechanics of composite materials

Macromechanics is the study of composite material behaviour wherein the material is assumed homogeneous (not necessarily isotropic) and the effects of the constituent materials are detected only as averaged apparent properties of the composite. Macromechanics is used for structural design and analysis.

3.3 CONSTITUTIVE EQUATIONS FOR LAMINATES

A composite laminate plate or shell usually consists of a number of layers bonded firmly with each other. Each layer is a lamina and it is flat for plates and curved for shells. A lamina is in (or parallel to) the x-y plane as shown in Fig. (3.3).

If x'-y'-z' are the material axes, where x' is usually in the fibre direction, then the properties of each lamina are given in terms of:

(i) $E_{x'}$, Young's modulus in fibre direction.

(ii) $E_{y'}$, Young's modulus in transverse direction.

(If $E_{z'}$ is required, the Young's modulus in z' direction, we take $E_{z'} = E_{y'}$)

(iii) $\nu_{x\backslash y\backslash}$, major Poisson's ratio, minor Poisson's ratio $\nu_{y\backslash x\backslash}$ can be obtained from:

$$\frac{\nu_{x\backslash y\backslash}}{E_{x\backslash}} = \frac{\nu_{y\backslash x\backslash}}{E_{y}}$$

(iv) $\mu_{x\backslash y\backslash}$, shear modulus in x$\backslash$-y$\backslash$ plane

(v) $\mu_{y\backslash z\backslash} = \mu_{z\backslash x\backslash}$, transverse shear moduli (not always given)

The stress and strain states at any point inside a layer may be defined in terms of the following stress and engineering strain vectors, (El-Zafrany, 1995):

$$\underline{\sigma} = \{\sigma_x \quad \sigma_y \quad \sigma_z \quad \tau_{xy} \quad \tau_{yz} \quad \tau_{zx}\} \tag{3.1}$$

$$\underline{\varepsilon} = \{\varepsilon_x \quad \varepsilon_y \quad \varepsilon_z \quad \gamma_{xy} \quad \gamma_{yz} \quad \gamma_{zx}\} \tag{3.2}$$

The elastic stress-strain equations may be expressed with respect to x$\backslash$-y$\backslash$-z$\backslash$ coordinate system as follows:

$$\underline{\varepsilon}^{\backslash} = \underline{C}^{\backslash}\ \underline{\sigma}^{\backslash} \tag{3.3}$$

and $$\underline{\sigma}^{\backslash} = \underline{D}^{\backslash}\ \underline{\varepsilon}^{\backslash} \tag{3.4}$$

where

$$\underline{D}^{\backslash} = \underline{C}^{\backslash -1} \tag{3.5}$$

and $$\underline{D}^{\backslash} = \begin{bmatrix} \underline{d}^{\backslash}_{3x3} & \underline{0}_{3x3} \\ \underline{0}_{3x3} & \begin{matrix} \mu_{x'y'} & 0 & 0 \\ 0 & \mu_{y'z'} & 0 \\ 0 & 0 & \mu_{z'x'} \end{matrix} \end{bmatrix} \tag{3.6}$$

where

$$\underline{d}'_{3x3} = \frac{1}{Q}\begin{bmatrix} E_x(1-\nu_{y'z}\nu_{zy}) & E_{x'}(\nu_{x'y}+\nu_{xz}\nu_{zy'}) & E_x(\nu_{x'z}+\nu_{x'y}\nu_{yz}) \\ E_{y'}(\nu_{yx}+\nu_{yz}\nu_{zx'}) & E_y(1-\nu_{xz}\nu_{z'x'}) & E_y(\nu_{y'z'}+\nu_{y'x}\nu_{xz}) \\ E_{z'}(\nu_{zx'}+\nu_{zy'}\nu_{y'x'}) & E_z(\nu_{zy'}+\nu_{zx'}\nu_{x'y}) & E_{z'}(1-\nu_{xy}\nu_{yx'}) \end{bmatrix}$$

$$Q = 1-\nu_{x'y'}\nu_{y'x}-\nu_{yz}\nu_{zy'}-\nu_{z'x'}\nu_{xz'}-\nu_{xy}\nu_{yz}\nu_{zx}-\nu_{xz}\nu_{zy}\nu_{yx}$$

In general laminated composites, the fibres in a ply are aligned in different directions relative to the reference axes to achieve the desired properties in the appropriate directions. When the ply material axes do not coincide with the reference axes, the ply is called generally orthotropic ply. The stress-strain relationship of a generally orthotropic ply is determined by taking the following points into consideration:

- The stress transformations from material axes to local axes.
- The strain transformations from material axes to local axes.
- The stress-strain relationship of an especially orthotropic ply.

The directional cosines of x'-y'-z' axes with respect to the x, y, z axes are:

$$(\cos\theta\ ,\ \sin\theta\ ,\ 0)\ \ ,(-\sin\theta\ ,\ \cos\theta\ ,\ 0)\ \ ,(0\ ,\ 0,\ 1)$$

and

$$\underline{R} = \begin{bmatrix} \cos\theta & \sin\theta & 0 \\ -\sin\theta & \cos\theta & 0 \\ 0 & 0 & 1 \end{bmatrix}$$

where $\underline{R}$ represents the rotation matrix from of x'-y'-z' coordinate system to the x, y, z coordinate system.

3.3.1 Stress transformation

The stress vector with respect to material axes can be expressed in terms of the stress vector with respect to local axes as follows, (El-Zafrany, 1995):

$$\underline{\sigma}^{\backslash} = \underline{R}_{\sigma}\,\underline{\sigma} \tag{3.7}$$

where $\underline{R}_{\sigma}$ is the stress transformation matrix:

$$\underline{R}_{\sigma} = \begin{bmatrix} m^2 & n^2 & 0 & 2mn & 0 & 0 \\ n^2 & m^2 & 0 & -2mn & 0 & 0 \\ 0 & 0 & 1 & 0 & 0 & 0 \\ -mn & mn & 0 & m^2 - n^2 & 0 & 0 \\ 0 & 0 & 0 & 0 & m & -n \\ 0 & 0 & 0 & 0 & n & m \end{bmatrix}$$

where, $m = \cos\theta$ $\quad$ $n = \sin\theta$

From equation (3.7), it is clear that:

$$\underline{\sigma} = \underline{R}_{\sigma}^{-1}\,\underline{\sigma}^{\backslash} \tag{3.8}$$

3.3.2 Strain transformation

Similarly, the strain vector with respect to material axes can be expressed in terms of the strain vector with respect to local axes as follows:

$$\underline{\varepsilon}^{\backslash} = \underline{R}_{\varepsilon}\,\underline{\varepsilon} \tag{3.9}$$

where $\underline{R}_{\varepsilon}$ is the strain transformation matrix:

$$\underline{R}_{\varepsilon} = \begin{bmatrix} m^2 & n^2 & 0 & mn & 0 & 0 \\ n^2 & m^2 & 0 & -mn & 0 & 0 \\ 0 & 0 & 1 & 0 & 0 & 0 \\ -2mn & 2mn & 0 & m^2 - n^2 & 0 & 0 \\ 0 & 0 & 0 & 0 & m & -n \\ 0 & 0 & 0 & 0 & n & m \end{bmatrix}$$

and from equation (3.9), it is clear that:

$$\underline{\varepsilon} = \underline{R}_{\varepsilon}^{-1} \underline{\varepsilon}^{\backslash} \tag{3.10}$$

3.3.3 D matrix transformation

It is clear from the definition of the $\underline{D}$ matrix that the following matrix equation can be employed with respect to the x-y-z coordinate system:

$$\underline{\sigma} = \underline{D}\ \underline{\varepsilon} \tag{3.11}$$

and similarly, one can define a stiffness matrix $\underline{D}^{\backslash}$ with respect to the $x^{\backslash}$-$y^{\backslash}$-$z^{\backslash}$ coordinate system such that:

$$\underline{\sigma}^{\backslash} = \underline{D}^{\backslash}\ \underline{\varepsilon}^{\backslash} \tag{3.12}$$

Substituting from equation (3.7) and (3.9) into (3.12) then

$$\underline{R}_{\sigma}\ \underline{\sigma} = \underline{D}^{\backslash}\ \underline{R}_{\varepsilon}\ \underline{\varepsilon}$$

i.e. $$\underline{\sigma} = \underline{R}_{\sigma}^{-1}\ \underline{D}^{\backslash}\ \underline{R}_{\varepsilon}\ \underline{\varepsilon} \tag{3.13}$$

Comparing equation (3.11) with (3.13) it can be deduced that

$$\underline{D} = \underline{R}_{\sigma}^{-1}\ \underline{D}^{\backslash}\ \underline{R}_{\varepsilon} \tag{3.14}$$

Explicit values of $\underline{D}$ matrix have been given in appendix "A".

The D matrix can be divided into two independent separate parts for transverse shear stress $\underline{\tau}$ and x-y stress $\underline{\sigma}_{xy}$, in terms of transverse shear strain $\underline{\gamma}$ and x-y strain $\underline{\varepsilon}_{xy}$.

The transverse shear stress and strain vectors are defined as follows:

$$\underline{\tau} = \{\tau_{xz} \quad \tau_{yz}\} \tag{3.15}$$

$$\underline{\gamma} = \{\gamma_{xz} \quad \gamma_{yz}\} \tag{3.16}$$

Hence, it is clear from equations (3.1), (3.2), (3.11), and (3.14) that:

$$\underline{\tau} = \underline{\mu}_{2x2} \ \underline{\gamma} \tag{3.17}$$

where

$$\underline{\mu}_{2x2} = \begin{bmatrix} d_{66} & d_{65} \\ d_{56} & d_{55} \end{bmatrix} \tag{3.18}$$

The x-y stress and strain components are defined as follows:

$$\underline{\sigma}_{xy} = \{\sigma_x \quad \sigma_y \quad \tau_{xy}\} \tag{3.19}$$

$$\underline{\varepsilon}_{xy} = \{\varepsilon_x \quad \varepsilon_y \quad \gamma_{xy}\} \tag{3.20}$$

If σ_z is negligible (plane stress) then:

$$\sigma_z = d_{31}\varepsilon_x + d_{32}\varepsilon_y + d_{34}\varepsilon_{xy} + d_{33}\varepsilon_z \approx 0$$

$$\text{i.e.} \qquad \varepsilon_z = \frac{1}{d_{33}}(d_{31}\varepsilon_x + d_{32}\varepsilon_y + d_{34}\varepsilon_{xy}) \tag{3.21}$$

Hence the x-y stress components can be obtained from equations (3.21), (3.11), and (3.14) as:

$$\underline{\sigma}_{xy} = \underline{D}_{xy} \ \underline{\varepsilon}_{xy} \tag{3.22}$$

where $\underline{D}_{xy} = \begin{bmatrix} d_{11} - \frac{d_{13}\,d_{31}}{d_{33}} & d_{12} - \frac{d_{13}\,d_{32}}{d_{33}} & d_{14} - \frac{d_{13}\,d_{34}}{d_{33}} \\ d_{21} - \frac{d_{23}\,d_{31}}{d_{33}} & d_{22} - \frac{d_{23}\,d_{32}}{d_{33}} & d_{24} - \frac{d_{23}\,d_{34}}{d_{33}} \\ d_{41} - \frac{d_{43}\,d_{31}}{d_{33}} & d_{42} - \frac{d_{43}\,d_{32}}{d_{33}} & d_{44} - \frac{d_{43}\,d_{34}}{d_{33}} \end{bmatrix}$

3.4 DAMAGE OF COMPOSITE MATERIALS

From the advantages of composite materials, it may pass through different modes of failure before reaching the complete failure (fracture). In this work, our concentration will be on the damage occurs due to cyclic load which is the fatigue damage.

3.4.1 Damage development of composite materials

Different failure modes of composite materials are defined in the literature: matrix cracking, crack coupling and interfacial debonding, delamination and fibre breaking (Reifsnider, 1991). Any one of those damage modes may cause a complete damage of the material. In the general case, the failure is caused by a combination of two or three modes. Figure (3.4) shows a schematic representation of the development of damage during the fatigue life of a composite laminate reported by Reifsnider (1991).

The initial stage of this development is the matrix cracking, which is initiated from flaws in the matrix and grows until the crack reaches an interface. The growth of this crack depends upon the stress value at the crack tip. The delay of this growth means the stress at the crack tip is insufficient to break the fibre. This crack generally occurs in composite materials, which have brittle matrix materials, such as graphite/epoxy and glass/epoxy, and it also occurs under fatigue load in composite materials, which have ductile matrix components, if the matrix cracks are long enough to create small cracks through the interface between plies, which lead to failure of the interface.

The next stage is the delamination, which is the debonding from one ply to another. It is caused by the discontinuities in the path of the load due to the matrix cracks and the small cracks through the interface.

The critical stage of the damage development of composite materials, which leads to complete failure, is fibre breaking. The fibre may fail at the weakest point along its length or at a point of high stress concentration at the crack tip.

The fracture is the final stage of damage development, which represents a complete failure of a component due to rapid progression of the damage modes.

3.4.2 Fatigue damage growth of composite materials

Fatigue damage is a feature of failure due to cyclic load. Fatigue damage phenomenon is defined as the reduction of the strength and the subsequent failure of materials subjected to repeated load. The fatigue damage of composite materials is more complex and difficult to predict than that of metals.

In fact, the fatigue behaviour is dependent on the type of composite materials and its constituents as well as the geometry, load conditions and environment. The treatment of this phenomenon begins with a description and discussion of failure modes of composite materials, which are responsible for the fatigue process in composite materials of various types.

A structure subjected to fatigue load generally goes through three stages during its fatigue life: fatigue damage initiation, fatigue damage growth, and fracture. Due to applying this type of load, energy is accumulated near flaws and defects that grow and unite, forming small cracks (fatigue initiation). In some applications, the fatigue damage initiation is considered a complete failure state of a structure, especially for those applications designed by fail-safe design criterion, (Carl, 1982).

Fatigue damage initiation does not necessarily imply total failure of the structure, but is only the beginning of an interactive and progressive failure process. Fatigue damage growth process is considered a better way to understand the fatigue phenomena; especially in the

applications which have stress concentration effects. The fatigue damage growth process is controlled by two important factors: the damage growth rate and the linear elastic fracture mechanics concepts (LEFM).

The fracture is the final stage, which represents a complete failure of a component due to rapid progression of the damage modes.

Figure (3.5) shows the three development stages during the fatigue life and represents the relation between the damage growth rate and the stress intensity range, (Gdoutos, 1993). Region I represents the initiation stage below which there is no observable crack growth. The damage growth is represented by region II where the relation between the damage rate and the stress intensity range is linear on the logarithmic chart.

One of the most widely used fatigue crack growth laws in metals and alloys is that proposed by Paris and Erdogan (1963) and it is usually known as the Paris law. That equation represents a linear relationship between the stress intensity factor range and the crack growth rate in logarithmic scale as shown in region II of Figure (3.5) and is used to describe the fatigue crack growth behaviour. It can be represented as follows, (Gdoutos, 1993):

$$\frac{da}{dN} = C\ (\Delta K)^m \tag{3.23}$$

where da/dN is the crack growth rate, ΔK is the stress intensity factor range, and C and m are material constants determined experimentally.

The basic concepts of linear elastic fracture mechanics have been represented by two approaches, stress approach and energy balance approach. Stress approach is defined by the stress intensity factor K to represent the relation between load configuration, crack shape and crack mode as well as to describe the stress distribution around a damaged area. The energy approach is defined by energy release rate G. In that approach, the damage instability occurs as soon as the total energy no longer increases with increasing damage area.

The fatigue damage behaviour in composites is quite difficult to assess and it is usually caused by more than one mode of failure. Consequently, the energy balance approach is used to analyse the fatigue damage growth in composites.

The fatigue damage behaviour of composites has been investigated by Feng et al. (1997) using the strain energy release rate derived by Nairn and Hu (1985) to formulate a matrix micro crack in cross-ply laminates which is given by:

$$G = \frac{1}{2}\sigma_{90}^2\, t_{90} \sqrt{C_1\left(C_4 - C_2 + 2\sqrt{C_1 C_3}\right)} \tag{3.24}$$

where

$$C_1 = \frac{1}{E_1^{(90)}} + \frac{1}{\lambda E_1^{(s)}}$$

$$C_2 = \frac{\nu_{13}^{(90)}}{E_1^{(90)}}\left(\lambda + \frac{2}{3}\right) - \frac{\lambda \nu_{13}^{(s)}}{3E_1^{(s)}}$$

$$C_3 = \frac{1}{60\, E_3^{(90)}}\left(15\lambda^2 + 20\lambda + 8\right) + \frac{\lambda^3}{20E_3^{(s)}}$$

$$C_4 = \frac{1}{3\, G_{13}^{(90)}} + \frac{\lambda}{3\, G_{13}^{(s)}}$$

where σ_{90} is the tensile stress in the transverse direction within the 90^o plies, t_{90} is the thickness of all 90^o plies. The term $\lambda = t_s/t_{90}$, where t_s is the sum of the thickness of the sub laminates. $E^{(90)}$, $G^{(90)}$ and $\nu^{(90)}$ represent the material properties of the 90^o plies and $E^{(s)}$, $G^{(s)}$ and $\nu^{(s)}$ are the material properties of the sub laminates.

That study has concentrated on micro cracking in 90^o plies and reviewed micro crack in $[0/90]_s$ and $[90/0]_s$ laminates. The main problem of that model is that it is limited only to one type of stacking sequence which is the cross-ply laminates. The details of fatigue damage theories employed in this thesis are discussed in chapter 6.

3.5 MANUFACTURING PROCESS

Two types of fibre reinforced materials have been used in this work, carbon/epoxy (Fiberite 977-2 toughened epoxy resin) by Cytec Fiberite Ltd. and glass/epoxy (Fibredux 914G-E-5-30%) by CIBA-GEIGY Ltd.

Typical applications for the Fiberite 977-2 include aircraft primary and secondary structures, space structures, ballistics, cryogenic tanks, or any application where impact resistance and light weight are required.

The Fibredux 914 is a highly successful modified epoxy matrix which is used extensively in high temperature resistant primary aircraft structures. The controlled melt viscosity and excellent matrix rheology of the Fibredux 914 permit a wide range of processing conditions for high quality components.

The materials are delivered in a prepregs form where the reinforcing fibre are produced in a sheet form. The prepregs form is complete in itself ready for component manufacture and it has the following advantages:

- Being ready formulated, they reduce the chemical knowledge required by a component manufacturer
- No worries about stocking various resins, hardeners and reinforcements
- Greater design freedom due to the simplicity of cutting irregular shapes
- Waste material is almost completely eliminated
- Reproducible quality
- Automated mass production methods used

A varity of manufacturing methods suitable for several applications are available. From them, the vacuum bag and autoclave methods are applied.

A typical vacuum bag is shown in Figure (3.6). The normal contact moulding is the first to be carried out. Before curing has advanced, a flexible membrane is placed over the component (flexible bag e.g. polvinyl, nylon); all joints are sealed and a vacuum is created. This results in subjecting the moulding surface up to one atmospheric pressure and thus forcing out air (voids) and excess resin.

An autoclave consists of a cylindrical vessel constructed to withstand high pressure and temperature. A typical autoclave is shown in Figure (3.7). The application of heat results in an initial reduction of resin viscosity and hence resins flow. A pressure plate is used to aid in the application of uniform pressure over the component surface. The pressure plate is separated from the bleed layers by a non-porous release film.

3.6 EXPERIMENTAL SETUP

Some experimental work is presented in this work to verify the natural frequency and buckling analysis and to provide fatigue life curves (S-N diagrams) for the two types of laminates mentioned earlier in section 3.5. The material is prepared in panel forms with different stacking sequences based on the types of test.

3.6.1 Material preparation

The final form of the specimens used with this experimental work is shown in Figure (3.8) after cutting the large panels to small specimens and making some preparation (sticking grips, drilling, ... etc.) to be ready for test. The configuration of the test specimen is critical in order to achieve reproducible results. Specimen configuration is generally specified for each test procedure.

The fatigue test specimens are straight-sided coupons of constant cross section. Figure (3.9) shows the geometry of the specimen as described in ASTM D3039-76 (1989). Recommended thickness is 0.5 to 2.5 mm (0.02 to 0.1 in) usually six plies for the longitudinal specimen and at least eight plies for the transverse one. However, it was necessary to modify the

configuration in order to obtain acceptable values (to ensure failure in the gauge area and not within the area in contact with the test grips).

3.6.2 Natural frequency test

The hammer test is applied in the natural frequency test, as shown in Figure (3.10). The test is applied on the two types of composite with three different dimensions. The specimen was clamped from one end and free from the other one. The position of the applied load and the response is selected carefully to avoid any node position. The output measurements is recorded by the FFT analyzer through the force transducer and accelerometer.

The dimensions of the specimens and the results will be presented and discussed later in chapter 8.

3.6.3 Buckling test

The fatigue testing machine shown in Figure (3.11), which was manufactured by Denison Mayes Group is used in the buckling and fatigue test. This machine is well-suited for measuring the fatigue properties of various materials under the testing modes of tension, compression, and tension-compression alternating loads. The machine can also be used with 100 kN as a maximum allowable load. The buckling test is applied on the two types of composites with three different dimensions. The buckling analysis is carried out by increasing the applied compression load to the buckling mode is observed. The dimensions of the specimens and the results will be presented and discussed later in chapter 8.

3.6.4 Fatigue test

The main purpose of this test is to provide fatigue life diagrams (S-N Diagrams). The axial fatigue test is used to determine the effect of variations in material, geometry, surface condition, stress, ... etc., on the fatigue resistance of materials subjected to direct stress for relatively large numbers of cycles. The test results (S-N diagrams) may be used as a guide in the proposed finite element package to the selection of materials for service under conditions of repeated direct stress.

The type of specimens used depends on the objective of the test program, the type of equipment capacity and the form in which the material is available. However, the design must meet certain general criteria, (Daniel and Ishai, 1994):

- Failure occurs in the test section.
- The absolute maximum stress should not be less than 25% of the machine operating stress range being used and the absolute minimum stress should not be less than < 2.5% of the machine operating range being used.

At least three specimens are applied at each certain level of stress with frequency 10 [Hz]. Samples of the failed specimens are shown in Figure (3.12).

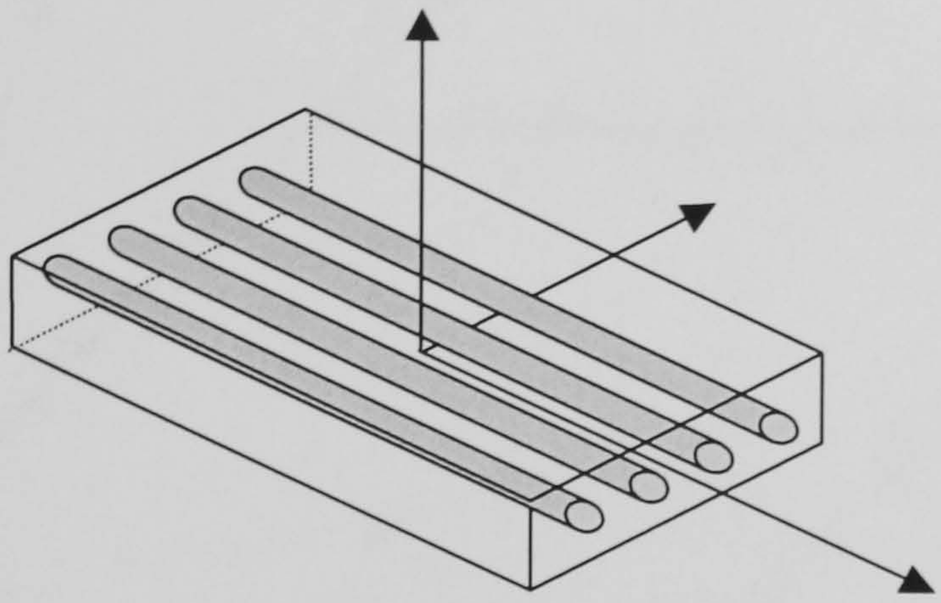

Figure (3.1) Lamina with unidirectional fibres

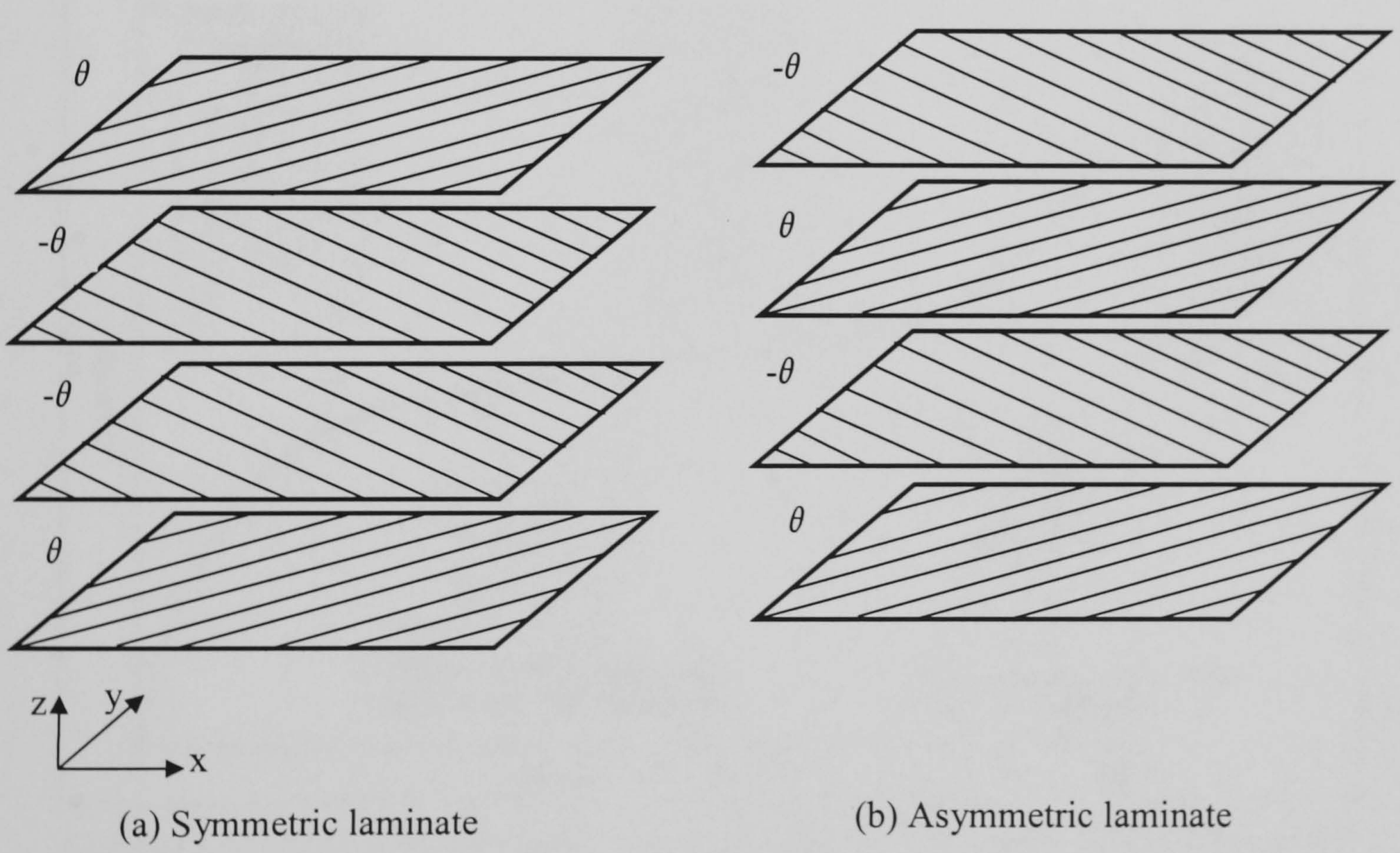

(a) Symmetric laminate (b) Asymmetric laminate

Figure (3.2) Laminates with various fibre orientations

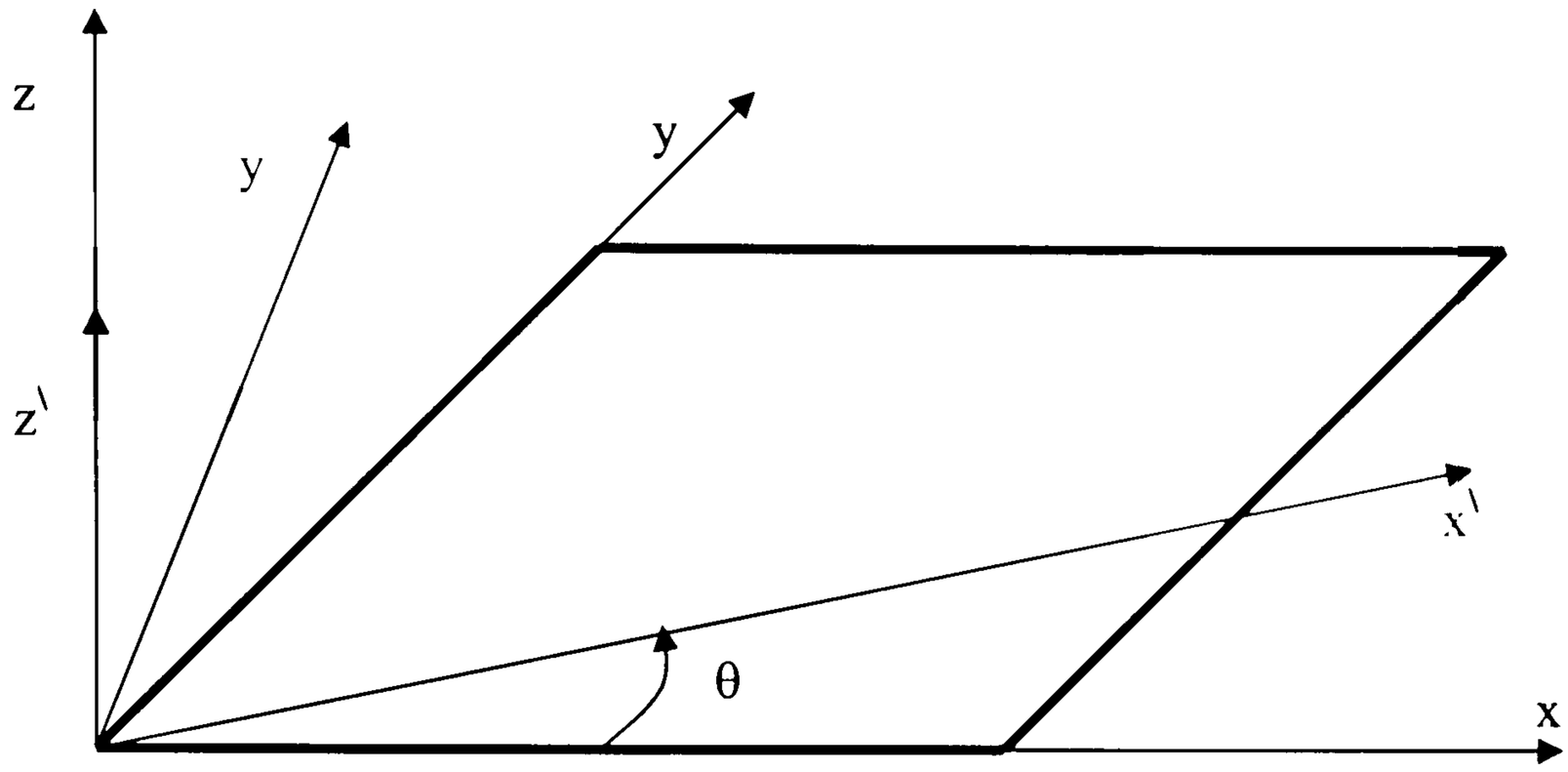

Figure (3.3) Local and material axes of lamina

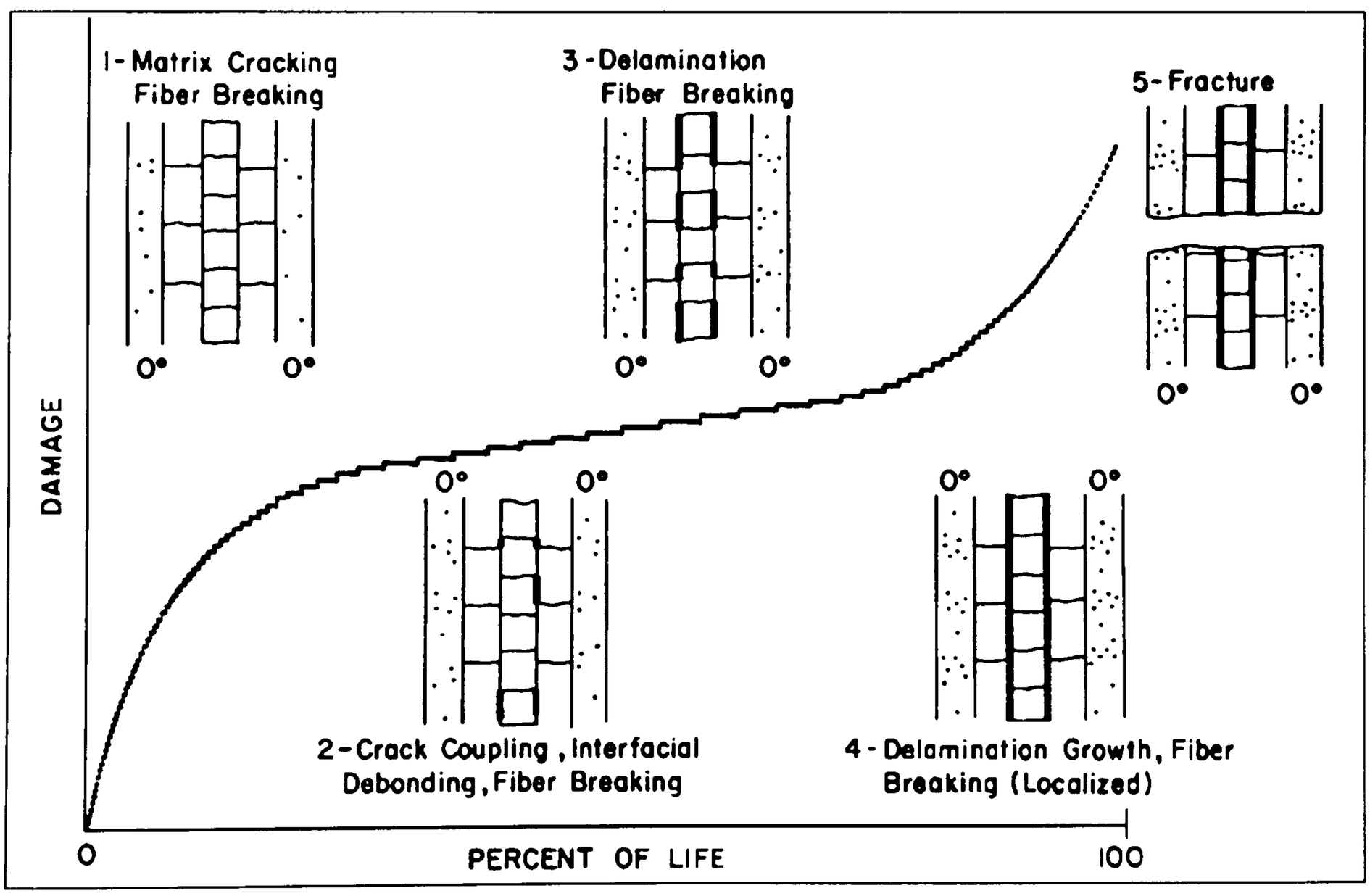

Figure (3.4) Damage development of composite material laminate during fatigue life

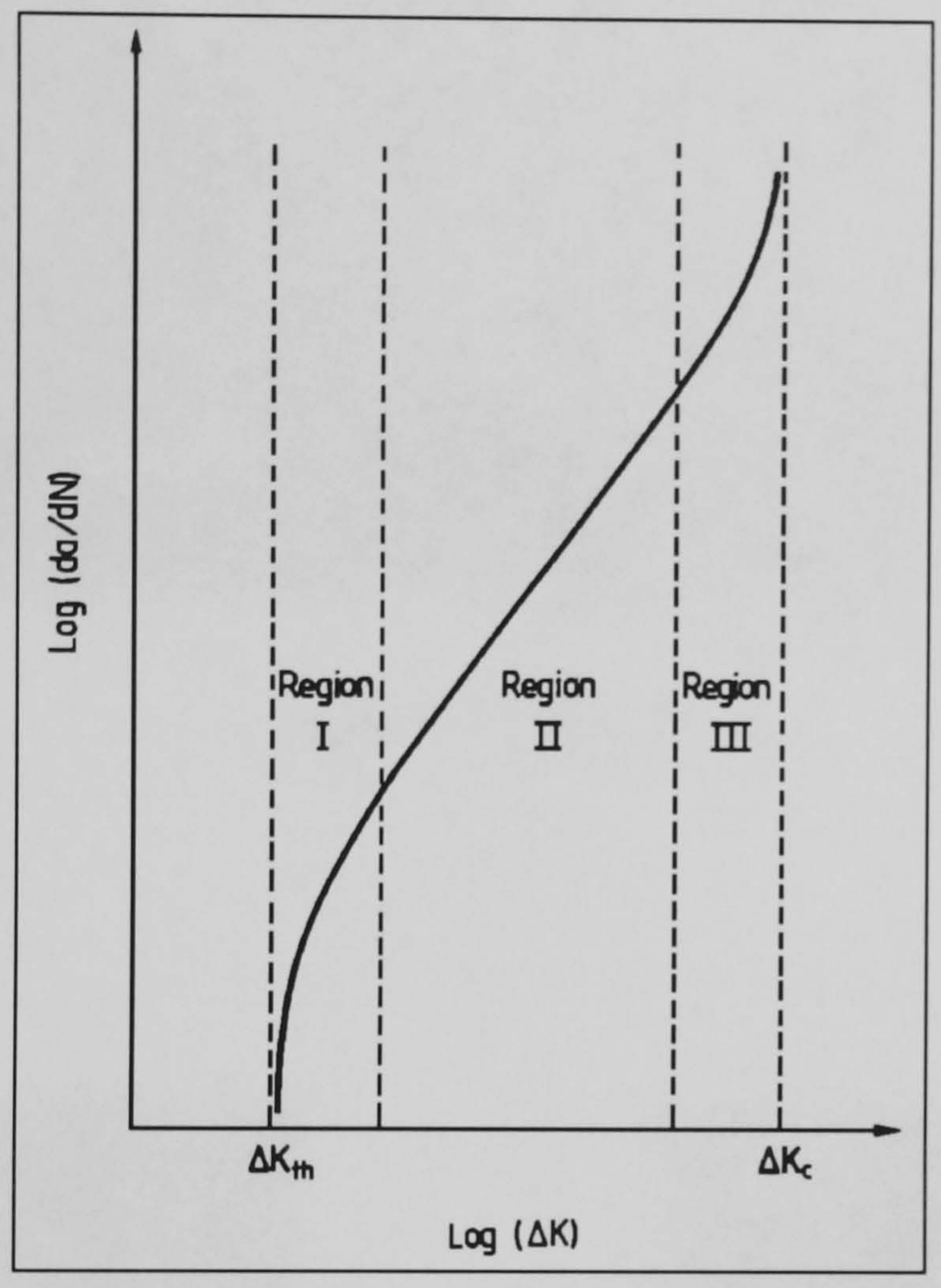

Figure (3.5) Fatigue crack growth rate

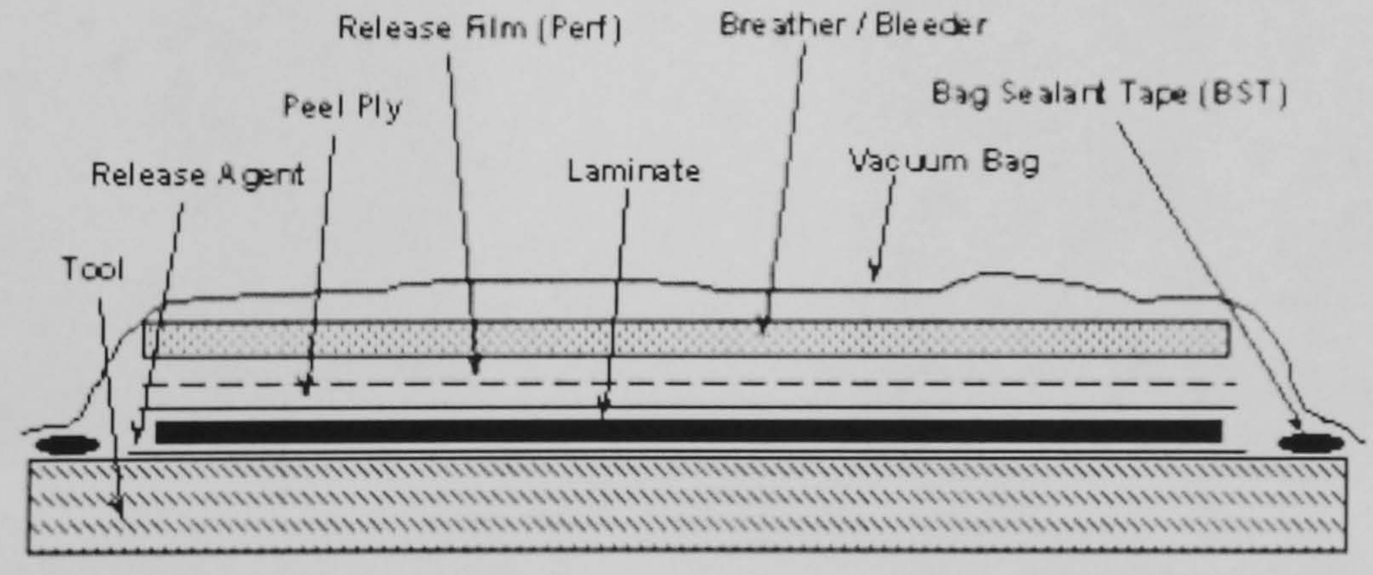

Figure (3.6) Schematic diagram of vacuum bag

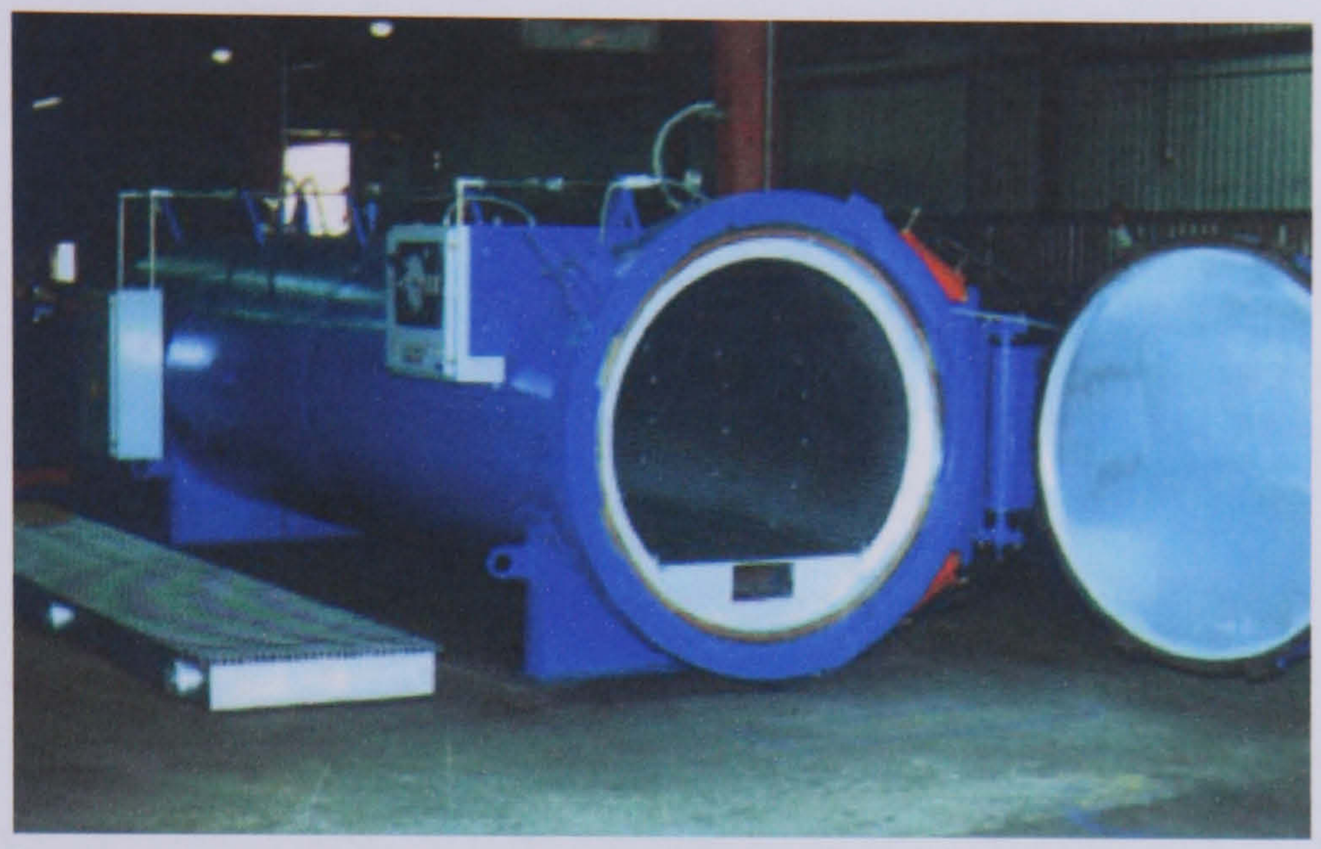

Figure (3.7) Autoclave

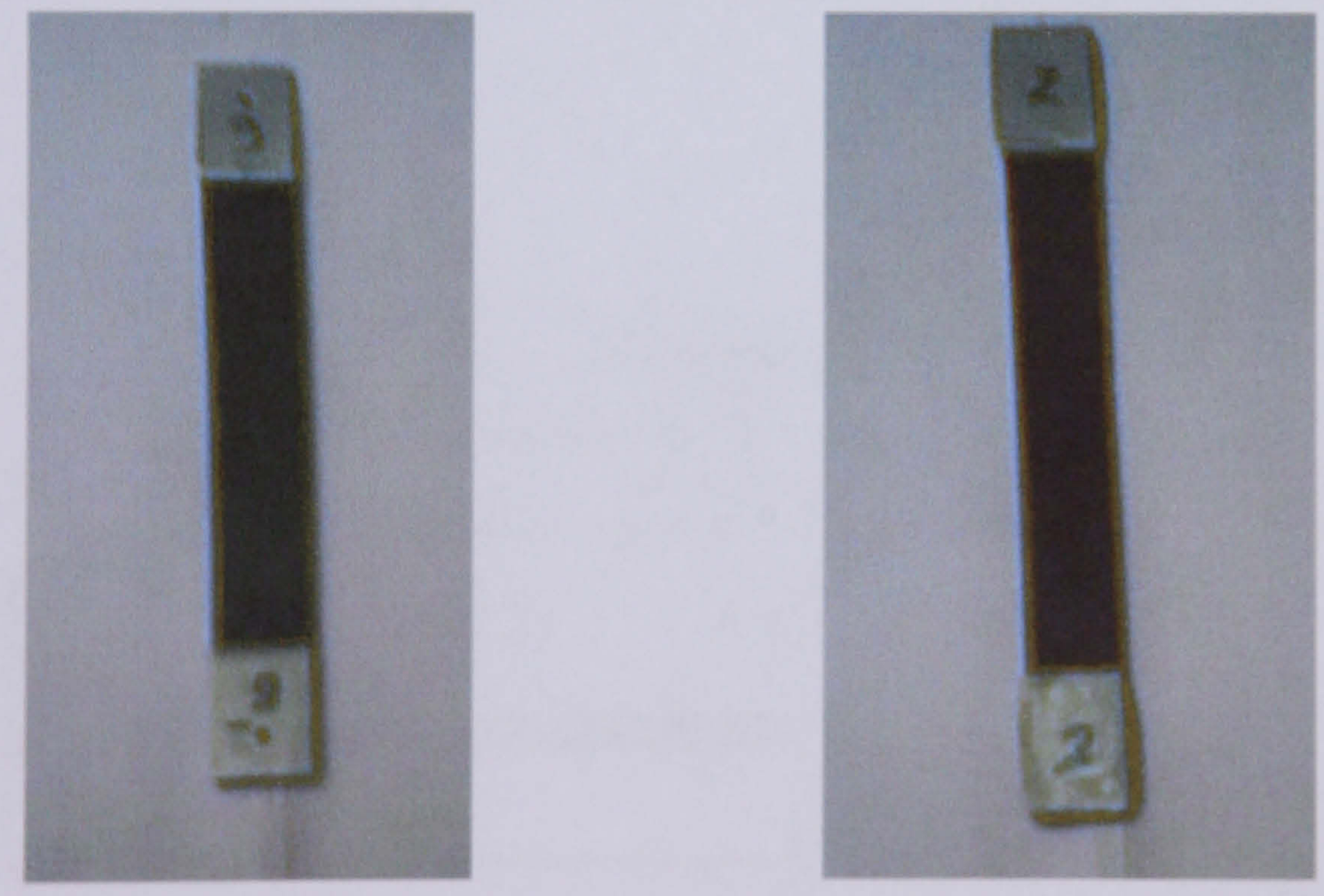

(a) Carbon/epoxy specimen (b) Glass/epoxy specimen

Figure (3.8) Geometry of specimens used with the fatigue test

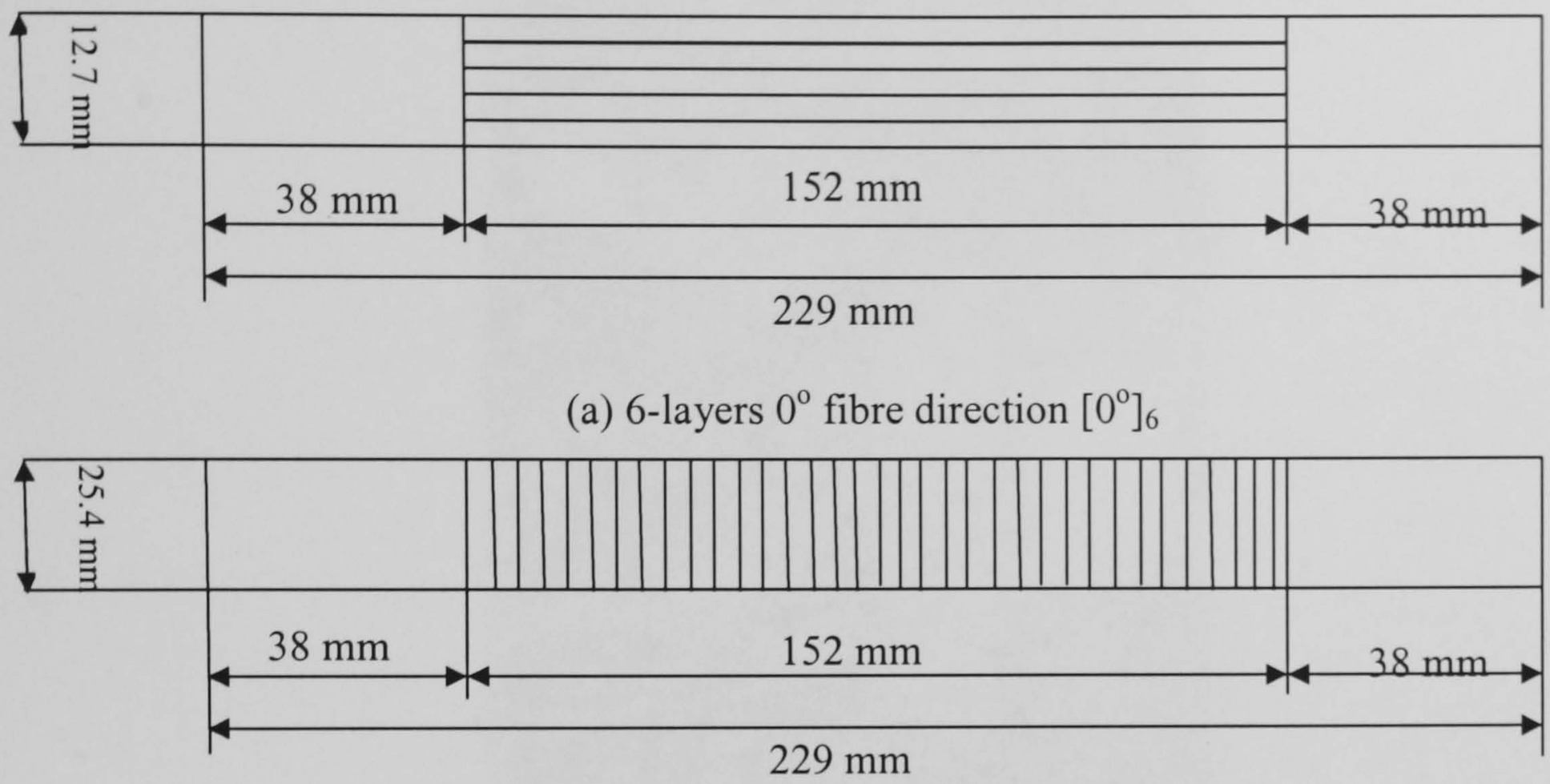

(a) 6-layers 0^o fibre direction $[0^o]_6$

(b) 8-layers 90^o fibre direction $[90^o]_8$

Figure (3.9) Geometry of specimens used with the fatigue test

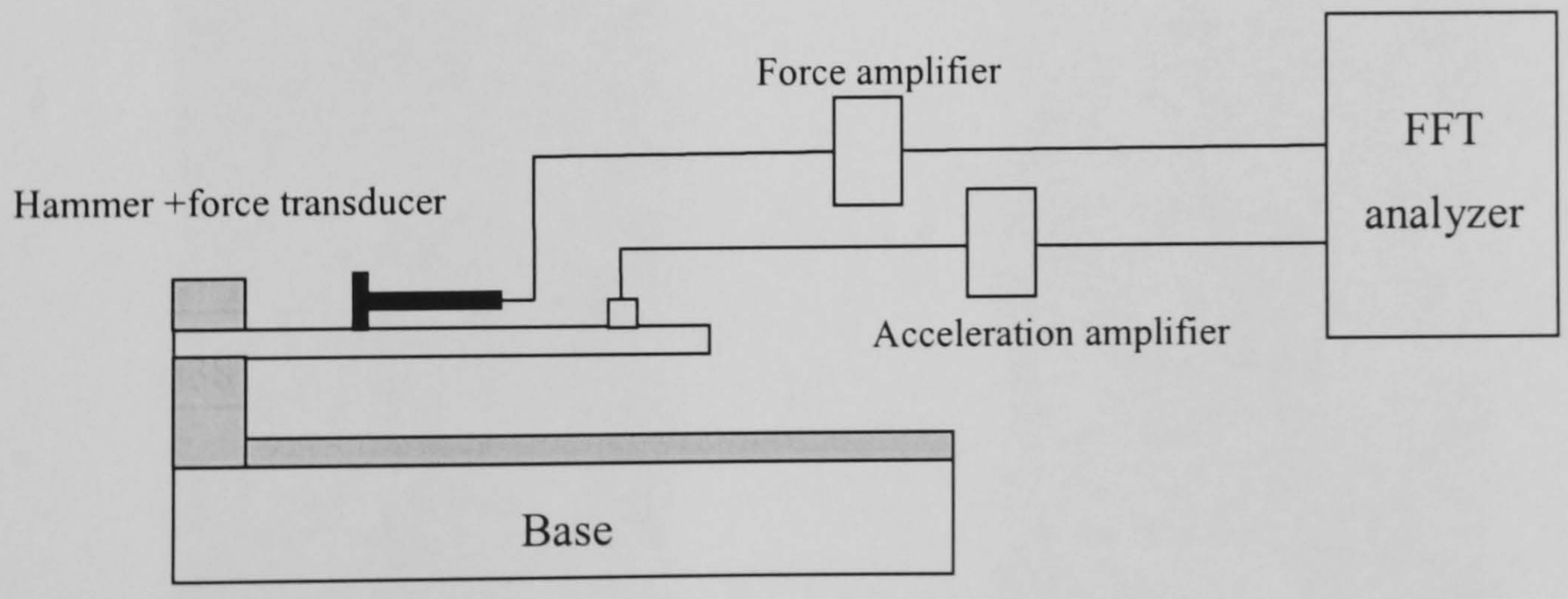

Figure (3.10) Instrumentation setup for the natural frequency test

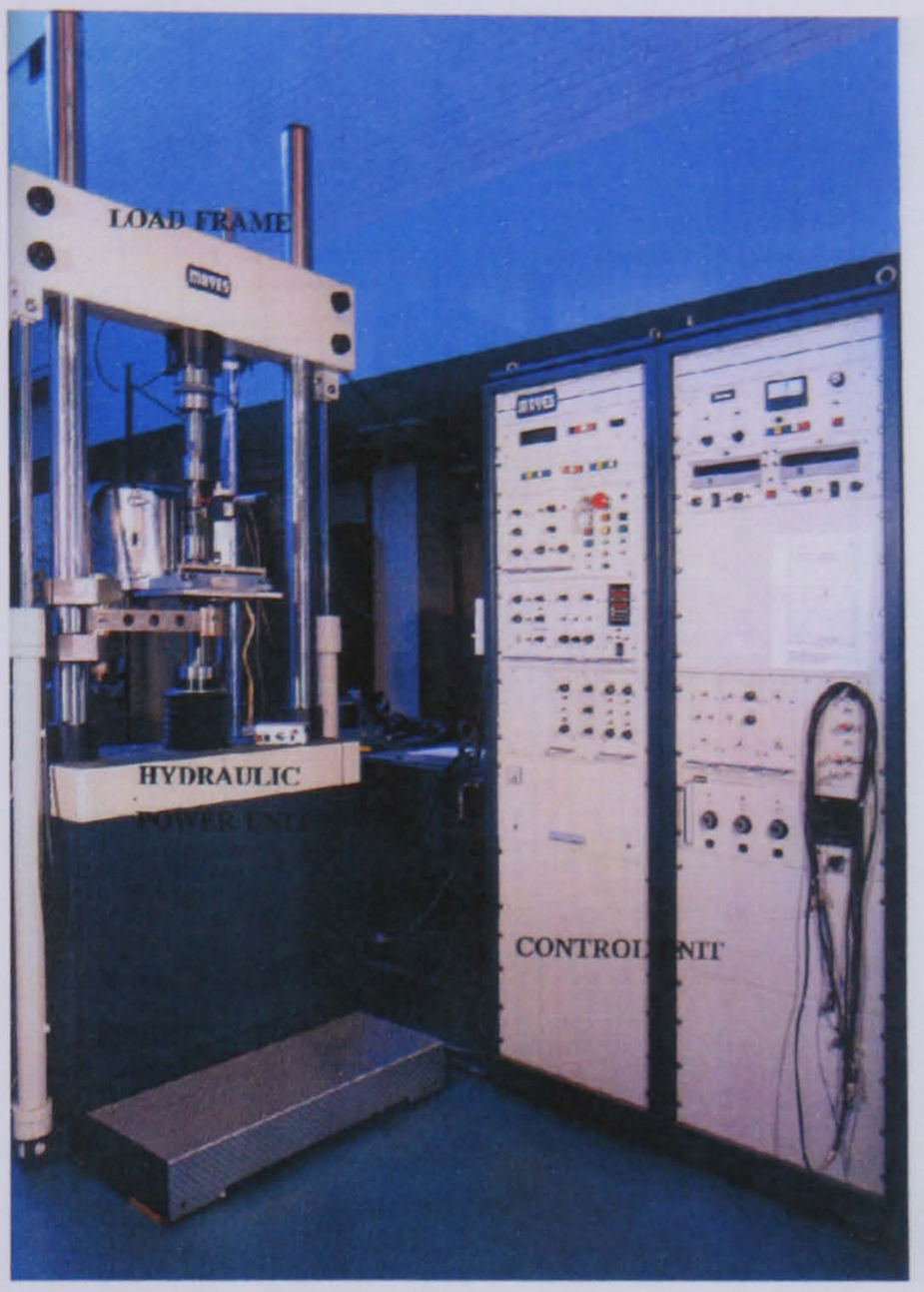

Figure (3.11) Fatigue testing machine

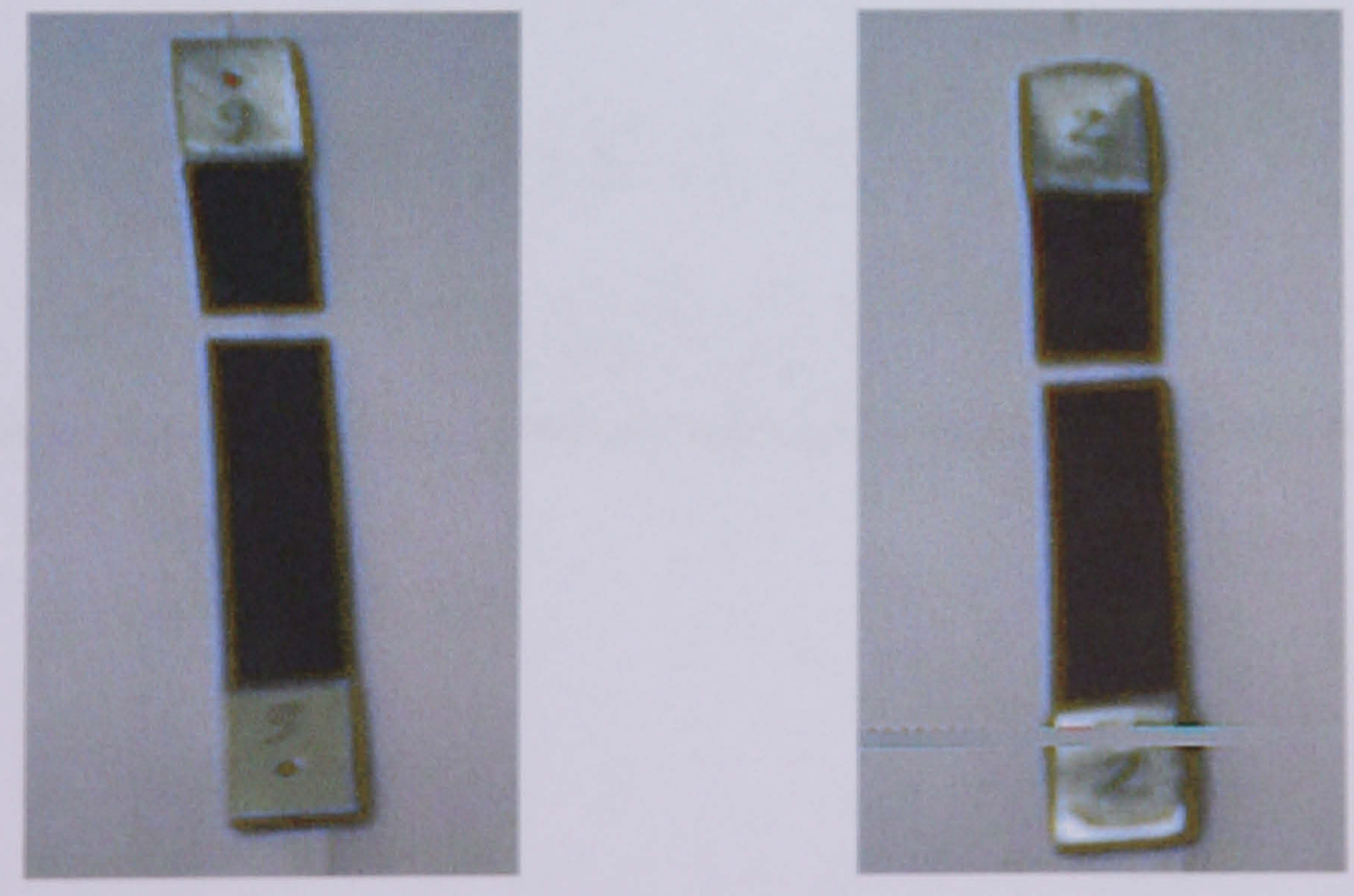

(a) Carbon/epoxy specimen (b) Glass/epoxy specimen

Figure (3.12) Failed specimens due to axial fatigue load

4

DEFORMATION THEORY OF HIGH-ORDER SHEAR ELEMENT

4.1 INTRODUCTION

Plate and shell elements are considered the ideal finite elements to represent any structure where the thickness is small compared with other dimension. Plates and shells are structural elements with upper and lower surfaces z_U and z_L respectively, and they are usually defined in terms of a midplane or midsurface and thickness distribution. The thickness is much smaller than other dimensions and is measured in the direction normal to the midsurface. The plates and shells may be classified into thin and thick according to the thickness to span length ratio.

Stress analysis parameters defined within plate or shell domains are usually modelled in the finite element theory by a two-dimensional piecewise interpolation in terms of midplane parameters, together with analytical expressions in the direction of thickness.

4.2 DISPLACEMENT FORMULATION

Some assumptions have been taken into consideration to formulate the displacement equations, as follows:

- The composite layered plate or shell consists of a number of orthotropic layers and the shell is modelled in terms of a number of facets.
- The midplane is the local Cartesian x-y plane and the total thickness at any point (x , y) on the midplane is t.
- The transverse shear strain is assumed to be continuous function of z.
- The composite layers are considered to be firmly connected together; hence the distributions of displacement components are continuous with respect to the z direction.
- The transverse normal stress σ_z is small compared with other stress components and can be neglected.

4.2.1 Transverse strains

Figure (4.1) shows the upper and lower surfaces of a plate element with thickness t. The boundary conditions around the total thickness, t, of the plate can be summarized as follows:

At the upper and lower surfaces $z = \pm t/2$, the transverse shear stresses $\tau_{xz} = \tau_{yz} = 0$, hence, it can be also be deduced that, the transverse shear strains $\gamma_{xz} = \gamma_{yz} = 0$

Consider φ_x and φ_y to be the values of γ_{xz} and γ_{yz} at the midplane $z = 0$, respectively, then by using a three-point Lagrangian interpolation at $z = -t/2$, $z = 0$ and $z = t/2$ as follows:

$$\gamma_{xz} = \frac{(z - z_1)(z - z_3)}{(z_2 - z_1)(z_2 - z_3)} \varphi_x$$

hence,

$$\gamma_{xz} = \varphi_x \left(1 - \frac{4z^2}{t^2}\right) \tag{4.1}$$

Similarly, it can be shown that:

$$\gamma_{yz} = \varphi_y \left(1 - \frac{4z^2}{t^2}\right) \tag{4.2}$$

To simplify the problem, transverse shear stresses and strains averaged over the thickness may be employed without violating equilibrium or strain energy contributions. The average transverse shear stresses $\bar{\tau}_{xz}$, $\bar{\tau}_{yz}$ so as to maintain internal equilibrium, (El-Zafrany, 1995) are such that:

$$\int_{-t/2}^{t/2} \bar{\tau}_{xz}\, dz = \int_{-t/2}^{t/2} \tau_{xz}\, dz \tag{4.3}$$

and

$$\tau_{xz} = \mu_{xz}\, \gamma_{xz} \tag{4.4}$$

where μ_{xz} is the modulus of rigidity in x-z plane.

Substituting from equations (4.1) and (4.4) into (4.3), then:

$$\bar{\tau}_{xz} = \frac{2}{3} \mu_{xz} \varphi_x \tag{4.5}$$

Similarly,

$$\bar{\tau}_{yz} = \frac{2}{3} \mu_{yz} \varphi_y \tag{4.6}$$

where μ_{yz} is the modulus of rigidity in y-z plane.

The average transverse shear strains $\bar{\gamma}_{xz}$, $\bar{\gamma}_{yz}$ so as to maintain strain energy contributions, lead to:

$$\int_{-t/2}^{t/2} \bar{\tau}_{xz} \bar{\gamma}_{xz} \, dz = \int_{-t/2}^{t/2} \tau_{xz} \gamma_{xz} \, dz \tag{4.7}$$

Substituting from equations (4.1), (4.4) and (4.5) into (4.7) and integrating then:

$$\bar{\gamma}_{xz} = \frac{6 \tau_{xz}}{5 \mu_{xz}} \tag{4.8}$$

Substituting from equation (4.5) into (4.8) then

$$\bar{\gamma}_{xz} = \frac{4}{5} \varphi_x \tag{4.9}$$

Similarly,

$$\bar{\gamma}_{yz} = \frac{4}{5} \varphi_y \tag{4.10}$$

Substituting from equations (4.9) and (4.10) into equations (4.1) and (4.2), then:

$$\gamma_{xz} = \frac{5 \bar{\gamma}_{xz}}{4} \left(1 - \frac{4 z^2}{t^2} \right) \tag{4.11}$$

$$\gamma_{yz} = \frac{5 \bar{\gamma}_{yz}}{4} \left(1 - \frac{4 z^2}{t^2} \right) \tag{4.12}$$

4.2.2 Average slope angles

If the normal to the section remains straight but not necessarily normal, bending deformation becomes:

$$\bar{u} = z\ \theta_y \qquad \bar{v} = -z\ \theta_x$$

From the equations of average strains, it can be deduced that

$$\bar{\gamma}_{xz} = \frac{\partial \bar{u}}{\partial z} + \frac{\partial w}{\partial x} = \frac{\partial w}{\partial x} + \theta_y$$

and $$\bar{\gamma}_{yz} = \frac{\partial \bar{v}}{\partial z} + \frac{\partial w}{\partial y} = \frac{\partial w}{\partial y} - \theta_x$$

Hence,

$$\theta_x = \left(\frac{\partial w}{\partial y} - \bar{\gamma}_{yz} \right) \tag{4.13}$$

$$\theta_y = -\left(\frac{\partial w}{\partial x} - \bar{\gamma}_{xz} \right) \tag{4.14}$$

For simplicity of notation, we shall define

$$\psi_x = -\bar{\gamma}_{yz} \qquad \text{and} \qquad \psi_y = \bar{\gamma}_{xz}$$

where

θ_x , θ_y represent average rotation angles in x and y directions, respectively, as shown in Figures (4.2) and (4.3).

ψ_x , ψ_y are the additional rotation due to transverse shear deformation, in x and y directions, respectively, as shown in Figures(4.2) and (4.3).

Hence, $\theta_x = \left(\frac{\partial w}{\partial y}\right) + \psi_x$ (4.15)

$\theta_y = \left(-\frac{\partial w}{\partial x}\right) + \psi_y$ (4.16)

and equations (4.11) and (4.12) can be rewritten as:

$\gamma_{xz} = \frac{5\psi_y}{4}\left(1 - \frac{4z^2}{t^2}\right)$ (4.17)

$\gamma_{yz} = -\frac{5\psi_x}{4}\left(1 - \frac{4z^2}{t^2}\right)$ (4.18)

Equations (4.17) and (4.18) can also be written in vectorial form as

$\underline{\gamma} = -\frac{5}{4}\left(1 - \frac{4z^2}{t^2}\right)\hat{\underline{\gamma}}$ (4.19)

where

$\underline{\gamma} = \{\gamma_{xz} \quad \gamma_{yz}\}$ and $\hat{\underline{\gamma}} = \{-\psi_y \quad \psi_x\}$

4.2.3 Displacement components

The displacement components at a general point inside the plate may be resolved into u, v (in-plane displacements) and w (out-of plane displacement). From the transverse shear strain equations (4.17) and (4.18), the displacement components can be derived as follows:

$\gamma_{xz} = \frac{5\psi_y}{4}\left(1 - \frac{4z^2}{t^2}\right) = \frac{\partial w}{\partial x} + \frac{\partial u}{\partial z}$

and

$\gamma_{yz} = -\frac{5\psi_x}{4}\left(1 - \frac{4z^2}{t^2}\right) = \frac{\partial w}{\partial y} + \frac{\partial v}{\partial z}$

By integration and substitution from equations (4.15) and (4.16), then

$$u(x,y,z) = u_0(x,y) + z\ \theta_y(x,y) + f(z)\,\psi_y(x,y) \tag{4.20}$$

and

$$v(x,y,z) = v_0(x,y) - z\ \theta_x(x,y) - f(z)\,\psi_x(x,y) \tag{4.21}$$

where

u_0, v_0 are the displacement components at the midplane, along the x and y directions, respectively

and

$$f(z) = \frac{1}{4}\left(z - \frac{20\ z^3}{3\ t^2} \right)$$

The lateral displacement w is approximated in terms of its value w_0 at the midplane z = 0 as follows:

$$w(x,y,z) \cong w_0(x,y) \tag{4.22}$$

4.3 NODAL PARAMETERS AND INTERPOLATED DISPLACEMENT COMPONENTS

For an n-node element, the degrees of freedom at any point on the midplane are defined in terms of in-plane displacements, out-of plane displacements, and transverse shear strains. The nodal displacement vector of the element is defined as follows:

$$\underline{\delta} = \{\underline{\delta}_0 \quad \underline{\delta}_b \quad \underline{\delta}_t\} \tag{4.23}$$

where

$$\underline{\delta}_0 = \{(u_0)_1 \quad (v_0)_1 \quad (u_0)_2 \quad (v_0)_2 \quad \cdots \quad (u_0)_n \quad (v_0)_n\} \tag{4.24}$$

$$\underline{\delta}_b = \{(w_0)_1 \quad (\theta_x)_1 \quad (\theta_y)_2 \quad (\theta_z)_2 \quad \cdots \quad (w_0)_n \quad (\theta_x)_n \quad (\theta_y)_n \quad (\theta_z)_n\} \tag{4.25}$$

$$\underline{\delta}_t = \{(\psi_x)_1 \quad (\psi_y)_1 \quad (\psi_x)_2 \quad (\psi_y)_2 \quad \cdots \quad (\psi_x)_n \quad (\psi_y)_n\} \tag{4.26}$$

For an n-node element, Lagrangian interpolation is used with in-plane and transverse shear components as follows:

$$u_0(x,y) = \sum_{i=1}^{n} N_i(x,y)\ (u)_i \tag{4.27}$$

$$v_0(x,y) = \sum_{i=1}^{n} N_i(x,y)\ (v)_i \tag{4.28}$$

$$\psi_x(x,y) = \sum_{i=1}^{n} N_i(x,y)\ (\psi_x)_i \tag{4.29}$$

$$\psi_y(x,y) = \sum_{i=1}^{n} N_i(x,y)\ (\psi_y)_i \tag{4.30}$$

where i represents node number and N_i is a Lagrangian shape function i, and $(\ )_i$ represents values at node i on the midplane.

The out-of plane components are expressed in terms of w (x, y) and is interpolated by means of Hermitian interpolation, which can be expressed for an n-node element in terms of intrinsic coordinates (ξ,η) as follows:

$$w(x,y) = \sum_{i=1}^{n}\left[f_i(\xi,\eta)\, w_i + g_i(\xi,\eta)\, w_{i,\xi} + h_i(\xi,\eta)\, w_{i,\eta} + p_i(\xi,\eta)\, w_{i,\xi\eta}\right] \tag{4.31}$$

where f_i, g_i, h_i, and p_i represent Hermitian shape functions and:

$$w_{i,\xi} = \frac{\partial w_i}{\partial \xi} \quad , \quad w_{i,\eta} = \frac{\partial w_i}{\partial \eta} \quad \text{and} \quad w_{i,\xi\eta} = \frac{\partial^2 w_i}{\partial \xi \partial \eta}$$

There are two types of Hermitian interpolation, (Zienkiewicz, 1977), conforming which is available for rectangular elements, and non-conforming which is available for triangular and quadrilateral sub-parametric elements where $p_i(\xi,\eta) = 0$.

The transformation from (ξ,η) intrinsic system to (x, y) Cartesian system can be represented as follows:

$$\begin{bmatrix} \frac{\partial w}{\partial \xi} \\ \frac{\partial w}{\partial \eta} \end{bmatrix} = \begin{bmatrix} \frac{\partial x}{\partial \xi} & \frac{\partial y}{\partial \xi} \\ \frac{\partial x}{\partial \eta} & \frac{\partial y}{\partial \eta} \end{bmatrix} \begin{bmatrix} \frac{\partial w}{\partial x} \\ \frac{\partial w}{\partial y} \end{bmatrix}$$

where the transformation 2x2 matrix is called the Jacobian matrix $\underline{J}$.

The out-of plane displacement can be represented in terms of the nodal parameters as follows, (El-Zafrany, 1995):

$$w(x,y) = \sum_{i=1}^{n} \Big[F_i(\xi,\eta)\, w_i + H_i(\xi,\eta)\,(\theta_x)_i - G_i(\xi,\eta)\,(\theta_y)_i + P_i(\xi,\eta)\,(\theta_z)_i \Big] + \Big[- H_i(\xi,\eta)\,(\psi_x)_i + G_i(\xi,\eta)\,(\psi_y)_i \Big] \tag{4.32}$$

where

$F_i = f_i$ $\quad G_i = g_i\, J_{11} + h_i\, J_{21}$ $\quad H_i = g_i\, J_{12} + h_i\, J_{22}$

$P_i = 0$ for non-conforming element

$P_i = J_{11}\, J_{22}\, p_i$ for rectangular conforming element

Explicit expressions for Hermitian shape functions can be found in El-Zafrany & Cookson (1986a) and (1986b).

4.4 DISPLACEMENT, VELOCITY AND ACCELERATION COMPONENTS

Dynamic equations will be derived at an instant of time t, in a way similar to that employed for static equations, but all nodal values are measured at that instant of time. The displacement components at any point (x,y,z) inside the element, and at an instant of time t can be expressed similar to equations (4.20), (4.21) and (4.22):

$$u(x,y,z,t) = u_0(x,y,z,t) + z\ \theta_y(x,y,z,t) + f(z)\,\psi_y(x,y,z,t) \tag{4.33}$$

$$v(x,y,z,t) = v_0(x,y,z,t) - z\ \theta_x(x,y,z,t) - f(z)\,\psi_x(x,y,z,t) \tag{4.34}$$

$$w(x,y,z,t) = w_0(x,y,z,t) \tag{4.35}$$

For an n-node element, the degrees of freedom at any point on the midplane (z=0) are defined in terms of in-plane displacements, out-of-plane displacements and transverse shear strain.

(i) In-plane vector

$$\underline{q}_o(x,y,t)=\begin{bmatrix} u_o(x,y,t) \\ v_o(x,y,t) \end{bmatrix} \tag{4.36}$$

(ii) Out-of-plane vector

$$\underline{q}_b(x,y,t)=\begin{bmatrix} w(x,y,t) \\ \theta_x(x,y,t) \\ \theta_y(x,y,t) \\ \theta_z(x,y,t) \end{bmatrix} \tag{4.37}$$

(iii) Transverse shear strain vector

$$\underline{q}_t(x,y,t)=\begin{bmatrix} \psi_x(x,y,t) \\ \psi_y(x,y,t) \end{bmatrix} \tag{4.38}$$

They can be defined in terms of nodal displacements and shape function matrices by using equations (4.27-32) as follows:

$$\underline{q}_o=\begin{bmatrix} u_o \\ v_o \end{bmatrix}=\underline{N}_o(x,y)\,\underline{\delta}_o(t) \tag{4.39}$$

$$\text{where}\quad \underline{N}_o=\begin{bmatrix} N_1 & 0 & \dots & \dots \\ 0 & N_1 & \dots & \dots \end{bmatrix} \tag{4.40}$$

$$\text{and}\quad \underline{q}_b=\begin{bmatrix} w \\ \theta_x \\ \theta_y \\ \theta_z \end{bmatrix}=\underline{N}_b(x,y)\,\underline{\delta}_b(t)+\underline{N}_t(x,y)\,\underline{\delta}_t(t) \tag{4.41}$$

$$\text{where}\quad \underline{N}_b=\begin{bmatrix} F_1 & H_1 & -G_1 & P_1 & \dots\dots \\ \dfrac{\partial F_1}{\partial y} & \dfrac{\partial H_1}{\partial y} & -\dfrac{\partial G_1}{\partial y} & \dfrac{\partial P_1}{\partial y} & \dots\dots \\ -\dfrac{\partial F_1}{\partial x} & -\dfrac{\partial H_1}{\partial x} & \dfrac{\partial G_1}{\partial x} & -\dfrac{\partial P_1}{\partial x} & \dots\dots \\ \dfrac{\partial^2 F_1}{\partial x\partial y} & \dfrac{\partial^2 H_1}{\partial x\partial y} & -\dfrac{\partial^2 G_1}{\partial x\partial y} & \dfrac{\partial^2 P_1}{\partial x\partial y} & \dots\dots \end{bmatrix} \tag{4.42}$$

and $$\underline{N}_t = \begin{bmatrix} -H_1 & G_1 & \cdots \\ N_1 - \dfrac{\partial H_1}{\partial y} & \dfrac{\partial G_1}{\partial y} & \cdots \\ \dfrac{\partial H_1}{\partial x} & N_1 - \dfrac{\partial G_1}{\partial x} & \cdots \\ -\dfrac{\partial^2 H_1}{\partial x \partial y} & \dfrac{\partial^2 G_1}{\partial x \partial y} & \cdots \end{bmatrix} \tag{4.43}$$

and $$\underline{q}_t = \begin{bmatrix} \psi_x \\ \psi_y \end{bmatrix} = \underline{N}_o(x,y)\,\underline{\delta}_t(t) \tag{4.44}$$

Hence, the displacement equations (4.33-35) can be rewritten in the following matrix form using equations (4.39), (4.41) and (4.44) as follows:

$$\underline{q}(x,y,z,t) = \begin{bmatrix} u \\ v \\ w \end{bmatrix} = \underline{I}_2\ \underline{q}_o + \underline{Z}\ \underline{q}_b + \underline{f}\ \underline{q}_t \tag{4.45}$$

where $$\underline{I}_2 = \begin{bmatrix} 1 & 0 \\ 0 & 1 \\ 0 & 0 \end{bmatrix} \qquad \underline{Z} = \begin{bmatrix} 0 & 0 & z & 0 \\ 0 & -z & 0 & 0 \\ 1 & 0 & 0 & 0 \end{bmatrix} \qquad \underline{f} = \begin{bmatrix} 0 & f \\ -f & 0 \\ 0 & 0 \end{bmatrix}$$

Velocity and acceleration components can be obtained by differentiating the displacement components once and twice respectively as follows:

$$\dot{\underline{q}} = \underline{I}_2\ \dot{\underline{q}}_o + \underline{Z}\ \dot{\underline{q}}_b + \underline{f}\ \dot{\underline{q}}_t \tag{4.46}$$

and $$\ddot{\underline{q}} = \underline{I}_2\ \ddot{\underline{q}}_o + \underline{Z}\ \ddot{\underline{q}}_b + \underline{f}\ \ddot{\underline{q}}_t \tag{4.47}$$

where $\dot{\underline{q}}$ and $\ddot{\underline{q}}$ represent the velocity and acceleration components respectively

and $$\dot{\underline{q}}(x,y,z,t) = \begin{bmatrix} \dot{u} \\ \dot{v} \\ \dot{w} \end{bmatrix} \qquad \ddot{\underline{q}}(x,y,z,t) = \begin{bmatrix} \ddot{u} \\ \ddot{v} \\ \ddot{w} \end{bmatrix}$$

4.5 STRAIN-DISPLACEMENT RELATIONS

The strains are defined in terms of two separate vectors:

- x-y components vector, which will now be simplified as:

$$\underline{\varepsilon} = \{\varepsilon_x \quad \varepsilon_y \quad \gamma_{xy}\} \tag{4.48}$$

- Transverse shear vector:

$$\underline{\gamma} = \{\gamma_{xz} \quad \gamma_{yz}\} \tag{4.49}$$

The $\underline{\gamma}$ equation has been already given by equation (4.19). According to Green's strain displacement equations the x-y strain components can be expressed as follows:

$$\varepsilon_x = \frac{\partial u}{\partial x} + \frac{1}{2}\left[\left(\frac{\partial u}{\partial x}\right)^2 + \left(\frac{\partial v}{\partial x}\right)^2 + \left(\frac{\partial w}{\partial x}\right)^2\right] \tag{4.50}$$

$$\varepsilon_y = \frac{\partial v}{\partial y} + \frac{1}{2}\left[\left(\frac{\partial u}{\partial y}\right)^2 + \left(\frac{\partial v}{\partial y}\right)^2 + \left(\frac{\partial w}{\partial y}\right)^2\right] \tag{4.51}$$

$$\gamma_{xy} = \frac{\partial u}{\partial y} + \frac{\partial v}{\partial x} + \left[\left(\frac{\partial u}{\partial x}\right)\left(\frac{\partial u}{\partial y}\right) + \left(\frac{\partial v}{\partial x}\right)\left(\frac{\partial v}{\partial y}\right) + \left(\frac{\partial w}{\partial x}\right)\left(\frac{\partial w}{\partial y}\right)\right] \tag{4.52}$$

Hence, the vector of x-y strain components can be partitioned as follows:

$$\underline{\varepsilon} = \underline{\varepsilon}_S + \underline{\varepsilon}_L \tag{4.53}$$

where the subscript "s" represents small strains and "L" represents the additional terms of "Large" strains.

Hence,

$$\underline{\varepsilon}_s = \begin{bmatrix} \dfrac{\partial u}{\partial x} \\ \dfrac{\partial v}{\partial y} \\ \dfrac{\partial u}{\partial y} + \dfrac{\partial v}{\partial x} \end{bmatrix} \tag{4.54}$$

and $$\underline{\varepsilon}_L = \frac{1}{2}\begin{bmatrix} \left(\frac{\partial u}{\partial x}\right)^2 + \left(\frac{\partial v}{\partial x}\right)^2 + \left(\frac{\partial w}{\partial x}\right)^2 \\ \left(\frac{\partial u}{\partial y}\right)^2 + \left(\frac{\partial v}{\partial y}\right)^2 + \left(\frac{\partial w}{\partial y}\right)^2 \\ 2\left(\frac{\partial u}{\partial x}\right)\left(\frac{\partial u}{\partial y}\right) + 2\left(\frac{\partial v}{\partial x}\right)\left(\frac{\partial v}{\partial y}\right) + 2\left(\frac{\partial w}{\partial x}\right)\left(\frac{\partial w}{\partial y}\right) \end{bmatrix} \qquad (4.55)$$

Substituting from equations (4.20-22) into (4.54) hence, the small strain vector can be expressed as follows:

$$\underline{\varepsilon}_S = \underline{\varepsilon}_0 - z\ \underline{\varepsilon}_b + g(z)\,\underline{\varepsilon}_t \qquad (4.56)$$

where $g(z) = z + f(z) = \frac{5}{4}\left(z - \frac{4z^3}{3t^2}\right)$,

$\underline{\varepsilon}_0$ represents the strain components due to in-plane effect, i.e.

$$\underline{\varepsilon}_o = \begin{bmatrix} \frac{\partial u_o}{\partial x} \\ \frac{\partial v_o}{\partial y} \\ \frac{\partial u_o}{\partial y} + \frac{\partial v_o}{\partial x} \end{bmatrix} \qquad (4.57)$$

$\underline{\varepsilon}_b$ represents the strain component due to bending effect, i.e.

$$\underline{\varepsilon}_b = \begin{bmatrix} \frac{\partial^2 w}{\partial x^2} \\ \frac{\partial^2 w}{\partial y^2} \\ 2\frac{\partial^2 w}{\partial x\,\partial y} \end{bmatrix} \qquad (4.58)$$

and $\underline{\varepsilon}_t$ represents the strain component due to transverse shear effect:

$$\underline{\varepsilon}_t = \begin{bmatrix} \dfrac{\partial \psi_y}{\partial x} \\ -\dfrac{\partial \psi_x}{\partial y} \\ \dfrac{\partial \psi_y}{\partial y} - \dfrac{\partial \psi_x}{\partial x} \end{bmatrix} \tag{4.59}$$

Similarly by substituting from equations (4.20-22) into (4.55), the large strain vector can be expressed as follows:

$$\underline{\varepsilon}_L = \underline{\varepsilon}_m + \underline{\varepsilon}_w + z^2 \ \underline{\varepsilon}_\theta + g^2(z)\ \underline{\varepsilon}_\psi - z\ \underline{\varepsilon}_{m\theta} + g(z)\ \underline{\varepsilon}_{m\psi} + z\ g(z)\ \underline{\varepsilon}_{\theta\psi} \tag{4.60}$$

where

$\underline{\varepsilon}_m$ represents the strain component due to in-plane effect in large deformation:

$$\underline{\varepsilon}_m = \frac{1}{2}\begin{bmatrix} \left(\dfrac{\partial u_o}{\partial x}\right)^2 + \left(\dfrac{\partial v_o}{\partial x}\right)^2 \\ \left(\dfrac{\partial u_o}{\partial y}\right)^2 + \left(\dfrac{\partial v_o}{\partial y}\right)^2 \\ 2\left(\dfrac{\partial u_o}{\partial x}\right)\left(\dfrac{\partial u_o}{\partial y}\right) + 2\left(\dfrac{\partial v_o}{\partial x}\right)\left(\dfrac{\partial v_o}{\partial y}\right) \end{bmatrix} \tag{4.61}$$

$\underline{\varepsilon}_w$, $\underline{\varepsilon}_\theta$ represent the strain components due to bending effect in large deformation:

$$\underline{\varepsilon}_w = \frac{1}{2}\begin{bmatrix} \left(\dfrac{\partial w}{\partial x}\right)^2 \\ \left(\dfrac{\partial w}{\partial y}\right)^2 \\ 2\left(\dfrac{\partial w}{\partial x}\right)\left(\dfrac{\partial w}{\partial y}\right) \end{bmatrix} \tag{4.62}$$

$$\underline{\varepsilon}_{\theta} = \frac{1}{2}\begin{bmatrix} \left(\frac{\partial^2 w}{\partial x^2}\right)^2 + \left(\frac{\partial^2 w}{\partial x \partial y}\right)^2 \\ \left(\frac{\partial^2 w}{\partial x \partial y}\right)^2 + \left(\frac{\partial^2 w}{\partial y^2}\right)^2 \\ 2\left(\frac{\partial^2 w}{\partial x^2}\right)\left(\frac{\partial^2 w}{\partial x \partial y}\right) + 2\left(\frac{\partial^2 w}{\partial x \partial y}\right)\left(\frac{\partial^2 w}{\partial y^2}\right) \end{bmatrix} \tag{4.63}$$

$\underline{\varepsilon}_{\psi}$ represents the strain components due to transverse shear effect in large deformation:

$$\underline{\varepsilon}_{\psi} = \frac{1}{2}\begin{bmatrix} \left(\frac{\partial \psi_x}{\partial x}\right)^2 + \left(\frac{\partial \psi_y}{\partial x}\right)^2 \\ \left(\frac{\partial \psi_x}{\partial y}\right)^2 + \left(\frac{\partial \psi_y}{\partial y}\right)^2 \\ 2\left(\frac{\partial \psi_y}{\partial x}\right)\left(\frac{\partial \psi_y}{\partial y}\right) + 2\left(\frac{\partial \psi_x}{\partial x}\right)\left(\frac{\partial \psi_x}{\partial y}\right) \end{bmatrix} \tag{4.64}$$

$\underline{\varepsilon}_{m\theta}$, $\underline{\varepsilon}_{m\psi}$, $\underline{\varepsilon}_{\theta\psi}$ represent the strain components due to the coupling effect of in-plane, bending and transverse shear in large deformation:

$$\underline{\varepsilon}_{m\theta} = \begin{bmatrix} \frac{\partial u_o}{\partial x}\frac{\partial^2 w}{\partial x^2} + \frac{\partial v_o}{\partial x}\frac{\partial^2 w}{\partial x \partial y} \\ \frac{\partial u_o}{\partial y}\frac{\partial^2 w}{\partial x \partial y} + \frac{\partial v_o}{\partial y}\frac{\partial^2 w}{\partial y^2} \\ \frac{\partial u_o}{\partial x}\frac{\partial^2 w}{\partial x \partial y} + \frac{\partial u_o}{\partial y}\frac{\partial^2 w}{\partial x^2} + \frac{\partial v_o}{\partial x}\frac{\partial^2 w}{\partial y^2} + \frac{\partial v_o}{\partial y}\frac{\partial^2 w}{\partial x \partial y} \end{bmatrix} \tag{4.65}$$

$$\underline{\varepsilon}_{m\psi} = \begin{bmatrix} \frac{\partial u_o}{\partial x}\frac{\partial \psi_y}{\partial x} - \frac{\partial v_o}{\partial x}\frac{\partial \psi_x}{\partial x} \\ \frac{\partial u_o}{\partial y}\frac{\partial \psi_y}{\partial y} - \frac{\partial v_o}{\partial y}\frac{\partial \psi_x}{\partial y} \\ \frac{\partial u_o}{\partial x}\frac{\partial \psi_y}{\partial y} + \frac{\partial u_o}{\partial y}\frac{\partial \psi_y}{\partial x} - \frac{\partial v_o}{\partial x}\frac{\partial \psi_x}{\partial y} - \frac{\partial v_o}{\partial y}\frac{\partial \psi_x}{\partial x} \end{bmatrix} \tag{4.66}$$

$$\underline{\varepsilon}_{\theta\psi} = \begin{bmatrix} \dfrac{\partial\psi_x}{\partial x}\dfrac{\partial^2 w}{\partial x\partial y} - \dfrac{\partial\psi_y}{\partial x}\dfrac{\partial^2 w}{\partial x^2} \\ \dfrac{\partial\psi_x}{\partial y}\dfrac{\partial^2 w}{\partial y^2} - \dfrac{\partial\psi_y}{\partial y}\dfrac{\partial^2 w}{\partial x\partial y} \\ \dfrac{\partial\psi_x}{\partial y}\dfrac{\partial^2 w}{\partial x\partial y} + \dfrac{\partial\psi_x}{\partial x}\dfrac{\partial^2 w}{\partial y^2} - \dfrac{\partial\psi_y}{\partial y}\dfrac{\partial^2 w}{\partial x^2} - \dfrac{\partial\psi_y}{\partial x}\dfrac{\partial^2 w}{\partial x\partial y} \end{bmatrix} \tag{4.67}$$

Using the interpolation equations (4.27-31), the infinitesimal strain components can be defined in terms of nodal displacements and shape function matrices $\underline{B}$ as follows:

$$\hat{\underline{\gamma}} = \underline{B}_\gamma(x,y)\ \underline{\delta}_t \tag{4.68}$$

$$\underline{\varepsilon}_0 = \underline{B}_0(x,y)\ \underline{\delta}_0 \tag{4.69}$$

$$\underline{\varepsilon}_b = \underline{B}_b(x,y)\ \underline{\delta}_b + \underline{B}_{bt}(x,y)\ \underline{\delta}_t \tag{4.70}$$

$$\underline{\varepsilon}_t = \underline{B}_t(x,y)\ \underline{\delta}_t \tag{4.71}$$

where

$$\underline{B}_\gamma(x,y) = \begin{bmatrix} 0 & -N_1 & \dots & \dots \\ N_1 & 0 & \dots & \dots \end{bmatrix} \tag{4.72}$$

$$\underline{B}_0(x,y) = \begin{bmatrix} \dfrac{\partial N_1}{\partial x} & 0 & \dots & \dots \\ 0 & \dfrac{\partial N_1}{\partial y} & \dots & \dots \\ \dfrac{\partial N_1}{\partial y} & \dfrac{\partial N_1}{\partial x} & \dots & \dots \end{bmatrix} \tag{4.73}$$

$$\underline{B}_b(x,y) = \begin{bmatrix} \dfrac{\partial^2 F_1}{\partial x^2} & \dfrac{\partial^2 H_1}{\partial x^2} & -\dfrac{\partial^2 G_1}{\partial x^2} & \dfrac{\partial^2 P_1}{\partial x^2} & \dots & \dots \\ \dfrac{\partial^2 F_1}{\partial y^2} & \dfrac{\partial^2 H_1}{\partial y^2} & -\dfrac{\partial^2 G_1}{\partial y^2} & \dfrac{\partial^2 P_1}{\partial y^2} & \dots & \dots \\ 2\dfrac{\partial^2 F_1}{\partial x\partial y} & 2\dfrac{\partial^2 H_1}{\partial x\partial y} & -2\dfrac{\partial^2 G_1}{\partial x\partial y} & 2\dfrac{\partial^2 P_1}{\partial x\partial y} & \dots & \dots \end{bmatrix} \tag{4.74}$$

$$\underline{B}_{bt}(x, y) = \begin{bmatrix} -\frac{\partial^2 H_1}{\partial x^2} & \frac{\partial^2 G_1}{\partial x^2} & \cdots & \cdots \\ -\frac{\partial^2 H_1}{\partial y^2} & \frac{\partial^2 G_1}{\partial y^2} & \cdots & \cdots \\ -2\frac{\partial^2 H_1}{\partial x \partial y} & 2\frac{\partial^2 G_1}{\partial x \partial y} & \cdots & \cdots \end{bmatrix} \tag{4.75}$$

$$\underline{B}_{t}(x, y) = \begin{bmatrix} 0 & \frac{\partial N_1}{\partial x} & \cdots & \cdots \\ -\frac{\partial N_1}{\partial y} & 0 & \cdots & \cdots \\ -\frac{\partial N_1}{\partial x} & \frac{\partial N_1}{\partial y} & \cdots & \cdots \end{bmatrix} \tag{4.76}$$

Similarly, the large or finite strain components can also be expressed in terms of rotation vectors $\underline{\theta}$ and matrices $\underline{A}$ as follows:

$$\underline{\varepsilon}_m = \frac{1}{2}\underline{A}_m \ \underline{\theta}_m \tag{4.77}$$

$$\underline{\varepsilon}_w = \frac{1}{2}\underline{A}_w \ \underline{\theta}_w \tag{4.78}$$

$$\underline{\varepsilon}_\theta = \frac{1}{2}\underline{A}_\theta \ \underline{\theta}_\theta \tag{4.79}$$

$$\underline{\varepsilon}_\psi = \frac{1}{2}\underline{A}_\psi \ \underline{\theta}_\psi \tag{4.80}$$

$$\underline{\varepsilon}_{m\theta} = \underline{A}_\theta \, \underline{\theta}_m = \underline{A}_m \, \underline{\theta}_\theta \tag{4.81}$$

$$\underline{\varepsilon}_{m\psi} = \underline{A}_\psi \, \underline{\theta}_m = \underline{A}_m \, \underline{\theta}_\psi \tag{4.82}$$

$$\underline{\varepsilon}_{\theta\psi} = -\underline{A}_\theta \, \underline{\theta}_\psi = -\underline{A}_\psi \, \underline{\theta}_\theta \tag{4.83}$$

where

$$\underline{\theta}_m = \left\{ \frac{\partial u_0}{\partial x} \quad \frac{\partial v_0}{\partial x} \quad \frac{\partial u_0}{\partial y} \quad \frac{\partial v_0}{\partial y} \right\} \tag{4.84}$$

$$\underline{\theta}_\psi = \left\{ \frac{\partial \psi_y}{\partial x} \quad -\frac{\partial \psi_x}{\partial x} \quad \frac{\partial \psi_y}{\partial y} \quad -\frac{\partial \psi_x}{\partial y} \right\} \tag{4.85}$$

$$\underline{\theta}_\theta = \left\{ \frac{\partial^2 w}{\partial x^2} \quad \frac{\partial^2 w}{\partial x \partial y} \quad \frac{\partial^2 w}{\partial x \partial y} \quad \frac{\partial^2 w}{\partial^2 y} \right\} \tag{4.86}$$

$$\underline{\theta}_w = \left\{ \frac{\partial w}{\partial x} \quad \frac{\partial w}{\partial y} \right\} \tag{4.87}$$

$$\underline{A}_m = \begin{bmatrix} \frac{\partial u_0}{\partial x} & \frac{\partial v_0}{\partial x} & 0 & 0 \\ 0 & 0 & \frac{\partial u_0}{\partial y} & \frac{\partial v_0}{\partial y} \\ \frac{\partial u_0}{\partial y} & \frac{\partial v_0}{\partial y} & \frac{\partial u_0}{\partial x} & \frac{\partial v_0}{\partial x} \end{bmatrix} \tag{4.88}$$

$$\underline{A}_\theta = \begin{bmatrix} \frac{\partial w^2}{\partial x^2} & \frac{\partial w^2}{\partial x \partial y} & 0 & 0 \\ 0 & 0 & \frac{\partial w^2}{\partial x \partial y} & \frac{\partial w^2}{\partial y^2} \\ \frac{\partial w^2}{\partial x \partial y} & \frac{\partial w^2}{\partial y^2} & \frac{\partial w^2}{\partial x^2} & \frac{\partial w^2}{\partial x \partial y} \end{bmatrix} \tag{4.89}$$

$$\underline{A}_\psi = \begin{bmatrix} \frac{\partial \psi_y}{\partial x} & -\frac{\partial \psi_x}{\partial x} & 0 & 0 \\ 0 & 0 & \frac{\partial \psi_y}{\partial y} & -\frac{\partial \psi_x}{\partial y} \\ \frac{\partial \psi_y}{\partial y} & -\frac{\partial \psi_x}{\partial y} & \frac{\partial \psi_y}{\partial x} & -\frac{\partial \psi_x}{\partial x} \end{bmatrix} \tag{4.90}$$

$$\underline{A}_w = \begin{bmatrix} \frac{\partial w}{\partial x} & 0 \\ 0 & \frac{\partial w}{\partial y} \\ \frac{\partial w}{\partial y} & \frac{\partial w}{\partial x} \end{bmatrix} \tag{4.91}$$

From these $\underline{\theta}$ vectors and $\underline{A}$ matrices we have some properties. For any $\underline{\theta} = \{\theta_1 \quad \theta_2 \quad \theta_3 \quad \theta_4\}$ except $\underline{\theta}_w$ there is a corresponding $\underline{A}$ matrix as follows:

$$\underline{A} = \begin{bmatrix} \theta_1 & \theta_2 & 0 & 0 \\ 0 & 0 & \theta_3 & \theta_4 \\ \theta_3 & \theta_4 & \theta_1 & \theta_2 \end{bmatrix}$$

and if we have any stress vector $\underline{\sigma} = \{\sigma_x \quad \sigma_y \quad \tau_{xy}\}$ then, $\underline{A}^T \underline{\sigma}$ can be rearranged as follows:

$$\underline{A}^T \underline{\sigma} = \underline{S}\,\underline{\theta} \tag{4.92}$$

where $\underline{S} = \begin{bmatrix} \sigma_x \underline{I}_2 & \tau_{xy} \underline{I}_2 \\ \tau_{xy} \underline{I}_2 & \sigma_y \underline{I}_2 \end{bmatrix}$

and $\underline{I}_2$ is the identity 2x2 matrix = $\begin{bmatrix} 1 & 0 \\ 0 & 1 \end{bmatrix}$.

With respect to $\underline{A}_w$, it can be shown that:

$$\underline{A}_w^T \underline{\sigma} = \underline{S}_{ww}\,\underline{\theta}_w \tag{4.93}$$

where $\underline{S}_{ww} = \begin{bmatrix} \sigma_x & \tau_{xy} \\ \tau_{xy} & \sigma_y \end{bmatrix}$

Also, from the differentiation properties of those vectors and matrices

$$d\left(\frac{1}{2}\underline{A}\,\underline{\theta}\right) = \frac{1}{2}\left(d\underline{A}\,\underline{\theta} + \underline{A}\,d\underline{\theta}\right)$$

and $$d\underline{A}\,\underline{\theta} = \underline{A}\,d\underline{\theta}$$

i.e. $$d\left(\frac{1}{2}\underline{A}\,\underline{\theta}\right) = \underline{A}\,d\underline{\theta} \tag{4.94}$$

Hence, the following equations can be obtained

$$d\underline{\varepsilon}_m = \underline{A}_m\ d\underline{\theta}_m \tag{4.95}$$

$$d\underline{\varepsilon}_w = \underline{A}_w\ d\underline{\theta}_w \tag{4.96}$$

$$d\underline{\varepsilon}_\theta = \underline{A}_\theta\ d\underline{\theta}_\theta \tag{4.97}$$

$$d\underline{\varepsilon}_\psi = \underline{A}_\psi\ d\underline{\theta}_\psi \tag{4.98}$$

$$d\underline{\varepsilon}_{m\theta} = \underline{A}_\theta\, d\underline{\theta}_m + \underline{A}_m\, d\underline{\theta}_\theta \tag{4.99}$$

$$d\underline{\varepsilon}_{m\psi} = \underline{A}_\psi\, d\underline{\theta}_m + \underline{A}_m\, d\underline{\theta}_\psi \tag{4.100}$$

$$d\underline{\varepsilon}_{\theta\psi} = -\underline{A}_\theta\, d\underline{\theta}_\psi - \underline{A}_\psi\, \underline{\theta}_\theta \tag{4.101}$$

Using the interpolation equations (4.27-32) the rotation vectors $\underline{\theta}$ can be related to the nodal displacement $\underline{\delta}$ as follows:

$$\underline{\theta}_m = \underline{G}_m \underline{\delta}_0 \tag{4.102}$$

$$\underline{\theta}_w = \underline{G}_w \underline{\delta}_b + \underline{G}_{wt} \underline{\delta}_t \tag{4.103}$$

$$\underline{\theta}_\psi = \underline{G}_\psi \underline{\delta}_t \tag{4.104}$$

$$\underline{\theta}_\theta = \underline{G}_\theta \underline{\delta}_b + \underline{G}_{\theta t} \underline{\delta}_t \tag{4.105}$$

where

$$\underline{G}_m = \begin{bmatrix} \frac{\partial N_1}{\partial x} & 0 & \dots & \dots \\ 0 & \frac{\partial N_1}{\partial x} & \dots & \dots \\ \frac{\partial N_1}{\partial y} & 0 & \dots & \dots \\ 0 & \frac{\partial N_1}{\partial y} & \dots & \dots \end{bmatrix} \tag{4.106}$$

$$\underline{G}_\psi = \begin{bmatrix} 0 & \frac{\partial N_1}{\partial x} & \dots & \dots \\ -\frac{\partial N_1}{\partial x} & 0 & \dots & \dots \\ 0 & \frac{\partial N_1}{\partial y} & \dots & \dots \\ -\frac{\partial N_1}{\partial y} & 0 & \dots & \dots \end{bmatrix} \tag{4.107}$$

$$\underline{G}_w = \begin{bmatrix} \frac{\partial F_1}{\partial x} & \frac{\partial H_1}{\partial x} & -\frac{\partial G_1}{\partial x} & \frac{\partial P_1}{\partial x} & \dots & \dots \\ \frac{\partial F_1}{\partial y} & \frac{\partial H_1}{\partial y} & -\frac{\partial G_1}{\partial y} & \frac{\partial P_1}{\partial y} & \dots & \dots \end{bmatrix} \tag{4.108}$$

$$\underline{G}_{wt} = \begin{bmatrix} -\frac{\partial H_1}{\partial x} & \frac{\partial G_1}{\partial x} & \dots & \dots \\ -\frac{\partial H_1}{\partial y} & \frac{\partial G_1}{\partial y} & \dots & \dots \end{bmatrix} \tag{4.109}$$

$$\underline{G}_\theta = \begin{bmatrix} \frac{\partial^2 F_1}{\partial x^2} & \frac{\partial^2 F_1}{\partial x^2} & -\frac{\partial^2 G_1}{\partial x^2} & \frac{\partial^2 P_1}{\partial x^2} & \dots & \dots \\ \frac{\partial^2 F_1}{\partial x \partial y} & \frac{\partial^2 F_1}{\partial x \partial y} & -\frac{\partial^2 G_1}{\partial x \partial y} & \frac{\partial^2 P_1}{\partial x \partial y} & \dots & \dots \\ \frac{\partial^2 F_1}{\partial x \partial y} & \frac{\partial^2 F_1}{\partial x \partial y} & -\frac{\partial^2 G_1}{\partial x \partial y} & \frac{\partial^2 P_1}{\partial x \partial y} & \dots & \dots \\ \frac{\partial^2 F_1}{\partial y^2} & \frac{\partial^2 F_1}{\partial y^2} & -\frac{\partial^2 G_1}{\partial y^2} & \frac{\partial^2 P_1}{\partial y^2} & \dots & \dots \end{bmatrix} \tag{4.110}$$

$$\underline{G}_{\theta t} = \begin{bmatrix} -\dfrac{\partial^2 H_1}{\partial x^2} & \dfrac{\partial^2 G_1}{\partial x^2} & \cdots & \cdots \\ -\dfrac{\partial^2 H_1}{\partial x \partial y} & \dfrac{\partial^2 G_1}{\partial x \partial y} & \cdots & \cdots \\ -\dfrac{\partial^2 H_1}{\partial x \partial y} & \dfrac{\partial^2 G_1}{\partial x \partial y} & \cdots & \cdots \\ -\dfrac{\partial^2 H_1}{\partial y^2} & \dfrac{\partial^2 G_1}{\partial y^2} & \cdots & \cdots \end{bmatrix} \tag{4.111}$$

Substituting from equations (4.102-105) into equations (4.77-83) to represent the finite strain components in terms of nodal displacement $\underline{\delta}$, it can be shown that

$$\underline{\varepsilon}_m = \frac{1}{2} \underline{A}_m \ \underline{G}_m \ \underline{\delta}_0 \tag{4.112}$$

$$\underline{\varepsilon}_w = \frac{1}{2} (\underline{A}_w \ \underline{G}_w \ \underline{\delta}_b + \underline{A}_w \ \underline{G}_{wt} \ \underline{\delta}_t) \tag{4.113}$$

$$\underline{\varepsilon}_\theta = \frac{1}{2} (\underline{A}_\theta \ \underline{G}_\theta \ \underline{\delta}_b + \underline{A}_\theta \ \underline{G}_{\theta t} \ \underline{\delta}_t) \tag{4.114}$$

$$\underline{\varepsilon}_\psi = \frac{1}{2} \underline{A}_\psi \ \underline{G}_\psi \ \underline{\delta}_t \tag{4.115}$$

$$\underline{\varepsilon}_{m\theta} = \underline{A}_\theta \ \underline{G}_m \ \underline{\delta}_0 = \underline{A}_m \ \underline{G}_\theta \ \underline{\delta}_b + \underline{A}_m \ \underline{G}_{\theta t} \ \underline{\delta}_t \tag{4.116}$$

$$\underline{\varepsilon}_{m\psi} = \underline{A}_\psi \ \underline{G}_m \ \underline{\delta}_0 = \underline{A}_m \ \underline{G}_\psi \ \underline{\delta}_t \tag{4.117}$$

$$\underline{\varepsilon}_{\theta\psi} = - \underline{A}_\theta \ \underline{G}_\psi \ \underline{\delta}_t = - \underline{A}_\psi \ \underline{G}_\theta \ \underline{\delta}_b - \underline{A}_\psi \ \underline{G}_{\theta t} \ \underline{\delta}_t \tag{4.118}$$

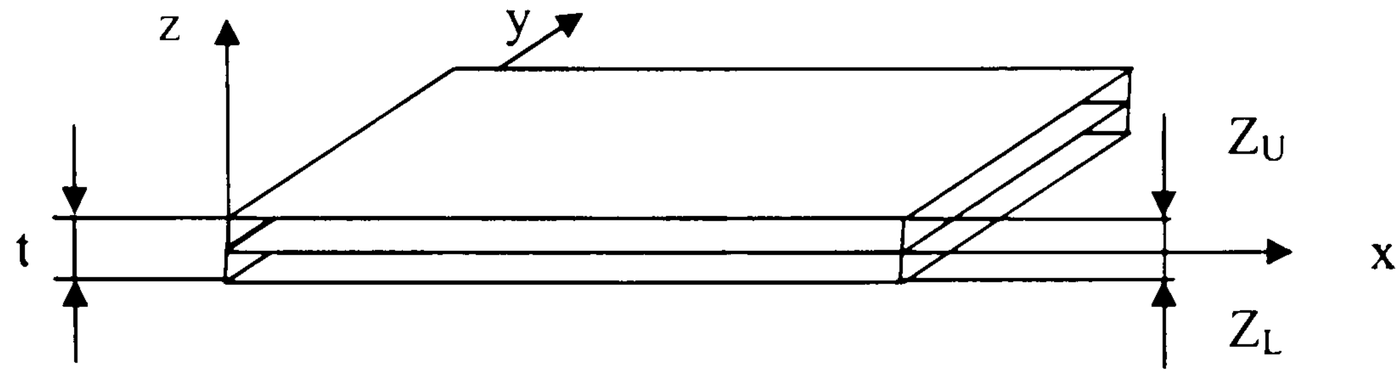

Figure (4.1) Plate with local xyz axes

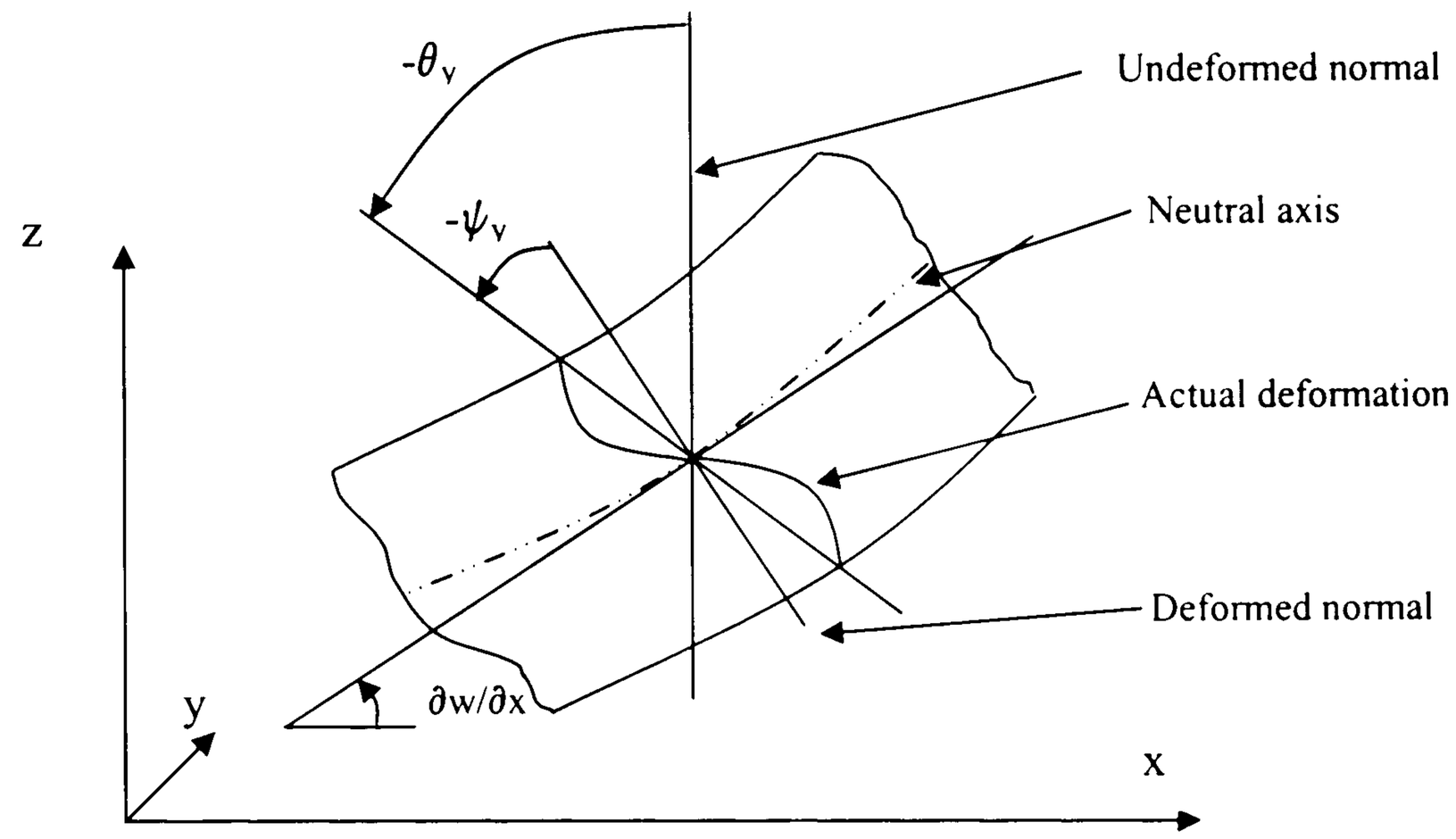

Figure (4.2) Deformation in x-z plane

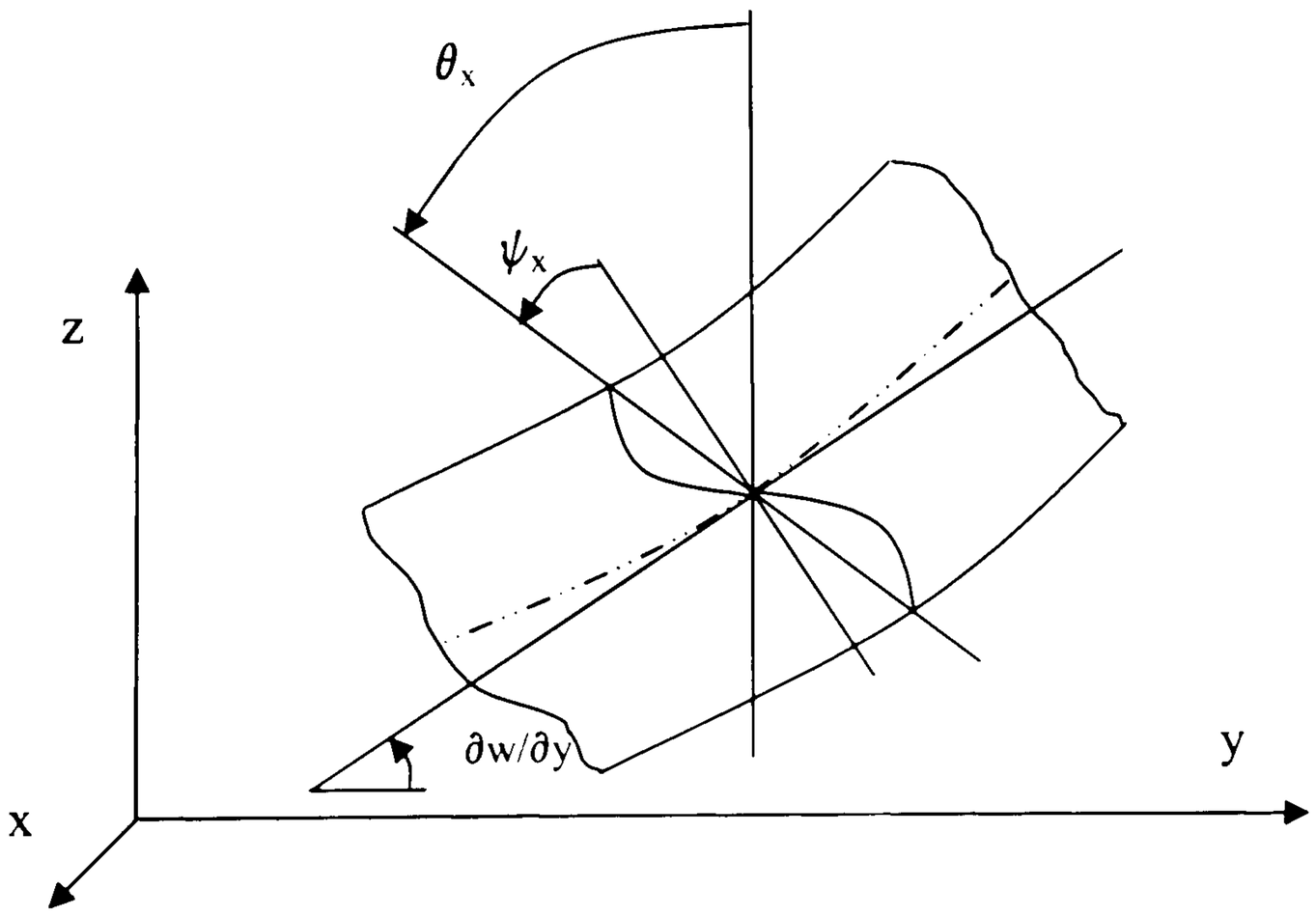

Figure (4.3) Deformation in y-z plane

5

FINITE ELEMENT EQUATIONS

5.1 INTRODUCTION

The deformation theory of high order elements has been introduced in the previous chapter with a complete description of all stress and strain relations. In this chapter, the finite element matrices will be derived using some basic concepts, such as strain energy, D'Alembert's principle, and the principle of virtual work.

For the completion of the work description, some basic types of finite element analyses employed in this work are also summarized in this chapter, such as nonlinear static and dynamic analysis and stability analysis. The fatigue damage analysis of composite materials will be discussed separately in the next chapter.

5.2 STRAIN ENERGY

Due to a differential displacement field, the corresponding change of strain energy density is,

$$d\overline{U} = d\underline{\varepsilon}^T \underline{\sigma} + d\underline{\gamma}^T \underline{\tau} \tag{5.1}$$

where $\underline{\sigma}$, $\underline{\tau}$ represent x-y stress and shear stress vectors, respectively, and:

$$\underline{\sigma} = \{\sigma_x \quad \sigma_y \quad \tau_{xy}\} \tag{5.2}$$

$$\underline{\tau} = \{\tau_{xz} \quad \tau_{yz}\} \tag{5.3}$$

The stress at any point inside a composite laminate can be related to strain as follows:

$$\underline{\sigma} = \underline{D}\,\underline{\varepsilon} \tag{5.4}$$

$$\underline{\tau} = \underline{\mu}\,\underline{\gamma} \tag{5.5}$$

where $\underline{D} \equiv \underline{D}_{xy}$, $\underline{\mu} \equiv \underline{\mu}_{2x2}$ as expressed in chapter 3.

Hence, the x-y stress vector can be partitioned similar to the strain vector in equation (4.53) as follows:

$$\underline{\sigma} = \underline{\sigma}_S + \underline{\sigma}_L \tag{5.6}$$

where $\underline{\sigma}_S$, $\underline{\sigma}_L$ represent the stress vectors due to infinitesimal and large strains, respectively, i.e.

$$\underline{\sigma}_S = \underline{D}\,\underline{\varepsilon}_S \quad , \quad \underline{\sigma}_L = \underline{D}\,\underline{\varepsilon}_L \tag{5.7}$$

Hence, the strain energy density can be written as follows:

$$d\overline{U} = d\underline{\varepsilon}_S^T\,\underline{\sigma}_S + d\underline{\varepsilon}_S^T\,\underline{\sigma}_L + d\underline{\varepsilon}_L^T\,\underline{\sigma} + d\underline{\gamma}^T\,\underline{\tau} \tag{5.8}$$

which can be rewritten as follows:

$$d\overline{U} = d\overline{U}_S + d\overline{U}_L + d\overline{U}_{SL} \tag{5.9}$$

where $d\overline{U}_S$ contains small or infinitesimal strain effect only and $d\overline{U}_L$, $d\overline{U}_{SL}$ contain finite or large strain effect, i.e.

$$d\overline{U}_S = d\underline{\varepsilon}_S^T\,\underline{\sigma}_S + d\underline{\gamma}^T\,\underline{\tau} \tag{5.10}$$

$$d\overline{U}_L = d\underline{\varepsilon}_L^T\,\underline{\sigma} \tag{5.11}$$

$$d\overline{U}_{SL} = d\underline{\varepsilon}_S^T\,\underline{\sigma}_L \tag{5.12}$$

then, the change of strain energy per unit area is defined as

$$dU' = \int_{z_L}^{z_U} d\overline{U}\,dz \tag{5.13}$$

By integrating equation (5.13) over the midplane, the change of element strain energy is obtained, i.e.

$$dU = \iint_{Area} dU'\,dxdy \tag{5.14}$$

5.3 INFINITESIMAL STIFFNESS MATRIX $\underline{K}$

From the change of small strain energy density $d\bar{U}_S$, equation (5.10), and by substituting from equation (4.56), then:

$$d\bar{U}_S = d\gamma^T\,\underline{\tau} + \left(d\underline{\varepsilon}_o - z\,d\underline{\varepsilon}_b + g(z)\,d\underline{\varepsilon}_t\right)^T \underline{D}\left(d\underline{\varepsilon}_o - z\,d\underline{\varepsilon}_b + g(z)\,d\underline{\varepsilon}_t\right) \tag{5.15}$$

Hence,

$$\begin{aligned} d\bar{U}_S = {} & d\underline{\gamma}^T\,\underline{\tau} + d\underline{\varepsilon}_o^T\,\underline{D}\,\underline{\varepsilon}_o + z^2\,d\underline{\varepsilon}_b^T\,\underline{D}\,\underline{\varepsilon}_b + g^2(z)\,d\underline{\varepsilon}_t^T\,\underline{D}\,\underline{\varepsilon}_t - z\,d\underline{\varepsilon}_o^T\,\underline{D}\,\underline{\varepsilon}_b - \\ & z\,d\underline{\varepsilon}_b^T\,\underline{D}\,\underline{\varepsilon}_o + g(z)\,d\underline{\varepsilon}_o^T\,\underline{D}\,\underline{\varepsilon}_t + g(z)\,d\underline{\varepsilon}_t^T\,\underline{D}\,\underline{\varepsilon}_o + z\,g(z)\,d\underline{\varepsilon}_b^T\,\underline{D}\,\underline{\varepsilon}_t + \\ & z\,g(z)\,d\underline{\varepsilon}_o^T\,\underline{D}\,\underline{\varepsilon}_o \end{aligned} \tag{5.16}$$

Substituting from the strain displacement equations given in chapter 4, into equation (5.16) then,

$$\begin{aligned} d\bar{U}_S = {} & d\underline{\delta}_t^T\,\underline{B}_\gamma^T\left[-\frac{5}{4}\left(1-\frac{4z^2}{h^2}\right)\right]^2 \underline{\mu}\,\underline{B}_\gamma\,\underline{\delta}_t + d\underline{\delta}_o^T\,\underline{B}_o^T\,\underline{D}\,\underline{B}_o\,\underline{\delta}_o + \\ & d\underline{\delta}_b^T\,\underline{B}_b^T\,z^2\,\underline{D}\,\underline{B}_b\,\underline{\delta}_b + d\underline{\delta}_b^T\,\underline{B}_b^T\,z^2\,\underline{D}\,\underline{B}_{bt}\,\underline{\delta}_t + \\ & d\underline{\delta}_t^T\,\underline{B}_{bt}^T\,z^2\,\underline{D}\,\underline{B}_b\,\underline{\delta}_b + d\underline{\delta}_t^T\,\underline{B}_{bt}^T\,z^2\,\underline{D}\,\underline{B}_{bt}\,\underline{\delta}_t + \\ & d\underline{\delta}_t^T\,\underline{B}_t^T\,g^2(z)\,\underline{D}\,\underline{B}_t\,\underline{\delta}_t - d\underline{\delta}_o^T\,\underline{B}_o^T\,z\,\underline{D}\,\underline{B}_b\,\underline{\delta}_b - \\ & d\underline{\delta}_o^T\,\underline{B}_o^T\,z\,\underline{D}\,\underline{B}_{bt}\,\underline{\delta}_t - d\underline{\delta}_b^T\,\underline{B}_b^T\,z\,\underline{D}\,\underline{B}_o\,\underline{\delta}_o - \\ & d\underline{\delta}_t^T\,\underline{B}_{bt}^T\,z\,\underline{D}\,\underline{B}_o\,\underline{\delta}_o + d\underline{\delta}_o^T\,\underline{B}_o^T\,g(z)\,\underline{D}\,\underline{B}_t\,\underline{\delta}_t + \\ & d\underline{\delta}_t^T\,\underline{B}_t^T\,g(z)\,\underline{D}\,\underline{B}_o\,\underline{\delta}_o - d\underline{\delta}_b^T\,\underline{B}_b^T\,z\,g(z)\,\underline{D}\,\underline{B}_t\,\underline{\delta}_t - \\ & d\underline{\delta}_t^T\,\underline{B}_{bt}^T\,z\,g(z)\,\underline{D}\,\underline{B}_t\,\underline{\delta}_t - d\underline{\delta}_t^T\,\underline{B}_t^T\,z\,g(z)\,\underline{D}\,\underline{B}_b\,\underline{\delta}_b - \\ & d\underline{\delta}_t^T\,\underline{B}_t^T\,z\,g(z)\,\underline{D}\,\underline{B}_{bt}\,\underline{\delta}_t \end{aligned} \tag{5.17}$$

Hence, the change of strain energy per unit area can be expressed by applying equation (5.13). leading to:

$$
\begin{aligned}
dU_S = {} & d\underline{\delta}_t^T \underline{B}_\gamma^T \underline{\mu}_{\gamma\gamma} \underline{B}_\gamma \underline{\delta}_t + d\underline{\delta}_o^T \underline{B}_o^T \underline{D}_{oo} \underline{B}_o \underline{\delta}_o + \\
& d\underline{\delta}_b^T \underline{B}_b^T \underline{D}_{bb} \underline{B}_b \underline{\delta}_b + d\underline{\delta}_b^T \underline{B}_b^T \underline{D}_{bb} \underline{B}_{bt} \underline{\delta}_t + \\
& d\underline{\delta}_t^T \underline{B}_{bt}^T \underline{D}_{bb} \underline{B}_b \underline{\delta}_b + d\underline{\delta}_t^T \underline{B}_{bt}^T \underline{D}_{bb} \underline{B}_{bt} \underline{\delta}_t + \\
& d\underline{\delta}_t^T \underline{B}_t^T \underline{D}_{tt} \underline{B}_t \underline{\delta}_t - d\underline{\delta}_o^T \underline{B}_o^T \underline{D}_{ob} \underline{B}_b \underline{\delta}_b - \\
& d\underline{\delta}_o^T \underline{B}_o^T \underline{D}_{ob} \underline{B}_{bt} \underline{\delta}_t - d\underline{\delta}_b^T \underline{B}_b^T \underline{D}_{bo} \underline{B}_o \underline{\delta}_o - \\
& d\underline{\delta}_t^T \underline{B}_{bt}^T \underline{D}_{bo} \underline{B}_o \underline{\delta}_o + d\underline{\delta}_o^T \underline{B}_o^T \underline{D}_{ot} \underline{B}_t \underline{\delta}_t + \\
& d\underline{\delta}_t^T \underline{B}_t^T \underline{D}_{to} \underline{B}_o \underline{\delta}_o - d\underline{\delta}_b^T \underline{B}_b^T \underline{D}_{bt} \underline{B}_t \underline{\delta}_t - \\
& d\underline{\delta}_t^T \underline{B}_{bt}^T \underline{D}_{bt} \underline{B}_t \underline{\delta}_t - d\underline{\delta}_t^T \underline{B}_t^T \underline{D}_{tb} \underline{B}_b \underline{\delta}_b - \\
& d\underline{\delta}_t^T \underline{B}_t^T \underline{D}_{tb} \underline{B}_{bt} \underline{\delta}_t
\end{aligned}
\tag{5.18}
$$

where $\underline{D}$ matrix may be different from layer to layer which need to be integrated over the thickness. Writing the integration of a general function f(z) over the total thickness in terms of integrations over different layers, i.e.

$$
\int_{z_L}^{z_U} f(z)\,dz = \sum_{m=1}^{N_l} \int_{z_L^{(m)}}^{z_U^{(m)}} f(z)\,dz \tag{5.19}
$$

where N_l is the number of layers and m is the layer number m, $z_U^{(m)}$, $z_L^{(m)}$ represent the upper and lower surfaces of layer m, respectively, hence, the $\underline{D}_{**}$ matrices can be defined as follows:

$$
\underline{\mu}_{\gamma\gamma} = \sum_{m=1}^{N_l} \int_{z_L^{(m)}}^{z_U^{(m)}} \frac{25}{16}\left(1 - \frac{4z^2}{h^2}\right) \underline{\mu}^{(m)}\,dz \tag{5.20}
$$

$$
\underline{D}_{oo} = \sum_{m=1}^{N_l} \int_{z_L^{(m)}}^{z_U^{(m)}} \underline{D}^{(m)}\,dz \tag{5.21}
$$

$$
\underline{D}_{bb} = \sum_{m=1}^{N_l} \int_{z_L^{(m)}}^{z_U^{(m)}} z^2\, \underline{D}^{(m)}\,dz \tag{5.22}
$$

$$
\underline{D}_{tt} = \sum_{m=1}^{N_l} \int_{z_L^{(m)}}^{z_U^{(m)}} g^2(z)\, \underline{D}^{(m)}\,dz \tag{5.23}
$$

$$\underline{D}_{ob} = \underline{D}_{bo} = \sum_{m=1}^{N_l} \int_{z_L^{(m)}}^{z_U^{(m)}} z\ \underline{D}^{(m)}\, dz \tag{5.24}$$

$$\underline{D}_{ot} = \underline{D}_{to} = \sum_{m=1}^{N_l} \int_{z_L^{(m)}}^{z_U^{(m)}} g(z)\ \underline{D}^{(m)}\, dz \tag{5.25}$$

$$\underline{D}_{bt} = \underline{D}_{tb} = \sum_{m=1}^{N_l} \int_{z_L^{(m)}}^{z_U^{(m)}} z\, g(z)\ \underline{D}^{(m)}\, dz \tag{5.26}$$

Applying equation (5.14) to obtain the strain energy change of the element it can be deduced that:

$$\begin{aligned} dU_S = {} & d\underline{\delta}_t^T\ \underline{K}_{\gamma\gamma}\ \underline{\delta}_t + d\underline{\delta}_o^T\ \underline{K}_{oo}\ \underline{\delta}_o + d\underline{\delta}_b^T\ \underline{K}_{bb}\ \underline{\delta}_b + \\ & d\underline{\delta}_b^T\ \underline{K}_{bbt}\ \underline{\delta}_t + d\underline{\delta}_t^T\ \underline{K}_{btb}\ \underline{\delta}_b + d\underline{\delta}_t^T\ \underline{K}_{btbt}\ \underline{\delta}_t + \\ & d\underline{\delta}_t^T\ \underline{K}_{tt}\ \underline{\delta}_t - d\underline{\delta}_o^T\ \underline{K}_{ob}\ \underline{\delta}_b - d\underline{\delta}_o^T\ \underline{K}_{obt}\ \underline{\delta}_t - \\ & d\underline{\delta}_b^T\ \underline{K}_{bo}\ \underline{\delta}_o - d\underline{\delta}_t^T\ \underline{K}_{bto}\ \underline{\delta}_o + d\underline{\delta}_o^T\ \underline{K}_{ot}\ \underline{\delta}_t + \\ & d\underline{\delta}_t^T\ \underline{K}_{to}\ \underline{\delta}_o - d\underline{\delta}_b^T\ \underline{K}_{bt}\ \underline{\delta}_t - d\underline{\delta}_t^T\ \underline{K}_{btt}\ \underline{\delta}_t - \\ & d\underline{\delta}_t^T\ \underline{K}_{tb}\ \underline{\delta}_b - d\underline{\delta}_t^T\ \underline{K}_{tbt}\ \underline{\delta}_t \end{aligned} \tag{5.27}$$

where

$$\underline{K}_{\gamma\gamma} = \iint_{\text{element}} \underline{B}_\gamma^T\ \underline{\mu}_{\gamma\gamma}\ \underline{B}_\gamma\, dxdy \tag{5.28}$$

$$\underline{K}_{oo} = \iint_{\text{element}} \underline{B}_o^T\ \underline{D}_{oo}\ \underline{B}_o\, dxdy \tag{5.29}$$

$$\underline{K}_{bb} = \iint_{\text{element}} \underline{B}_b^T\ \underline{D}_{bb}\ \underline{B}_b\, dxdy \tag{5.30}$$

$$\underline{K}_{bbt} = \iint_{\text{element}} \underline{B}_b^T\ \underline{D}_{bb}\ \underline{B}_{bt}\, dxdy \tag{5.31}$$

$$\underline{K}_{btb} = \iint_{\text{element}} \underline{B}_{bt}^T\ \underline{D}_{bb}\ \underline{B}_b\, dxdy \tag{5.32}$$

$$\underline{K}_{btbt} = \iint_{element} \underline{B}_{bt}^{T}\, \underline{D}_{bb}\, \underline{B}_{bt}\, dxdy \tag{5.33}$$

$$\underline{K}_{tt} = \iint_{element} \underline{B}_{t}^{T}\, \underline{D}_{tt}\, \underline{B}_{t}\, dxdy \tag{5.34}$$

$$\underline{K}_{ob} = \iint_{element} \underline{B}_{o}^{T}\, \underline{D}_{ob}\, \underline{B}_{b}\, dxdy \tag{5.35}$$

$$\underline{K}_{obt} = \iint_{element} \underline{B}_{o}^{T}\, \underline{D}_{ob}\, \underline{B}_{bt}\, dxdy \tag{5.36}$$

$$\underline{K}_{bo} = \iint_{element} \underline{B}_{b}^{T}\, \underline{D}_{bo}\, \underline{B}_{o}\, dxdy \tag{5.37}$$

$$\underline{K}_{bto} = \iint_{element} \underline{B}_{bt}^{T}\, \underline{D}_{bo}\, \underline{B}_{o}\, dxdy \tag{5.38}$$

$$\underline{K}_{ot} = \iint_{element} \underline{B}_{o}^{T}\, \underline{D}_{ot}\, \underline{B}_{t}\, dxdy \tag{5.39}$$

$$\underline{K}_{to} = \iint_{element} \underline{B}_{t}^{T}\, \underline{D}_{to}\, \underline{B}_{o}\, dxdy \tag{5.40}$$

$$\underline{K}_{bt} = \iint_{element} \underline{B}_{b}^{T}\, \underline{D}_{bt}\, \underline{B}_{t}\, dxdy \tag{5.41}$$

$$\underline{K}_{btt} = \iint_{element} \underline{B}_{bt}^{T}\, \underline{D}_{bt}\, \underline{B}_{t}\, dxdy \tag{5.42}$$

$$\underline{K}_{tb} = \iint_{element} \underline{B}_{t}^{T}\, \underline{D}_{tb}\, \underline{B}_{b}\, dxdy \tag{5.43}$$

$$\underline{K}_{tbt} = \iint_{element} \underline{B}_{t}^{T}\, \underline{D}_{tb}\, \underline{B}_{bt}\, dxdy \tag{5.44}$$

Equation (5.27) may also be rewritten as follows:

$$dU_S = d\underline{\delta}^{T}\, \underline{K}\, \underline{\delta} \tag{5.45}$$

where $\underline{K}$ represents the element stiffness matrix which is defined as follows:

$$\underline{K} = \left[\begin{array}{c|c|c} \underline{K}_{oo} & -\underline{K}_{ob} & \underline{K}_{ot} - \underline{K}_{obt} \\ \hline -\underline{K}_{bo} & \underline{K}_{bb} & \underline{K}_{bbt} - \underline{K}_{bt} \\ \hline \underline{K}_{to} - \underline{K}_{bto} & \underline{K}_{btb} - \underline{K}_{tb} & \underline{K}_{\gamma\gamma} + \underline{K}_{btbt} + \underline{K}_{tt} - \underline{K}_{btt} - \underline{K}_{tbt} \end{array}\right] \tag{5.46}$$

5.4 STRESS STIFFNESS MATRIX $\underline{K}^{\sigma}$

Equation (5.11) represents the change of strain energy density for large deflection. Substituting from equation (4.60) into equation (5.11), then:

$$\begin{aligned} d\overline{U}_L = (& d\underline{\varepsilon}_m + d\underline{\varepsilon}_w + z^2\, d\underline{\varepsilon}_\theta + g^2(z)\, d\underline{\varepsilon}_\psi - \\ & z\, d\underline{\varepsilon}_{m\theta} + g(z)\, d\underline{\varepsilon}_{m\psi} + z\, g(z)\, d\underline{\varepsilon}_{\theta\psi})^T\, \underline{\sigma} \end{aligned} \tag{5.47}$$

Substituting from equations (4.95-101) into equation (5.47), then:

$$\begin{aligned} d\overline{U}_L = & d\underline{\theta}_m^T\, \underline{A}_m^T\, \underline{\sigma} + d\underline{\theta}_w^T\, \underline{A}_w^T\, \underline{\sigma} + d\underline{\theta}_\theta^T\, \underline{A}_\theta^T\, z^2\, \underline{\sigma} + d\underline{\theta}_\psi^T\, \underline{A}_\psi^T\, g^2(z)\, \underline{\sigma} - \\ & d\underline{\theta}_m^T\, \underline{A}_\theta^T\, z\, \underline{\sigma} - d\underline{\theta}_\theta^T\, \underline{A}_m^T\, z\, \underline{\sigma} + d\underline{\theta}_\psi^T\, \underline{A}_m^T\, g(z)\, \underline{\sigma} + d\underline{\theta}_m^T\, \underline{A}_\psi^T\, g(z)\, \underline{\sigma} - \\ & d\underline{\theta}_\psi^T\, \underline{A}_\theta^T\, z\, g(z)\, \underline{\sigma} + d\underline{\theta}_\theta^T\, \underline{A}_\psi^T\, z\, g(z)\, \underline{\sigma} \end{aligned} \tag{5.48}$$

Applying equation (5.13) the change of strain energy per unit area is obtained as follows:

$$\begin{aligned} dU_L^{\backslash} = & d\underline{\theta}_m^T\, \underline{A}_m^T\, \underline{\sigma}_m + d\underline{\theta}_w^T\, \underline{A}_w^T\, \underline{\sigma}_w + d\underline{\theta}_\theta^T\, \underline{A}_\theta^T\, \underline{\sigma}_\theta + d\underline{\theta}_\psi^T\, \underline{A}_\psi^T\, \underline{\sigma}_\psi + \\ & d\underline{\theta}_m^T\, \underline{A}_\theta^T\, \underline{\sigma}_{m\theta} + d\underline{\theta}_\theta^T\, \underline{A}_m^T\, \underline{\sigma}_{m\theta} + d\underline{\theta}_\psi^T\, \underline{A}_m^T\, \underline{\sigma}_{m\psi} + d\underline{\theta}_m^T\, \underline{A}_\psi^T\, \underline{\sigma}_{m\psi} - \\ & d\underline{\theta}_\psi^T\, \underline{A}_\theta^T\, \underline{\sigma}_{\theta\psi} - d\underline{\theta}_\theta^T\, \underline{A}_\psi^T\, \underline{\sigma}_{\theta\psi} \end{aligned} \tag{5.49}$$

where

$$\underline{\sigma}_m = \int_{z_L}^{z_t} \underline{\sigma}\, dz \tag{5.50}$$

$$\underline{\sigma}_w = \int_{z_L}^{z_U} \underline{\sigma}\, dz = \underline{\sigma}_m \tag{5.51}$$

$$\underline{\sigma}_\theta = \int_{z_L}^{z_U} z^2\, \underline{\sigma}\, dz \tag{5.52}$$

$$\underline{\sigma}_\psi = \int_{z_L}^{z_U} g^2(z)\, \underline{\sigma}\, dz \tag{5.53}$$

$$\underline{\sigma}_{m\theta} = \int_{z_L}^{z_U} - z\, \underline{\sigma}\, dz \tag{5.54}$$

$$\underline{\sigma}_{m\psi} = \int_{z_L}^{z_U} g(z)\, \underline{\sigma}\, dz \tag{5.55}$$

$$\underline{\sigma}_{\theta\psi} = \int_{z_L}^{z_U} z\, g(z)\, \underline{\sigma}\, dz \tag{5.56}$$

Substituting from equations (5.4), (4.56) and (4.60) into (5.50-56), then for general non-linear analysis, it can be proved that:

$$\begin{aligned}\underline{\sigma}_m = {} & \underline{D}_{oo}\underline{\varepsilon}_o - \underline{D}_{ob}\underline{\varepsilon}_b + \underline{D}_{ot}\underline{\varepsilon}_t + \underline{D}_{oo}(\underline{\varepsilon}_m + \underline{\varepsilon}_w) + \\ & \underline{D}_{bb}\underline{\varepsilon}_\theta + \underline{D}_{tt}\underline{\varepsilon}_\psi - \underline{D}_{ob}\underline{\varepsilon}_{m\theta} + \underline{D}_{ot}\underline{\varepsilon}_{m\psi} + \underline{D}_{bt}\underline{\varepsilon}_{\theta\psi}\end{aligned} \tag{5.57}$$

$$\begin{aligned}\underline{\sigma}_\theta = {} & \underline{D}_{bb}(\underline{\varepsilon}_o + \underline{\varepsilon}_m + \underline{\varepsilon}_w) + \underline{D}_{\theta\theta}\underline{\varepsilon}_\theta - \underline{D}_{\theta b}(\underline{\varepsilon}_b + \underline{\varepsilon}_{m\theta}) + \\ & \underline{D}_{\theta\psi}\underline{\varepsilon}_\psi + \underline{D}_{\theta t}(\underline{\varepsilon}_t + \underline{\varepsilon}_{m\psi}) + \underline{D}_{\theta\theta\psi}\underline{\varepsilon}_{\theta\psi}\end{aligned} \tag{5.58}$$

$$\begin{aligned}\underline{\sigma}_\psi = {} & \underline{D}_{tt}(\underline{\varepsilon}_o + \underline{\varepsilon}_m + \underline{\varepsilon}_w) + \underline{D}_{\theta\psi}\underline{\varepsilon}_\theta - \underline{D}_{\psi b}(\underline{\varepsilon}_b + \underline{\varepsilon}_{m\theta}) + \\ & \underline{D}_{\psi\psi}\underline{\varepsilon}_\psi + \underline{D}_{\psi t}(\underline{\varepsilon}_t + \underline{\varepsilon}_{m\psi}) + \underline{D}_{\psi\theta\psi}\underline{\varepsilon}_{\theta\psi}\end{aligned} \tag{5.59}$$

$$\begin{aligned}\underline{\sigma}_{m\theta} = {} & -\underline{D}_{ob}(\underline{\varepsilon}_o + \underline{\varepsilon}_m + \underline{\varepsilon}_w) - \underline{D}_{\theta b}\underline{\varepsilon}_\theta + \underline{D}_{bb}(\underline{\varepsilon}_b + \underline{\varepsilon}_{m\theta}) - \\ & \underline{D}_{\psi b}\underline{\varepsilon}_\psi - \underline{D}_{bt}(\underline{\varepsilon}_t + \underline{\varepsilon}_{m\psi}) - \underline{D}_{\theta t}\underline{\varepsilon}_{\theta\psi}\end{aligned} \tag{5.60}$$

$$\underline{\sigma}_{m\psi} = \underline{D}_{ot}(\underline{\varepsilon}_o + \underline{\varepsilon}_m + \underline{\varepsilon}_w) + \underline{D}_{\theta t}\underline{\varepsilon}_\theta - \underline{D}_{bt}(\underline{\varepsilon}_b + \underline{\varepsilon}_{m\theta}) + \underline{D}_{\psi t}\underline{\varepsilon}_\psi + \underline{D}_{tt}(\underline{\varepsilon}_t + \underline{\varepsilon}_{m\psi}) + \underline{D}_{\theta\psi}\underline{\varepsilon}_{\theta\psi} \tag{5.61}$$

$$\underline{\sigma}_{\theta\psi} = \underline{D}_{bt}(\underline{\varepsilon}_o + \underline{\varepsilon}_m + \underline{\varepsilon}_w) + \underline{D}_{\theta\theta\psi}\underline{\varepsilon}_\theta - \underline{D}_{\theta t}(\underline{\varepsilon}_b + \underline{\varepsilon}_{m\theta}) + \underline{D}_{\psi\theta\psi}\underline{\varepsilon}_\psi + \underline{D}_{\psi b}(\underline{\varepsilon}_t + \underline{\varepsilon}_{m\psi}) + \underline{D}_{\theta\psi}\underline{\varepsilon}_{\theta\psi} \tag{5.62}$$

where

$$\underline{D}_{\theta\theta} = \sum_{m=1}^{N_l} \int_{z_L^{(m)}}^{z_U^{(m)}} z^4 \, \underline{D}^{(m)} \, dz \tag{5.63}$$

$$\underline{D}_{\theta b} = \sum_{m=1}^{N_l} \int_{z_L^{(m)}}^{z_U^{(m)}} z^3 \, \underline{D}^{(m)} \, dz \tag{5.64}$$

$$\underline{D}_{\theta\psi} = \sum_{m=1}^{N_l} \int_{z_L^{(m)}}^{z_U^{(m)}} z^2 g^2(z) \, \underline{D}^{(m)} \, dz \tag{5.65}$$

$$\underline{D}_{\theta t} = \sum_{m=1}^{N_l} \int_{z_L^{(m)}}^{z_U^{(m)}} z^2 g(z) \, \underline{D}^{(m)} \, dz \tag{5.66}$$

$$\underline{D}_{\theta\theta\psi} = \sum_{m=1}^{N_l} \int_{z_L^{(m)}}^{z_U^{(m)}} z^3 g(z) \, \underline{D}^{(m)} \, dz \tag{5.67}$$

$$\underline{D}_{\psi b} = \sum_{m=1}^{N_l} \int_{z_L^{(m)}}^{z_U^{(m)}} z \, g^2(z) \, \underline{D}^{(m)} \, dz \tag{5.68}$$

$$\underline{D}_{\psi\theta\psi} = \sum_{m=1}^{N_l} \int_{z_L^{(m)}}^{z_U^{(m)}} z \, g^3(z) \, \underline{D}^{(m)} \, dz \tag{5.69}$$

$$\underline{D}_{\psi t} = \sum_{m=1}^{N_l} \int_{z_L^{(m)}}^{z_U^{(m)}} g^3(z) \, \underline{D}^{(m)} \, dz \tag{5.70}$$

$$\underline{D}_{\psi\psi} = \sum_{m=1}^{N_l} \int_{z_L^{(m)}}^{z_U^{(m)}} g^4(z)\, \underline{D}^{(m)}\, dz \tag{5.71}$$

For stability or buckling analysis, the small or infinitesimal stress only is considered, where

$$\underline{\sigma}_m = \underline{D}_{oo}\, \underline{\varepsilon}_o - \underline{D}_{ob}\, \underline{\varepsilon}_b + \underline{D}_{ot}\, \underline{\varepsilon}_t \tag{5.72}$$

$$\underline{\sigma}_\theta = \underline{D}_{bb}\, \underline{\varepsilon}_o + \underline{D}_{\theta b}\, \underline{\varepsilon}_b + \underline{D}_{\theta t}\, \underline{\varepsilon}_t \tag{5.73}$$

$$\underline{\sigma}_\psi = \underline{D}_{tt}\, \underline{\varepsilon}_o + \underline{D}_{\psi b}\, \underline{\varepsilon}_b + \underline{D}_{\psi t}\, \underline{\varepsilon}_t \tag{5.74}$$

$$\underline{\sigma}_{m\theta} = -\underline{D}_{ob}\, \underline{\varepsilon}_o + \underline{D}_{bb}\, \underline{\varepsilon}_b - \underline{D}_{bt}\, \underline{\varepsilon}_t \tag{5.75}$$

$$\underline{\sigma}_{m\psi} = \underline{D}_{ot}\, \underline{\varepsilon}_o - \underline{D}_{bt}\, \underline{\varepsilon}_b + \underline{D}_{tt}\, \underline{\varepsilon}_t \tag{5.76}$$

$$\underline{\sigma}_{\theta\psi} = \underline{D}_{bt}\, \underline{\varepsilon}_o - \underline{D}_{\theta t}\, \underline{\varepsilon}_b + \underline{D}_{\psi b}\, \underline{\varepsilon}_t \tag{5.77}$$

Using the properties of $\underline{A}$ and $\underline{\theta}$ in equations (4.92) and (4.93) then equation (5.49) can be rewritten as follows:

$$\begin{aligned} dU_L^{\backslash} = {} & d\underline{\theta}_m^T\, \underline{S}_{mm}\, \underline{\theta}_m + d\underline{\theta}_w^T\, \underline{S}_{ww}\, \underline{\theta}_w + d\underline{\theta}_\theta^T\, \underline{S}_{\theta\theta}\, \underline{\theta}_\theta + d\underline{\theta}_\psi^T\, \underline{S}_{\psi\psi}\, \underline{\theta}_\psi + \\ & d\underline{\theta}_m^T\, \underline{S}_{m\theta}\, \underline{\theta}_\theta + d\underline{\theta}_\theta^T\, \underline{S}_{\theta m}\, \underline{\theta}_m + d\underline{\theta}_\psi^T\, \underline{S}_{\psi m}\, \underline{\theta}_m + d\underline{\theta}_m^T\, \underline{S}_{m\psi}\, \underline{\theta}_\psi - \\ & d\underline{\theta}_\psi^T \underline{S}_{\psi\theta}\, \underline{\theta}_\theta - d\underline{\theta}_\theta^T \underline{S}_{\theta\psi}\, \underline{\theta}_\psi \end{aligned} \tag{5.78}$$

where $\underline{S}_{..}$ matrix represent a stress matrix which is defined in section (4.5) and corresponding to the stress values $\underline{\sigma}_{..}$ which is defined in this section.

Substituting from equations (4.102-105) into (5.68) and applying equation (5.14), the change of the element large strain energy can be expressed as:

$$
\begin{aligned}
dU_L = {} & d\underline{\delta}_o^T \underline{K}_{mm}^{\sigma} \underline{\delta}_o + d\underline{\delta}_b^T \underline{K}_{ww}^{\sigma} \underline{\delta}_b + d\underline{\delta}_b^T \underline{K}_{wwt}^{\sigma} \underline{\delta}_t + \\
& d\underline{\delta}_t^T \underline{K}_{wtw}^{\sigma} \underline{\delta}_b + d\underline{\delta}_t^T \underline{K}_{wtwt}^{\sigma} \underline{\delta}_t + d\underline{\delta}_b^T \underline{K}_{\theta\theta}^{\sigma} \underline{\delta}_b + \\
& d\underline{\delta}_b^T \underline{K}_{\theta\theta t}^{\sigma} \underline{\delta}_t + d\underline{\delta}_t^T \underline{K}_{\theta t\theta}^{\sigma} \underline{\delta}_b + d\underline{\delta}_t^T \underline{K}_{\theta t\theta t}^{\sigma} \underline{\delta}_t + \\
& d\underline{\delta}_t^T \underline{K}_{\psi\psi}^{\sigma} \underline{\delta}_t + d\underline{\delta}_o^T \underline{K}_{m\theta}^{\sigma} \underline{\delta}_b + d\underline{\delta}_o^T \underline{K}_{m\vartheta t}^{\sigma} \underline{\delta}_t - \\
& d\underline{\delta}_b^T \underline{K}_{\theta m}^{\sigma} \underline{\delta}_o - d\underline{\delta}_t^T \underline{K}_{\theta tm}^{\sigma} \underline{\delta}_o + d\underline{\delta}_o^T \underline{K}_{m\psi}^{\sigma} \underline{\delta}_t + \\
& d\underline{\delta}_t^T \underline{K}_{\psi m}^{\sigma} \underline{\delta}_o - d\underline{\delta}_b^T \underline{K}_{\theta\psi}^{\sigma} \underline{\delta}_t - d\underline{\delta}_t^T \underline{K}_{\theta t\psi}^{\sigma} \underline{\delta}_t - \\
& d\underline{\delta}_t^T \underline{K}_{\psi\theta}^{\sigma} \underline{\delta}_b - d\underline{\delta}_t^T \underline{K}_{\psi\theta t}^{\sigma} \underline{\delta}_t
\end{aligned}
\tag{5.79}
$$

where

$$\underline{K}_{mm}^{\sigma} = \iint_{element} \underline{G}_m^T \underline{S}_{mm} \underline{G}_m \, dxdy \tag{5.80}$$

$$\underline{K}_{ww}^{\sigma} = \iint_{element} \underline{G}_w^T \underline{S}_{ww} \underline{G}_w \, dxdy \tag{5.81}$$

$$\underline{K}_{wwt}^{\sigma} = \iint_{element} \underline{G}_w^T \underline{S}_{ww} \underline{G}_{wt} \, dxdy \tag{5.82}$$

$$\underline{K}_{wtw}^{\sigma} = \iint_{element} \underline{G}_{wt}^T \underline{S}_{ww} \underline{G}_w \, dxdy \tag{5.83}$$

$$\underline{K}_{wtwt}^{\sigma} = \iint_{element} \underline{G}_{wt}^T \underline{S}_{ww} \underline{G}_{wt} \, dxdy \tag{5.84}$$

$$\underline{K}_{\theta\theta}^{\sigma} = \iint_{element} \underline{G}_{\theta}^T \underline{S}_{\theta\theta} \underline{G}_{\theta} \, dxdy \tag{5.85}$$

$$\underline{K}_{\theta\theta t}^{\sigma} = \iint_{element} \underline{G}_{\theta}^T \underline{S}_{\theta\theta} \underline{G}_{\theta t} \, dxdy \tag{5.86}$$

$$\underline{K}_{\theta t\theta}^{\sigma} = \iint_{element} \underline{G}_{\theta t}^T \underline{S}_{\theta\theta} \underline{G}_{\theta} \, dxdy \tag{5.87}$$

$$\underline{K}_{\theta t\theta t}^{\sigma} = \iint_{element} \underline{G}_{\theta t}^T \underline{S}_{\theta\theta} \underline{G}_{\theta t} \, dxdy \tag{5.88}$$

$$\underline{K}^{\sigma}_{\psi\psi} = \iint_{element} \underline{G}^{T}_{\psi} \underline{S}_{\psi\psi} \underline{G}_{\psi} \, dxdy \tag{5.89}$$

$$\underline{K}^{\sigma}_{m\theta} = \iint_{element} \underline{G}^{T}_{m} \underline{S}_{m\theta} \underline{G}_{\theta} \, dxdy \tag{5.90}$$

$$\underline{K}^{\sigma}_{m\theta t} = \iint_{element} \underline{G}^{T}_{m} \underline{S}_{m\theta} \underline{G}_{\theta t} \, dxdy \tag{5.91}$$

$$\underline{K}^{\sigma}_{\theta m} = \iint_{element} \underline{G}^{T}_{\theta} \underline{S}_{\theta m} \underline{G}_{m} \, dxdy \tag{5.92}$$

$$\underline{K}^{\sigma}_{\theta t m} = \iint_{element} \underline{G}^{T}_{\theta t} \underline{S}_{\theta m} \underline{G}_{m} \, dxdy \tag{5.93}$$

$$\underline{K}^{\sigma}_{m\psi} = \iint_{element} \underline{G}^{T}_{m} \underline{S}_{m\psi} \underline{G}_{\psi} \, dxdy \tag{5.94}$$

$$\underline{K}^{\sigma}_{\psi m} = \iint_{element} \underline{G}^{T}_{\psi} \underline{S}_{\psi m} \underline{G}_{m} \, dxdy \tag{5.95}$$

$$\underline{K}^{\sigma}_{\theta\psi} = \iint_{element} \underline{G}^{T}_{\theta} \underline{S}_{\theta\psi} \underline{G}_{\psi} \, dxdy \tag{5.96}$$

$$\underline{K}^{\sigma}_{\theta t\psi} = \iint_{element} \underline{G}^{T}_{\theta t} \underline{S}_{\theta\psi} \underline{G}_{\psi} \, dxdy \tag{5.97}$$

$$\underline{K}^{\sigma}_{\psi\theta} = \iint_{element} \underline{G}^{T}_{\psi} \underline{S}_{\psi\theta} \underline{G}_{\theta} \, dxdy \tag{5.98}$$

$$\underline{K}^{\sigma}_{\psi\theta t} = \iint_{element} \underline{G}^{T}_{\psi} \underline{S}_{\psi\theta} \underline{G}_{\theta t} \, dxdy \tag{5.99}$$

Equation (5.79) may be rewritten as follows:

$$dU_{L} = d\underline{\delta}^{T} \underline{K}^{\sigma} \underline{\delta} \tag{5.100}$$

where $\underline{K}^{\sigma}$ represents the stress stiffness matrix which is defined as follows:

$$\underline{K}^{\sigma} = \left[\begin{array}{c|c|c} \underline{K}^{\sigma}_{mm} & \underline{K}^{\sigma}_{m\theta} & \underline{K}^{\sigma}_{m\psi} + \underline{K}^{\sigma}_{m\theta t} \\ \hline \underline{K}^{\sigma}_{\theta m} & \underline{K}^{\sigma}_{ww} + \underline{K}^{\sigma}_{\theta\theta} & \underline{K}^{\sigma}_{wwt} + \underline{K}^{\sigma}_{\theta\theta t} - \underline{K}^{\sigma}_{\theta\psi} \\ \hline \underline{K}^{\sigma}_{\psi m} + \underline{K}^{\sigma}_{\theta t m} & \underline{K}^{\sigma}_{wtw} + \underline{K}^{\sigma}_{\theta t\theta} - \underline{K}^{\sigma}_{\psi\theta} & \underline{K}^{\sigma}_{wtwt} + \underline{K}^{\sigma}_{\theta t\theta t} + \underline{K}^{\sigma}_{\psi\psi} - \underline{K}^{\sigma}_{\theta t\psi} - \underline{K}^{\sigma}_{\psi\theta t} \end{array}\right] \tag{5.101}$$

5.5 FINITE FORCE VECTOR $\underline{F}_L$

Equation (5.12) represents the coupling effect of small and large effect on the strain energy density. Substituting from equation (4.56) into equation (5.12).

$$d\overline{U}_{SL} = \left(d\underline{\varepsilon}_o - z\, d\underline{\varepsilon}_b + g(z)\, d\underline{\varepsilon}_t\right)^T \underline{\sigma}_L \tag{5.102}$$

By integrating equation (5.102) over the thickness, the strain energy per unit area is obtained as.

$$d\overline{U}_S = d\underline{\varepsilon}_o^T\, \underline{\sigma}_o - d\underline{\varepsilon}_b^T\, \underline{\sigma}_b + d\underline{\varepsilon}_t^T\, \underline{\sigma}_t \tag{5.103}$$

where

$$\underline{\sigma}_o = \int_{z_L}^{z_U} \underline{\sigma}_L\, dz \tag{5.104}$$

$$\underline{\sigma}_b = -\int_{z_L}^{z_U} z\, \underline{\sigma}_L\, dz \tag{5.105}$$

$$\underline{\sigma}_t = \int_{z_L}^{z_U} g(z)\, \underline{\sigma}_L\, dz \tag{5.106}$$

Substituting from equation (5.7) and (4.60) into equations (5.104-106) then it can be shown that:

$$\underline{\sigma}_o = \underline{D}_{oo}(\underline{\varepsilon}_m + \underline{\varepsilon}_w) + \underline{D}_{bb}\,\underline{\varepsilon}_\theta - \underline{D}_{ob}\,\underline{\varepsilon}_{m\theta} + \underline{D}_{tt}\,\underline{\varepsilon}_\psi + \underline{D}_{ot}\,\underline{\varepsilon}_{m\psi} + \underline{D}_{bt}\,\underline{\varepsilon}_{\theta\psi} \tag{5.107}$$

$$\underline{\sigma}_b = -\underline{D}_{ob}(\underline{\varepsilon}_m + \underline{\varepsilon}_w) - \underline{D}_{\theta b}\underline{\varepsilon}_\theta + \underline{D}_{bb}\underline{\varepsilon}_{m\theta} - \underline{D}_{\psi b}\underline{\varepsilon}_\psi - \underline{D}_{bt}\underline{\varepsilon}_{m\psi} - \underline{D}_{\theta t}\underline{\varepsilon}_{\theta\psi} \tag{5.108}$$

$$\underline{\sigma}_t = \underline{D}_{ot}(\underline{\varepsilon}_m + \underline{\varepsilon}_w) + \underline{D}_{\theta t}\underline{\varepsilon}_\theta - \underline{D}_{bt}\underline{\varepsilon}_{m\theta} + \underline{D}_{\psi t}\underline{\varepsilon}_\psi + \underline{D}_{tt}\underline{\varepsilon}_{m\psi} + \underline{D}_{\psi b}\underline{\varepsilon}_{\theta\psi} \tag{5.109}$$

Substituting from the strain equations, section (4.5), into equation (5.103) then,

$$dU_{SL}^{\backslash} = d\underline{\delta}_o^T\,\underline{B}_o^T\,\underline{\sigma}_o + d\underline{\delta}_b^T\,\underline{B}_b^T\,\underline{\sigma}_b + d\underline{\delta}_t^T\,\underline{B}_t^T\,\underline{\sigma}_t + d\underline{\delta}_t^T\,\underline{B}_{bt}^T\,\underline{\sigma}_b \tag{5.110}$$

By integrating equation (5.110) over the midplane then:

$$dU_{SL} = d\underline{\delta}_o^T\,\underline{F}_o^L + d\underline{\delta}_b^T\,\underline{F}_b^L + d\underline{\delta}_t^T\,\underline{F}_t^L + d\underline{\delta}_t^T\,\underline{F}_{bt}^L \tag{5.111}$$

where

$$\underline{F}_o^L = \iint_{element}\underline{B}_o^T\,\underline{\sigma}_o\,dxdy \tag{5.112}$$

$$\underline{F}_b^L = \iint_{element}\underline{B}_b^T\,\underline{\sigma}_b\,dxdy \tag{5.113}$$

$$\underline{F}_{bt}^L = \iint_{element}\underline{B}_{bt}^T\,\underline{\sigma}_b\,dxdy \tag{5.114}$$

$$\underline{F}_t^L = \iint_{element}\underline{B}_t^T\,\underline{\sigma}_t\,dxdy \tag{5.115}$$

Equation (5.111) may also be rewritten as follows:

$$dU_{SL} = d\underline{\delta}^T\,\underline{F}_L \tag{5.116}$$

where $\underline{F}_L$ represents the element force vector due to coupling effect which is defined as follows:

$$\underline{F}_L = \begin{bmatrix} \underline{F}_o^L \\ \underline{F}_b^L \\ \underline{F}_t^L + \underline{F}_{bt}^L \end{bmatrix} \tag{5.117}$$

5.6 ELEMENT MASS MATRIX M

We shall assume that different layers of the element are made of the same composite material but with different fibre orientations, i.e. the density of every layer is the same.

Using D'Alembert's principle, the inertial force vector acting on an infinitesimal volume dxdydz due to acceleration $\vec{a}$ is:

$$d\vec{F} = -\rho \vec{a}\, dx\, dy\, dz \tag{5.118}$$

Hence, the work done by the inertia forces due to an infinitesimal virtual displacement field $\delta\vec{q}$ is:

$$\delta W_a = -\iiint_{volume} \rho\, \delta\vec{q} \,.\, \ddot{\vec{q}}\, dx\, dy\, dz$$

or in matrix form

$$\delta W_a = -\iiint_{volume} \rho\, \delta\underline{q}^T\, \ddot{\underline{q}}\, dx\, dy\, dz \tag{5.119}$$

Substituting from equations (4.45) and (4.47) into equation (5.119), then:

$$\delta W_a = -\iiint \rho\, (\underline{I}_2\, \delta\underline{q}_o + \underline{Z}\, \delta\underline{q}_b + \underline{f}\, \delta\underline{q}_t)^T (\underline{I}_2\, \ddot{\underline{q}}_o + \underline{Z}\, \ddot{\underline{q}}_b + \underline{f}\, \ddot{\underline{q}}_t)\, dxdydz$$

which leads to,

$$\begin{aligned}\delta W_a = -\iiint [\, & \delta\underline{q}_o^T \rho\, \underline{I}_g\, \ddot{\underline{q}}_o + \delta\underline{q}_o^T \rho\, \underline{I}_Z\, \ddot{\underline{q}}_b + \delta\underline{q}_o^T \rho\, \underline{I}_f\, \ddot{\underline{q}}_t + \\ & \delta\underline{q}_b^T \rho\, \underline{Z}_g\, \ddot{\underline{q}}_b + \delta\underline{q}_b^T \rho\, \underline{Z}_l\, \ddot{\underline{q}}_o + \delta\underline{q}_b^T \rho\, \underline{Z}_f\, \ddot{\underline{q}}_t + \\ & \delta\underline{q}_t^T \rho\, \underline{f}_g\, \ddot{\underline{q}}_t + \delta\underline{q}_t^T \rho\, \underline{f}_l\, \ddot{\underline{q}}_o + \delta\underline{q}_t^T \rho\, \underline{f}_Z\, \ddot{\underline{q}}_b\,]\, dxdydz\end{aligned} \tag{5.120}$$

where

$$\underline{I}_g = \underline{I}_2^T \underline{I}_2 = \begin{bmatrix} 1 & 0 \\ 0 & 1 \end{bmatrix} \tag{5.121}$$

$$\underline{Z}_g = \underline{Z}^T \underline{Z} = \begin{bmatrix} 1 & 0 & 0 & 0 \\ 0 & z^2 & 0 & 0 \\ 0 & 0 & z^2 & 0 \\ 0 & 0 & 0 & 0 \end{bmatrix} \tag{5.122}$$

$$\underline{f}_g = \underline{f}^T \underline{f} = \begin{bmatrix} f^2(z) & 0 \\ 0 & f^2(z) \end{bmatrix} \tag{5.123}$$

$$\underline{I}_Z = \underline{Z}_1^T = \underline{I}_2^T \underline{Z} = \begin{bmatrix} 0 & 0 & z & 0 \\ 0 & -z & 0 & 0 \end{bmatrix} \tag{5.124}$$

$$\underline{I}_f = \underline{f}_1^T = \underline{I}_2^T \underline{f} = \begin{bmatrix} 0 & f(z) \\ -f(z) & 0 \end{bmatrix} \tag{5.125}$$

$$\underline{Z}_f = \underline{f}_Z^T = \underline{Z}^T \underline{f} = \begin{bmatrix} 0 & 0 \\ z\,f(z) & 0 \\ 0 & z\,f(z) \\ 0 & 0 \end{bmatrix} \tag{5.126}$$

Integrating equation (5.120) over the thickness, then:

$$\begin{aligned} \delta W_a = -\iint [\, & \delta \underline{q}_o^T \underline{R}_{oo} \ddot{\underline{q}}_o + \delta \underline{q}_o^T \underline{R}_{ob} \ddot{\underline{q}}_b + \delta \underline{q}_o^T \underline{R}_{ot} \ddot{\underline{q}}_t + \\ & \delta \underline{q}_b^T \underline{R}_{bb} \ddot{\underline{q}}_b + \delta \underline{q}_b^T \underline{R}_{bo} \ddot{\underline{q}}_o + \delta \underline{q}_b^T \underline{R}_{bt} \ddot{\underline{q}}_t + \\ & \delta \underline{q}_t^T \underline{R}_{tt} \ddot{\underline{q}}_t + \delta \underline{q}_t^T \underline{R}_{to} \ddot{\underline{q}}_o + \delta \underline{q}_t^T \underline{R}_{tb} \ddot{\underline{q}}_b \,] dxdy \end{aligned} \tag{5.127}$$

where

$$\underline{R}_{oo} = \int_{z_L}^{z_U} \rho \underline{I}_g dz = \sum_{m=1}^{N_l} \int_{z_L^{(m)}}^{z_m^{(m)}} \rho \underline{I}_g dz \tag{5.128}$$

$$\underline{R}_{ob} = \int_{z_L}^{z_U} \rho \underline{I}_Z dz = \sum_{m=1}^{N_l} \int_{z_L^{(m)}}^{z_m^{(m)}} \rho \underline{I}_Z dz \tag{5.129}$$

$$\underline{R}_{ot} = \int_{z_L}^{z_U} \rho \underline{I}_f dz = \sum_{m=1}^{N_l} \int_{z_L^{(m)}}^{z_m^{(m)}} \rho \underline{I}_f dz \tag{5.130}$$

$$\underline{R}_{bb} = \int_{z_L}^{z_U} \rho \underline{Z}_g dz = \sum_{m=1}^{N_l} \int_{z_L^{(m)}}^{z_m^{(m)}} \rho \underline{Z}_g dz \tag{5.131}$$

$$\underline{R}_{bo} = \underline{R}_{ob}^T \tag{5.132}$$

$$\underline{R}_{bt} = \int_{z_L}^{z_U} \rho \underline{Z}_f dz = \sum_{m=1}^{N_l} \int_{z_L^{(m)}}^{z_m^{(m)}} \rho \underline{Z}_f dz \tag{5.133}$$

$$\underline{R}_{tt} = \int_{z_L}^{z_U} \rho \underline{f}_g dz = \sum_{m=1}^{N_l} \int_{z_L^{(m)}}^{z_m^{(m)}} \rho \underline{f}_g dz \tag{5.134}$$

$$\underline{R}_{to} = \underline{R}_{ot}^T \tag{5.135}$$

$$\underline{R}_{tb} = \underline{R}_{bt}^T \tag{5.136}$$

Substituting from equations (4.39), (4.41) and (4.44) into equation (5.127).

$$\begin{aligned}\delta W_a = -\iint [\, & d\underline{\delta}_o^T \underline{N}_o^T \underline{R}_{oo} \underline{N}_o \ddot{\underline{\delta}}_o + d\underline{\delta}_o^T \underline{N}_o^T \underline{R}_{ob} \underline{N}_b \ddot{\underline{\delta}}_b + d\underline{\delta}_o^T \underline{N}_o^T \underline{R}_{ob} \underline{N}_t \ddot{\underline{\delta}}_t + \\ & d\underline{\delta}_o^T \underline{N}_o^T \underline{R}_{ot} \underline{N}_o \ddot{\underline{\delta}}_t + d\underline{\delta}_b^T \underline{N}_b^T \underline{R}_{bb} \underline{N}_b \ddot{\underline{\delta}}_b + d\underline{\delta}_b^T \underline{N}_b^T \underline{R}_{bb} \underline{N}_t \ddot{\underline{\delta}}_t + \\ & d\underline{\delta}_t^T \underline{N}_t^T \underline{R}_{bb} \underline{N}_b \ddot{\underline{\delta}}_b + d\underline{\delta}_t^T \underline{N}_t^T \underline{R}_{bb} \underline{N}_t \ddot{\underline{\delta}}_t + d\underline{\delta}_b^T \underline{N}_b^T \underline{R}_{bo} \underline{N}_o \ddot{\underline{\delta}}_o + \\ & d\underline{\delta}_t^T \underline{N}_t^T \underline{R}_{bo} \underline{N}_o \ddot{\underline{\delta}}_o + d\underline{\delta}_b^T \underline{N}_b^T \underline{R}_{bt} \underline{N}_o \ddot{\underline{\delta}}_t + d\underline{\delta}_t^T \underline{N}_t^T \underline{R}_{bt} \underline{N}_o \ddot{\underline{\delta}}_t + \\ & d\underline{\delta}_t^T \underline{N}_o^T \underline{R}_{tt} \underline{N}_o \ddot{\underline{\delta}}_t + d\underline{\delta}_t^T \underline{N}_o^T \underline{R}_{to} \underline{N}_o \ddot{\underline{\delta}}_o + d\underline{\delta}_t^T \underline{N}_o^T \underline{R}_{tb} \underline{N}_b \ddot{\underline{\delta}}_b + \\ & d\underline{\delta}_t^T \underline{N}_o^T \underline{R}_{tb} \underline{N}_t \ddot{\underline{\delta}}_t \,] dxdy\end{aligned} \tag{5.137}$$

Hence, it can be deduced that

$$\begin{aligned}\delta W_a = -[& d\underline{\delta}_o^T \underline{M}_{oooo} \ddot{\underline{\delta}}_b + d\underline{\delta}_o^T \underline{M}_{oobb} \ddot{\underline{\delta}}_b + d\underline{\delta}_o^T \underline{M}_{oobt} \ddot{\underline{\delta}}_t + d\underline{\delta}_o^T \underline{M}_{oott} \ddot{\underline{\delta}}_t + \\ & d\underline{\delta}_b^T \underline{M}_{bbbb} \ddot{\underline{\delta}}_b + d\underline{\delta}_b^T \underline{M}_{bbbt} \ddot{\underline{\delta}}_t + d\underline{\delta}_t^T \underline{M}_{tbbb} \ddot{\underline{\delta}}_b + d\underline{\delta}_t^T \underline{M}_{tbbt} \ddot{\underline{\delta}}_t + \\ & d\underline{\delta}_b^T \underline{M}_{bboo} \ddot{\underline{\delta}}_o + d\underline{\delta}_t^T \underline{M}_{tboo} \ddot{\underline{\delta}}_o + d\underline{\delta}_b^T \underline{M}_{bbtt} \ddot{\underline{\delta}}_t + d\underline{\delta}_t^T \underline{M}_{tbtt} \ddot{\underline{\delta}}_t + \\ & d\underline{\delta}_t^T \underline{M}_{tttt} \ddot{\underline{\delta}}_t + d\underline{\delta}_t^T \underline{M}_{ttoo} \ddot{\underline{\delta}}_o + d\underline{\delta}_t^T \underline{M}_{ttbb} \ddot{\underline{\delta}}_b + d\underline{\delta}_t^T \underline{M}_{ttbt} \ddot{\underline{\delta}}_t \,]\end{aligned} \tag{5.138}$$

where

$$\underline{M}_{oooo} = \iint_{element} \underline{N}_o^T \underline{R}_{oo} \underline{N}_o dxdy \tag{5.139}$$

$$\underline{M}_{oobb} = \iint_{element} \underline{N}_o^T \underline{R}_{ob} \underline{N}_b dxdy \tag{5.140}$$

$$\underline{M}_{oobt} = \iint_{element} \underline{N}_o^T \underline{R}_{ob} \underline{N}_t dxdy \tag{5.141}$$

$$\underline{M}_{oott} = \iint_{element} \underline{N}_o^T \underline{R}_{ot} \underline{N}_t dxdy \tag{5.142}$$

$$\underline{M}_{bbbb} = \iint_{element} \underline{N}_b^T \underline{R}_{bb} \underline{N}_b dxdy \tag{5.143}$$

$$\underline{M}_{bbbt} = \iint_{element} \underline{N}_b^T \underline{R}_{bb} \underline{N}_t dxdy \tag{5.144}$$

$$\underline{M}_{tbbb} = \iint_{element} \underline{N}_t^T \underline{R}_{bb} \underline{N}_b dxdy \tag{5.145}$$

$$\underline{M}_{tbbt} = \iint_{element} \underline{N}_t^T \underline{R}_{bb} \underline{N}_t dxdy \tag{5.146}$$

$$\underline{M}_{bboo} = \iint_{element} \underline{N}_b^T \underline{R}_{bo} \underline{N}_o dxdy \tag{5.147}$$

$$\underline{M}_{tboo} = \iint_{element} \underline{N}_t^T \underline{R}_{bo} \underline{N}_o dxdy \tag{5.148}$$

$$\underline{M}_{bbtt} = \iint_{element} \underline{N}_b^T \underline{R}_{bt} \underline{N}_o dxdy \tag{5.149}$$

$$\underline{M}_{tbtt} = \iint_{element} \underline{N}_t^T \underline{R}_{bt} \underline{N}_o dxdy \tag{5.150}$$

$$\underline{M}_{tttt} = \iint_{element} \underline{N}_o^T \underline{R}_{tt} \underline{N}_o dxdy \tag{5.151}$$

$$\underline{M}_{ttoo} = \iint_{element} \underline{N}_o^T \underline{R}_{to} \underline{N}_o dxdy \tag{5.152}$$

$$\underline{M}_{ttbb} = \iint_{element} \underline{N}_o^T \underline{R}_{tb} \underline{N}_b dxdy \tag{5.153}$$

$$\underline{M}_{ttbt} = \iint_{element} \underline{N}_o^T \underline{R}_{tb} \underline{N}_t dxdy \tag{5.154}$$

Equation (5.138) may be rewritten as follows:

$$\delta W_a = - d\underline{\delta}^T \underline{M} \ddot{\underline{\delta}} \tag{5.155}$$

where $\underline{M}$ represent the element mass matrix, which is defined as follows:

$$\underline{M} = \left[\begin{array}{c|c|c} \underline{M}_{oooo} & \underline{M}_{oobb} & \underline{M}_{oobt} + \underline{M}_{oott} \\ \hline \underline{M}_{bboo} & \underline{M}_{bbbb} & \underline{M}_{bbbt} + \underline{M}_{bbtt} \\ \hline \underline{M}_{tboo} + \underline{M}_{ttoo} & \underline{M}_{tbbb} + \underline{M}_{ttbb} & \underline{M}_{tbbt} + \underline{M}_{tbtt} + \underline{M}_{tttt} + \underline{M}_{ttbt} \end{array}\right] \tag{5.156}$$

5.7 FINITE ELEMENT ANALYSES

5.7.1 Nonlinear static analysis

An equivalent nodal force vector $\underline{F}$ can be defined such that the work done by the actual applied force due to a virtual displacement field is the same as that done by $\underline{F}$.

$$\text{i.e.} \qquad dW = d\delta^T \underline{F} \tag{5.157}$$

where dW represents the work done by the applied force $\underline{F}$.

Due to the same virtual displacement field, the corresponding change of the strain energy can be deduced from the previous definitions of the strain energies as follows:

$$dU = dU_S + dU_L + dU_{SL} \tag{5.158}$$

where dU_S, dU_L and dU_{SL} are defined by equations (5.44), (5.100) and (5.116), respectively.

Applying the principle of virtual work, then;

$$d\chi = dU - dW = 0 \tag{5.159}$$

Substituting, from equations (5.157) and (5.158) into equation (5.159), then;

$$\left(\underline{K} + \underline{K}^{\sigma}\right)\underline{\delta} + \underline{F}_L = \underline{F} \tag{5.160}$$

which represents the generalized equations of equilibrium. Let $\underline{\delta} + \Delta\underline{\delta}$ represent the exact solution of the equilibrium equation, then

$$\left(\underline{K} + \underline{K}^{\sigma}\right)\Delta\underline{\delta} = \underline{F} - \left(\underline{K} + \underline{K}^{\sigma}\right)\underline{\delta} - \underline{F}_L = \underline{R} \tag{5.161}$$

where the residual nodal force vector $\underline{R}$ can be defined as follows:

$$\underline{R} = \underline{F} - \left(\underline{K} + \underline{K}^{\sigma}\right)\underline{\delta} - \underline{F}_L$$

Equation (5.161) can be solved by means of an iterative algorithm as follows:

(1) First initial value (neglecting non-linear effect)

$$\underline{K}\ \underline{\delta}^0 = \underline{F}$$

(2) Hence, calculate updated values of:

$$\underline{\varepsilon}^0 = \underline{\varepsilon}_S + \underline{\varepsilon}_L \qquad \underline{\sigma}^0 = \underline{\sigma}_S + \underline{\sigma}_L$$

$$\underline{K}_0^\sigma = \underline{K}^\sigma(\underline{\sigma}^0) \qquad \underline{F}_L = \underline{F}_L(\underline{\sigma}^0)$$

all of these value corresponding to $\underline{\delta}^0$

(3) Calculate the residual vector

$$\underline{R} = \underline{F} - \left(\underline{K} + \underline{K}_0^\sigma\right) \underline{\delta}^0 - \underline{F}_L^0$$

(4) Solve equation (5.161) to obtain the incremental displacement:

$$\left(\underline{K} + \underline{K}_0^\sigma\right) \Delta\underline{\delta} = \underline{R}$$

(5) Calculate the new value of

$$\underline{\delta}_{new} = \underline{\delta}_{old} + \Delta\underline{\delta}$$

(6) Calculate the value of the error

$$\text{error} = \frac{\left|\underline{\delta}_{new} - \underline{\delta}_{old}\right|}{\left|\underline{\delta}_{old}\right|}$$

(7) If the error is greater than a certain acceptable value then repeat the procedure from step 2 using $\underline{\delta}_{new}$ instead of $\underline{\delta}_{old}$ until the value of the error reaches the acceptable value.

5.7.2 Stability analysis

In general, only at the critical load large deflection is assumed. Thus, a small deflection analysis can be carried out with a small load representing the distribution of actual load, and has equivalent nodal loading vector $\underline{F}_0$ and $\underline{K}^\sigma$ is proportional to the stress level. Just before instability, the strains can be considered infinitesimal, and instability may occur at $\underline{F} = \lambda\ \underline{F}_0$, where λ denotes the factor on stresses necessary to achieve neutral equilibrium. This means that the matrix $\left(\underline{K} + \lambda\ \underline{K}^\sigma\right)$ is no longer positive definite, i.e. the value of λ can be obtained by solving the eigenvalue problem

$$\underline{K}\ \underline{\delta} = (-\lambda)\ \underline{K}^\sigma\ \underline{\delta} \tag{5.162}$$

5.7.3 Non linear dynamic analysis

Applying an infinitesimal virtual displacement field $dq(x,y,z,t)$ at an instant of time t, then the work done by applied loads F(t) can be expressed as follows:

$$dW_F(t) = d\underline{\delta}^T(t)\ \underline{F}(t)$$

where F(t) represents a nodal loading vector equivalent to actual applied loads.

The work done due to inertia can be expressed as follows:

$$dW_a(t) = -\,d\underline{\delta}^T(t)\ \underline{M}\ \ddot{\underline{\delta}}(t)$$

The work done due to viscous and/or structural damping will be assumed to be represented by the following equation:

$$dW_d(t) = -\,d\underline{\delta}^T(t)\ \underline{C}\ \dot{\underline{\delta}}(t)$$

where $\underline{C}$ represents element damping matrix

The corresponding change in the strain energy

$$dU(t) = d\underline{\delta}^T(t)\ \left(\underline{K} + \underline{K}^\sigma\right)\ \underline{\delta}(t) + d\underline{\delta}^T(t)\ \underline{F}_L(t)$$

Applying the principle of virtual work in equation (5.159) at the instant of time t, then:

$$d\underline{\delta}^T(t)\ \left[\left(\underline{K} + \underline{K}^\sigma\right)\ \underline{\delta}(t) + \underline{F}_L(t) + \underline{M}\ \ddot{\underline{\delta}}(t) + \underline{C}\ \dot{\underline{\delta}}(t) - \underline{F}(t)\right] = 0$$

which leads to the following nonlinear dynamic equations:

$$\underline{M}\ \ddot{\underline{\delta}}(t) + \underline{C}\ \dot{\underline{\delta}}(t) + \left(\underline{K} + \underline{K}^\sigma\right)\ \underline{\delta}(t) + \underline{F}_L(t) = \underline{F}(t) \qquad (5.162)$$

If the damping and the coupling force effects on the natural frequency are negligible, then the previous equation can be reduced to:

$$\underline{M}\ \ddot{\underline{\delta}}(t) + \left(\underline{K} + \underline{K}^\sigma\right)\ \underline{\delta}(t) = \underline{F}(t) \qquad (5.163)$$

Hence, it can be assumed that, at a natural mode of vibration

$$\delta(t) = \hat{\delta}\cos\omega t \qquad (5.164)$$

where $\hat{\delta}$ represents the mode shape vector. Substituting from equation (5.164) into equation (5.163) then,

$$\left[\left(\underline{K} + \underline{K}^\sigma\right) - \omega^2\ \underline{M}\right]\ \hat{\delta} = \underline{0} \qquad (5.165)$$

This matrix equation represents a system of homogeneous simultaneous equations which have a non-trivial solution, if λ satisfies the following condition:

$$\left|\left(\underline{K} + \underline{K}^\sigma\right) - \lambda\ \underline{M}\right| = 0 \qquad (5.166)$$

where λ represent the eigenvalue which is equal to ω^2

6

FATIGUE DAMAGE OF COMPOSITE MATERIALS

6.1 INTRODUCTION

The word "Fatigue" is the normal description of fracture due to repeated stresses. It was introduced in 1850 to describe failures occurring from repeated loads. This phenomenon is defined as the reduction of the strength, stiffness and the subsequent failure of materials subjected to cyclic load. The fatigue process is usually divided into three phases: crack initiation, crack growth and fracture.

Crack initiation usually takes place at surfaces or corners of high stress concentration, if they exist, and where corrosive environment and changes in geometry exist.

The fatigue crack growth phase is governed primarily by several factors, such as the size of the initial crack relative to the structure geometry, the yield strength of the material, the applied load, ... etc. The fatigue crack propagates primarily along a plane normal to the maximum local tensile stress and is controlled by the stress intensity factor at the crack tip.

It is unusual for fatigue cracks to progress gradually across the complete component section. The fracture is the final phase of the fatigue process, which represents a complete failure of a component due to rapid progression of the cracks.

In order to reduce the failure probability, several criteria for fatigue design have been applied successfully, depending on the application.

Safe-life design criterion represents the designing for a finite life. It is used in many industrial applications (e.g. pressure vessels, jet engines, ... etc.). The safe-life design includes a degree of freedom for unexpected factors. The calculations may be based on stress-life relations (S/N diagram), strain-life relations (ε/N diagram) or crack growth relations.

Fail-safe design criterion recognises that fatigue cracks may occur and arrange the structure so that cracks will not lead to failure of the structure before they are detected and repaired. Fail-safe design criterion was developed by aircraft engineers and applied mainly to airframes (wings, control surfaces, ...etc.).

Fatigue of composite materials is more complex and difficult to predict than that of metals. The fatigue processes, which reduce strength in these materials, are generally very complex, involving the accumulation of multiple damage modes that may combine in a variety of ways to produce numerous failure modes. Due to the degradation of the stiffness properties during fatigue life, stresses are continuously redistributed across the composite construction, which is clearly not the case for metals.

For the treatment of the fatigue phenomena, an assessment of the physical mechanisms of failure, which are responsible for the fatigue process in composite materials, has to be carried out. In fact, the fatigue behaviour of composite materials is depending on some parameters, such as the type of the constituent materials, geometry, load and environment. Consequently, the fatigue response can only be determined with the aid of experimental data. The fatigue life for composite materials is still excellent compared to metals. Therefore, composite materials may be useful in many applications (industrial, military, ... etc.).

In this chapter, two types of fatigue damage assessments have been carried out, fatigue damage by initiation and fatigue damage by crack growth. The two assessments are illustrated step by step and described using flowcharts to illustrate the procedures followed in the modelling.

The material degradation rules used with fatigue damage by crack growth are explained based on some assumptions collected from the literature. The failure conditions and the damaged area calculations to achieve the failure strains of the matrix and fibre are also discussed.

Experimental S/N diagrams are used to predict the number of cycles to failure in the fatigue damage by initiation assessment. The energy balance approach has been engaged to study the damage growth model in composites. The energy balance approach is defined by the energy release rate G, where a modified form of Paris law is used for the calculation of the number of cycles to failure with the fatigue damage by crack growth assessment.

6.2 PRELIMINARY ANALYSES OF FATIGUE ASSESSMENTS

Fatigue damage studies are usually based on three major factors: model preparation, stress analysis and failure analysis. Two assessments of fatigue damage have been investigated in the present work: fatigue damage by initiation and fatigue damage growth. Some basic assumptions are adopted in this study.

- As mentioned before in chapter 3, the fatigue damage modes of composite materials are matrix cracking, crack coupling and interface, delamination and fibre breaking. Any one of these damage modes may cause fatigue failure of the material. The failure is generally caused by a combination of two or more of those modes. This work will assume that the failure is caused by matrix cracking only, which has been considered the dominant damage mode for fatigue failure of composite materials.

- The applied fatigue load has a uniform cycle with a frequency f [Hz]

- The opening mode of failure has been considered

- The linear elastic fracture mechanics theory has been applied in fatigue damage growth assessment to predict the fatigue life of the composite materials.

- Stress analysis with geometrical nonlinearity is considered for fatigue damage growth.

6.2.1 Cyclic load definition

The load definition is a very important step as the fatigue process is basically dependent on a cyclic load. This load is usually sinusoidal with constant amplitude and frequency.

The fatigue load is represented by two factors, a constant load vector $\underline{F}$ and a load ratio α. Figure (6.1) shows the variation of load ratio α with respect to time t. The actual value of load vector at any time t can be defined as follows:

$$\underline{F}(t) = \alpha(t)\ \hat{\underline{F}} \tag{6.1}$$

The maximum and minimum loads can be defined as follows:

$$\underline{F}_{max} = \alpha_{max} \hat{\underline{F}} \tag{6.2}$$

$$\underline{F}_{min} = \alpha_{min} \hat{\underline{F}} \tag{6.3}$$

The two common stress ratios R and A can be defined as follows:

$$R = \frac{\alpha_{min}}{\alpha_{max}} \tag{6.4}$$

$$A = \frac{\alpha_a}{\alpha_m} \tag{6.5}$$

where α_a , α_m are the alternating and mean load ratios, respectively.

$$\alpha_a = \frac{\alpha_{max} - \alpha_{min}}{2} \tag{6.6}$$

$$\alpha_m = \frac{\alpha_{max} + \alpha_{min}}{2} \tag{6.7}$$

6.2.2 Stress analysis

Stress analysis is considered a basic step for any fatigue study. The finite element method will be used to analyse the stresses in composite laminates with consideration of geometric nonlinearly and based on high order shear theory. The finite element theory is explained in detail earlier in chapter 4 and 5. For achieving higher accuracy, a fine mesh has to be used at the critical areas, which have a stress concentration.

The failure analysis is performed based on the stress and strain values in longitudinal (fibre direction) and transverse (matrix direction) directions of the composite. For this purposes, all the stress and strain values are calculated with respect to the local axes and transformed to the material axes by a proper way.

6.3 FATIGUE DAMAGE BY INITIATION OF COMPOSITE MATERIALS

The initiation of a crack does not mean a complete failure of a structure but it gives an indication of the start of the fatigue process that leads to complete failure. The fatigue initiation does not lead to complete failure of a structure before it is detected and repaired. Special components in some industrial applications have to be repaired or replaced when fatigue crack initiation is detected, especially in aerospace applications.

The fail-safe fatigue design criterion is a suitable design criterion in such situations to protect the components by using suitable means, such as multiple load path, strengthening of the components, crack stoppers, ... etc.

An assessment of fatigue damage by initiation is studied in this work to simulate the fatigue behaviour of unidirectional composite laminates under cyclic load conditions and to predict the fatigue life of these laminates under this type of load.

This study is carried out to establish a technique to use experimental data from unidirectional ply under uniaxial cyclic load to simulate the fatigue behaviour of laminates, which have the same constituents of that ply. On the other hand, this technique can give an early warning on the initiation of the fatigue damage and to estimate the number of cycles needed for the crack to start or grow in general applications under general load conditions.

Fig. (6.2) shows a flowchart that describes the strategy followed to develop the fatigue model so as to achieve such requirements.

6.3.1 Fatigue analysis

The fatigue analysis will be based upon experimental data in fibre and matrix materials of the composite and the fatigue theory of metals. The experimental data needed for this model are the stress-life S/N curves for fibre and matrix materials. The S/N curve is usually a curve between the alternating stress σ_a and the number of cycles to failure N. The measurement process is repeated several times at each level of stress to obtain a more accurate S/N diagram based on average value.

However, if the specimen does not fail, the applied load creates a stress under the endurance limit of the fibre and matrix of the composite laminate. The endurance limit of the fibre (matrix) is the highest stress, which the fibre (matrix) could withstand for an infinite number of load cycles without failure. The endurance limit of composite materials has enormous range depending on several factors, such as constitution of the material, size of the specimen, type of load, … etc.

6.3.2 The fatigue damage by initiation assessment in steps

Consider that it is required to investigate the fatigue behaviour of a composite laminate under general applied cyclic load. Since no actual cracks are assumed, linear stress analysis can be considered for this type of fatigue damage.

Step 1: preparations and basic assumptions

The fatigue load is applied uniformly with frequency f [Hz]. The maximum and minimum load ratios α_{max} and α_{min} are defined to represent the maximum and minimum load, respectively, as shown in Fig. (6.1).

The load is represented by the load vector $\underline{F}$ and the load ratio α where the actual value at any time is defined by equation (6.1).

Step 2: stress analysis using finite element method

Finite element method is used to analyse and evaluate the stresses and strains at any node (i) with respect to local coordinate system. A suitable transformation process is used to transfer the stresses $\underline{\sigma}_i$ and strains $\underline{\varepsilon}_i$ to the material coordinate system in the fibre and matrix directions. The actual stress value at any time and at any node (i) can be defined similar to the force vector in equation (6.1) as follows:

$$\underline{\sigma}_i(t) = \alpha(t)\ \underline{\sigma}_i \tag{6.8}$$

The maximum and minimum stresses can be defined similar to the load in equations (6.2) and (6.3) as follows:

$$\underline{\sigma}_{max})_i = \alpha_{max} \ \underline{\sigma}_i \tag{6.9}$$

$$\underline{\sigma}_{min})_i = \alpha_{min} \ \underline{\sigma}_i \tag{6.10}$$

Using the alternating and mean load ratios in equations (6.6) and (6.7) the alternating and mean stresses at node (i) can be represented as follows:

$$\underline{\sigma}_a)_i = \alpha_a \ \underline{\sigma}_i \tag{6.11}$$

$$\underline{\sigma}_m)_i = \alpha_m \ \underline{\sigma}_i \tag{6.12}$$

Hence, the critical values of alternating $\underline{\sigma}_a)_{cr}$ and mean $\underline{\sigma}_m)_{cr}$ stress can be obtained at critical node points.

Step 3: Stress checking

Before the fatigue analysis takes place, stress checking has to be completed. The stress checking is to ensure that the stress values occur between the endurance and ultimate stress limits of the material and satisfy the following condition:

$$\sigma_u < (\sigma_a)_{cr} < \sigma_e \tag{6.13}$$

where

σ_u is the ultimate stress of the material

σ_e is the endurance limit.

Step 4: Fatigue analysis

As a first approximation, Goodman relationship, which is an empirical relationship between the applied stress and the fatigue stress, (Fuchs & Stephens, 1980), is employed and can be defined as follows:

$$\frac{\sigma_a}{\sigma_N} + \frac{\sigma_m}{\sigma_u} = 1 \tag{6.14}$$

where σ_a, σ_m are the alternating and mean stresses, respectively, σ_N is the fatigue stress which corresponding to the number of cycles to failure, and σ_u is the ultimate stress of the material. For more accurate analysis, specific S/N diagrams have to be measured at different mean stress levels.

Applying equation (6.14) in the fibre and matrix directions separately for the failed elements as follows:

$$\frac{(\sigma_{a,f})_{cr}}{\sigma_{Nf}} + \frac{(\sigma_{m,f})_{cr}}{\sigma_{uf}} = 1 \tag{6.15}$$

$$\frac{(\sigma_{a,m})_{cr}}{\sigma_{Nm}} + \frac{(\sigma_{m,m})_{cr}}{\sigma_{um}} = 1 \tag{6.16}$$

The parameters of the previous equations are defined as the parameters of equation (6.14) where the subscripts f and m mean fibre and matrix, respectively.

The fatigue stresses of the fibre σ_{Nf} and matrix σ_{Nm} can be obtained by applying equations (6.15) and (6.16), respectively. The corresponding number of cycles to fatigue of fibre N_f and matrix N_m can be obtained by using S/N diagram for fibre and matrix. The final number of cycles to fatigue of the composite laminate is the minimum value of the number of cycles to failure for fibre N_f and matrix N_m. A detailed case study will be discussed later in chapter 8 to illustrate the previous steps in numbers.

It is expected that the failure is caused by matrix cracking mode, which is considered the dominant damage mode for fatigue failure of composite materials, i.e. $N_m < N_f$.

6.4 FATIGUE DAMAGE GROWTH OF COMPOSITE MATERIALS

The fatigue damage behaviour in composites is quite difficult to assess and it is usually caused by more than one mode of failure. Consequently, the energy balance approach is used to analyse the fatigue damage growth in composites. A modified form of Paris law which relates the damage area, fatigue load and energy release rate is used.

Procedures and methods for the fatigue damage by crack growth assessment are illustrated by the flowchart of Figure (6.3). The main objects in that assessment are the material degradation method and the fracture analysis, which will be discussed in detail later.

6.4.1 Failure analysis

As mentioned in the literature, many analyses have been developed to predict the failure of composite laminates. Due to some complexities and restrictions of those types of analyses, a simple technique is used in this work to predict the failure of composite laminates. This technique is based on ultimate strain values of the laminate in fibre and matrix direction, which is quite similar to the maximum strain theory, (Reddy and Reddy, 1992).

The ultimate strain values of the fibre ε_{uf} and matrix ε_{um} can be obtained experimentally by applying the maximum possible load on a unidirectional ply with [0°], on-axes, and [90°], off-axes, respectively, as shown in Fig. (6.4), and measuring the corresponding strain values.

The failure analysis is performed based on some assumptions:

- A complete failure will occur when the strain value in the fibre direction at any element ε_f reaches the ultimate strain value of the fibre ε_{uf}.

$$\varepsilon_f \geq \varepsilon_{uf} \qquad \text{(Complete failure)} \qquad (6.17)$$

- While the strain value in the matrix direction ε_m reaches its ultimate value (ultimate strain of the matrix ε_{um}), this implies that matrix cracking has occurred and crack growth will develop.

$$\varepsilon_{um1} \leq \varepsilon_m \leq \varepsilon_{um2} \qquad \text{(Fatigue initiation)} \tag{6.18}$$

where ε_{um1} and ε_{um2} represent the range of the ultimate strain of the matrix during which the degradation process will take place, with ε_{um1} being the threshold value of degradation to start, and ε_{um2} is the value beyond which the degradation process reaches its ultimate.

6.4.2 Material degradation

Material degradation is the reduction of the material properties of the structure due to certain type of applied load. The material degradation rules of composite materials are mainly based on experimental data. Due to the difficulty of measurement process and the time consumed in the experimental work, some investigators tried to introduce a theoretical solution to this problem based on some assumptions as shown earlier in the literature review. Most of those investigators paid attention to cross ply composite laminates which have a special geometry $[0^o/90^o]_{ns}$ or $[90^o/0^o]_{ns}$. The governing assumption in those investigations is the mode of failure which may be fibre breakage, fibre and matrix shear, … etc.

For a laminated composite under fatigue loading conditions, in the first cycles, the strength of the plies can be higher than the stress state. Therefore, during the first cycles, there is no failure mode that can be detected. Once the number of cycles increases and the failure takes place in the material, the material properties at the damaged area have to be degraded by a set of degradation rules and based on some factors, such as the mode of failure, the original properties, the stress-strain state, the strength of the material, …etc. That type of degradation is called gradual material properties degradation.

The reduction of the maximum modulus of elasticity (longitudinal modulus in the fibre direction) depends on laminate structure and material properties. Laminates whose axial stiffness is dominated by many 0^o plies show a small modulus reduction. As the number of 90^o plies increase, the laminate modulus reduction increases where those plies play a greater role in the laminate stiffness.

As the density of damaged area increases, the stiffness of the laminate decreases. At saturation damaged area density, the total properties decrease as much as 50% for the longitudinal modulus and 25% for the shear modulus, as related by Hashin (1985). The degradation process for the matrix mode of failure is based on several reduction factors for longitudinal Young's modulus E_1, transverse Young's modulus E_2 and in-plane modulus of rigidity G_{12}, as mentioned by Daniel and Ishai (1994).

As soon as the failure condition of the matrix, which is represented by equation (6.18), has been satisfied with in the laminate, the degradation process of the material properties have to take place. Consequently, the damaged area will be increased up to a critical value which is the damaged area of the laminate corresponding to the failure condition of the fibre, equation (6.17).

Based on the literature, some assumptions are taken into consideration during the material degradation process, (Hashin, 1985):

- The material properties are gradually degraded.
- The minimum value of the modulus reduction factor of the matrix will be 25%.
- The minimum value of the modulus reduction factor of the fibre will be 50%.

Hence, the damaged area will be replaced with one having the following properties

$$\begin{aligned} (E_1)_{new} &= (E_1)_{old} \bullet Rf \\ (E_2)_{new} &= (E_2)_{old} \bullet Rm \\ (G_{12})_{new} &= (G_{12})_{old} \bullet Rm \\ (\nu_{12})_{new} &= (\nu_{12})_{old} \bullet Rf \end{aligned} \tag{6.19}$$

where Rf , Rm represent the material reduction factors. Based on the previous assumptions and some experimental data, they can be approximated as follows:

$$Rf = Rf_{min} + (1 - Rf_{min})\left(1 - \frac{\varepsilon_f}{\varepsilon_{uf}}\right) \tag{6.20}$$

$$Rm = Rm_{min} + (1 - Rm_{min})\left(\frac{\varepsilon_{um2} - \varepsilon_m}{\varepsilon_{um2} - \varepsilon_{um1}}\right) \tag{6.21}$$

where Rf_{min}, Rm_{min} represent the minimum values of the modulus reduction factor of the fibre and matrix. The maximum values of the modulus reduction factor at the start of the applied stress will be unity as there is no damaged area at this stage.

6.4.3 Fracture analysis

Fracture analysis will be applied to model the fatigue damage growth in composite materials, where the prediction of the remaining life of composites requires the estimation of the redistribution of stresses caused by the introduction of damage in conjunction with the damage growth conditions.

From the conclusions of the literature review in fatigue damage field, it seems that many authors have investigated the response of composite laminates under fatigue load. Those investigations have been restricted by some assumptions, some of which have been taken into our consideration. Ogin et al. (1985), Boniface and Ogin (1989), and Mark et al. (1991) others assumed that the matrix cracking is the dominant mode of failure and they used fracture mechanics theory to investigate the fatigue crack growth in composite materials.

As discussed earlier in chapter 3, one of the most widely used fatigue crack growth laws is that proposed by Paris and Erdogan (1963) and it is usually known by Paris law, (Gdoutos, 1993).

$$\frac{da}{dN} = C\ (\Delta K)^m \tag{6.22}$$

where da/dN is the crack growth rate, ΔK is the stress intensity factor range, and C and m are material constants determined experimentally.

For many cases, the stress intensity factor is an unattractive parameter to use for modelling the damage growth in composite materials. Damage in composite materials results from more than one mode of failure, for which it is difficult to estimate or detect the shape or the behaviour of the damaged area and derive stress intensity factor. Consequently, the energy balance approach has been engaged to study the damage growth model in composites. The energy balance approach is defined by the energy release rate G.

Feng et al. (1997) used the strain energy release rate derived by Nairn and Hu (1994) to formulate matrix microcracks in cross-ply laminates. That study has concentrated on microcracking in 90^{o} plies and reviewed microcrack in $[0/90]_s$ and $[\ 90/0]_s$ laminates. The main problem of that model it is limited only to the cross-ply laminates.

On the other hand, the energy release rate can be evaluated with a simple computational scheme, which makes it a potentially useful tool for studying damage growth in composite materials. The energy release rate is physically defined as the rate of change of energy of the system per damaged area and it can be defied as follows, (Ewalds and Wanhill, 1986):

$$G = \frac{d}{dA}(W - U) \tag{6.23}$$

where W is work done by external force, U is internal strain energy and A is damaged area.

Hence, The damage growth equation (6.18) can be modified as follows: (Feng et al., 1997)

$$\frac{dA}{dN} = D\ (\Delta G)^{n} \tag{6.24}$$

where dA/dN is the damage area growth rate, ΔG is the energy release rate range, and D and n are material constants determined experimentally.

6.4.4 Algorithm of fatigue damage growth in composite laminates

Consider that it is required to investigate the fatigue damage growth behaviour of a composite laminate under cyclic load, assuming that the laminate has stress concentration zones.

Step 1: preparations and basic assumptions

The same preparations of the fatigue damage by initiation assessment can be carried at this stage. The material constants D and n, in equation (6.24), are to be obtained based on experimental work such as that of Gilchrist (1996) and Feng et al. (1997).

Step 2: stress analysis using finite element method

The finite element method is employed to evaluate the stresses and strains for each element with respect to the fibre and matrix directions at the maximum applied load. Stress analysis with nonlinear geometry should be considered since finite strains may be encountered.

Step 3: failure analysis

Apply equation (6.17) to check first the complete failure state. If $\varepsilon_f \geq \varepsilon_{uf}$, complete failure occur and go to step 6, otherwise apply equation (6.18) to check the damage progress in the matrix. If the strain values (ε_m) at all elements are less than the threshold value ε_{uml}, then there is no damage progress, and fatigue damage should have been checked by means of the crack initiation approach. Otherwise, if $\varepsilon_m \geq \varepsilon_{uml}$, there is damage progress in the matrix, and go to next step.

Step 4: fracture analysis

For the case when $\varepsilon_f < \varepsilon_{uf}$ and $\varepsilon_m \geq \varepsilon_{uml}$, then matrix cracking occurs and will progress with the number of cycles due to material degradation. The damaged area A can be determined as the area of the elements which have $\varepsilon_m \geq \varepsilon_{uml}$. The corresponding energies of equation (6.23) can be calculated for the whole structure. Note also that:

$$W = \underline{\delta}^T \underline{F}$$

$$U = U_S + U_L + U_{SL}$$

which can be calculated from equations given in chapter 5.

Step 5: material degradation

As soon as the failure condition of the matrix is satisfied, the material properties of the damaged area will be replaced with the material properties estimated according to equation (6.19). Then, repeat stress analysis at step 2 using the new material properties.

Step 6: fracture analysis

When complete failure is reached, with the final damaged area A_f, this step is employed to determine the number of cycles to failure.

(i) The results of the previous steps may be tabulated for U_i, W_i, A_i where A_i here is the actual damaged area employed during the stress analysis leading to U_i and W_i, i.e. at $i = 1$, $A_1 = 0$.

(ii) Apply a simple finite difference approach to find the energy release rate from equation (6.23), i.e.

$$G_{i+\frac{1}{2}} = \frac{(W_{i+1} - U_{i+1}) - (W_i - U_i)}{A_{i+1} - A_i}$$

$$A_{i+\frac{1}{2}} = \frac{(A_{i+1} - A_i)}{2}.$$

An alternative approach is to plot W-U versus A, and obtain G at any A from the actual derivative of W-U versus A curve.

(iii) Use equation (6.24) to calculate the values of dA/dN at different values of A.

(iv) The values of dA/dN versus A represent a relationship between dA/dN and A, or dN/dA versus A. Hence, curve fitting is to be employed to find dN/dA as an algebraic polynomial of A.

(v) Integrating the fitted equation of dN/dA with respect to A from A_1=0, to A_{max}=A_f leads to the number of cycles to failure, i.e. $N_f = \int_0^{A_f} \left(\frac{dN}{dA} \right) dA$.

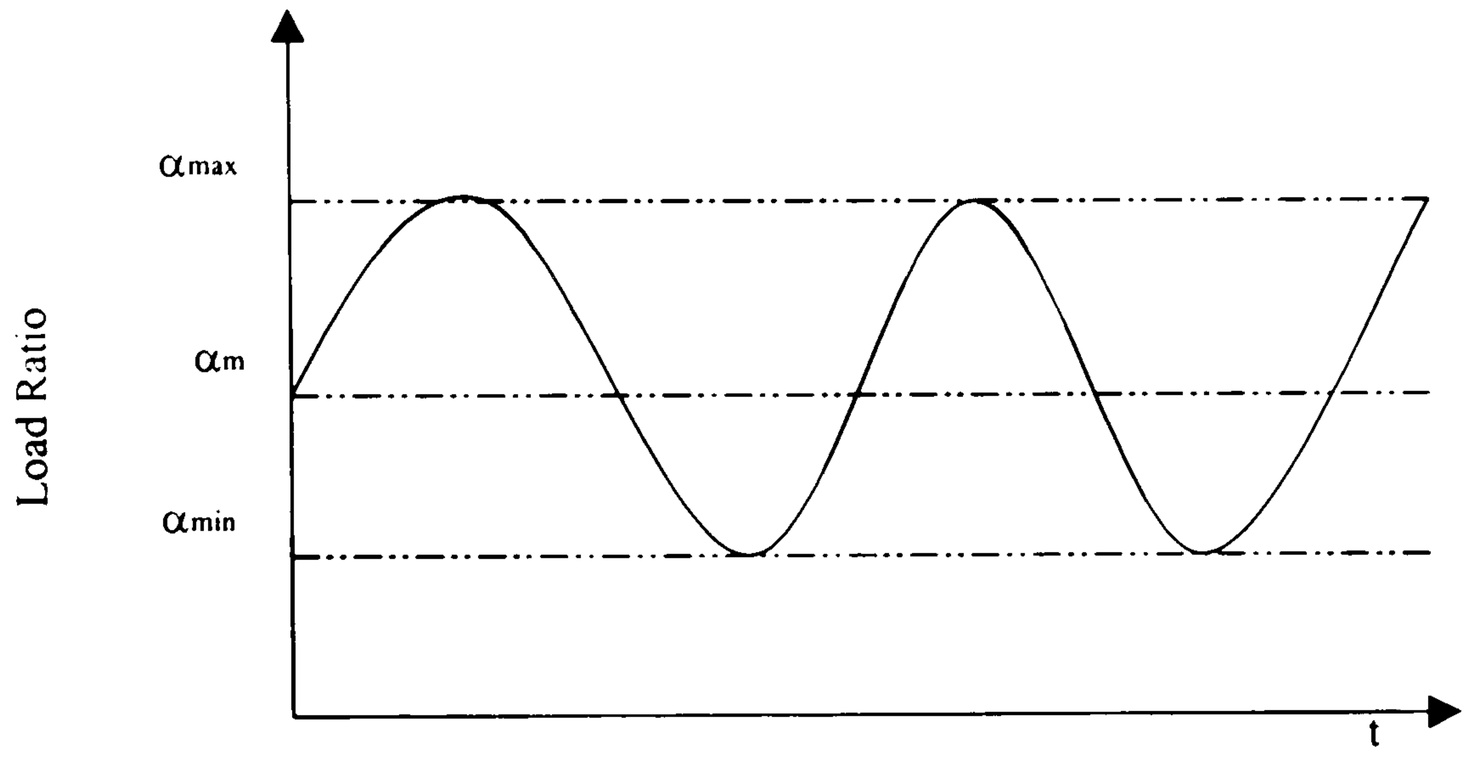

Figure (6.1) Load ratio versus time

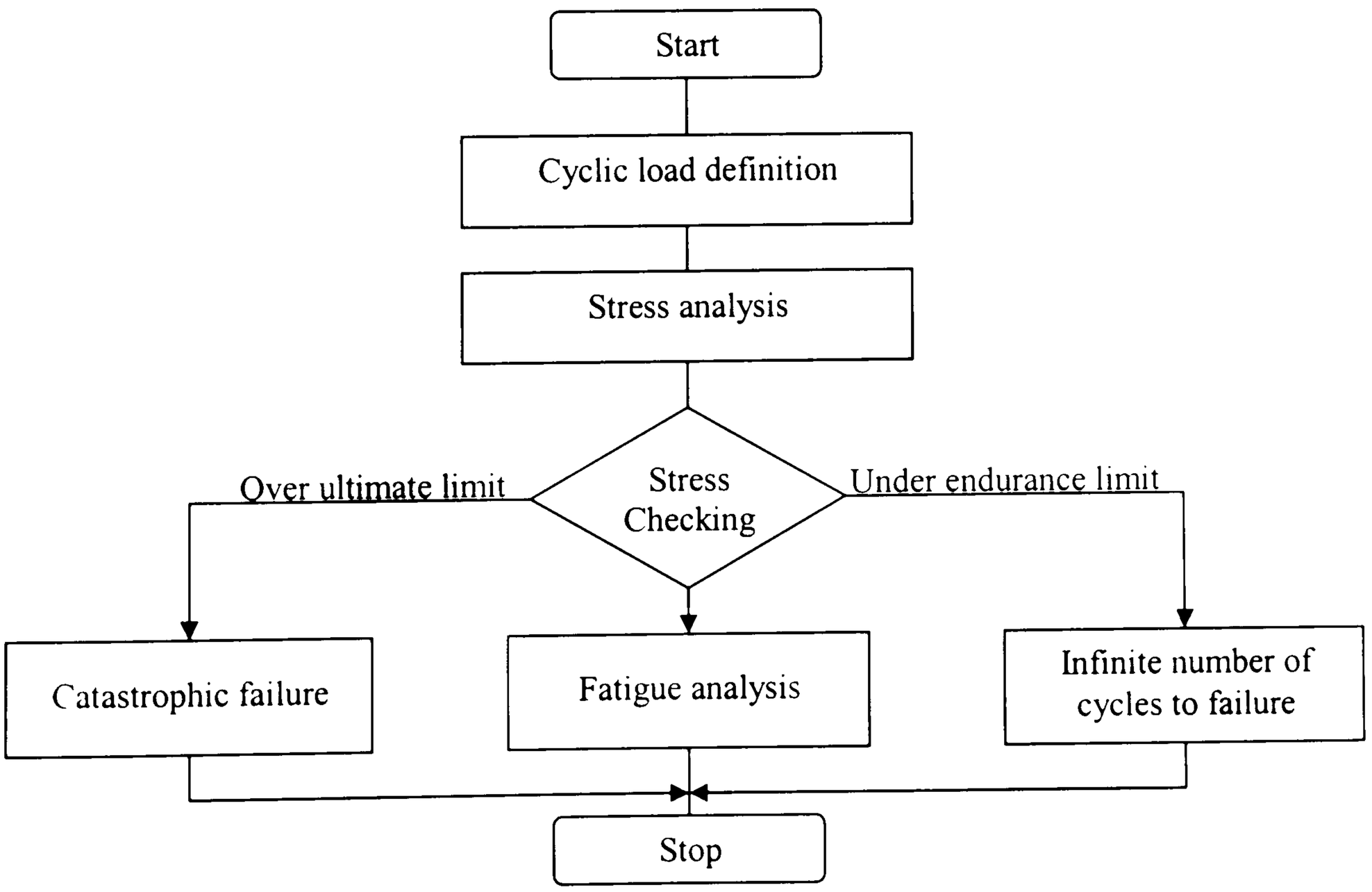

Figure (6.2) Flowchart of the fatigue damage by initiation assessment

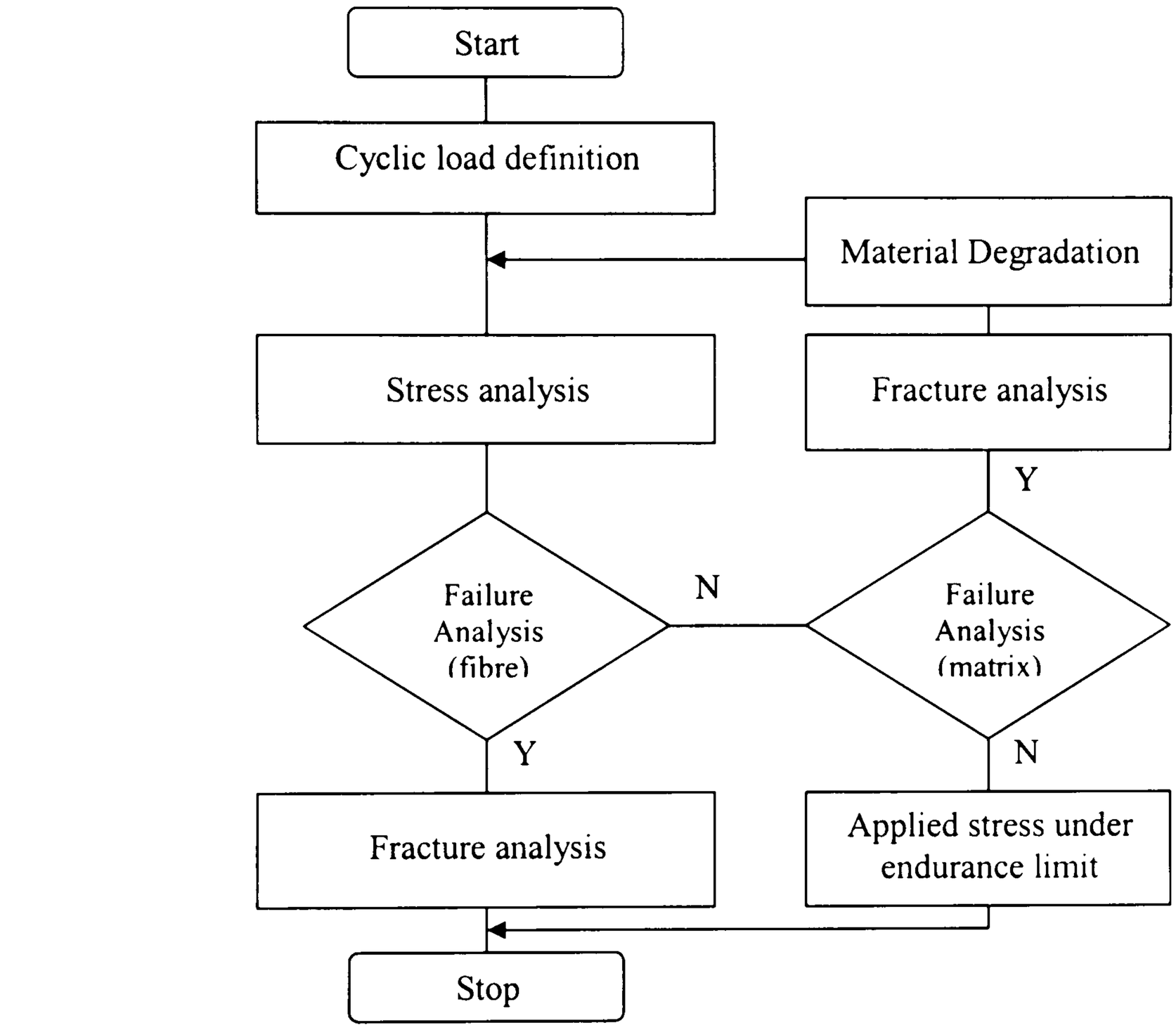

Figure (6.3) Flowchart of the fatigue damage growth assessment

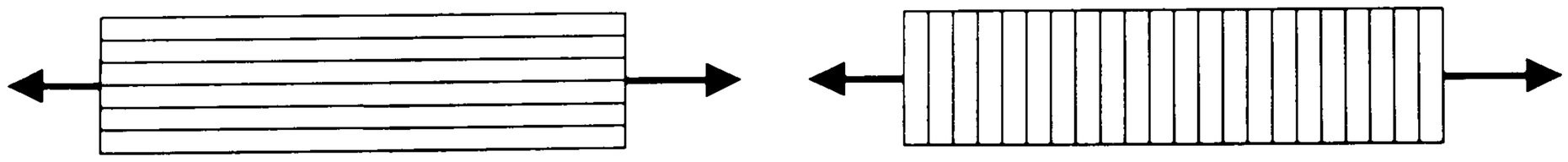

Fibre direction [0°] Matrix direction [90°]

Figure (6.4) Unidirectional ply under uniaxial tension load

7

FINITE ELEMENT COMPUTER PACKAGE

7.1 INTRODUCTION

A computer package was developed based on the finite element theory presented earlier in chapter 5 to carry out some analyses based on that theory. The package which is discussed in this work can be used to analyse shell or plate stress analysis applications, which may be linear or geometrically nonlinear.

The main types of analysis which are carried out in this package are static analysis (linear and nonlinear), dynamic analysis (eigenproblem), stability analysis (buckling) and fatigue damage analysis (damage by initiation or by damage growth).

The package was coded in Fortran 90 by means of Digital Visual FORTRAN V.6 under Microsoft Windows, and Salford Compiler under DOS.

7.2 PACKAGE STRUCTURE

The package was built as separate modules which give the flexibility to join any part of the package to another without changing the main structure of the package. Figure (7.1) illustrates the structure of the finite element package. As shown in the figure, the package has several options such as, type of application (plate or shell), type of element (first order Mindlin element or high-order shear deformation element), type of solver (ordinary, bandwidth or frontal), type of analysis (static, dynamic or fatigue) and type of dynamic and stability solver (simple iteration, standard Jacobi, general Jacobi or Householder method). In any finite element package there are two basic parts: data module and solution module

7.2.1 Data module

The main module in the package is the data module which is separated into three basic parts:

(i) The finite element problem description

This part is introduced to give information about the finite element problem such as, number of nodes and elements, load description (concentrated load or distributed load), boundary conditions and material properties.

(ii) Mathematical tools and axes definition

The numerical integration method used with the element matrices is Gauss integration method. The main function of this part from the data module is to provide the package with the number of Gauss quadrature points required for different integration processes.

In this package, three different new ways are used to define the local axes of each element. The first one is the definition by the element topology array. The second is defined by three points on each element. The last one is defined by three points on each set of elements which has the same definition of the local axes.

(iii) Type of analysis and output requirements

In this part, the type of analysis and the output form are identified. The output information is introduced through a set of nodes and elements at which the output is required. Several types of analyses are provided as shown in figure (7.1).

7.2.2 Solution module

The solution of the finite element problems considers the second step after the description of the data. In many existing commercial packages the user does not have any control on the type of solver, which is considered in most cases time and money consuming.

Several solver modes should be available to the user in the package to choose the suitable one for his problem. For this reason it is desirable to have a package which has different types of solvers. The proposed solvers in the package are mainly used to solve a set of linear equations and to solve the eigenproblem. The choice of the proper solver is based on some factors such as, the user experience, type of the problem, CPU time, computer limitation, ...etc. Three different solver modules have been used in this work to solve a set of linear equations:

(i) Ordinary solver

The ordinary solver is a popular direct method which is easy to understand. The ordinary solver is mainly based on the Gauss elimination method. The main

disadvantage of this method is the large CPU time and computer memory required, as it deals with full matrices.

(ii) Bandwidth solver

The bandwidth solver is used when the nodes are properly labeled. This method can lead to some reduction in the CPU time and computer memory because it deals with banded matrices.

(iii) Frontal solver

The frontal solver is used when the elements are properly labeled. The difficulty and complexity of this method is considered its main disadvantage, but it leads to a big reduction in the CPU time and computer memory.

In the natural frequency and stability problems, the subspace iteration method is used with one of the eigenproblem solvers because it deals with eigenproblems of large order. Four different eigenproblem solver modules have been used in this work, (Bathe and Edward, 1976):

(a) Simple iteration method

It can be employed for determining an eigenvalue which converges to its minimum value.

(b) Standard Jacobi method

It has been developed for the solution of standard eigenproblem (i.e. identity mass matrix). The standard Jacobi method is simple and stable and it can be used to calculate negative, zero or positive eigenvalues.

(c) General Jacobi method

The general Jacobi method has the same features of the standard Jacobi method but with a complete form of the eigenproblem.

(d) Householder QR iteration method

This method is restricted to the solution of the standard form like the standard Jacobi method. A basic difference to the Jacobi method is therefore that the matrix is first transformed without iteration into a tridiagonal form. This matrix can then be used effectively in the QR iterative solution, in which all eigenvalues are calculated. Finally, using inverse iteration the required eigenvectors of the tridiagonal matrix are calculated and transformed to obtain the eigenvectors.

7.3 STATIC ANALYSIS

Static analysis is basically carried out with all different types of analysis. It is coded within the package with several options based on the finite element problem such as, type of analysis (linear or nonlinear), the applied load (total load value or force increments by increasing load step by step) and type of solver (ordinary, bandwidth or frontal).

Figure (7.2) shows the main flowchart of the static analysis. The first step in this analysis is to generate the finite element stiffness matrix which is represented earlier by equation (5.46). For the nonlinear option, the finite element stress stiffness matrix and the finite element force due to nonlinear effect which are represented earlier by equations (5.101) and (5.117), respectively. The convergence check is carried out by the algorithm which has been introduced earlier in section 5.7.1

7.4 STABILITY AND NATURAL FREQUENCY ANALYSES

The stability and dynamic program modules are carried out to solve the eigenproblems which are represented earlier in chapter 5 by equations (5.161) and (5.166), respectively. Figure (7.3) illustrates the stability and natural frequency analyses structure.

The finite element stiffness matrices are firstly generated in the two types of analyses. The next step in the stability module is the generation of the finite element stress stiffness matrices by evaluating the stress state at Gauss quadrature points within each element. With respect to the dynamic module, the finite element mass matrices are generated.

The solution procedures are carried out by choosing the proper eigenproblem solver depending on the finite element problem as mentioned earlier.

7.5 FATIGUE DAMAGE BY INITIATION ANALYSIS

Fatigue damage by initiation program is represented by the structure as shown in Figure (7.4). Two data files are introduced in this module, one for the finite element description and the other one to provide the program by the fatigue stress life curves, S/N diagrams.

The maximum stress values at Gauss quadrature points are calculated within each element for linear and nonlinear static analysis based on the finite element problem. The stresses are represented with respect to the material axes.

The elements which have maximum stress in fibre and matrix direction are identified through the stress checking. The fatigue damage analysis is carried out on the damaged elements in fibre and matrix by comparing the stresses with the S/N data.

7.6 FATIGUE DAMAGE BY CRACK GROWTH ANALYSIS

The studying of the fatigue damage growth in composite laminates under cyclic load is considered one of the main objectives of this work. The fatigue damage growth program is represented within the package through the flowchart in Figure (7.5). As shown in the flowchart, the material is updated after reading of the finite element data and after the feedback from the stress analysis by certain ratios. The degradation ratios are calculated with respect to the strain value at the damaged area while their values are equal to unity at the first run.

The finite element static analysis (linear or nonlinear) is carried out to calculate the strain state in the fibre and matrix direction. The damage check is performed on the fibre and matrix to identify the damaged area and to apply the material degradation rules discussed in chapter 6. At each step the number of cycle to failure is calculated based on the fatigue damage growth relations as mentioned in chapter 6.

The previous steps will be automatically repeated until the complete failure of the structure occurs by failure of the first fibre in the laminate.

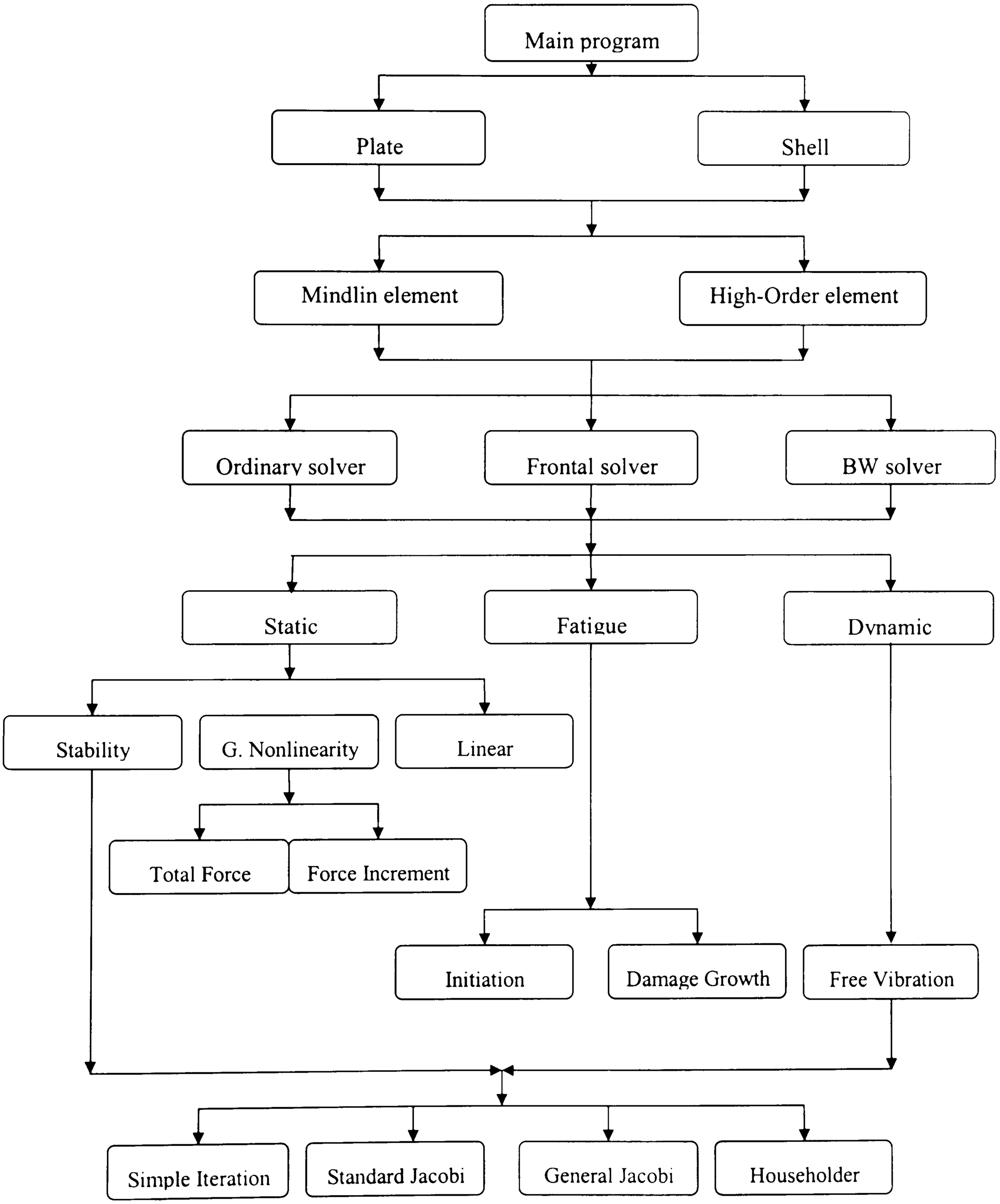

Figure (7.1) Package structure

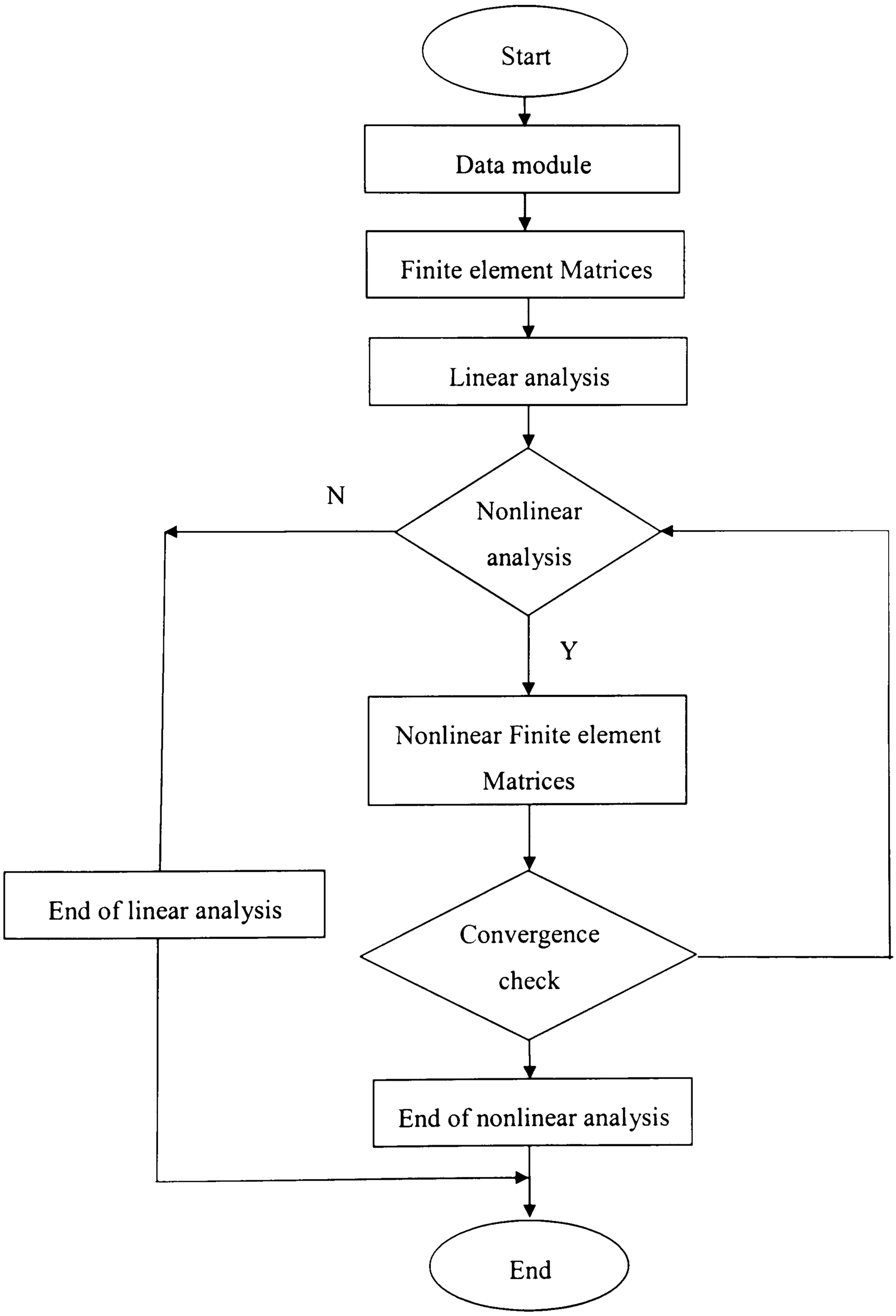

Figure (7.2) Static analysis structure

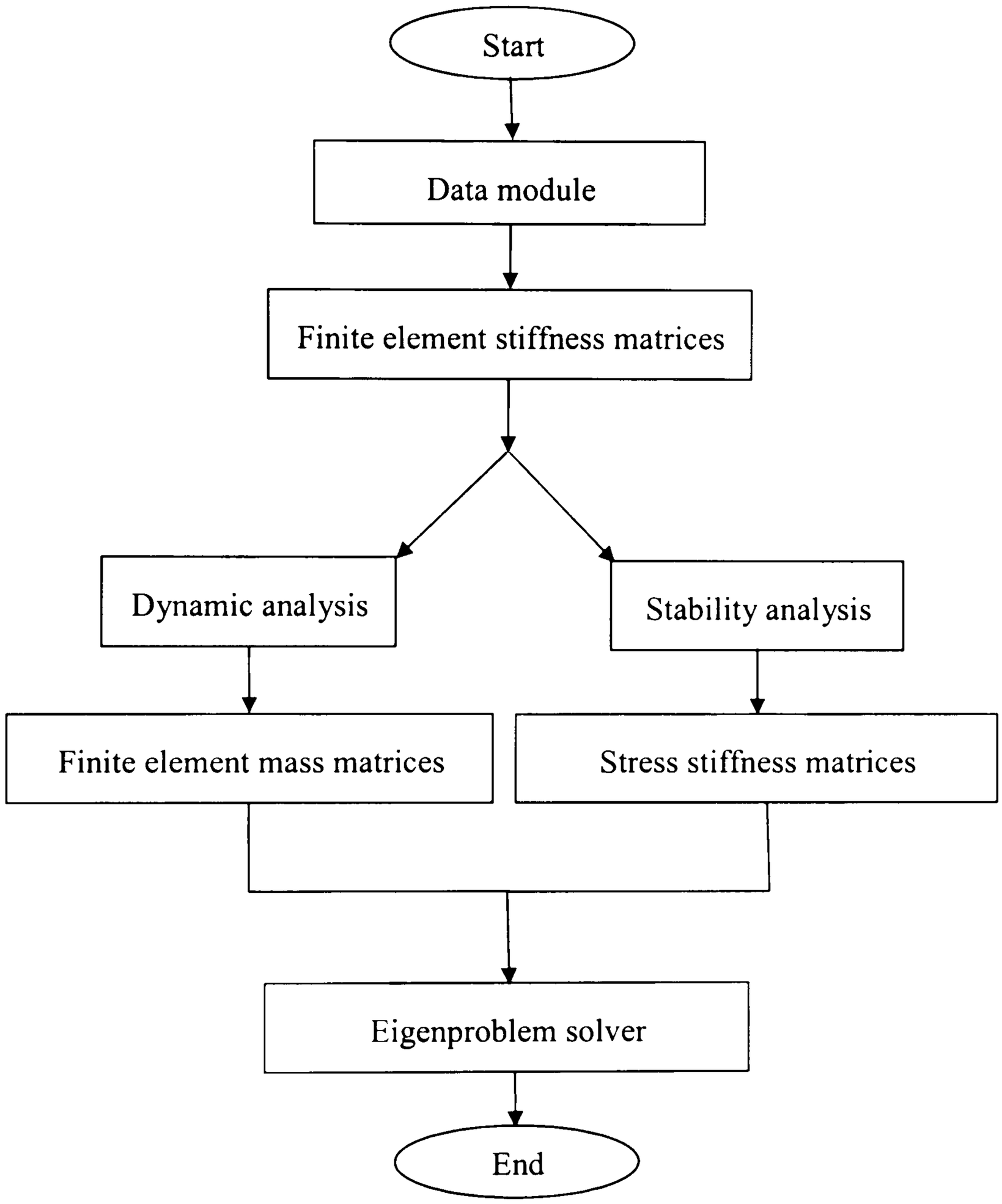

Figure (7.3) Dynamic and stability structure

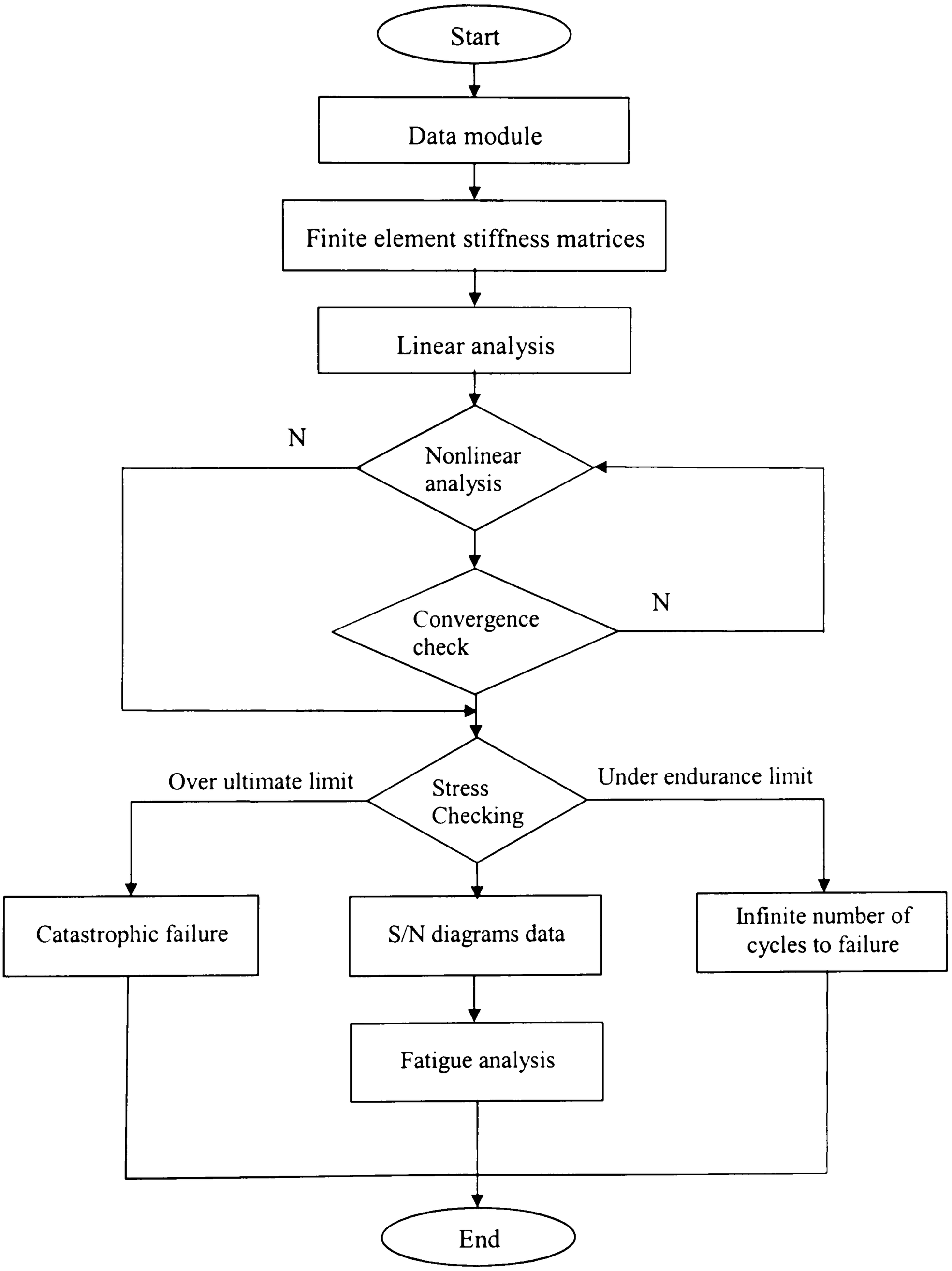

Figure (7.4) Fatigue damage by initiation structure

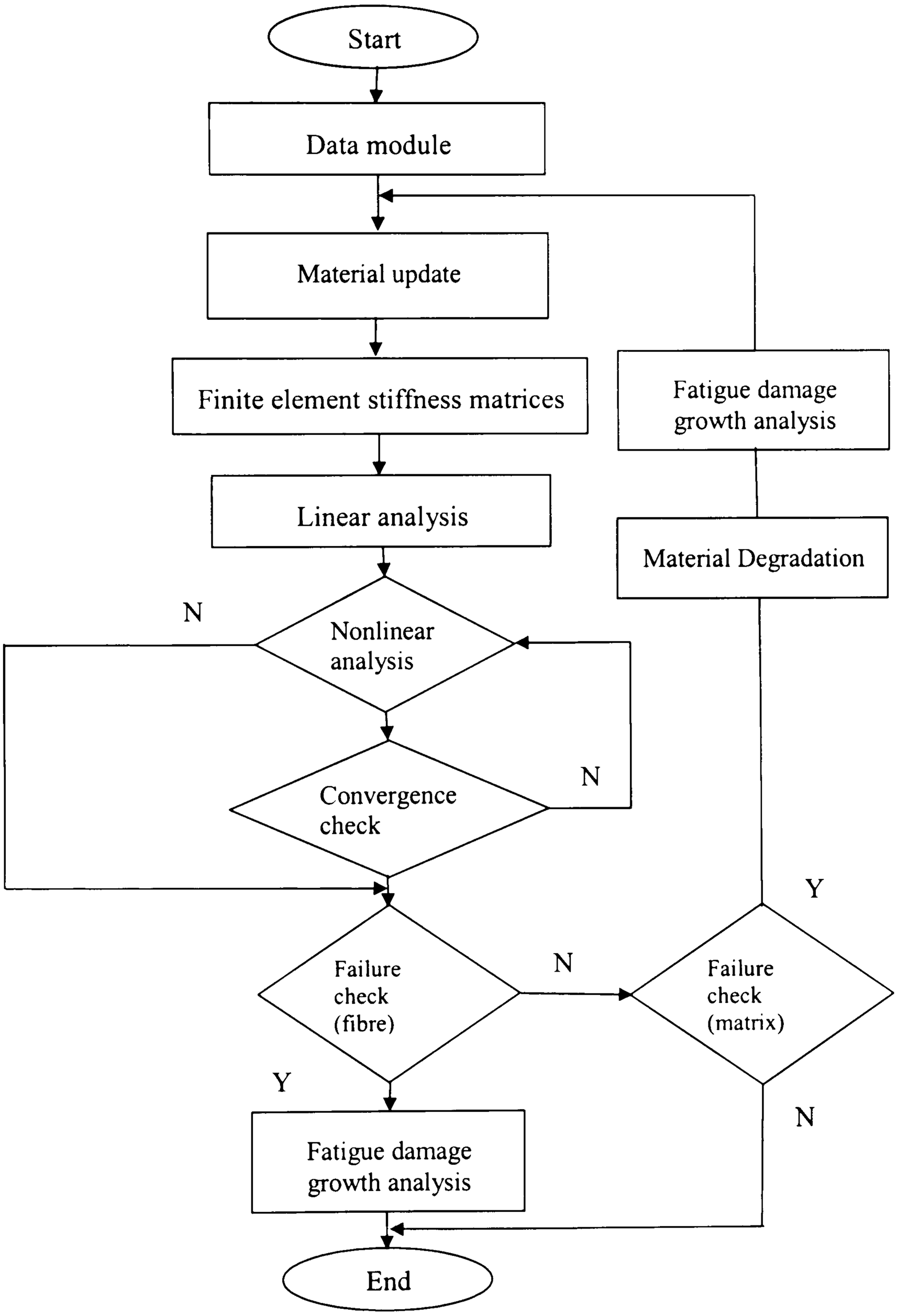

Figure (7.5) Fatigue damage growth structure

8

RESULTS AND DISCUSSIONS

8.1 INTRODUCTION

An adaptable finite element package has been presented for static, dynamic and fatigue analyses, based on the developed theory in chapters 4 and 5. A number of elements for plates and shells have been used with this package. The package facilities as employed for damage assessment are demonstrated in Figure (8.1). It is recommended that the stability analysis and the natural frequency analysis are carried out first before the fatigue damage analysis, to check the damage due to buckling effect and resonance effect, respectively.

This chapter demonstrates the validation procedures of the finite element package for different types of analyses using different case studies. The validation of all package aspects is very important factor before using it for the analysis of practical applications. The validation has been carried out by comparing the package results for different types of analyses with published, experimental (whenever available) and ABAQUS commercial package results.

A large number of investigations with the finite element package have been carried out to study the effect of some effective parameters on the types of analysis such as: mesh convergence, fibre orientation, number of layers, degree of orthotropy, aspect ratio (length to width ratio), length to thickness ratio and stiffener effect.

One of the main objectives of this work was to include the fatigue damage assessment with the finite element analysis. The fatigue damage assessment, depending on the case study, is presented with two approaches, fatigue damage by initiation and fatigue damage by crack growth. The fatigue damage assessment is validated by comparing the results with published results using ABAQUS commercial package and with published experimental work for the same case study.

Some experimental work has been carried out at Cranfield University laboratories in the School of Engineering (SOE) and the School of Industrial and Manufacturing Science (SIMS). Two types of composites with different degrees of orthotropy have been used with the experimental work, carbon/epoxy and glass/epoxy.

8.2 BASIC PACKAGE VALIDATION

In this section the basic aspects of the package, i.e. linear and nonlinear stress analysis, stability analysis and natural frequency analysis are to be validated. All package computations were carried out using a PC with Pentium II processor and double precision arithmetic.

8.2.1 Static validation and mesh convergence

Different static analyses have been carried out to ensure and validate the accuracy of the developed theory and its implementation in the programming package. One of the important problems in finite element analysis is the selection of the optimum finite element mesh so as to obtain accurate results with a reasonable number of elements. In this section, quadrilateral 4-node conforming and non-conforming elements and triangular 3-node non-conforming element have been used for the analyses with different meshes to validate the linear analysis and to study the mesh convergence.

8.2.1.1 Simply supported square plate

The square plate has been used before in many publications [(Pica et al., 1979), (Akay, 1979), (Phan and Reddy, 1985) and others]. Consider a laminate square plate with 8 layers $[0^o/45^o/-45^o/90^o]_s$ and the following material properties, (Phan & Reddy, 1985):

$E_1 = 40E_2$, $G_{12} = 0.6E_2$, $G_{23} = 0.5E_2$, $\nu_{12} = 0.25$, and it is assumed that $G_{13} = G_{12}$, $\nu_{13} = \nu_{12}$ and $\rho = 1$

where

E_1	longitudinal modulus of elasticity
E_2	transverse modulus of elasticity
G_{12}	shear modulus of rigidity in the x-y plane
G_{23}	shear modulus of rigidity in the y-z plane
G_{31}	shear modulus of rigidity in the z-x plane
ν_{12}	Poisson's ratio in x-y plane
ν_{13}	Poisson's ratio in x-z plane
ρ	density

The plate is subjected to two different types of transverse loadings, sinusoidal load, and uniform load with intensity q_o as shown in Figure (8.2, a, b) to test the package with different types of loads where the load has a shear force per unit area q represented as follows:

Uniform load $q(x, y) = q_o$

Sinusoidal load $q(x, y) = q_o \sin \frac{\pi x}{L}$

The plate is simply supported at all the four edges and the central deflections are represented by a non-dimensional deflection parameter $\overline{W}$ as follows:

$$\overline{W} = \frac{w_c E_2 t^3}{q_o L^4} x 10^2 \qquad (8.1)$$

where w_c is the central deflection, L and t are the side length and the thickness of the plate, respectively, as shown in Figure (8.2, c).

Due to the symmetry of the plate, a quarter-plate mesh is used. Two different types of mesh have been applied with this study, a coarse mesh (c.) and a fine mesh (f.) as shown in Figure (8.3) and Figure (8.4) to study the mesh convergence.

Tables (8.1,2,3) summarize the results by comparing the non-dimensional deflection parameter $\overline{W}$ of the simply supported square plate under uniform load using different elements with the published results of Phan & Reddy (1985) and the results obtained with the ABAQUS commercial package. It is clear from the results presented in the tables that all elements give good results, and the two types of meshes provide very close results to each other.

Figures (8.5,6,7) show the non dimensional deflection parameter $\overline{W}$ of the simply supported square plate under sinusoidal load using different elements as a function of the span-to-thickness ratio. As seen in the figures, the package results, which were obtained using the coarse mesh, have a good agreement with the corresponding results by ABAQUS package. While the published results of Phan & Reddy (1985) have a certain shift all over the span-to-thickness ratio range which is due to the approximations employed in their theory.

8.2.1.2 Curved shell case

An important factor, which has to be verified before the present package can be used safely for the analysis of shell structures, is the ability of the package to deal with composite structures with different local coordinate systems.

For this purpose, a curved shell clamped from one end and free from the other, as shown in Figure (8.8), has been studied. A distributed line load has been applied on the free end of the shell with intensity q_o as shown in Figure (8.8).

This case was discussed before by Attia (1996), where the material properties were isotropic properties expressed as orthotropic material properties. In that case the effect of different material axes in different layers does not appear as the material is actually isotropic. The curved shell considered here has 8 layers $[0°/90°/+45°/-45°]_s$ of E-glass/epoxy. Table (8.4) shows the material properties and the geometric properties of the curved shell, (Barbero, 1999).

Two different types of meshes were attempted; coarse meshes (c.) with 40 and 80, 4-node and 3-node elements, respectively, and fine meshes (f.) with 80 and 160, 4-node and 3-node elements, respectively, as shown in Figure (8.9) and Figure (8.10). For the purpose of validation the same meshes were also used in the ABAQUS commercial package with S4 and S3 elements.

Figures (8.11-13) show the variation of the nodal displacement shell in the z-direction of the curved shell with the polar coordinates θ (shown in Figure 8.8). The figures illustrate the comparison between the package results and the corresponding ABAQUS results with coarse and fine meshes.

The first observation is that the two types of meshes provide very close results to each other. It can also be seen in the figures that the package results have a good agreement with the ABAQUS commercial package results.

8.2.1.3 Clamped square plate

The proposed theory has also considered the effect of geometric nonlinearity or finite strain. A four-layer clamped square plate was employed to illustrate the accuracy of the proposed theory

with geometric nonlinearity analysis. The plate is clamped at all four edges and the history of maximum deflection at the centre with the load is represented by a non-dimensional deflection parameter $\overline{W}$ and a load parameter $\bar{q}$ as follows, (Reddy, 1982):

$$\overline{W} = \frac{w_c}{t} \tag{8.2}$$

$$\bar{q} = q_o \left(\frac{L}{t}\right)^4 10^{-1} / E_2 \tag{8.3}$$

where w_c is the central deflection and t is the thickness of the plate. A quarter-plate mesh has been used due to the symmetry of the plate, where the same meshes and material properties of the simply supported square case have been applied in this case. The package was tested with different types of stacking sequence of the fibre; cross-ply [0°/90°/0°/90°] and angle-ply [45°/-45°/45°/-45°] where the two plies form unsymmetrical composites. The plate is subjected to uniform distributed load where the span-to-thickness ratio L/t = 100.

Figures (8.14) and (8.15) demonstrate the central non-dimensional deflection parameter history of the angle-ply plate with the transverse load parameter for various elements. It is clear from the figures that a good agreement has been recognized between the results with the package elements and with the ABAQUS elements and the published results by Reddy (1982).

Figures (8.16) and (8.17) show the central non-dimensional deflection parameter history of the cross-ply plate with the transverse load parameter for various elements.

It is clear from the figures that the package elements give results that compare well with ABAQUS results and the published results by Reddy (1982) for the different types of composite stacking sequences. It can also be seen from the shown results that the proposed elements provide very close results to each other with the two types of meshes.

Hence, it was decided to use only the 4-node elements with coarse mesh for further validation analyses.

8.2.2 Stability validation

For the purpose of validation, experimental and numerical stability analyses have been carried out with some selected case studies. Experimental setup of the stability test is discussed earlier in section (3.6.3). Table (8.5) provides the material properties of two types of composites, carbon/epoxy and glass/epoxy, which are available for the experimental purpose.

Rectangular plates of length 180 [mm] and width 40 [mm] have been employed in the experimental tests and for the finite element package with coarse mesh (72 4-node elements). Table (8.6) shows the critical buckling load obtained experimentally and by the finite element package. It is clear from the results that the package results have a quite good agreement with the experimental results.

Numerical results were obtained for one [30°] and three [30°/-30°/30°] layers square and rectangular composite plates. The plates are made of E-glass/epoxy materials with the following material properties (Narita & Leissa, 1990):

E_1 =60.7 GPa, E_2 =24.8 GPa, G_{12} =12.0 GPa, G_{23} =12.0 GPa, G_{31} =12.0 GPa & ν_{12} = 0.23

The plates are simply supported on all four edges and subjected to in-plane uniform edge load as shown in Figure (8.18). The buckling analysis is numerically validated with thin (L/t =100) and thick (L/t = 10) plates for different number of layers, where L/t is the span-to-thickness ratio. The buckling analysis is represented by the buckling parameter λ as follows (Narita & Leissa, 1990):

$$\lambda = -\frac{F_c L^2}{D_o} \tag{8.4}$$

where

$$D_o = \frac{E_1 t^3}{12(1-\nu_{12}\nu_{21})}$$

and F_c is the critical buckling load per length. The critical buckling load N_c is obtained by solving an eigenvalue problem as shown in section (5.7.2). For practical purposes only the lowest mode of the eigenvalue problem is corresponding to the actual buckling load. In that case, the critical buckling load per length $F_c = N_c/b$.

The buckling parameters provided by the package are compared with the ABAQUS results and the published results by Narita & Leissa (1990) in Table (8.7), where results are shown for different element types, and different plate geometry. It can be seen from the table that the results of the package are in a good agreement with the ABAQUS and published results.

8.2.3 Natural frequency validation

For the purpose of validation, experimental and numerical natural frequency analyses have been carried out with some selected case studies. Experimental setup of the natural frequency test is discussed earlier in section (3.6.4). The materials used with this analysis are the same carbon/epoxy and glass/epoxy used with the previous analyses.

Rectangular plates of length 150 [mm] and width 40 [mm] have been employed in the experimental tests and for the finite element package with coarse mesh (60 4-node elements). Table (8.8) shows the natural frequencies obtained experimentally and by the finite element package. It is clear from the results that the package results have a good agreement with the experimental results which were slightly influenced by the effect of supports. Some modes of vibration were difficult to detect using this type of experiment.

Numerical validation of the natural frequency is carried out with a wide range of effective parameters. A laminate square plate with different number of layers, boundary conditions and material properties (degree of orthotropy, E_1/E_2) have been used in this validation.

Two different types of materials with different degrees of orthotropy have been used with the following material properties (Khdeir & Reddy, 1999):

(i) $E_1 = 40\ E_2$, $G_{12} = 0.6\ E_2$, $G_{23} = 0.5\ E_2$, $\nu_{12} = 0.25$, $G_{13} = G_{12}$, $\nu_{13} = \nu_{12}$, $\rho = 1$ and $E_2 = 1$

(ii) $E_1 = 25\ E_2$, $G_{12} = 0.5\ E_2$, $G_{23} = 0.2\ E_2$, $\nu_{12} = 0.25$, $G_{13} = G_{12}$, $\nu_{13} = \nu_{12}$, $\rho = 1$ and $E_2 = 1$

Three different types of fibre stacking sequence and number of layers have been used; four layers angle- ply [45°/-45°/45°/-45°], three layers cross-ply [0°/90°/0°] and two layers cross-ply [0°/90°]. All layers are assumed to have the same thickness, density and made of the same orthotropic material.

The boundary conditions of the plates are applied as follows:

(i) Simply supported on all four edges (SSSS)

(ii) Simply supported on two edges facing each other and clamped on the other two (SSCC)

The natural frequency is represented by a non dimensional frequency parameter as follows (Khdeir & Reddy, 1999):

$$\bar{\omega} = \frac{\omega L^2}{t}\sqrt{\frac{\rho}{E_2}}$$

where

ω is the natural frequency in rad/sec.

Tables (8.9-11) show the lowest frequency parameter variation with the span-to-thickness ratio for different types of laminated plates. Generally, the package provides good results as compared with ABAQUS and the published results by Khdeir & Reddy (1999).

It is clear from Table (8.10) that the package results are very significantly more accurate than the published results by Khdeir & Reddy (1999) for simply supported-clamped (SSCC) case, compared with ABAQUS results. This validation shows that the package should be preferred for thin and thick laminate plates and the proposed theory is intended primarily for use with thin and thick laminated plates for different conditions.

8.3 PARAMETRIC INVESTIGATION

The cantilever plate is considered a useful structural component in industrial, military and aerospace fields, especially when it is made of composite laminated plates. Typical applications are aerodynamic lifting structures, missile stabilizing surfaces, fan blades and turbine blades.

This section provides a parametric study for composite laminated cantilever stiffened and unstiffened plates and demonstrates the effect of some parameters on the natural frequency and stability parameter.

The natural frequency analysis is shown in terms of the natural frequencies of the first three modes of free vibration and the stability analysis is in terms of the stability parameter in equation (8.4) under in-plane compression load.

The natural frequencies and the stability parameters are obtained for composite cantilever laminated plates with different numbers of layers: i.e. 4-layers, 8-layers and 12-layers with the same thickness. These analyses are carried out on stiffened and unstiffened plates to show the stiffener effect on these types of analyses. The geometry and boundary conditions of the unstiffened cantilever plate are shown in Figure (8.19) with length L, width b and thickness t while the plate is clamped at one end and free at the others.

A repeating element of the stiffened plate is shown in Figure (8.20) with length L, width b, height h and thickness t. The stiffened cantilever plate consists of four elements as shown in Figure (8.21) with the same boundary conditions of the unstiffened one. Fibre orientation angles are measured with respect to the local x-axis which is parallel to the stiffener direction. The laminated plates are composed of orthotropic layers of equal thickness. Each layer has the following non-dimension material properties, (Phan & Reddy, 1985), (Khdeir & Reddy, 1999):

$E_1 = 40E_2$, $G_{12} = 0.6E_2$, $G_{23} = 0.5E_2$, $\nu_{12} = 0.25$, and it is assumed that $G_{13} = G_{12}$, $\nu_{13} = \nu_{12}$ and $\rho = 1$ and $E_2 = 1$

The layers are arranged in two stacking sequence, symmetry, such as for 4-layers plate [θ/-θ/-θ/θ] and asymmetry, such as for 4-layers plate [θ/-θ/θ/-θ] to investigate the effect of stacking sequence where θ is the fibre orientation angle varied from 0° to 90° with 15° increments. Two different aspect ratios L/b have been used to represent a square plate L/b=1 and a rectangular plate L/b=2 with span-to-thickness ratios L/t=10 and 20, respectively. Coarse meshes for unstiffened and stiffened plates are used in this investigation as shown in Figures (8.22,26,30,34) for the reason discussed earlier in the static validation section. The 4-node non-conforming element has been used for the analyses of stiffened plate as the conforming one is only suitable for plates.

8.3.1 Effect of fibre orientation angles and number of layers on the natural frequency

Tables (8.12-14) and (8.15-17) show the first three natural frequencies of unstiffened and stiffened cantilever plate, respectively. The stacking sequence used in this investigation is asymmetric laminate with different number of layers having the same thickness. The tables illustrate the variation of the natural frequencies with the fibre orientation angles for two different aspect ratios (L/b=1 and 2) and with three different number of layers (4-layers, 8-layers and 12-layers).

It is clear from the results presented by these tables that the conforming and non-conforming elements have the same degree of accuracy with the unstiffened plate, as shown in Table (8.12-14). The plates with different number of layers have the same natural frequencies at fibre angle 0^o, and also at fibre angle 90^o.

The maximum natural frequency of the first mode of the unstiffened plate is found at fibre angle 0^o for the two aspect ratios as shown in Table (8.12). The maximum natural frequency of the first mode of the stiffened plate using non-conforming element is found at fibre angle 15^o for aspect ratio L/b=1 and at fibre angle 0^o for aspect ratio L/b=2 as shown in Table (8.15).

It is also observed that the natural frequency of the first mode of the unstiffened plate decreases gradually as the fibre angle θ increases. As well as, it is clear that the natural frequency of the first mode of the stiffened plate decreases gradually as the fibre angle $\theta+15^o$ increase using the non-conforming element.

The maximum natural frequencies of the second and third modes for the stiffened and unstiffened are found at certain fibre angles and the values gradually decrease as the fibre angle is far from that angle.

A general observation is that the natural frequencies decrease by increasing the number of surfaces where it is recognized that the natural frequencies of the unstiffened square plate are higher than the corresponding ones for the unstiffened rectangular plate and the natural frequencies of the stiffened square plate are also higher than those of the rectangular stiffenend plate.

Figures (8.23-25,27-29) show the first three mode shapes for the unstiffened square and rectangular plates with 8-layer asymmetric laminates and fibre angle $\theta = 30^{o}$. Similarly, Figures (8.31-33,35-37) display the first three mode shapes for stiffened square and rectangular plates with the same composite layout.

8.3.2 Effect of fibre angles and number of layers on the stability

The previous configurations have been employed with the stability analysis. Tables (8.18) and (8.19) show the stability parameter of unstiffened and stiffened cantilever plates, respectively, as a function of the fibre orientation angles, aspect ratios (L/b=1 and 2) and number of layers (4-layers, 8-layers and 12-layers). The stacking sequence used in this investigation is asymmetric laminate with different number of layers having the same thickness.

It is clear from the results presented by these tables that the conforming and non-conforming elements have the same degree of accuracy with the unstiffened plate, as shown in Table (8.18).

The stability parameters for different plates with different number of layers have the same value with fibre angle 0^{o} and 90^{o} for stiffened and unstiffened plates.

The maximum value of the stability parameter for the unstiffened plate is found at fibre angle 0^{o} for the two aspect ratios as shown in Table (8.18). The maximum value of the stability parameter for the stiffened plate using is found at fibre angle 0^{o} for the two aspect ratios.

It is observed that the stability parameter of the unstiffened plate decreases gradually as the fibre angle θ increases. As well as, it is clear that the stability parameter of the stiffened plate decreases gradually as the fibre angle θ increases using non-conforming element.

In contrast with the natural frequencies, the stability parameter increases by increasing the number of surfaces where it is recognized that the stability parameter of stiffened rectangular plate is higher than that of the stiffened square plate. Similarly it is also higher than that of the unstiffened rectangular plate, which is higher than that of the square unstiffened plate.

Figures (8.38-41) show the buckling mode shape for unstiffened square and rectangular cantilever plates as well as stiffened square and rectangular plate. All plates have 12-layer asymmetry laminate with angle $\theta = 15^{o}$.

8.3.3 *Effect of stacking sequence on the natural frequency*

In this part of the investigation, the influence of the stacking sequence on the natural frequencies analysis is discussed. The stacking sequence is represented by symmetric and asymmetric laminates with fibre angles varying form 0^o to 90^o by increment 15^o.

Tables (8.20,21) and (8.22) illustrate the variation of the first three natural frequencies for the unstiffened and the stiffened cantilever plate, respectively. It is clear from the presented results that there is no effect of the stacking sequence for the unstiffened and the stiffened plates at fibre angles 0^o and 90^o. A small, not effective, difference has been observed between the natural frequencies for the symmetric and asymmetric stacking sequence at the rest of the fibre angles, 15^o, 30^o, 45^o, 60^o, 75^o.

8.3.4 *Effect of stacking sequence on the stability*

The previous configurations have been used for stability analysis to study the stacking sequence effect. The same stacking sequences used before in the previous investigation are used again with the stability analysis.

Tables (8.23) and (8.24) illustrate the variation of the stability parameter for the unstiffened and the stiffened cantilever plates, respectively. It is clear from the results that the stacking sequence has no effect on the stability analysis for the unstiffened and the stiffened plates at fibre angles 0^o and 90^o but a small, not effective, difference in the rest of the fibre angles, 15^o, 30^o, 45^o, 60^o, 75^o has been observed.

8.3.5 *Stiffener effect on the natural frequency*

The stiffened plates and shells are used in several applications, such as aircrafts and ships. The stiffened plate shown in Figure (8.21) has been used to investigate the stiffener effect on the natural frequency.

Figures (8.42-44) plot the first three natural frequencies of the stiffened and the unstiffened square cantilever plate with 8-layer symmetric (sym.) and asymmetric (asym.) laminates against the fibre orientation angles. It is clear from the figures that the natural frequencies of the stiffened

plates are lower than the unstiffened ones. There is no significant difference between the natural frequencies of symmetric and asymmetric laminates (with the same other configurations).

Figures (8.45-47) show the variation of the first three natural frequencies with the fibre orientation angles of the stiffened and the unstiffened rectangular cantilever plates with 8-layer symmetric (sym.) and asymmetric (asym.) laminates. Conclusions similar to those obtained for the square plates are observied.

These conclusions agree with the general observation in section (8.3.1) of the effect of fibre angle and number of layers investigation on the natural frequency analysis.

8.3.6 Stiffener effect on the stability

The stiffened plate shown in Figure (8.21) has also been used to investigate the stiffener effect on the stability parameters.

Figure (8.48) displays the stability parameter of the stiffened and the unstiffened square cantilever plates with 12-layer symmetric (sym.) and asymmetric (asym.) laminates against the fibre orientation angles. It is clear from the figures that the stability parameter of the stiffened plates is higher than the unstiffened ones. We can also observe that there is very small difference between the stability parameters of symmetric and asymmetric laminates with the same configurations.

Figure (8.49) shows the variation of the stability parameter with the fibre orientation angles of the stiffened and the unstiffened rectangular cantilever plates with 12-layer symmetric (sym.) and asymmetric (asym.) laminates. Observations similar to those found for the previous case can be noticed. These conclusions agree with the general observation in section (8.3.2) of the effect of fibre angle and number of layers investigation on the stability analysis.

8.4 FATIGUE DAMAGE ANALYSIS BY INITIATION

The previous sections illustrate the validation of the finite element package from several points of view (type of analysis, mesh selection, number of layers, fibre orientation angles, aspect ratio and span to thickness ratio). The finite element package is used in this section for the fatigue analysis by initiation in composite materials, which was discussed earlier in section (6.3).

Two symmetric 12-layer $[0°/90°/45°/0°/-45°/90°]_s$ composite plates have been used in this analysis, with two different types of materials, carbon/epoxy and glass/epoxy, which were also used in the experimental validation of natural frequency and stability analyses.

The square plate with aspect ratio L/b=1 and rectangular plate with aspect ratio L/b=2, which were employed in the previous parametric studies, have been used in this analysis with the same coarse meshes as shown in Figures (8.22) and (8.26), respectively. The plates were subjected to in-plane cyclic loads of $F_{min} < F < F_{max}$, with $F_{min}=0$, $F_{max} = 10$ kN for the glass/epoxy case study and $F_{max} = 50$ kN for the carbon/epoxy case. The boundary conditions applied on the edges of the plates are as follows:

$$\text{at } x = 0 : u = 0, v = 0, w = 0 \text{ and } \theta_y = 0 \quad \text{where at } x = L : v = 0, w = 0 \text{ and } \theta_y = 0$$

The experimental fatigue test analyses have been carried out as explained in Chapter 3 to obtain the fatigue life diagrams for carbon/epoxy and glass/epoxy materials. The S-N diagrams for carbon/epoxy and glass/epoxy are shown in Figure (8.50) and (8.51), respectively.

For more validation, the stress analyses carried out by the finite element package are compared with the results obtained with the ABAQUS commercial package. The maximum stress along the local x-direction σ_x and its node location for the two types of materials are shown by Tables (8.25) and (8.26), respectively, which confirm the excellent agreement between the package results and corresponding ABAQUS results.

The stress σ_x contours at lower surface are shown in Figures (8.52) and (8.53) for square and rectangular plates, respectively, for the carbon/epoxy case. The stress σ_x contours at lower surface are shown in Figures (8.54) and (8.55) for square and rectangular plates, respectively, for the glass/epoxy case. These figures illustrate the areas with the maximum stresses, which are in agreement with the results in Tables (8.25) and (8.26).

With respect to carbon/epoxy case, Figures (8.56) and (8.57) show the variation of the stress σ_x in the local x-direction across the total thickness of the plate at node 41 for the square plate and node 82 for rectangular plate, respectively, where the maximum stress occurred. Similarly for the glass/epoxy case, Figures (8.58) and (8.59) show the variation of σ_x across the total thickness of

the plate at node 41 for the square plate and node 72 for rectangular plate, respectively, where the maximum stress occurred.

It is clear from these tables and figures that very good agreements between the results of the finite element package and the corresponding results of ABAQUS package have been recognized for different aspect ratios and with different types of materials.

The stress analyses presented in this part are carried out under the effect of unit load as explained in chapter 6 by equation (6.1). The maximum and minimum stresses defined by equations (6.9) and (6.10), respectively, are obtained based on load ratios as follows:

for carbon/epoxy: $\alpha_{max} = 50$ $\alpha_{min} = 0$

for glass/epoxy: $\alpha_{max} = 10$ $\alpha_{min} = 0$

Tables (8.27) and (8.28) show the maximum stress values in fibre and matrix directions and it location (layer and element) relating to the previous load ratios with respect to carbon/epoxy and glass/epoxy types of materials, respectively. It can be observed from the results that the maximum fibre stresses observed in the 0^o layers (1, 4, 9 and12) and the maximum matrix stress observed in 90^o layers (2, 6, 7 and 11). The mean and alternating stresses values relating to the previous load ratios with respect to carbon/epoxy and glass/epoxy types of materials are presented in Tables (8.29) and (8.30), respectively.

By applying Goodman relationship in equations (6.15) and (6.16) with respect to the fibre and the matrix, respectively, Tables (8.31) and (8.32) give the fatigue stress and the corresponding number of cycles to failure from S-N diagrams for carbon/epoxy and glass/epoxy case studies, respectively.

The final number of cycles to failure of the composite laminates is the minimum value of cycles to failure for fibre and matrix as mentioned before in section (6.3) and as shown in Table (8.33).

8.5 FATIGUE DAMAGE BY CRACK GROWTH ANALYSIS

Fatigue damage growth is considered a better way to understand the fatigue phenomena; especially in applications which have stress concentration effects. The proposed fatigue damage

model, which is introduced in chapter 6, is applied to square and rectangular coupons with hole subjected to tensile load.

The square coupon with hole case is studied before by Feng et al. (1997) using ABAQUS commercial package for the finite element analysis, and it has been used to validate the proposed fatigue growth model. The rectangular coupon with hole case has been used to illustrate the fatigue behaviour during the fatigue life

8.5.1 Fatigue model validation

To predict the fatigue life of the coupon, a repeated load F is applied where $F_{max} < F < F_{min}$ and $F_{max} = 50$ kN and $F_{min} = 5$ kN. The geometry of the square coupon and the applied load are shown in Figure (8.60). The 4-node non-conforming element has been used with a coarse mesh of 96 elements as shown in Figure (8.61). Due to the symmetric property of the coupon, one quarter has been selected for the finite element analysis as shown in Figure (8.61) with the following boundary conditions:

at $x = 0 : u = 0$ and $\theta_y = 0$

at $x = L/2 : v = 0, w = 0$ and $\theta_x = 0$

at $y = 0 : v = 0$ and $\theta_x = 0$

The coupon is fabricated from carbon/epoxy composite material with the following material properties: the longitudinal modulus of elasticity $E_1 = 130$ GPa, the transverse modulus of elasticity $E_2 = 11$ GPa, the shear modulus of rigidity in x-y plane $G_{12} = 7$ GPa, the Poisson's ratio in x-y plane $\nu_{12} = 0.3$, and it is assumed that $G_{23} = G_{31} = G_{12}$. The coupon consists of 24 plies with thickness 0.125 mm for each and a stacking sequence $[0^o/-45^o/90^o]_{2s}[90^o/-45^o/0^o]_{2s}$ with respect to the local coordinates.

According to experimental data published by Fang et al. (1997), the material constants used in equation (6.24) are assumed as follows:

$D = 7.03 \times 10^{-20}$ and $n = 3.5$

The matrix damage (matrix cracking) starts to grow at ε_{um1} = 0.4% and reaches maximum damage at ε_{um2} = 0.8% for the carbon/epoxy composite used in this analysis. The complete failure occurs when the strain value in the fibre direction reaches the ultimate value ε_{uf} which is 1.3% for the carbon/epoxy composite used in this analysis.

Eight iteration steps have been observed during the finite element stress analysis. Each step has been carried out with new material properties for the damaged area as mentioned in the material degradation process in chapter 6. The main observation from the finite element analysis is that the damage occurred firstly in the 90° plies at the elements within the stress concentration zone. Figure (8.62) shows the damaged elements at the last iteration with one of the 90° plies (layer number 3). It is clear from that observation and Figure (8.62) that the finite element stress analysis results have a good agreement with the published results by Feng et al. (1997) as they proved that the damage occurred at the same zone.

From the previous finite element fatigue analysis, the predicted number of cycle to failure of the square coupon by the proposed fatigue model is approximately 8.2×10^6 cycles. The number of cycles to failure predicted by Feng et al. (1997) for the same case study is about 15×10^6 cycles. Fatigue experimental work was introduced by Enderby c. (1993) on the same case study where the fatigue life was terminated after 7.65×10^6 cycles.

Hence, it is clear that the predicted fatigue life by the developed finite element fatigue package has a better agreement with the experimental work, compared with Feng et al. (1997) results.

8.5.2 Fatigue behaviour of rectangular coupon subject to tensile load

A rectangular plate with hole fabricated from carbon/epoxy has been employed in this section. The plate consists of 13-layers with a stacking sequence [0°/90°/45°/0°/-45°/90°/0°/90°/-45°/0°/45°/90°/0°]. The plate has been fabricated for experimental work on carbon/epoxy composites. The material properties of the carbon/epoxy are illustrated before in Table (8.5). The plate geometry and the applied tensile load are shown in Figure (8.63). The applied tensile load F is a cyclic load with minimum value F_{min} = 0 and maximum value F_{max} = 10 kN. The 4-node non-conforming element has been used with a coarse mesh of 161 elements as shown in Figure (8.65), where a fine mesh is used near the hole as it is the stress concentration zone. Due to the

symmetric property of the plate, one quarter of the plate has been selected for the finite element analysis as shown in Figure (8.64) with the same boundary conditions of the previous case.

Thirty stress analysis iterations have been carried out with new material properties for each trial according to the degradation rule discussed later in section (6.4.2). The damaged areas are calculated at each trial. Figure (8.65) comprehensively illustrates the variation of the damaged areas with the number of iterations. However, the first group of iterations have demonstrated that the dominant damage occurred within the stress concentrated zone at the 90^{o} plies.

Table (8.34) illustrates the number of damaged elements per plies at iteration number one. Figures (8.66) and (8.67) show the damage zone of layer number two of the plate using the finite element package and ABAQUS package, respectively. The results provided by ABAQUS are obtained using input files generated automatically at each iteration by the developed package. It is seen from the figures that a good agreement between the finite element and ABAQUS results has been achieved.

The final group of iterations have illustrated that the damage starts to growth in the 0^{o} plies, exactly at iteration number 23 as shown in Table (8.35). Figures (8.68) and (8.69) show the damage zone of layer number two of the plate using the finite element package and ABAQUS package, respectively. A good agreement between the finite element and ABAQUS results can be seen from the figures.

A sample element, at this case, element number 14 has been used to show the changes of the strain and material properties in the longitudinal (fibre) and transverse (matrix) directions during the iterations. Element 14 has been chosen because it is in the damaged zone during all the analysis steps.

Figures (8.70-71) show the history of the longitudinal and transverse moduli of elasticity during the iterations for the element 14 within layer number 2. The main observation is that the variation of the transverse moduli of elasticity is faster and more effective than the longitudinal one.

Figure (8.72) shows the variation of the transverse strain (strain in matrix direction) with the first 23 iterations while Figure (8.73) shows its variation with the rest of iterations. As observed in Table (8.35), the damage occurrence in 0^{o} plies caused the variation in the transverse strain after

the 23rd iteration. Figure (8.74) shows the variation of the longitudinal strain (strain in fibre direction) during the iteration steps.

Tables (8.36) shows the strain energy and the work done by external force as a function of the damaged areas while an interpolation has been carried out to represent the strain energy and the work done as polynomial functions of the damaged area as follows:

$$U(A) = f(A) \qquad W(A) = g(A) \tag{8.5}$$

The area has to be given in [m^2] and the strain energy and work done in [N.mm], (Fuchs and Stephens, 1980). Using equation (6.23), the strain energy release rate G can be computed as a function of the damaged area, hence the energy release rate range in equation (6.24) can be calculated as well as.

$$G(A) = h(A) \tag{8.6}$$

Table (8.36) shows the variation of the energy release rate with the damaged area, for the present case. Once the equation (8.6) is established the number of cycles to failure can be easily computed from equation (6.24) at each step of iterations. The final number of cycles to failure is $N_f = 6.8 \times 10^6$ cycles.

The fatigue life calculations for every case study, including different iterations with material degradation, and derivations of equations (8.5), and (8.6) up to finding N_f, have been carried out automatically via a single run of the finite element package. This represents a major saving of user time and computer resources as compared with fatigue life assessments based on commercial finite element packages.

Table (8.1) Non dimensional deflection parameter of simply supported square plate subjected to uniform load using 4-node conforming element.

L/t	Phan & Reddy (1985)	ABAQUS S4 (c.)	ABAQUS S4 (f.)	4-Node Conf. (c.)	4-Node Conf. (f.)
4	1.634	1.672	1.669	1.794	1.806
10	0.590	0.644	0.644	0.686	0.679
20	0.434	0.470	0.470	0.496	0.486
50	0.386	0.404	0.405	0.423	0.413
100	0.377	0.387	0.389	0.405	0.395

Table (8.2) Non dimensional deflection parameter of simply supported square plate subjected to uniform load using 4-node non-conforming element.

L/t	Phan & Reddy (1985)	ABAQUS S4 (c.)	ABAQUS S4 (f.)	4-Node Non-Conf. (c.)	4-Node Non-Conf. (f.)
4	1.634	1.672	1.669	1.799	1.810
10	0.590	0.644	0.644	0.671	0.677
20	0.434	0.470	0.470	0.477	0.480
50	0.386	0.404	0.405	0.403	0.406
100	0.377	0.387	0.389	0.386	0.388

Table (8.3) Non dimensional deflection parameter of simply supported square plate subjected to uniform load using 3-node non-conforming element.

L/t	Phan & Reddy (1985)	ABAQUS S3 (c.)	ABAQUS S3 (f.)	3-Node Non-Conf. (c.)	3-Node Non-Conf. (f.)
4	1.634	1.666	1.668	1.790	1.805
10	0.590	0.636	0.641	0.669	0.676
20	0.434	0.461	0.468	0.477	0.480
50	0.386	0.394	0.401	0.405	0.407
100	0.377	0.380	0.385	0.389	0.390

Table (8.4) Material and geometric properties of the curved shell case.

Parameter	Value
Longitudinal Modulus E_1 [GPa]	45
Transverse Modulus E_2 [GPa]	12
Inplane Shear Modulus G_{12} [GPa]	5.5
Poisson's Ratio ν_{12}	0.19
Radius of the curved shell R [m]	0.1
Thickness of each layer [m]	0.002
Width of the curved shell B [m]	0.04
Load intensity q_o [kN/m]	0.08

Table (8.5) Material properties of Carbon/epoxy and Glass/epoxy.

Parameter	Carbon/epoxy	Glass/epoxy
Longitudinal Modulus E_1, [GPa]	128.0	35.0
Transverse Modulus E_2, [GPa]	11.0	8.22
Shear Modulus in x-y plane G_{12}, [GPa]	4.48	4.1
Shear Modulus in y-z plane G_{23}, [GPa]	4.48	4.1
Shear Modulus in z-x plane G_{31}, [GPa]	4.48	4.1
In-plane Poisson's Ratio ν_{12}	0.25	0.26
Number of layers	13	12
Thickness of each layer, [mm]	0.25	0.15
Stacking sequence	$[0^o/90^o/45^o/0^o/-45^o/90^o/0^o/90^o/-45^o/0^o/45^o/90^o/0^o]$	$[0^o/90^o/45^o/0^o/-45^o/90^o]_s$
Density ρ, [kg/m^3]	1500	2000

Table (8.6) Critical buckling load of carbon/epoxy and glass/epoxy composite materials.

		Carbon/epoxy	Glass/epoxy
Finite element package	4-node conf.	7964.24 [N]	545.53 [N]
	4-node nonconf.	8107.48 [N]	551.65 [N]
Experimental		8200.00 [N]	510.00 [N]

Table (8.7) Buckling parameter λ of one [30°] and three [30°/-30°/30°] layers composite plates with different aspect ratios and span-to-thickness ratios.

		No. of Layers	Narita & Leissa (1990)	ABAQUS S4	4-node Conf.	4-node Non-Conf.
L/t = 100	L/b = 1	1	25.17	25.64	25.19	24.98
		3	25.40	25.75	25.31	25.09
	L/b = 2	1	100.9	101.77	99.93	99.05
		3	101.8	102.51	100.73	99.83
L/t =10	L/b = 1	1	---	22.84	22.01	21.91
		3	---	22.96	22.13	22.04
	L/b = 2	1	---	74.49	70.89	70.43
		3	---	75.38	71.88	71.47

Table (8.8) Natural frequencies in [Hz] of carbon/epoxy and glass/epoxy composite materials.

		Carbon/epoxy			Glass/epoxy		
		mode 1	mode 2	mode 3	mode 1	mode 2	mode 3
Finite element package	4-node Conf.	15.2	94.9	263.7	4.41	27.73	76.8
	4-node nonconf.	15.2	94.9	264.2	4.41	27.76	76.9
Experimental		17		278	3	34	

Table (8.9) Frequency parameter $\bar{\omega}$ of a 4-layer [45°/-45°/45°/-45°] square plate using material (i).

L/t		5	10	20	50	100
SSSS	Conf. 4-node	8.73	16.95	20.49	22.64	23.25
	Non Conf. 4-node	8.73	16.92	20.49	22.59	23.16
	Khdeir & Reddy (1999)	12.93	18.67	21.95	23.25	23.46
	ABAQUS S4	8.60	16.02	20.19	22.71	23.37
SSCC	Conf. 4-node	12.73	19.78	25.81	29.63	30.52
	Non Conf. 4-node	12.72	19.83	25.83	29.50	30.33
	Khdeir & Reddy (1999)	13.46	20.89	26.77	29.98	30.60
	ABAQUS S4	11.16	18.34	25.14	29.74	30.82

Table (8.10) Frequency parameter $\bar{\omega}$ of a 3-layer [0°/90°/0°] square plate material (ii).

L/t		5	10	20	50	100
SSSS	Conf. 4-node	8.19	11.75	14.04	15.01	15.17
	Non Conf. 4-node	8.13	11.66	13.93	14.90	15.06
	Khdeir & Reddy (1999)	9.09	12.53	14.38	15.08	15.19
	ABAQUS S4	7.70	11.49	14.00	15.10	15.29
SSCC	Conf. 4-node	9.54	13.60	16.07	17.10	17.27
	Non Conf. 4-node	9.48	13.50	15.94	16.96	17.12
	Khdeir & Reddy (1999)	10.20	17.46	25.43	30.89	31.99
	ABAQUS S4	8.31	12.8	15.87	17.24	17.47

Table (8.11) Frequency parameter $\bar{\omega}$ of a 2-layer [0°/90°] square plate material (ii).

L/t		5	10	20	50	100
SSSS	Conf. 4-node	7.46	9.02	9.68	9.92	9.96
	Non Conf. 4-node	7.41	8.96	9.63	9.86	9.90
	Khdeir & Reddy (1999)	7.61	9.00	9.50	9.67	-----
	ABAQUS S4	6.04	8.24	9.43	9.91	10.00
SSCC	Conf. 4-node	9.08	12.77	15.10	16.11	16.28
	Non Conf. 4-node	9.06	12.73	15.03	16.00	16.16
	Khdeir & Reddy (1999)	9.38	12.96	15.02	15.84	-----
	ABAQUS S4	6.81	10.73	14.12	16.04	16.40

Table (8.12) The first natural frequency of unstiffened cantilever plate.

aspect Ratio	fibre angle	4 layers		8 layers		12 layers	
		conf.	non-conf	conf.	non-conf	conf.	non-conf
L/b = 1	0	5.6189	5.6163	5.6189	5.6163	5.6189	5.6163
	15	4.9183	4.9107	5.18	5.1712	5.2274	5.2183
	30	3.8396	3.827	4.0644	4.0499	4.1046	4.0898
	45	2.5021	2.4932	2.6288	2.6188	2.6515	2.6413
	60	1.4807	1.4766	1.5243	1.5197	1.5322	1.5275
	75	1.0542	1.0533	1.0586	1.0576	1.0594	1.0584
	90	1.0036	1.0036	1.0036	1.0036	1.0036	1.0036
L/b = 2	0	1.5398	1.5397	1.5398	1.5397	1.5398	1.5397
	15	1.3123	1.3115	1.387	1.3861	1.4004	1.3994
	30	0.93522	0.93369	0.98621	0.98443	0.99525	0.99342
	45	0.55913	0.55826	0.58092	0.57997	0.58479	0.58382
	60	0.33935	0.33884	0.34597	0.34542	0.34716	0.3466
	75	0.26129	0.26113	0.26194	0.26177	0.26206	0.26189
	90	0.25204	0.25203	0.25204	0.25203	0.25204	0.25203

Table (8.13) The second natural frequency of unstiffened cantilever plate.

aspect ratio	Fibre Angle	4 layers		8 layers		12 layers	
		conf.	non-conf	Conf.	non-conf	conf.	non-conf
L/b = 1	0	6.1632	6.1547	6.1632	6.1547	6.1632	6.1547
	15	7.0145	6.9977	7.2899	7.2709	7.3406	7.3211
	30	8.2313	8.2223	8.6661	8.6563	8.7452	8.7353
	45	8.4857	8.4839	8.9569	8.9551	9.0424	9.0405
	60	7.4248	7.4253	7.8413	7.8419	7.9164	7.917
	75	5.0634	5.0648	5.3109	5.3126	5.3554	5.3573
	90	2.8924	2.8934	2.8924	2.8934	2.8924	2.8934
L/b = 2	0	2.1084	2.1086	2.1084	2.1086	2.1084	2.1086
	15	2.964	2.9633	3.105	3.1041	3.1306	3.1296
	30	3.8451	3.8438	4.0696	4.0682	4.1101	4.1086
	45	3.2628	3.2714	3.3861	3.3952	3.4082	3.4175
	60	2.0747	2.0776	2.117	2.12	2.1246	2.1277
	75	1.6189	1.6192	1.6228	1.6231	1.6235	1.6238
	90	1.3007	1.3008	1.3007	1.3008	1.3007	1.3008

Table (8.14) The third natural frequency of unstiffened cantilever plate.

aspect ratio	Fibre Angle	4 layers		8 layers		12 layers	
		conf.	non-conf	Conf.	non-conf	conf.	Non-conf
L/b = 1	0	11.641	9.5747	9.6272	9.5747	9.6272	9.5747
	15	11.819	11.787	12.161	12.128	12.225	12.192
	30	14.276	14.324	14.818	14.872	14.921	14.976
	45	12.201	12.292	12.653	12.751	12.737	12.836
	60	8.3303	8.3758	8.531	8.5805	8.5676	8.6179
	75	6.3321	6.3412	6.3539	6.364	6.358	6.3682
	90	6.0771	6.0774	7.1725	6.0774	6.0771	6.0774
L/b = 2	0	5.4717	5.4717	5.4717	5.4717	5.4717	5.4717
	15	6.8727	6.8956	7.1654	7.1911	7.2183	7.2445
	30	5.0897	5.1082	5.3176	5.3379	5.3587	5.3793
	45	4.0915	4.091	4.3142	4.3143	4.319	4.3191
	60	2.9807	2.9811	2.9969	2.9969	2.9998	2.9998
	75	2.4213	2.4216	2.4858	2.4858	2.4867	2.4867
	90	1.5648	1.5648	1.5648	1.5648	1.5648	1.5648

Table (8.15) The first natural frequency of stiffened cantilever plate.

Aspect Ratio	Fibre Angle	4 layers	8 layers	12 layers
L/b=1	0	2.2225	2.2225	2.2225
	15	2.4219	2.4734	2.4825
	30	1.9479	1.9982	2.0072
	45	1.3779	1.419	1.4264
	60	0.93742	0.96209	0.96656
	75	0.63404	0.63704	0.63759
	90	0.50007	0.50007	0.50007
L/b=2	0	0.67794	0.67794	0.67794
	15	0.64745	0.66306	0.66579
	30	0.47686	0.48906	0.49122
	45	0.33117	0.3408	0.34254
	60	0.2291	0.23512	0.23621
	75	0.15873	0.15945	0.15959
	90	0.12669	0.12669	0.12669

Table (8.16) The second natural frequency of stiffened cantilever plate.

Aspect Ratio	Fibre Angle	4 layers	8 layers	12 layers
L/b=1	0	2.3052	2.3052	2.3052
	15	2.7562	2.8201	2.8316
	30	2.8388	2.947	2.9667
	45	2.7069	2.8329	2.8559
	60	2.2868	2.397	2.4171
	75	1.5752	1.6383	1.6498
	90	0.95765	0.95765	0.95765
L/b=2	0	0.78249	0.78249	0.78249
	15	0.99861	1.0324	1.0385
	30	1.182	1.2385	1.2487
	45	1.1692	1.2163	1.2239
	60	0.89394	0.90282	0.9042
	75	0.68496	0.70812	0.71185
	90	2.3052	2.3052	2.3052

Table (8.17) The third natural frequency of stiffened cantilever plate.

Aspect Ratio	Fibre Angle	4 layers	8 layers	12 layers
L/b=1	0	2.9665	2.9664	2.9664
	15	3.7502	3.839	3.8555
	30	4.5232	4.6815	4.7111
	45	4.865	4.9026	4.9092
	60	3.3458	3.3667	3.3704
	75	2.6546	2.6689	2.6713
	90	2.0984	2.0984	2.0984
L/b=2	0	1.5016	1.5015	1.5015
	15	2.2258	2.2687	2.2766
	30	2.2172	2.2404	2.2443
	45	1.3444	1.3703	1.3759
	60	1.0654	1.1183	1.1281
	75	0.79543	0.8077	0.81038
	90	0.68853	0.68853	0.68853

Table (8.18) Stability parameter of unstiffened cantilever plate.

aspect ratio	fibre angle	4 layers		8 layers		12 layers	
		conf.	non-conf	conf.	non-conf	conf.	non-conf
L/b = 1	0	2.1149	2.1118	2.1149	2.1118	2.1149	2.1118
	15	1.4248	1.4238	1.7094	1.7079	1.764	1.7624
	30	0.75087	0.74845	0.93235	0.92968	0.96755	0.96486
	45	0.30004	0.29891	0.3536	0.35243	0.36367	0.3625
	60	0.11326	0.11292	0.12104	0.12069	0.12242	0.12207
	75	6.59E-02	6.58E-02	6.65E-02	6.64E-02	6.66E-02	6.65E-02
	90	6.12E-02	6.12E-02	6.12E-02	6.12E-02	6.12E-02	6.12E-02
L/b = 2	0	2.3669	2.3666	2.3669	2.3666	2.3669	2.3666
	15	1.4608	1.4609	1.8111	1.8115	1.8796	1.8799
	30	0.64248	0.64191	0.79767	0.79699	0.82774	0.82704
	45	0.22141	0.22121	0.2534	0.25318	0.25925	0.25902
	60	9.51E-02	9.50E-02	9.99E-02	9.98E-02	0.10074	0.10061
	75	6.48E-02	6.48E-02	6.52E-02	6.52E-02	6.53E-02	6.53E-02
	90	6.15E-02	6.15E-02	6.15E-02	6.15E-02	6.15E-02	6.15E-02

Table (8.19) Stability parameter of stiffened cantilever plate.

Aspect Ratio	Fibre Angle	4 layers	8 layers	12 layers
L/b=1	0	3.5841	3.5841	3.5841
	15	3.4053	3.8477	3.9288
	30	1.8816	2.212	2.2747
	45	0.95317	1.1113	1.1412
	60	0.48369	0.53264	0.54154
	75	0.23869	0.24434	0.24532
	90	0.15372	0.15372	0.15372
L/b=2	0	4.8074	4.8074	4.8074
	15	3.5886	4.1608	4.2683
	30	1.7461	2.0875	2.1531
	45	0.87329	1.0181	1.0453
	60	0.46394	0.51024	0.51863
	75	0.23831	0.24393	0.2449
	90	0.15586	0.15586	0.15586

Table (8.20) The variation of the natural frequencies of unstiffened plate with the stacking sequence using conforming element.

Aspect Ratio	fibre angle	symmetric composite			asymmetric composite		
		mode1	mode2	mode3	mode1	mode2	mode3
L/b = 1	0	5.6189	6.1632	9.6272	5.6189	6.1632	9.6272
	15	5.1687	7.2284	12.07	5.18	7.2899	12.161
	30	4.0374	8.532	14.657	4.0644	8.6661	14.818
	45	2.6063	8.7835	12.503	2.6288	8.9569	12.653
	60	1.515	7.6562	8.4677	1.5243	7.8413	8.531
	75	1.058	5.1746	6.3491	1.0586	5.3109	6.3539
	90	1.0036	2.8924	6.0771	1.0036	2.8924	6.0771
L/b = 2	0	1.5398	2.1084	5.4717	1.5398	2.1084	5.4717
	15	1.3787	3.0711	7.1811	1.387	3.105	7.1654
	30	0.97636	3.9937	5.2738	0.98621	4.0696	5.3176
	45	0.5752	3.3463	4.2311	0.58092	3.3861	4.3142
	60	0.34403	2.1026	3.0021	0.34597	2.117	2.9969
	75	0.26181	1.6218	2.4874	0.26194	1.6228	2.4858
	90	0.25204	1.3007	1.5648	0.25204	1.3007	1.5648

Table (8.21) The variation of the natural frequencies of unstiffened plate with the stacking sequence using non-conforming element.

Aspect Ratio	fibre angle	symmetric composite			asymmetric composite		
		mode1	mode2	mode3	mode1	mode2	mode3
L/b = 1	0	5.6163	6.1547	9.5747	5.6163	6.1547	9.5747
	15	5.1614	7.2081	12.036	5.1712	7.2709	12.128
	30	4.0228	8.5217	14.712	4.0499	8.6563	14.872
	45	2.5958	8.781	12.609	2.6188	8.9551	12.751
	60	1.5102	7.6571	8.5194	1.5197	7.8419	8.5805
	75	1.0569	5.1763	6.3592	1.0576	5.3126	6.364
	90	1.0036	2.8934	6.0774	1.0036	2.8934	6.0774
L/b = 2	0	1.5397	2.1086	5.4717	1.5397	2.1086	5.4717
	15	1.3777	3.0702	7.2099	1.3861	3.1041	7.1911
	30	0.97432	3.9922	5.2968	0.98443	4.0682	5.3379
	45	0.57408	3.3562	4.2308	0.57997	3.3952	4.3143
	60	0.34342	2.1058	3.0021	0.34542	2.12	2.9969
	75	0.26164	1.6221	2.4874	0.26177	1.6231	2.4858
	90	0.25203	1.3008	1.5648	0.25203	1.3008	1.5648

Table (8.22) The variation of the natural frequencies of stiffened plate with the stacking sequence using non-conforming element.

aspect ratio	fibre angle	symmetric composite			asymmetric composite		
		mode1	mode2	mode3	mode1	mode2	mode3
L/b = 1	0	2.2225	2.3052	2.9664	2.2225	2.3052	2.9664
	15	2.4766	2.8155	3.8225	2.4734	2.8201	3.839
	30	2.002	2.9259	4.6377	1.9982	2.947	4.6815
	45	1.4258	2.7922	4.9127	1.419	2.8329	4.9026
	60	0.96811	2.3495	3.371	0.96209	2.397	3.3667
	75	0.63786	1.6018	2.6722	0.63704	1.6383	2.6689
	90	0.50007	0.95765	2.0984	0.50007	0.95765	2.0984
L/b = 2	0	0.67794	0.78249	1.5015	0.67794	0.78249	1.5015
	15	0.66444	1.0299	2.2654	0.66306	1.0324	2.2687
	30	0.49008	1.2216	2.2468	0.48906	1.2385	2.2404
	45	0.34249	1.198	1.3634	0.3408	1.2163	1.3703
	60	0.23669	0.90142	1.091	0.23512	0.90282	1.1183
	75	0.15966	0.69421	0.8011	0.15945	0.70812	0.8077
	90	0.12669	0.40642	0.68853	0.12669	0.40642	0.68853

Table (8.23) The variation of the stability parameter of unstiffened plate with the stacking sequence at different fibre angles.

Aspect Ratio	fibre angle	symmetric composite		asymmetric composite	
		Conf.	non-conf.	Conf.	non-conf.
L/b = 1	0	2.1149	2.1118	2.1149	2.1118
	15	1.7203	1.7183	1.7094	1.7079
	30	0.94312	0.93989	0.93235	0.92968
	45	0.35433	0.35298	0.3536	0.35243
	60	0.1204	0.12	0.12104	0.12069
	75	6.64E-02	6.64E-02	6.65E-02	6.64E-02
	90	6.12E-02	6.12E-02	6.12E-02	6.12E-02
L/b = 2	0	2.3669	2.3666	2.3669	2.3666
	15	1.8226	1.8224	1.8111	1.8115
	30	0.80622	0.80508	0.79767	0.79699
	45	0.25417	0.25383	0.2534	0.25318
	60	9.97E-02	9.95E-02	9.99E-02	9.98E-02
	75	6.52E-02	6.52E-02	6.52E-02	6.52E-02
	90	6.15E-02	6.15E-02	6.15E-02	6.15E-02

Table (8.24) The variation of the stability parameter of stiffened plate with the stacking sequence at different fibre angles.

Aspect Ratio	Fibre Angle	symmetric composite	asymmetric composite
L/b=1	0	3.5841	3.5841
	15	3.9334	3.8477
	30	2.2924	2.212
	45	1.1544	1.1113
	60	0.54663	0.53264
	75	0.24598	0.24434
	90	0.15372	0.15372
L/b=2	0	4.8074	4.8074
	15	4.2928	4.1608
	30	2.1787	2.0875
	45	1.0595	1.0181
	60	0.52396	0.51024
	75	0.24559	0.24393
	90	0.15586	0.15586

Table (8.25) Maximum stress along the local x-direction σ_x for carbon/epoxy case study.

			Finite element	ABAQUS
aspect ratio	L/b = 1	Max. stress [MPa]	3.868	3.875
		Node number	41	41
	L/b = 2	Max. stress [MPa]	3.796	3.804
		Node number	82	82

Table (8.26) Maximum stress along the local x-direction σ_x for glass/epoxy case study.

			Finite element	ABAQUS
aspect ratio	L/b = 1	Max. stress [MPa]	5.333	5.346
		Node number	41	41
	L/b = 2	Max. stress [MPa]	5.222	5.233
		Node number	72	72

Table (8.27) Maximum stress along the fibre and matrix directions for carbon/epoxy case study.

			Max. stress [MPa]	Layer No.	Element No.
aspect ratio	L/b = 1	Fibre	3.866	1,4,9,12	28
		Matrix	0.3164	2,6,7,11	44
	L/b = 2	Fibre	3.799	1,4,9,12	100
		Matrix	0.3141	2,6,7,11	122

Table (8.28) Maximum stress along the fibre and matrix directions for glass/epoxy case study.

			Max. stress [MPa]	Layer No.	Element No.
aspect ratio	L/b = 1	Fibre	5.332	1,4,9,12	28
		Matrix	1.201	2,6,7,11	44
	L/b = 2	Fibre	5.226	1,4,9,12	100
		Matrix	1.188	2,6,7,11	117

Table (8.29) Mean and alternating stresses along the fibre and matrix direction for carbon/epoxy case study.

			Mean stress [MPa]	Alternating stress [MPa]
aspect ratio	L/b = 1	Fibre	96.65	96.65
		Matrix	7.91	7.91
	L/b = 2	Fibre	94.99	94.99
		Matrix	7.852	7.852

Table (8.30) Mean and alternating stresses along the fibre and matrix direction for glass/epoxy case study.

			Mean stress [MPa]	Alternating stress [MPa]
aspect ratio	L/b = 1	Fibre	26.66	26.66
		Matrix	6.003	6.003
	L/b = 2	Fibre	26.13	26.13
		Matrix	5.939	5.939

Table (8.31) Failure stresses and the corresponding number of cycles for carbon/epoxy.

			Failure stress [MPa]	Number of cycles
aspect ratio	L/b = 1	Fibre	101.3	$1.5x10^{11}$
		Matrix	8.75	$2.61x10^{6}$
	L/b = 2	Fibre	99.48	$1.79x10^{11}$
		Matrix	8.678	$2.86x10^{6}$

Table (8.32) Failure stresses and the corresponding number of cycles for glass/epoxy.

			Failure stress [MPa]	Number of cycles
aspect ratio	L/b = 1	Fibre	27.33	$1.4x10^{17}$
		Matrix	7.096	$1.41x10^{5}$
	L/b = 2	Fibre	26.78	$1.95x10^{17}$
		Matrix	7.005	$1.57x10^{5}$

Table (8.33) Number of cycles to failure for different case studies.

Case study	Number of cycles to failures
Square carbon/epoxy	2.6×10^{6} [cycle]
Square glass/epoxy	1.41×10^{5} [cycle]
Rectangular carbon/epoxy	2.86×10^{6} [cycle]
Rectangular glass/epoxy	1.57×10^{5} [cycle]

Table (8.34) Number of damaged elements per plies at iteration number one.

Layer number	Element number								
2, 6, 8, 12	9	10	11	12	13	14			
	21	22	23	24	25	26	27	28	
	35	36	37	38	39	40	41	42	
	48	49	50	51	52	53	54	55	56
	62	63	64	65	66	67	68	69	70
	76	77	78	79	80	81	82		
	93	107	108						
3, 11	8	9	10	11	12				

Table (8.35) Number of damaged elements per plies at iteration number 23.

Layer number	Element number								
1, 4, 7, 10	35								
2, 6, 8, 12	9	10	11	12	13	14			
	21	22	23	24	25	26	27	28	
	35	36	37	38	39	40	41	42	
	48	49	50	51	52	53	54	55	56
	62	63	64	65	66	67	68	69	70
	76	77	78	79	80	81	82		
	91	92	93	94					
	105	106	107	108	119				
3	9	10	11						
11	8	9	10	11	12				

Table (8.36) Strain energy, work done by external force and energy release rate as a function of the damaged areas.

Damaged area [mm^2]	Strain energy [N.mm]	Work done [N.mm]	Energy release rate [N/mm]
1742.689	3416.290887	6832.582	23448.42
1822.111	3424.242278	6848.485	42271.99
2087.422	3441.535654	6883.071	105152.6
2208.083	3446.166735	6892.333	133750
2362.077	3474.718671	6949.437	170247.7
2506.728	3506.780616	7013.561	204531
2530.304	3510.841006	7021.682	210118.8
2559.67	3521.871341	7043.743	217078.6
2583.959	3529.234569	7058.469	222835.2
2683.959	3539.458268	7078.917	246535.9
2780.256	3564.915991	7129.832	269359.1
2813.136	3580.284328	7160.569	277151.9

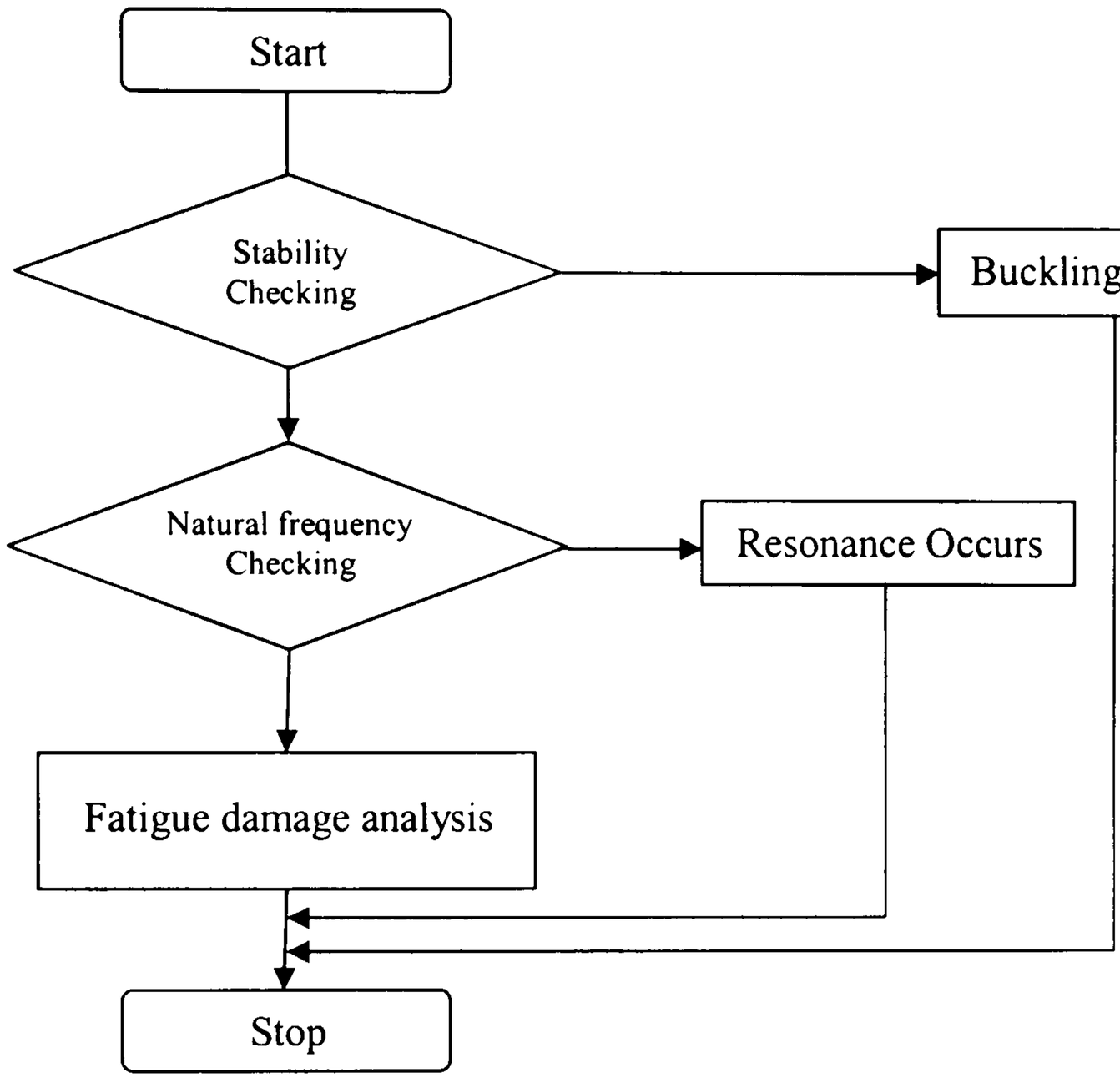

Figure (8.1) Flowchart of damage assessment.

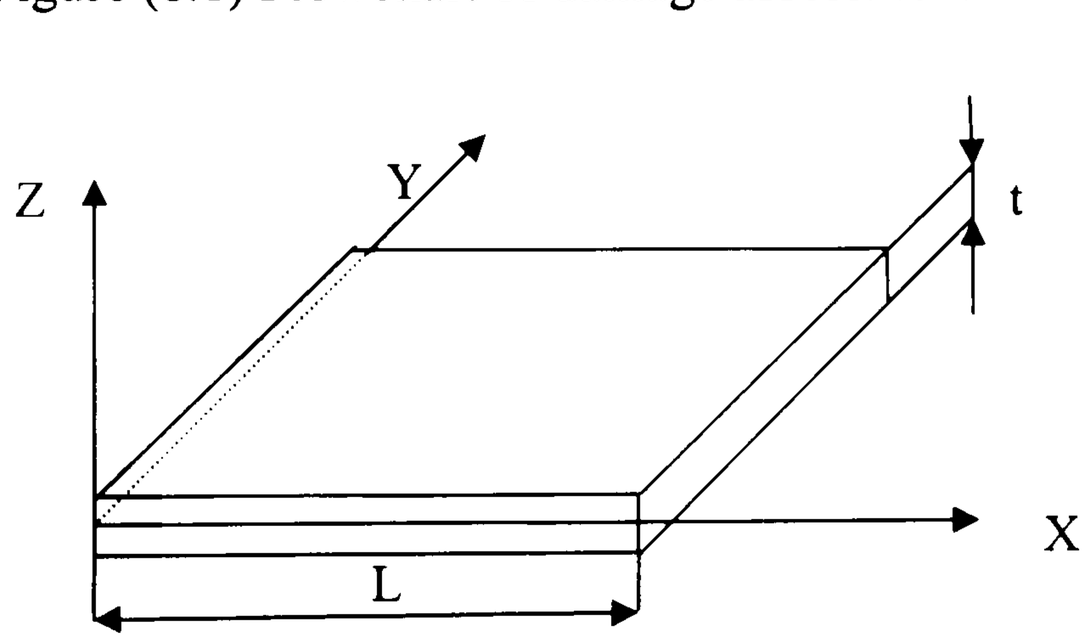

(c) Plate geometry.

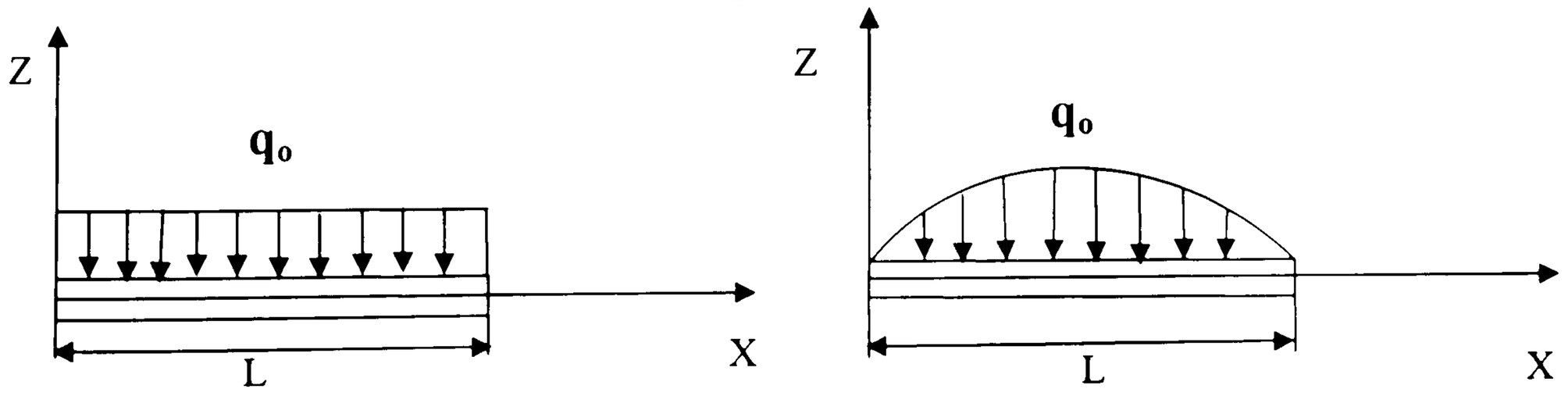

(a) Uniform load.

(b) Sinusoidal load.

Figure (8.2) Square plate under two different types of loads.

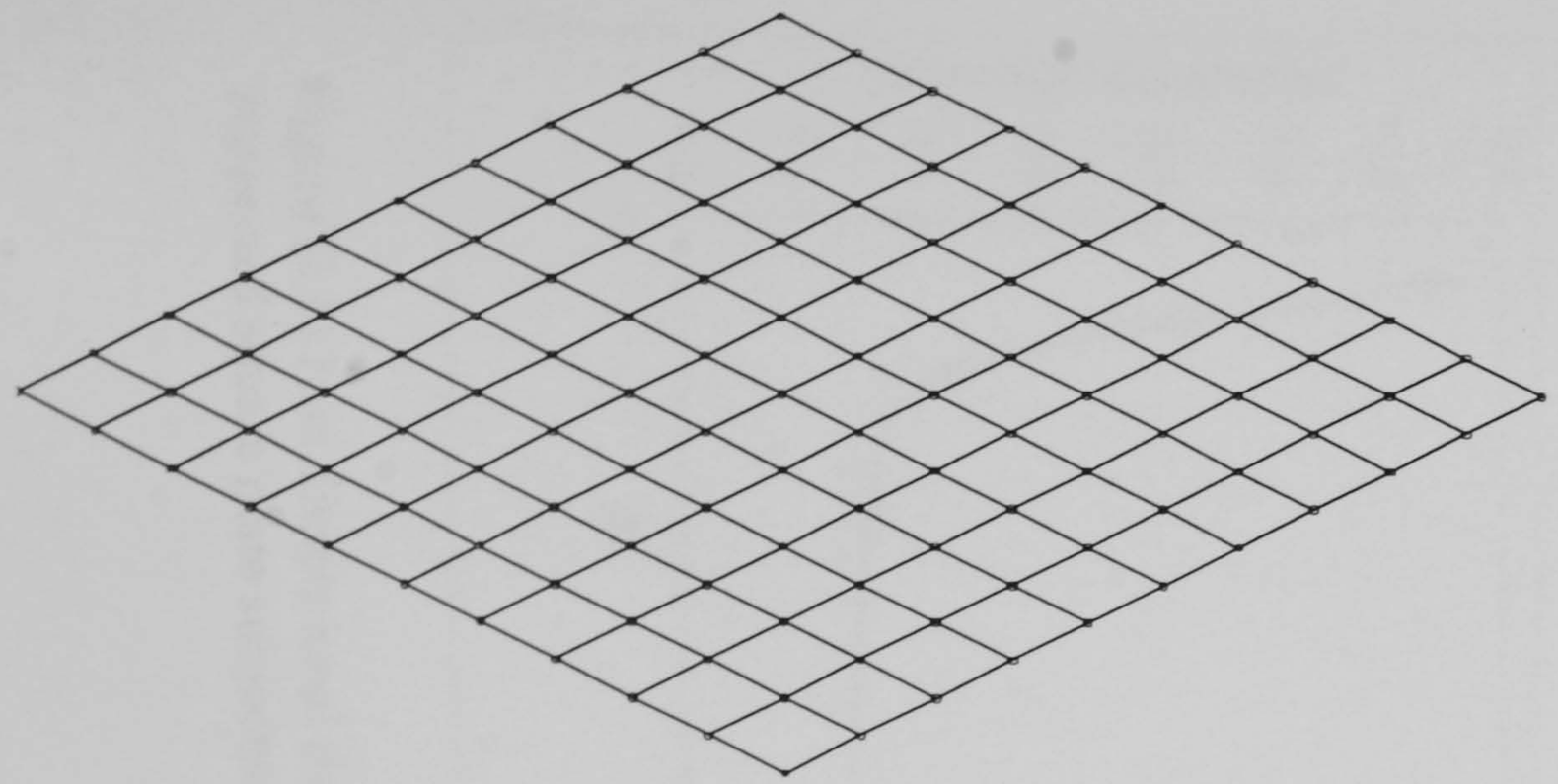

(a) Coarse mesh (c.) with 100 elements.

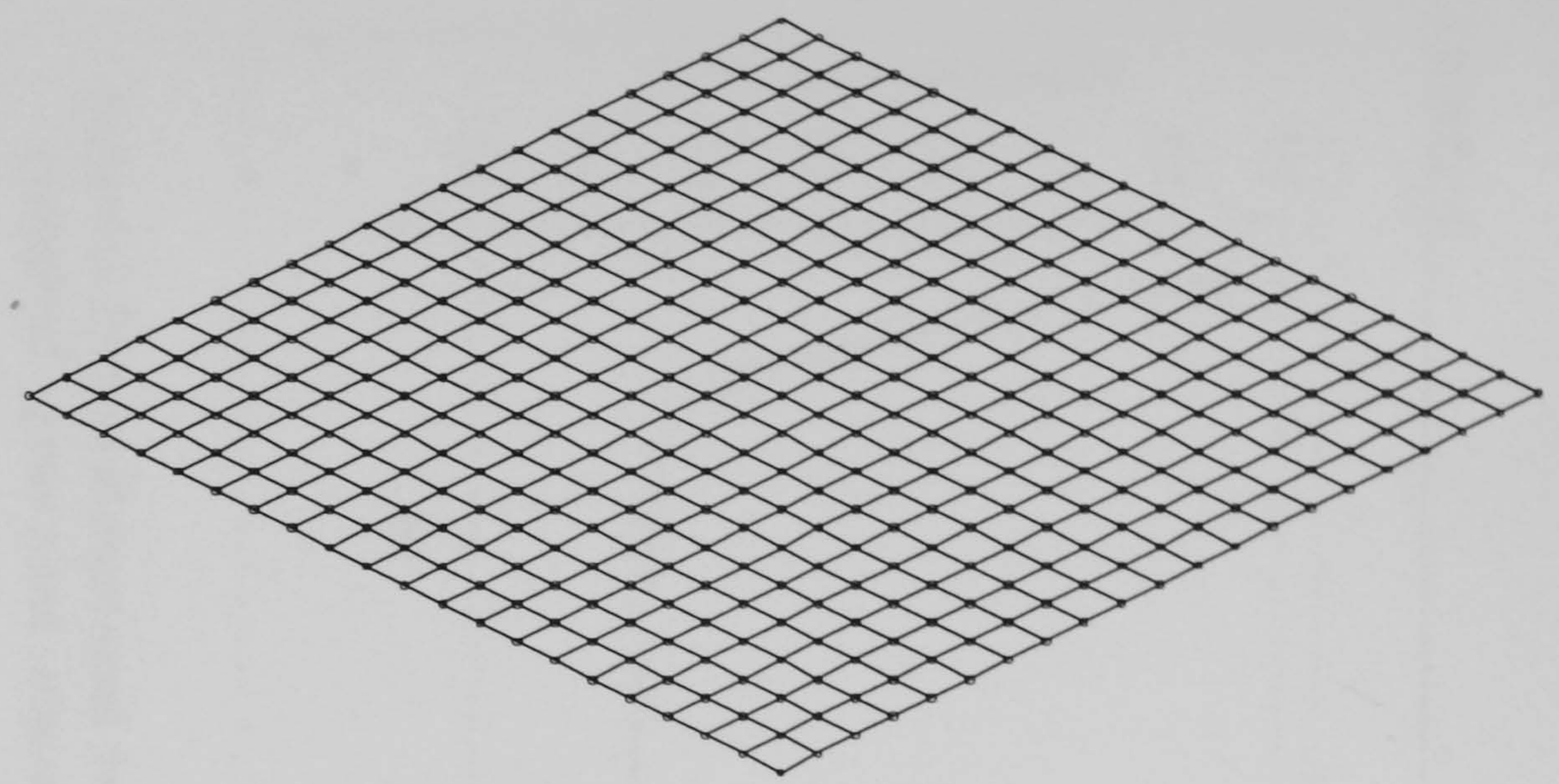

(b) Fine mesh (f.) with 400 elements.

Figure (8.3) Meshes of a square plate with 4-node quadrilateral elements.

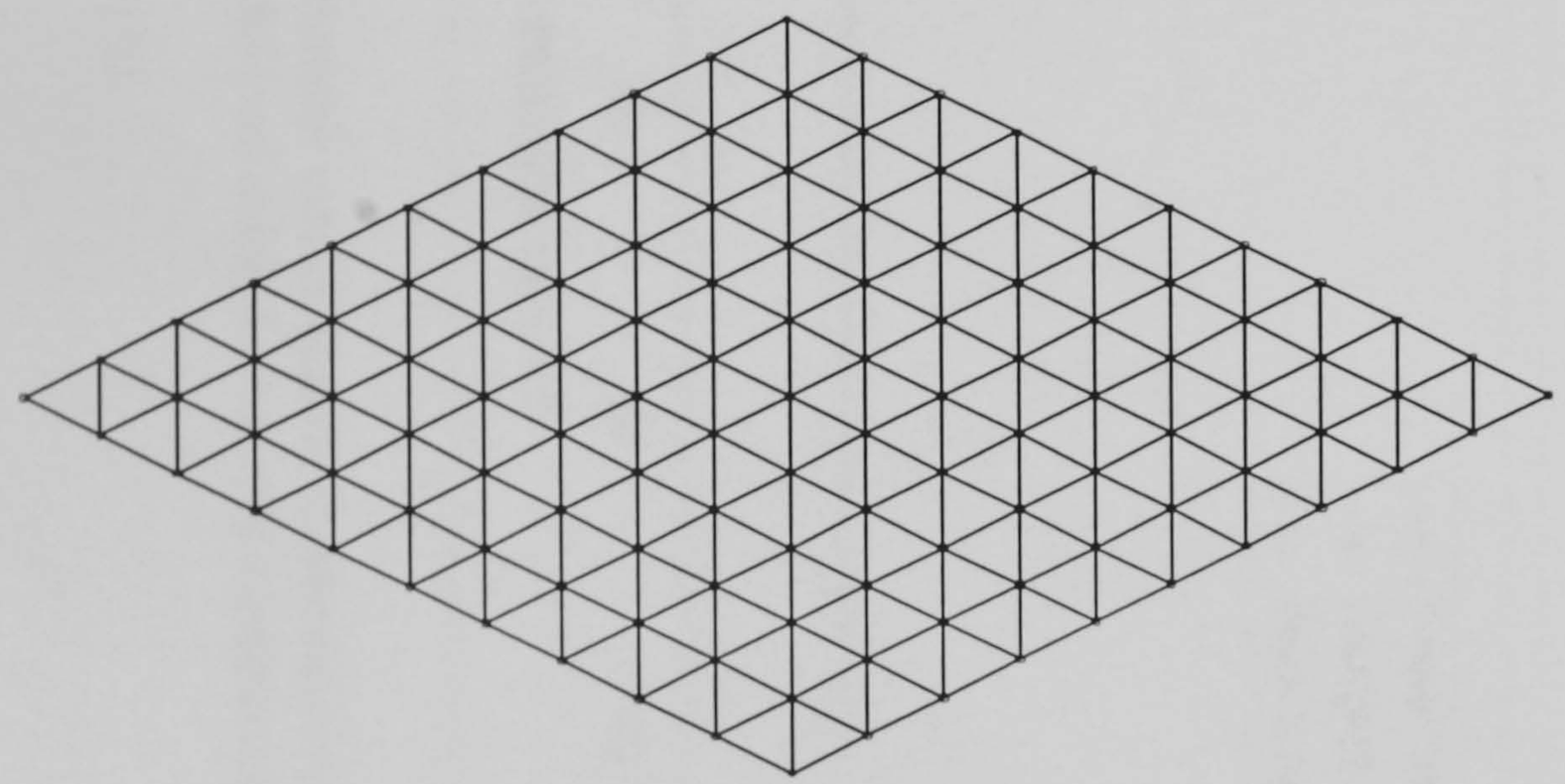

(a) Coarse mesh (c.) with 200 elements.

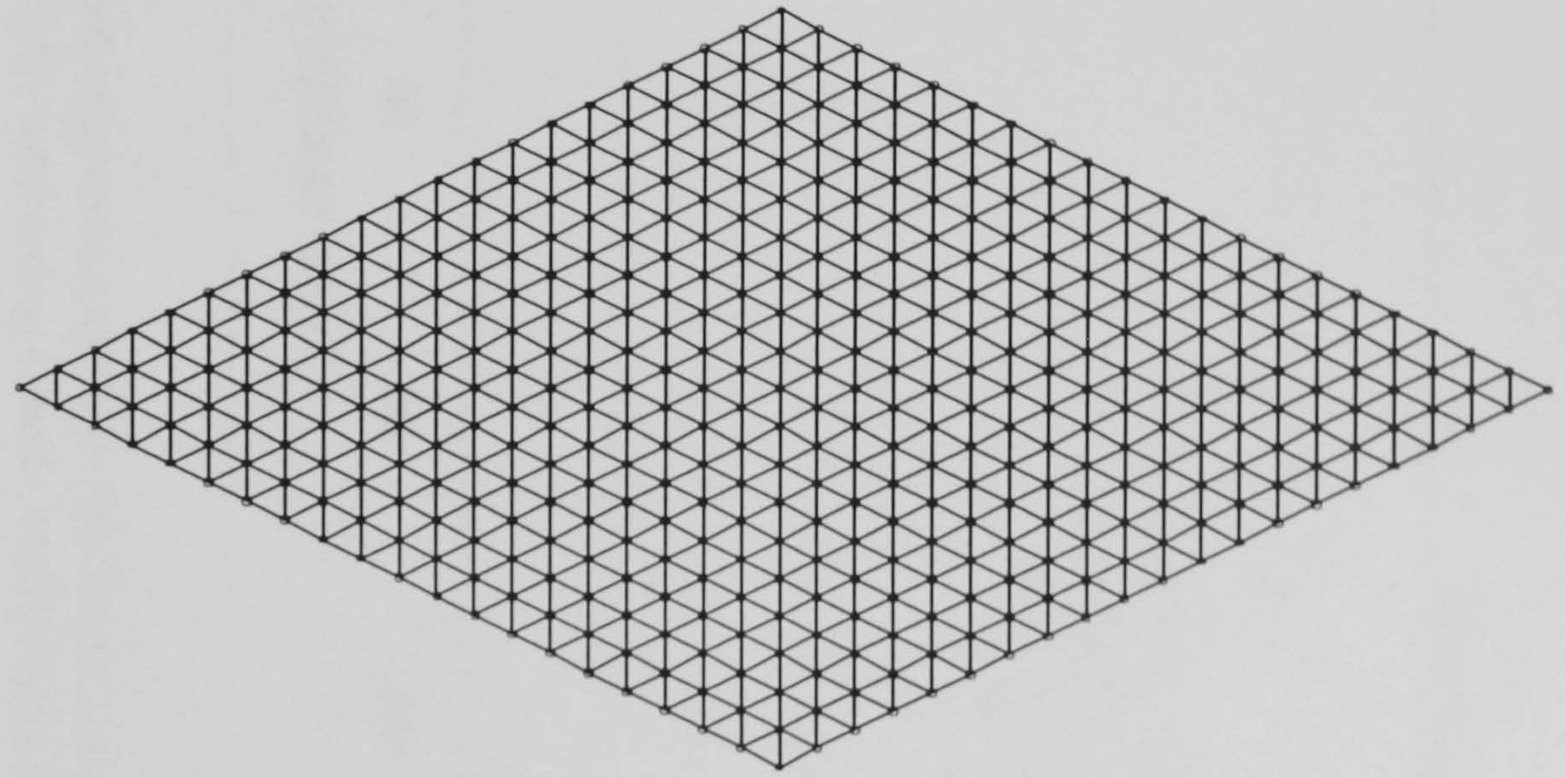

(b) Fine mesh (f.) with 800 elements.

Figure (8.4) Meshes of a square plate with 3-node triangle element.

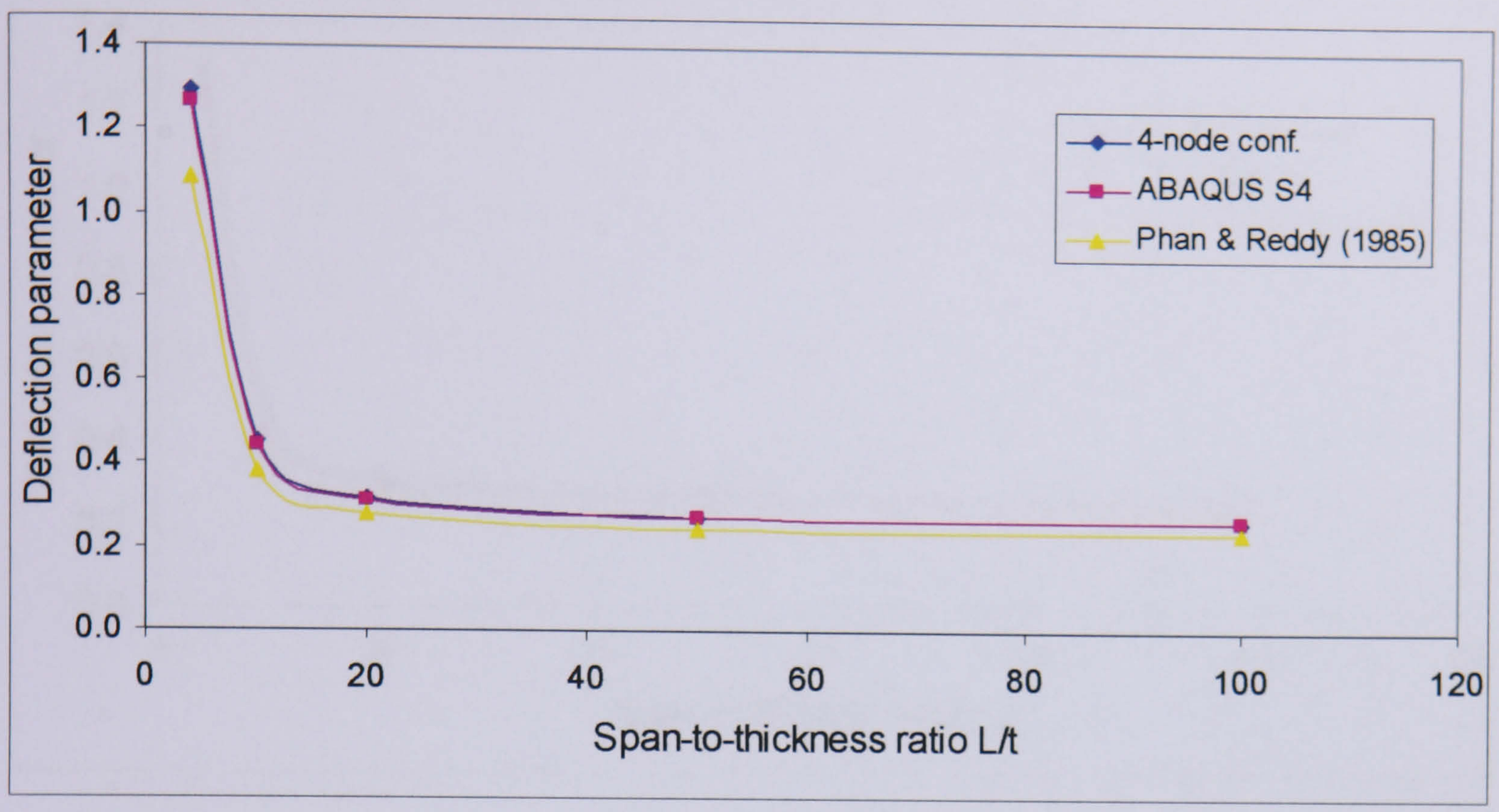

Figure (8.5) Non dimensional deflection parameter versus span-to-thickness ratio of simply supported square plate subjected to sinusoidal load using 4-node conforming element.

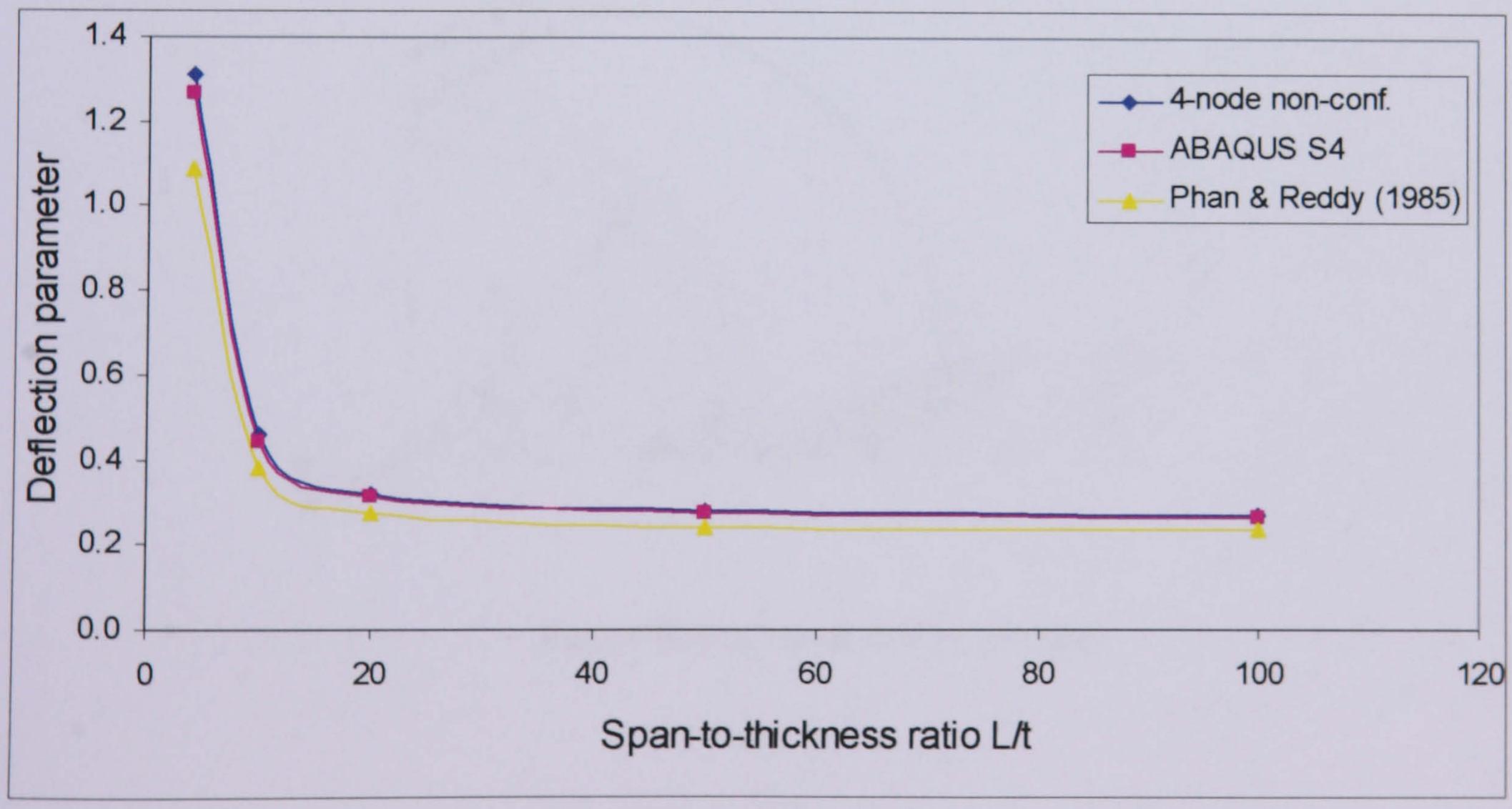

Figure (8.6) Non dimensional deflection parameter versus span-to-thickness ratio of simply supported square plate subjected to sinusoidal load using 4-node non-conforming element.

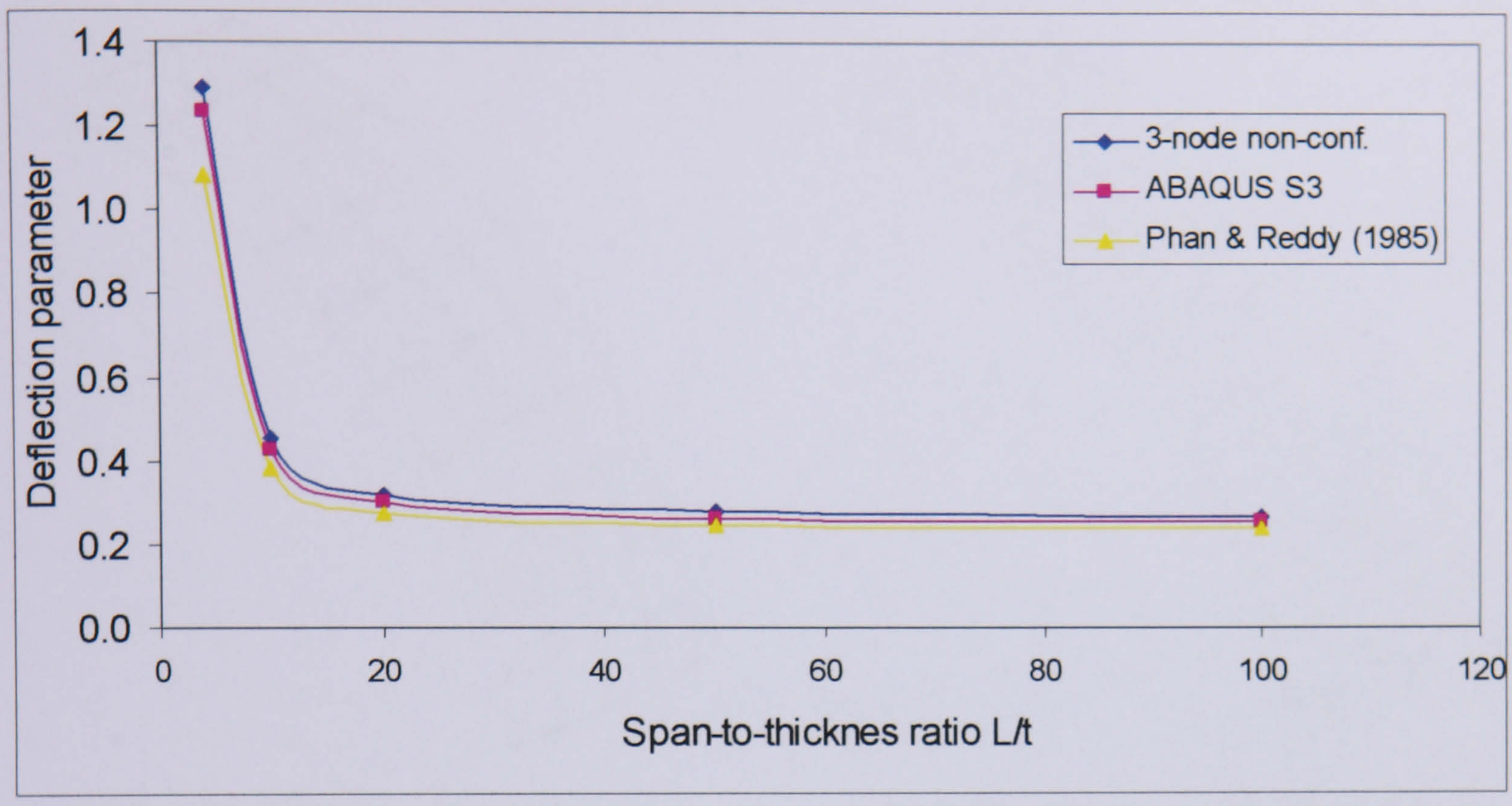

Figure (8.7) Non dimensional deflection parameter versus span-to-thickness ratio of simply supported square plate subjected to sinusoidal load using 3-node non-conforming element.

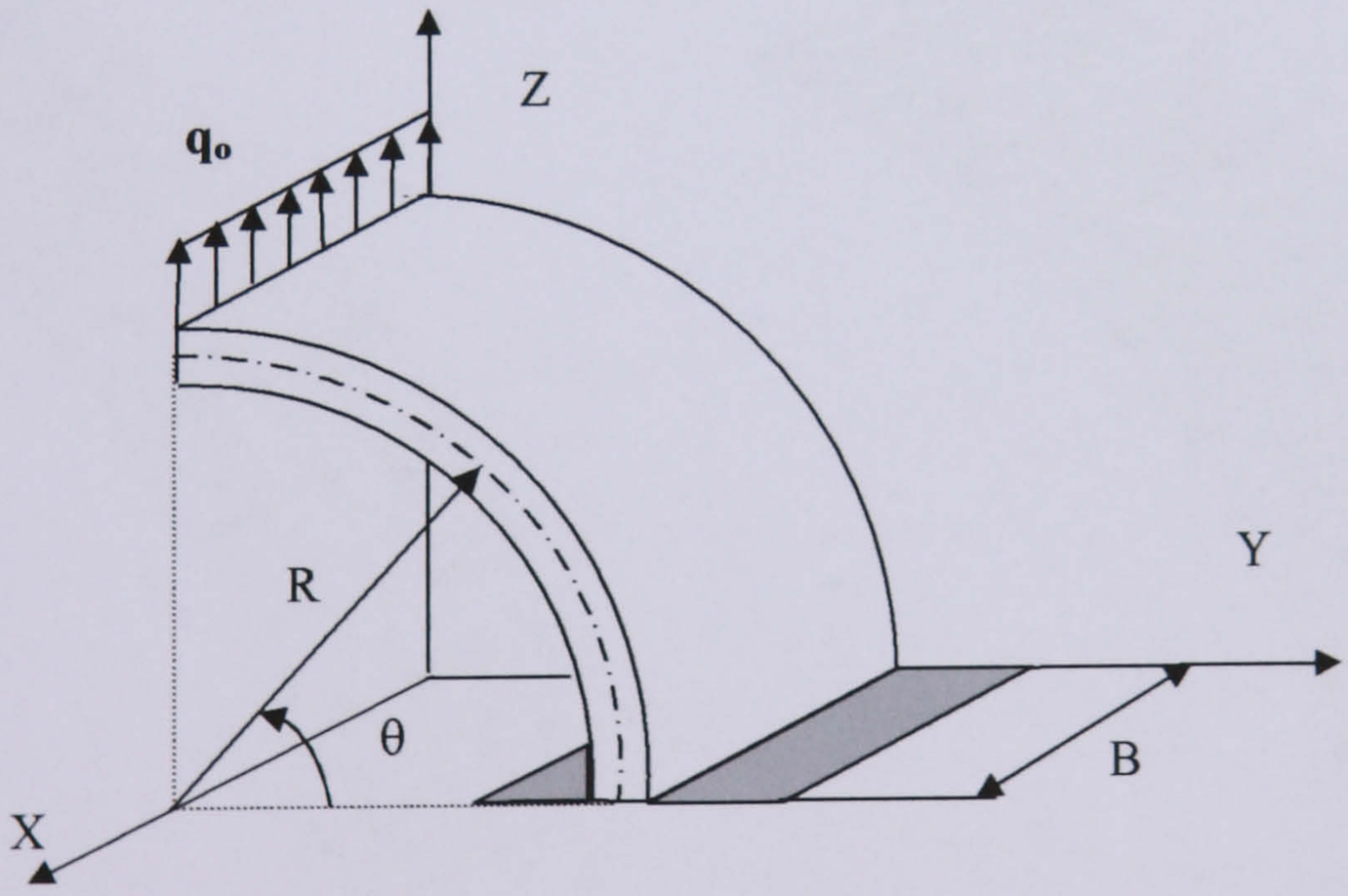

Figure (8.8) Curved shell case study.

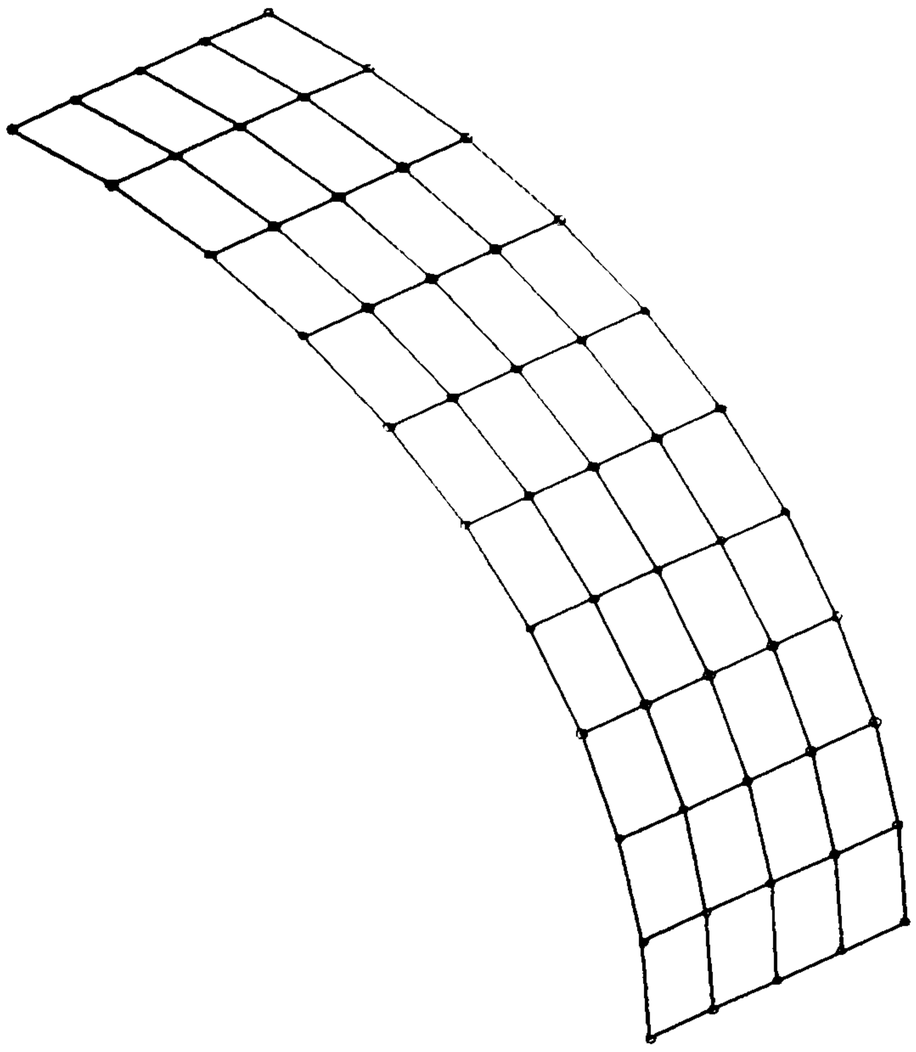

(a) Coarse mesh (c.) with 40 elements.

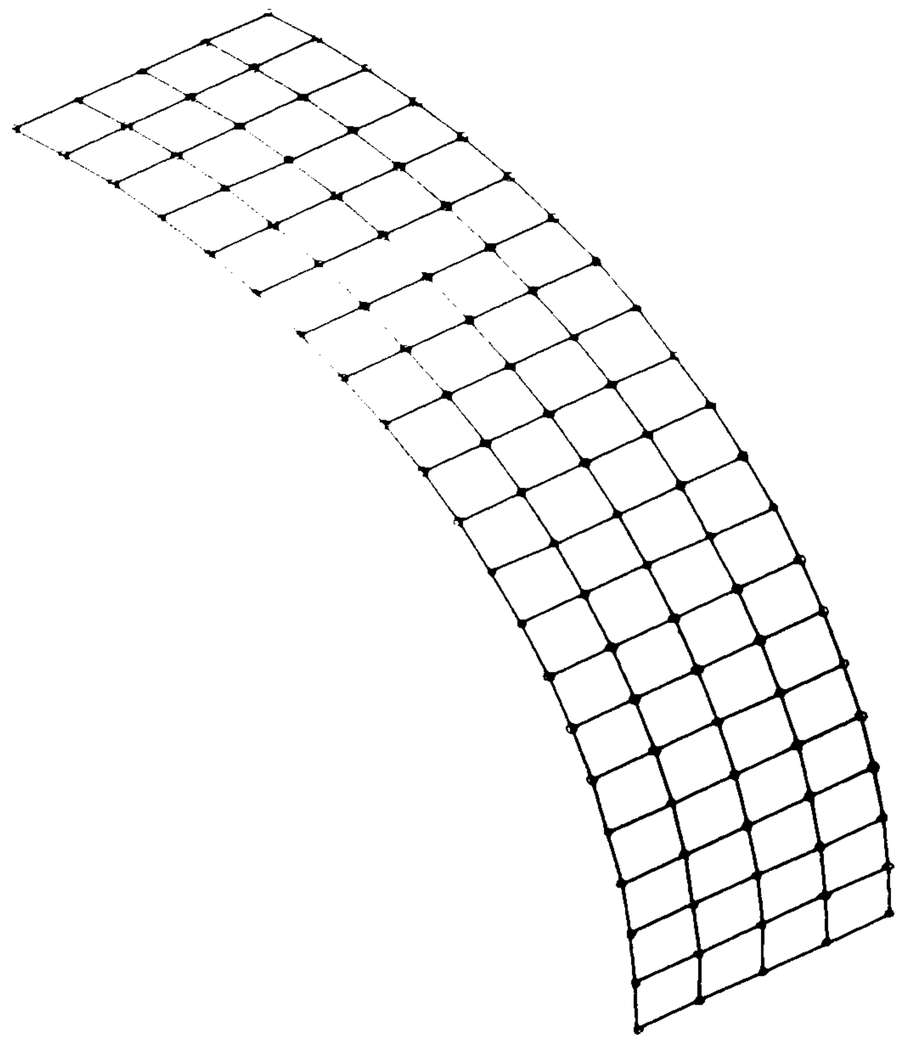

(b) Fine mesh (f.) with 80 elements.

Figure (8.9) Meshes of a curved shell with 4-node quadrilateral elements.

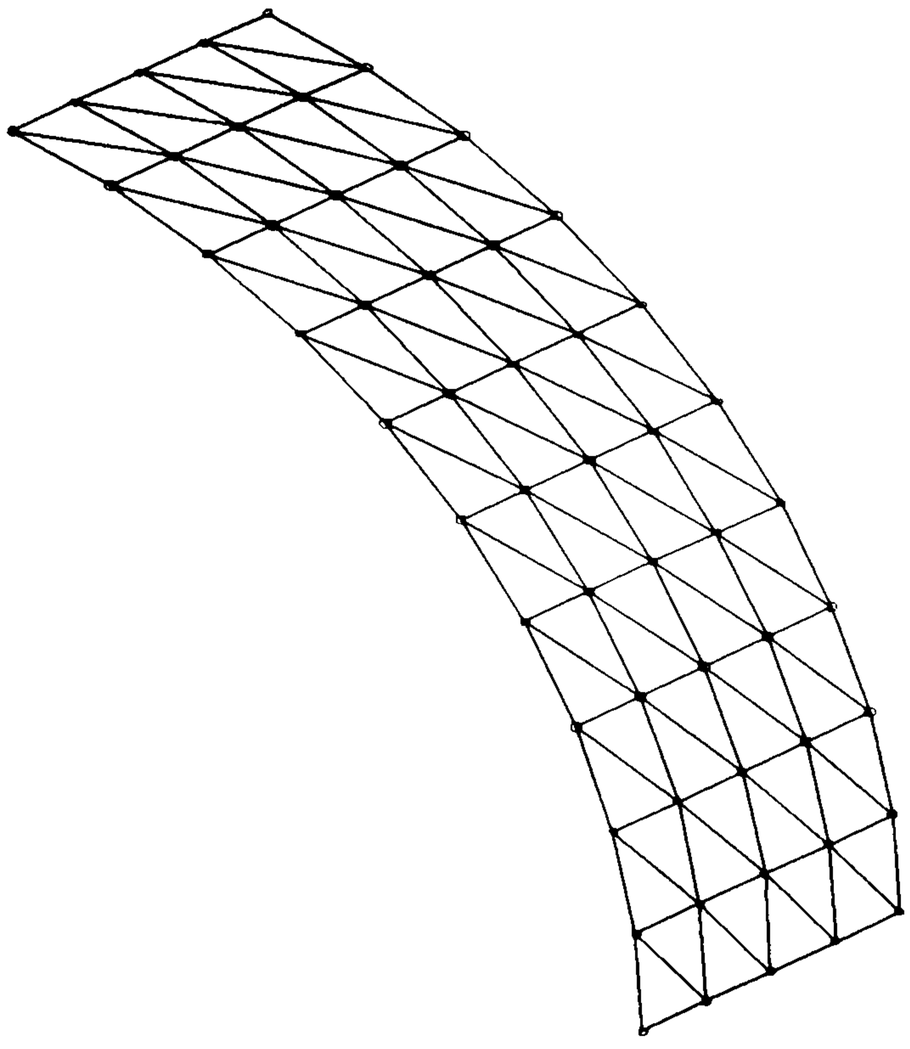

(a) Coarse mesh (c.) with 80 elements.

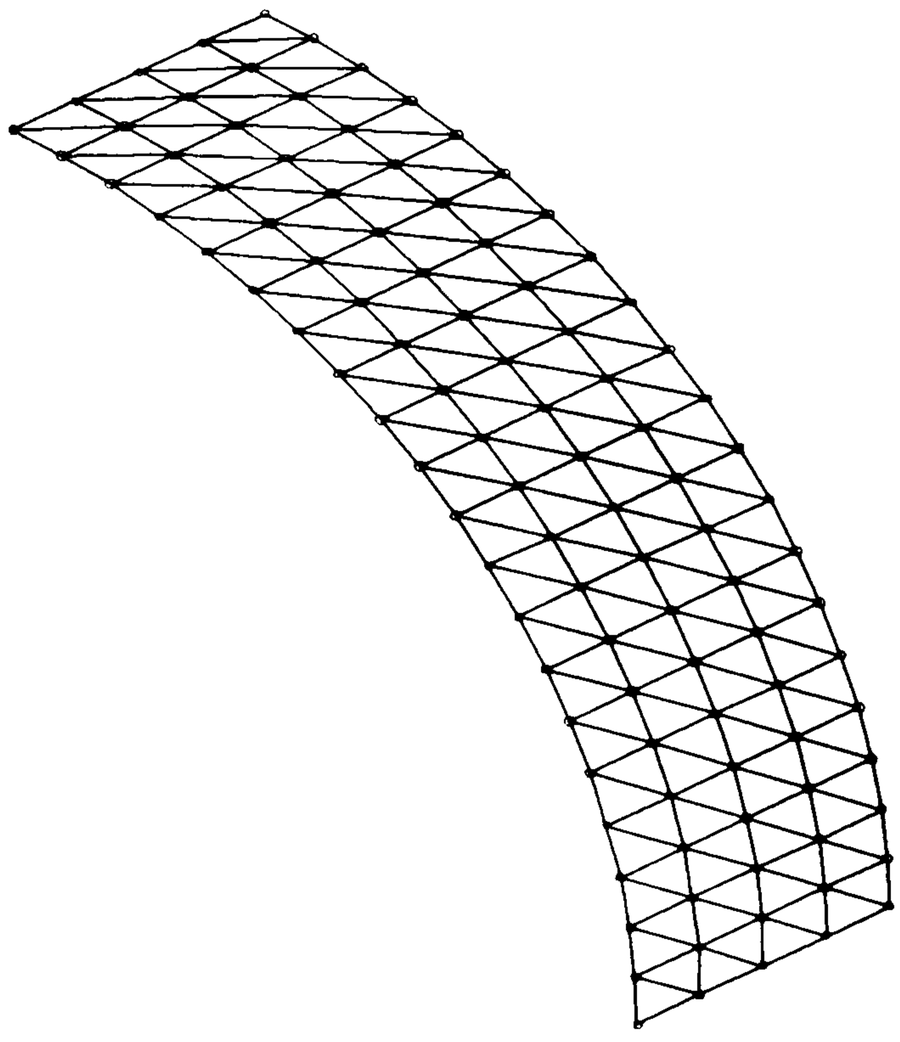

(b) Fine mesh (f.) with 160 elements.

Figure (8.10) Meshes of a curved shell with 3-node triangle elements.

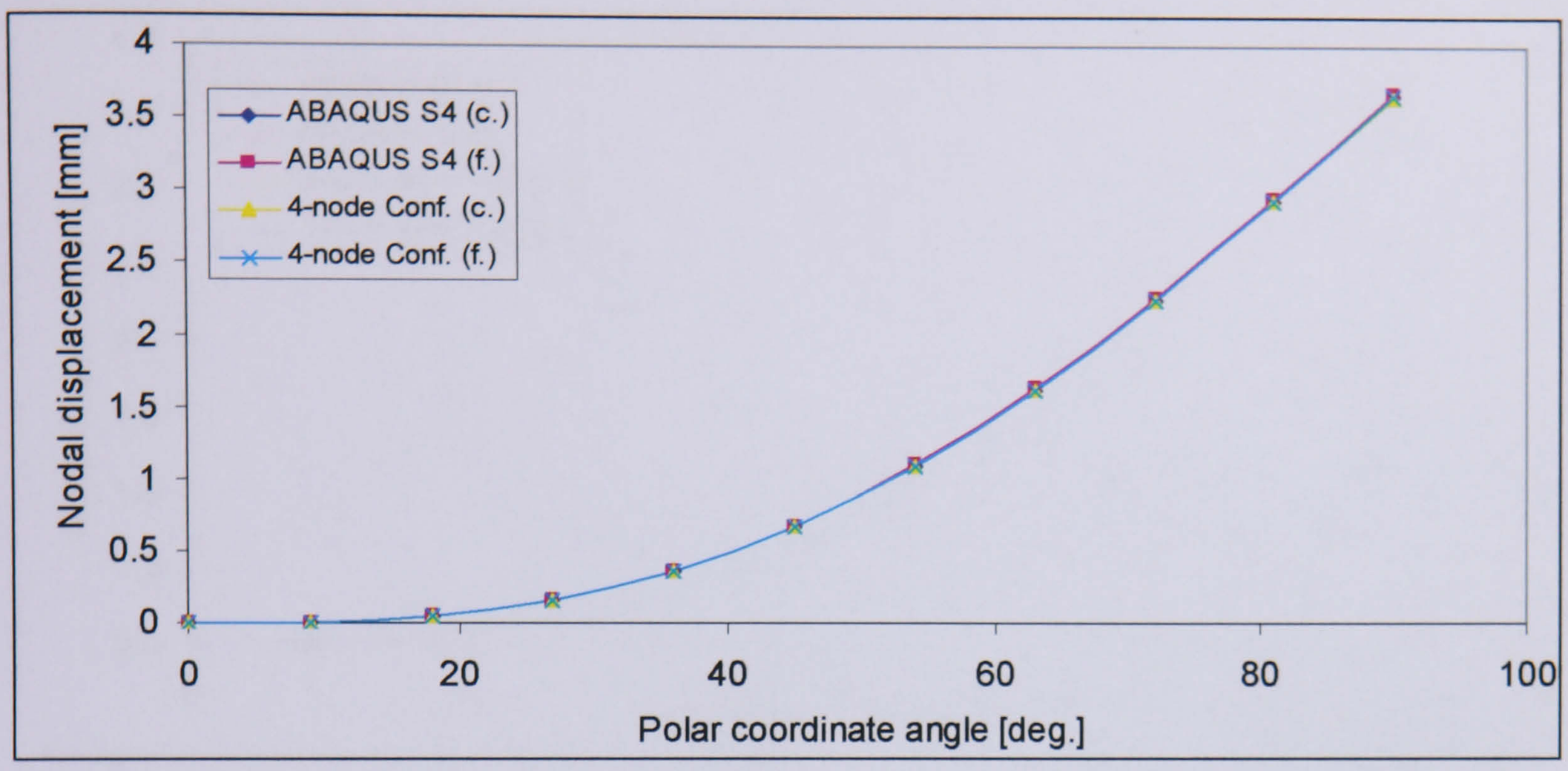

Figure (8.11) Nodal deflection in z-direction versus θ for a clamped-free curved shell subjected to distributed line force using 4-node conforming element.

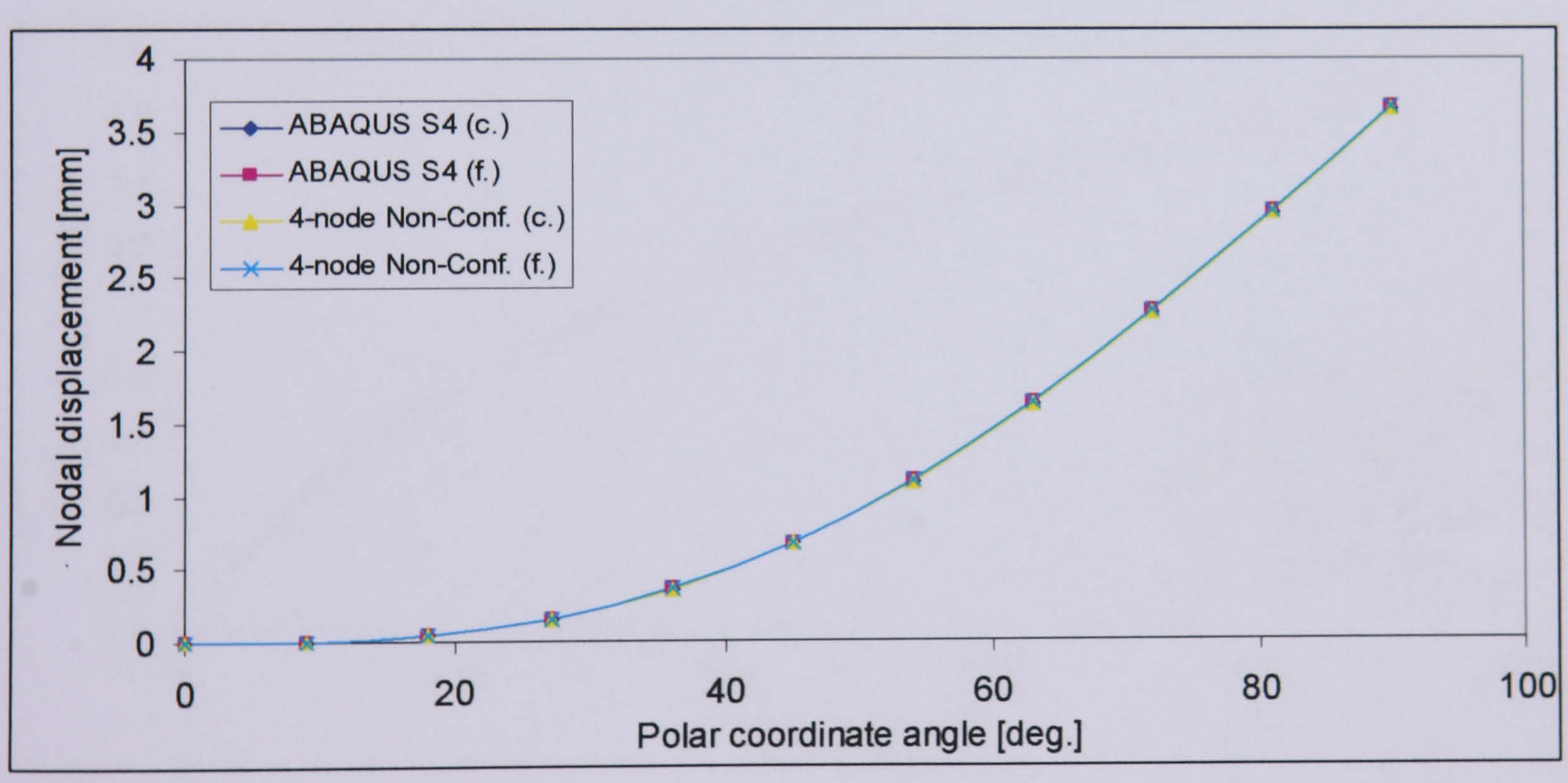

Figure (8.12) Nodal deflection in z-direction versus θ for a clamped-free curved shell subjected to distribute line force using 4-node non-conforming element.

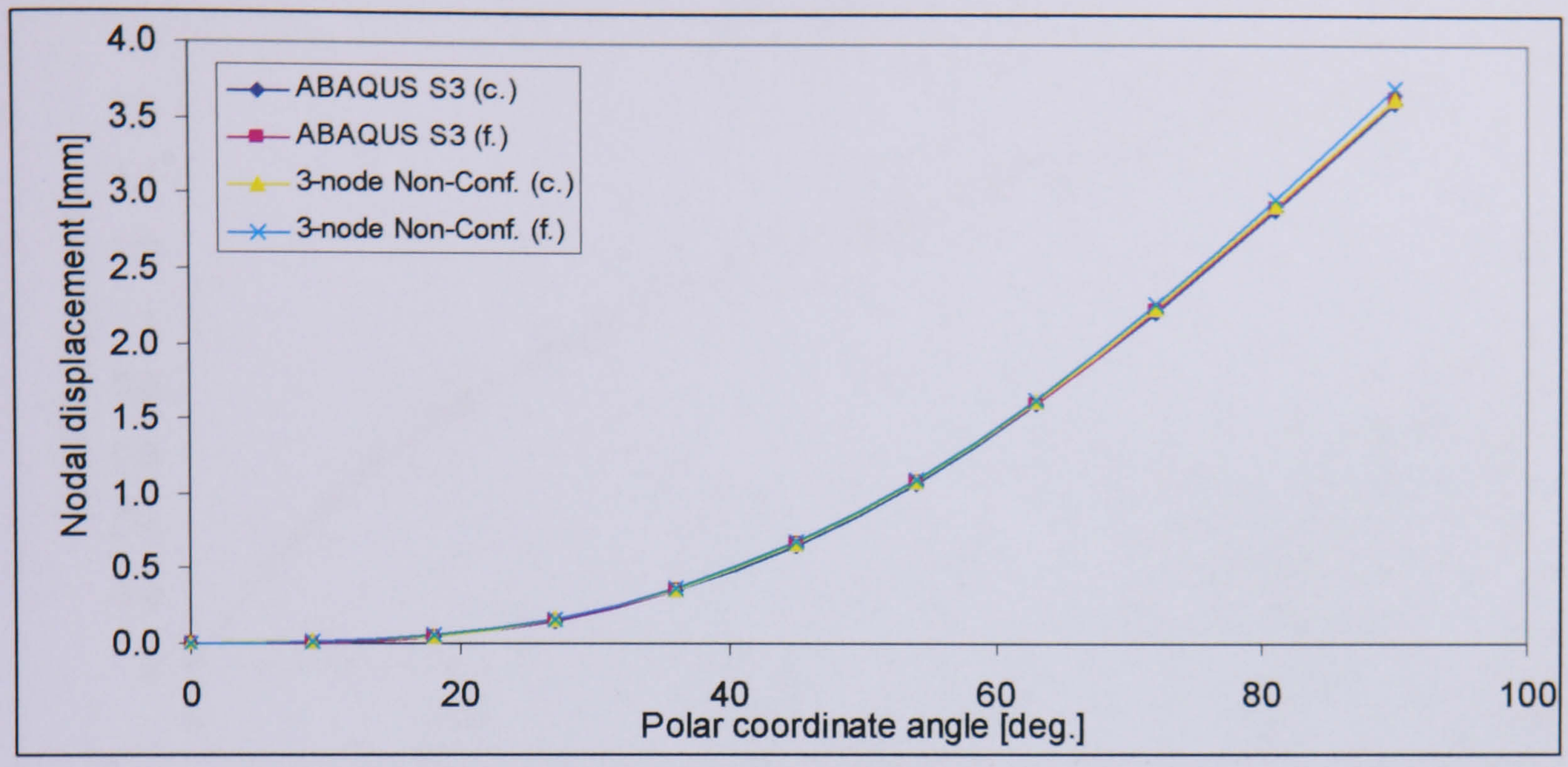

Figure (8.13) Nodal deflection in z-direction versus θ for a clamped-free curved shell subjected to distribute line force using 3-node non-conforming element.

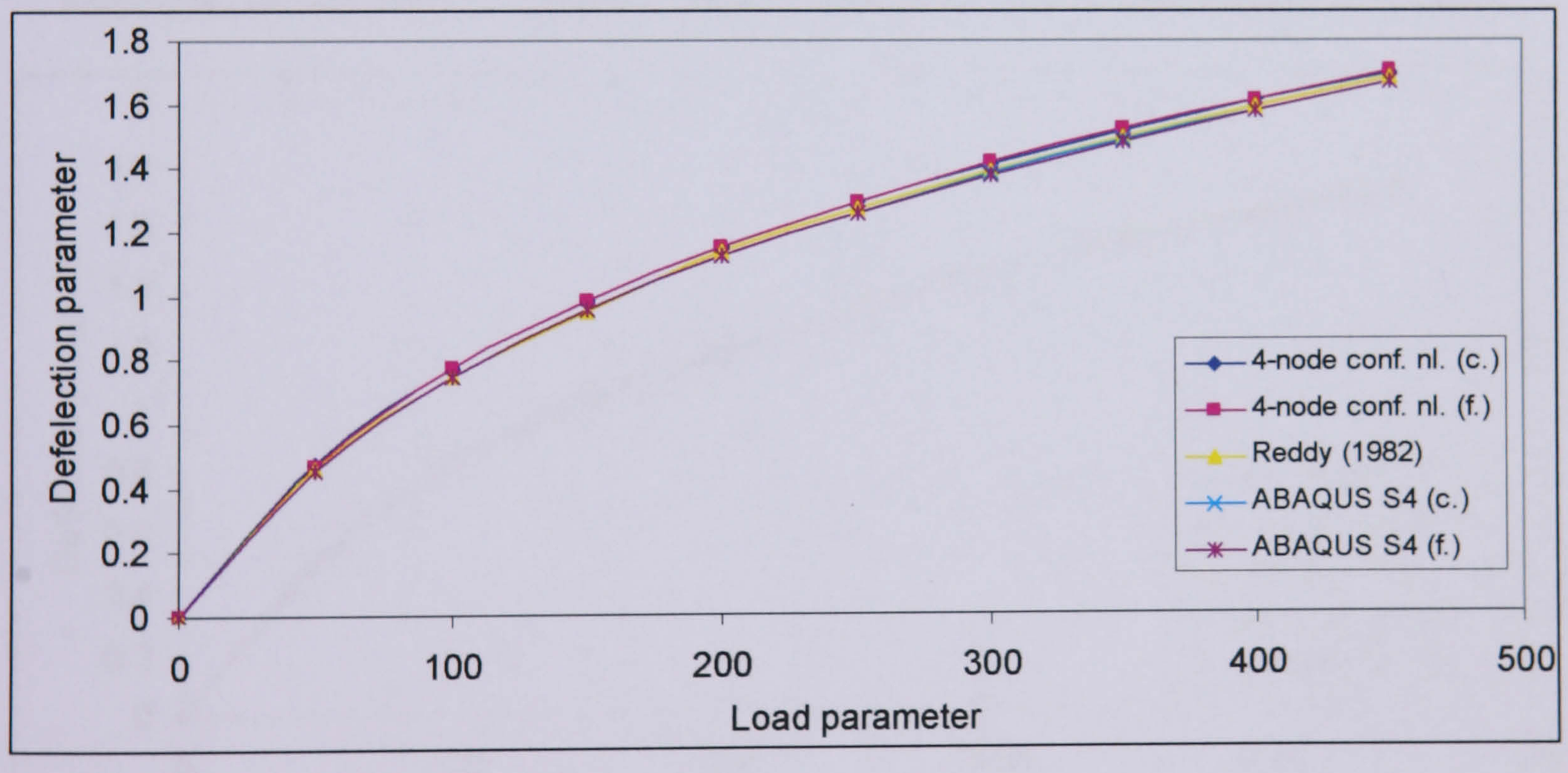

Figure (8.14) Non dimensional deflection parameter $\overline{W}$ history with load parameter $\bar{q}$ of the angle-ply [45°/-45°/45°/-45°] clamped square plate using 4-node conforming element.

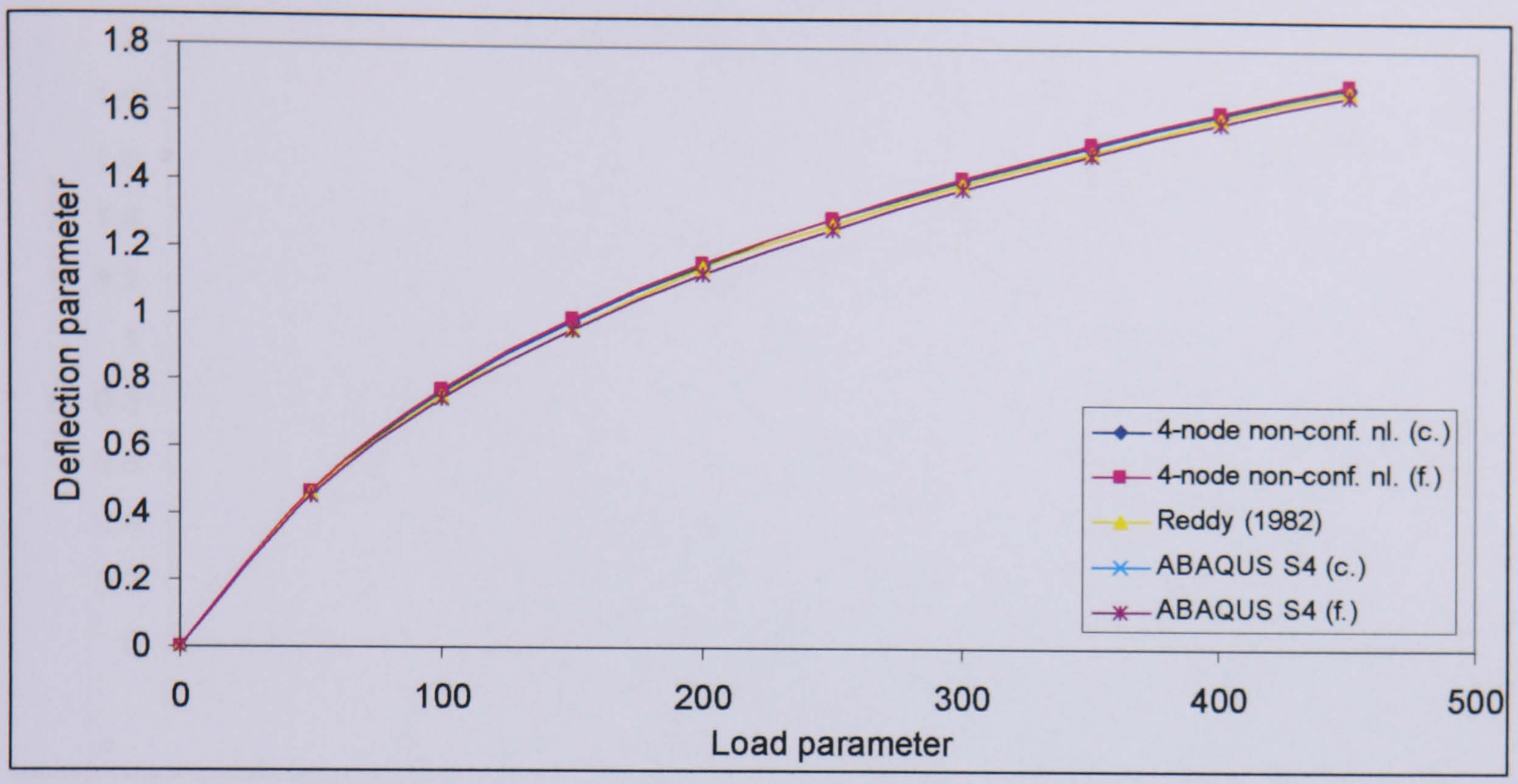

Figure (8.15) Non dimensional deflection parameter $\overline{W}$ history with load parameter $\bar{q}$ of the angle-ply [45°/-45°/45°/-45°] clamped square plate using 4-node non-conforming element.

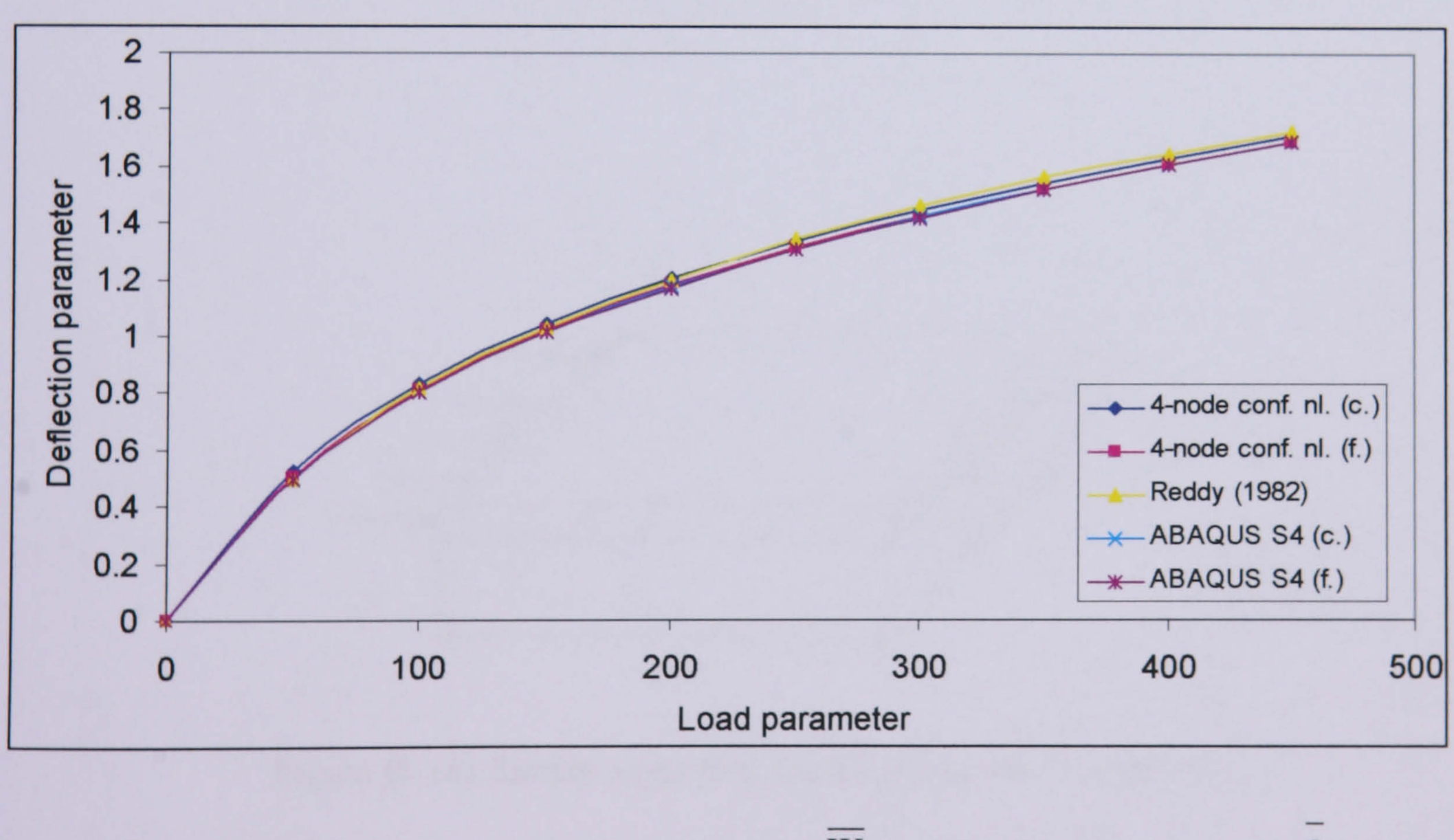

Figure (8.16) Non dimensional deflection parameter $\overline{W}$ history with load parameter $\bar{q}$ of the cross-ply [0°/90°/0°/90°] clamped square plate using 4-node conforming element.

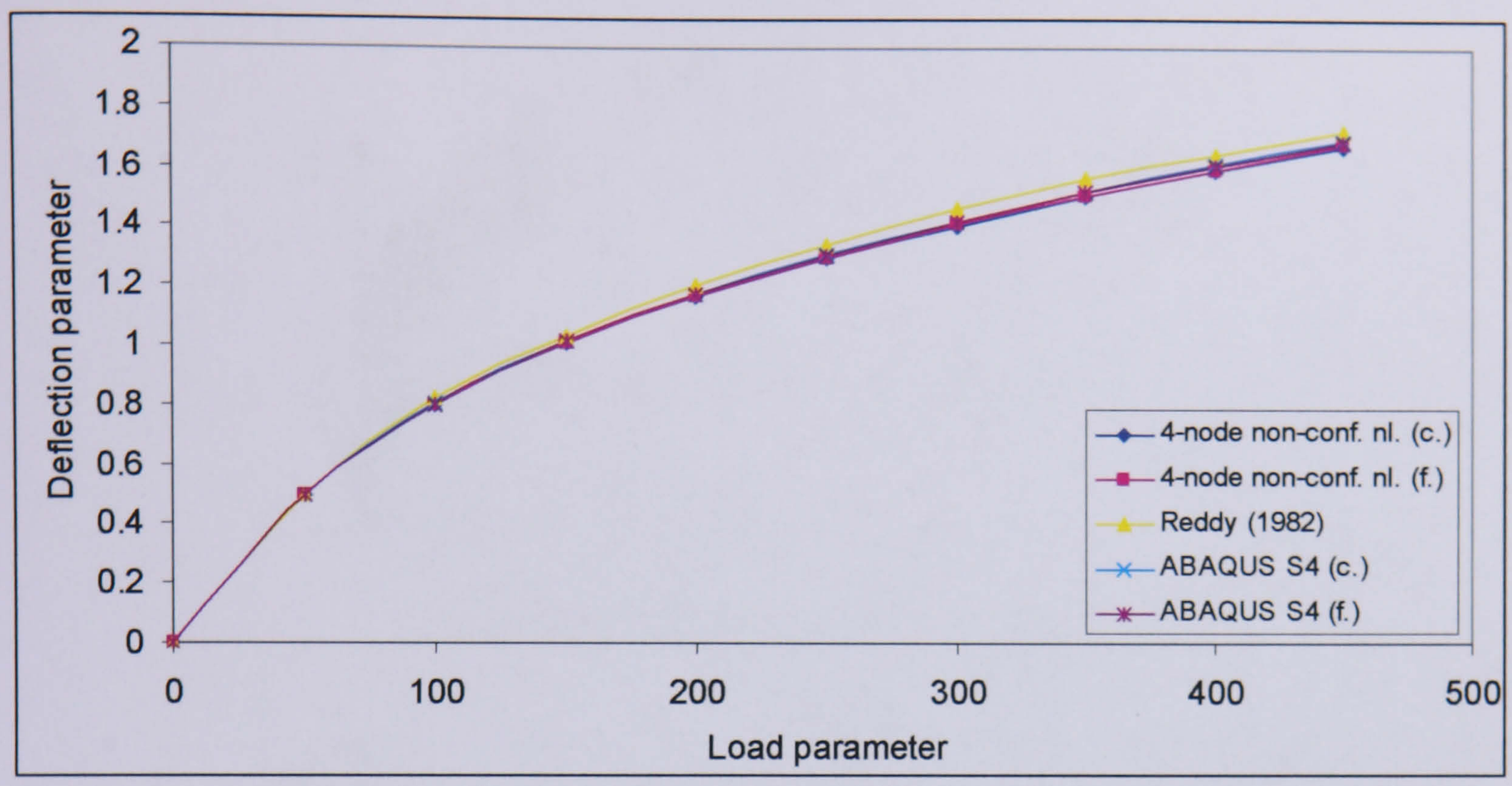

Figure (8.17) Non dimensional deflection parameter $\overline{W}$ history with load parameter $\bar{q}$ of the cross-ply [0°/90°/0°/90°] clamped square plate using 4-node non-conforming element.

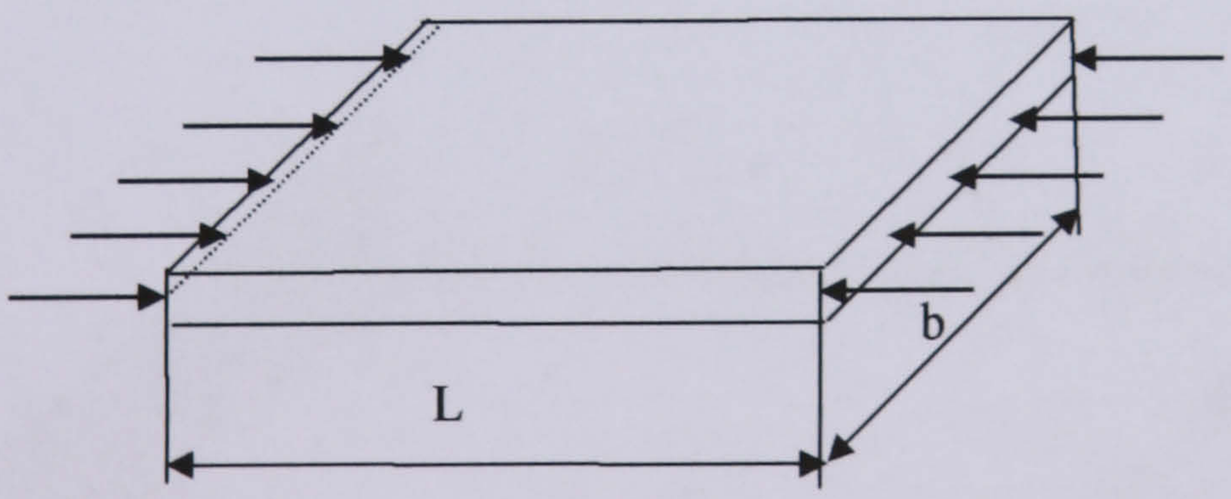

Figure (8.18) Simply supported plate subjected to in-plane load.

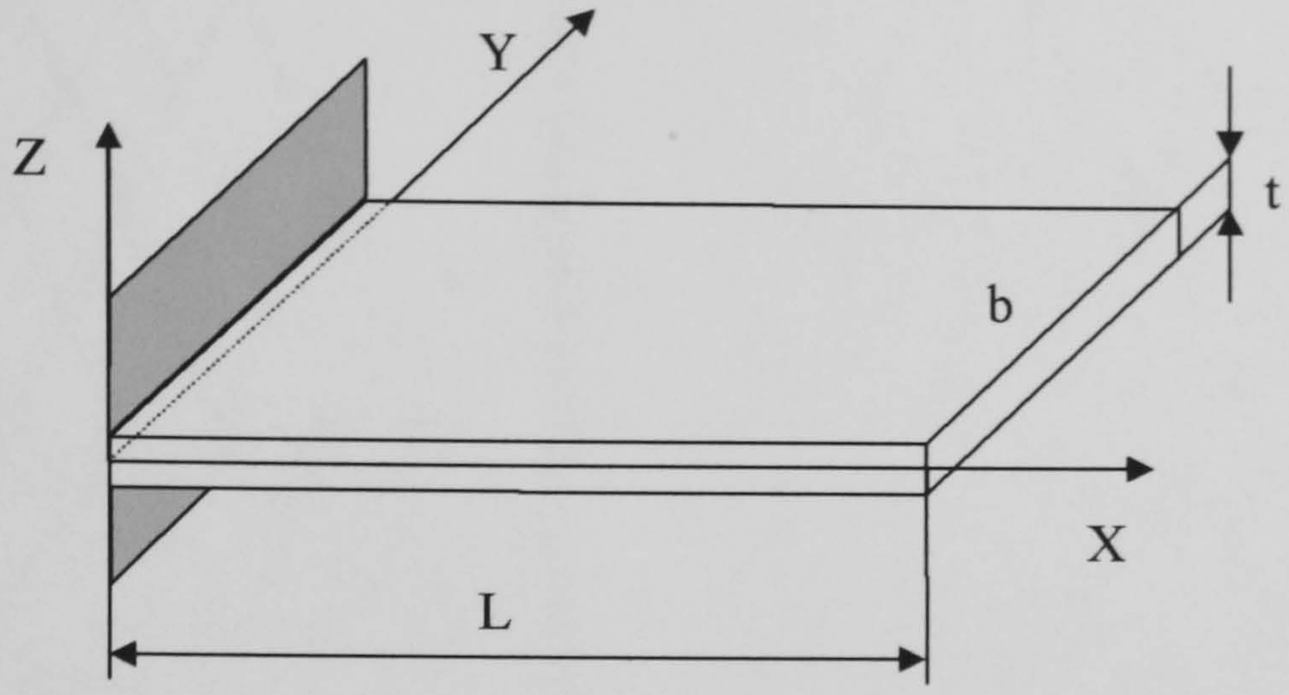

Figure (8.19) Unstiffened cantilever plate.

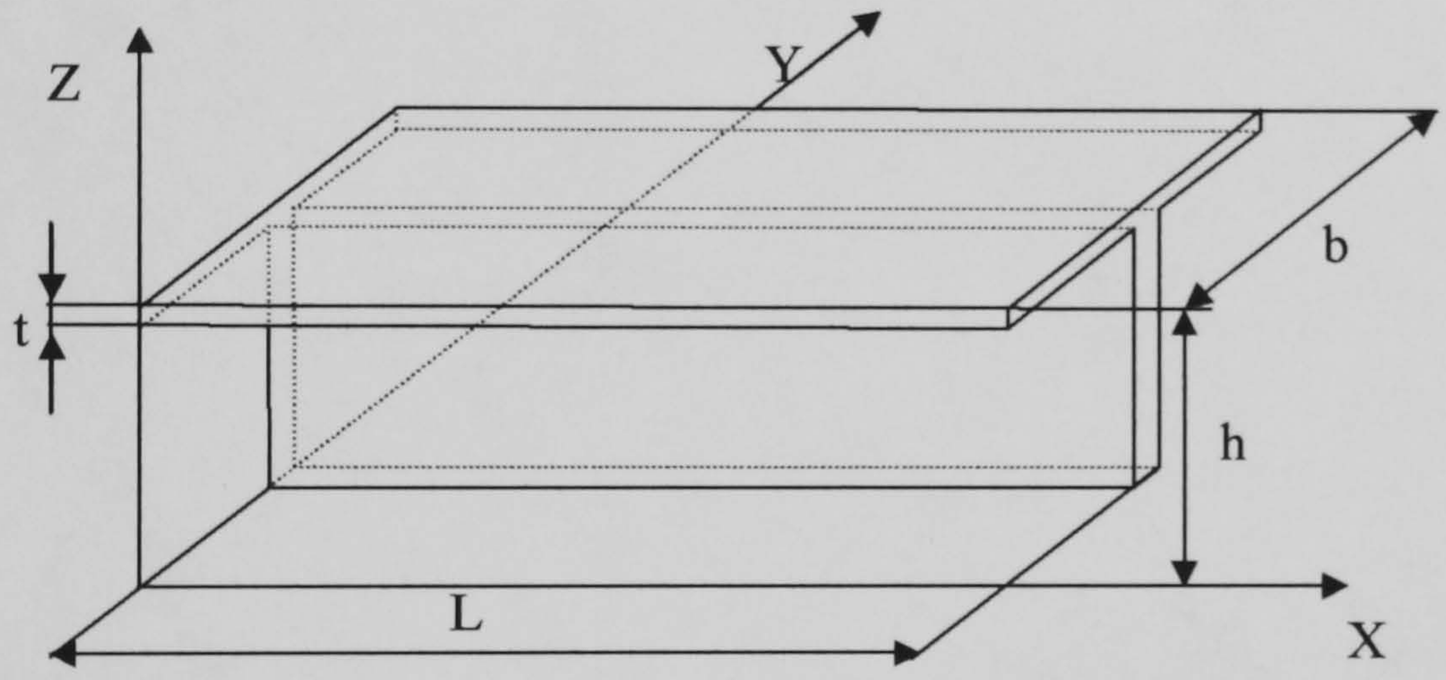

Figure (8.20) Repeating element for stiffened plate.

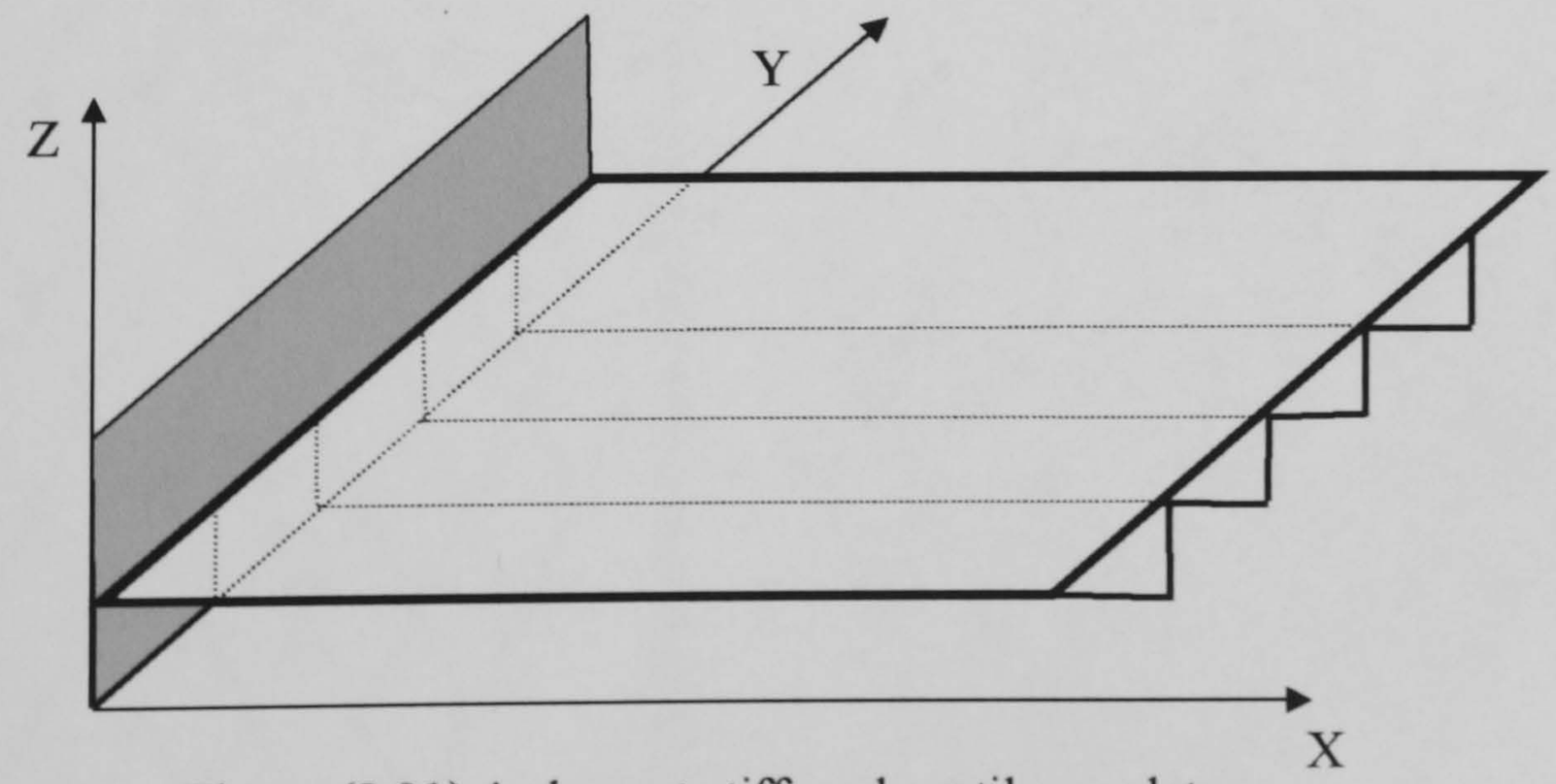

Figure (8.21) 4-element stiffened cantilever plate.

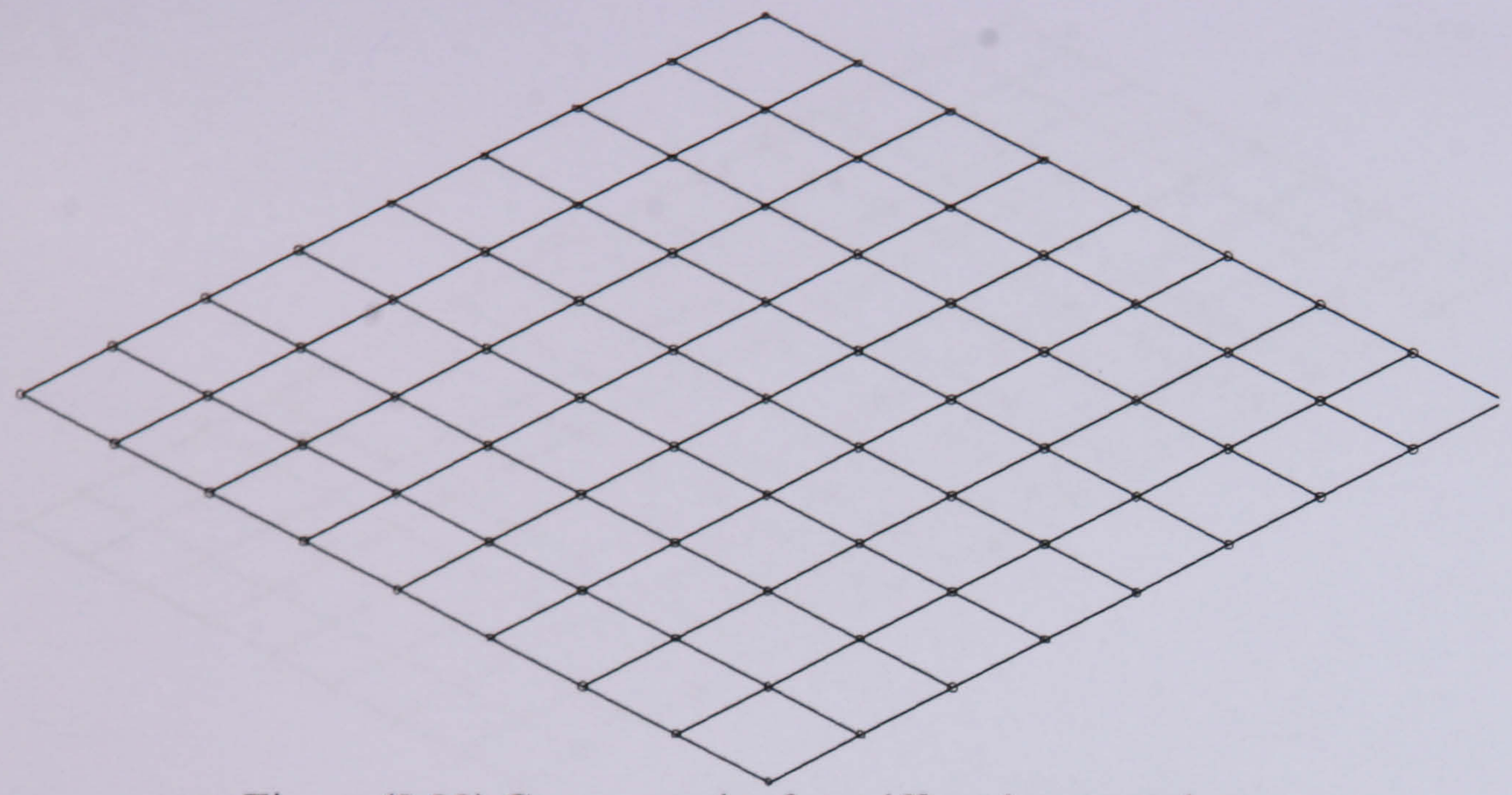

Figure (8.22) Coarse mesh of unstiffened square plate.

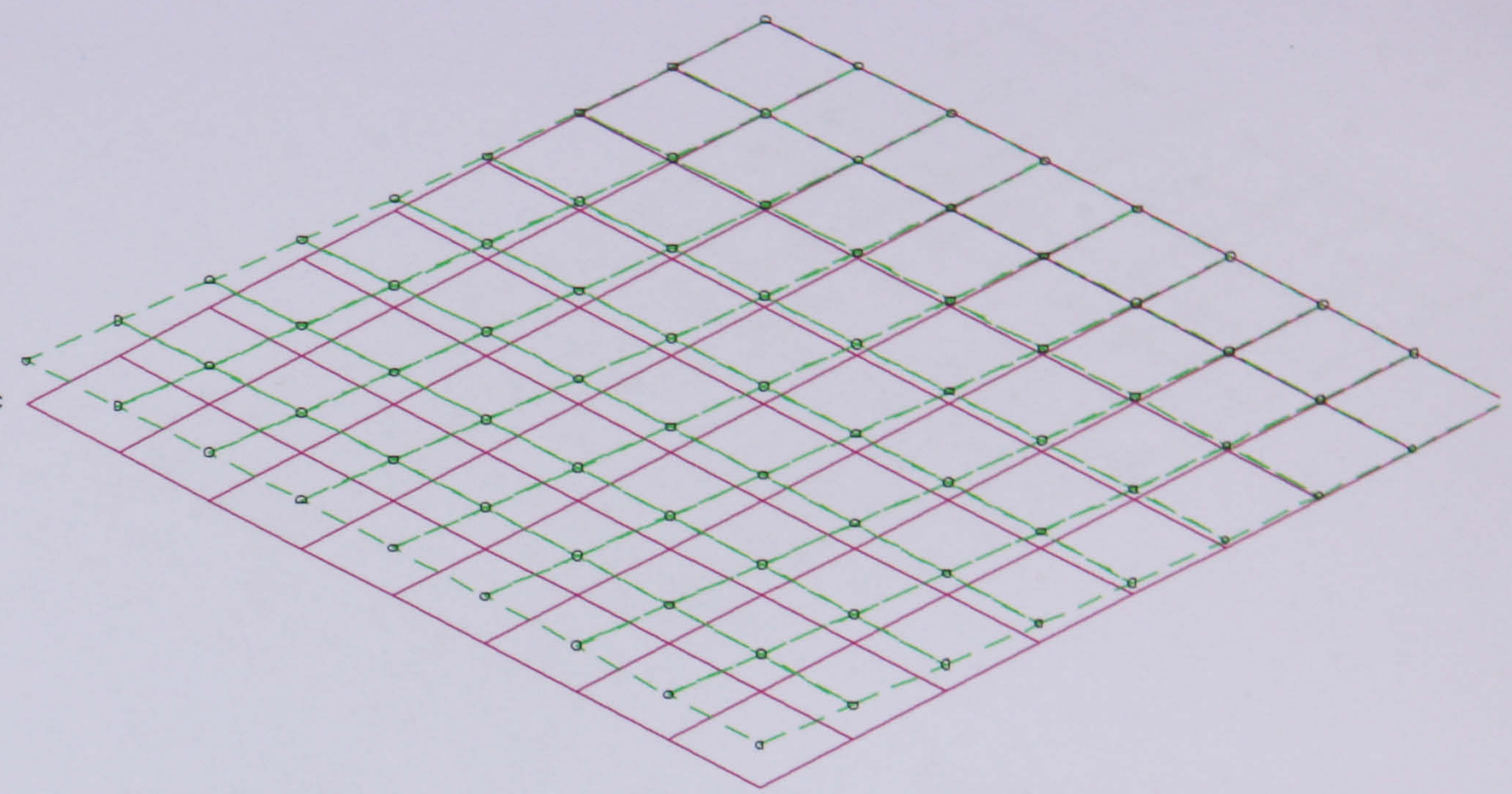

Figure (8.23) First mode shape of 8-layer unstiffened square plate.

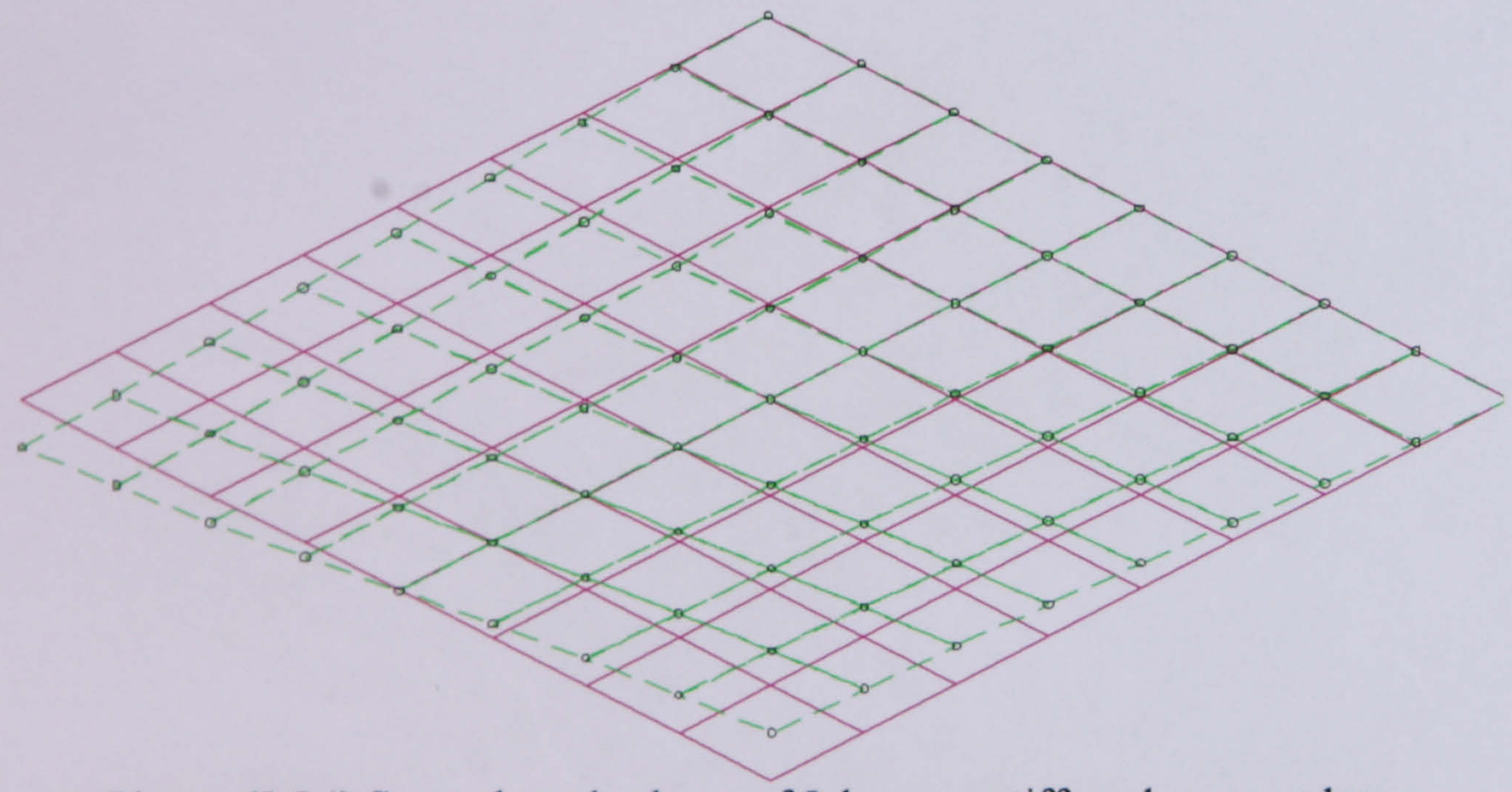

Figure (8.24) Second mode shape of 8-layer unstiffened square plate.

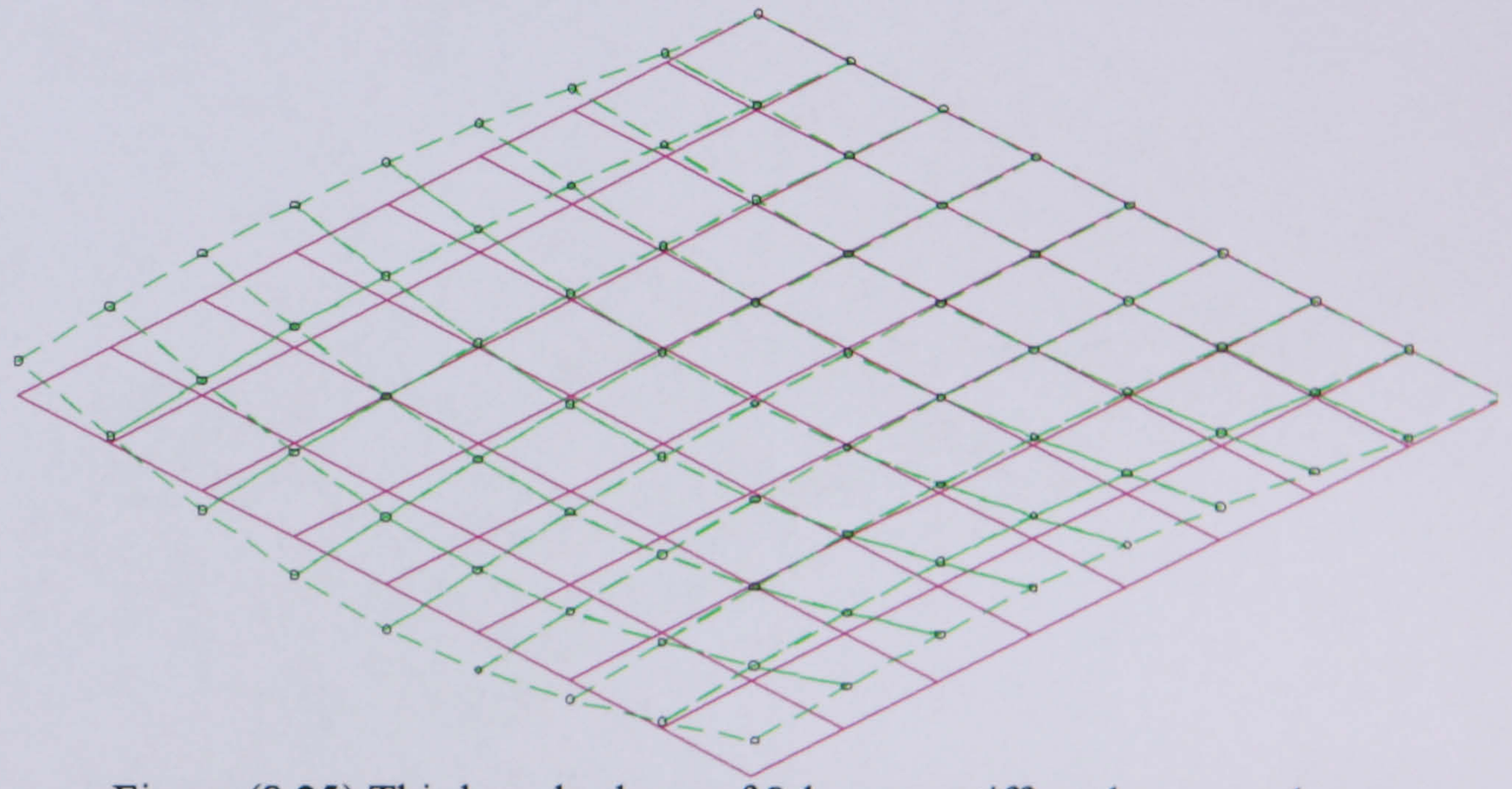

Figure (8.25) Third mode shape of 8-layer unstiffened square plate.

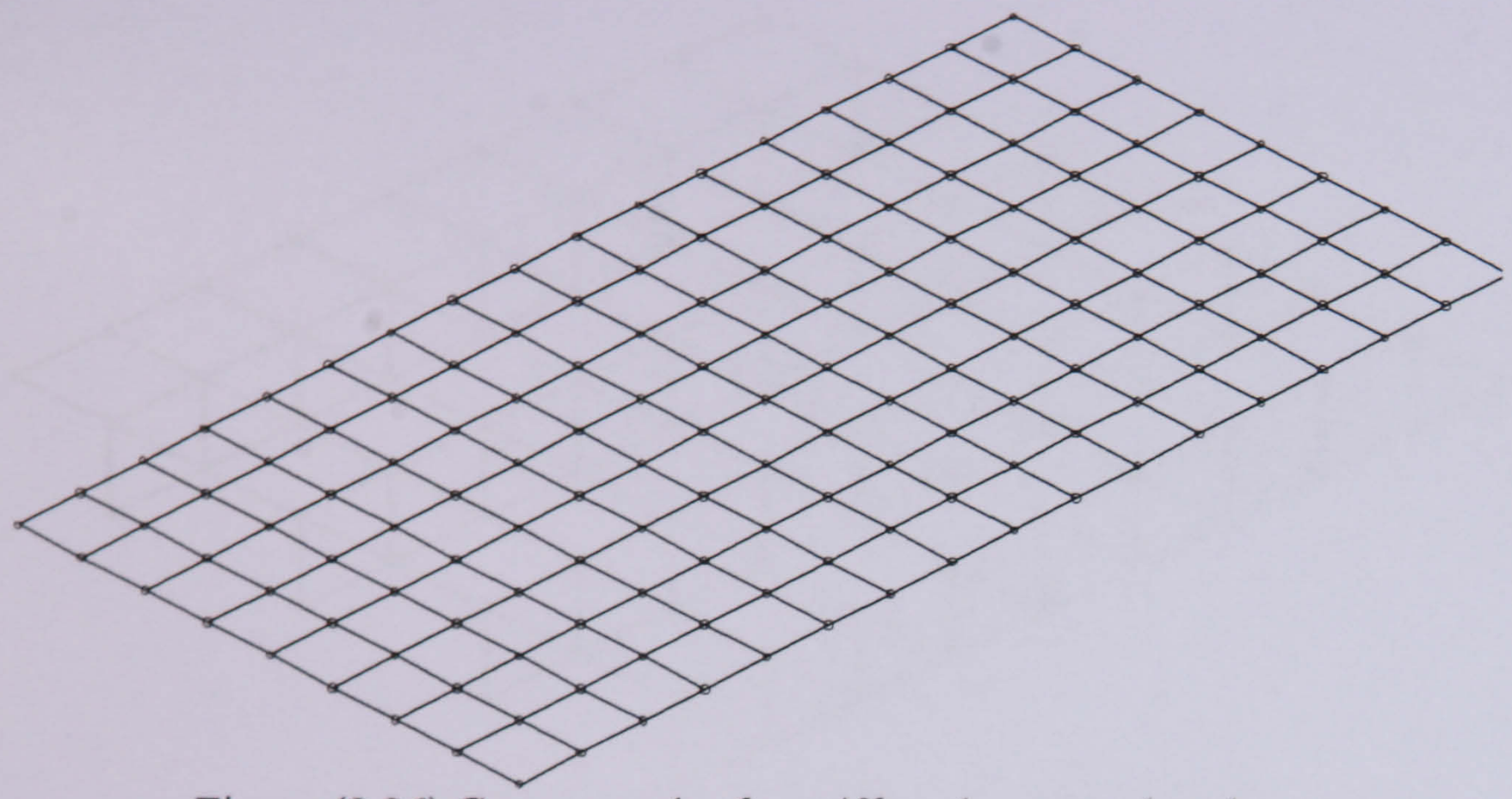

Figure (8.26) Coarse mesh of unstiffened rectangular plate.

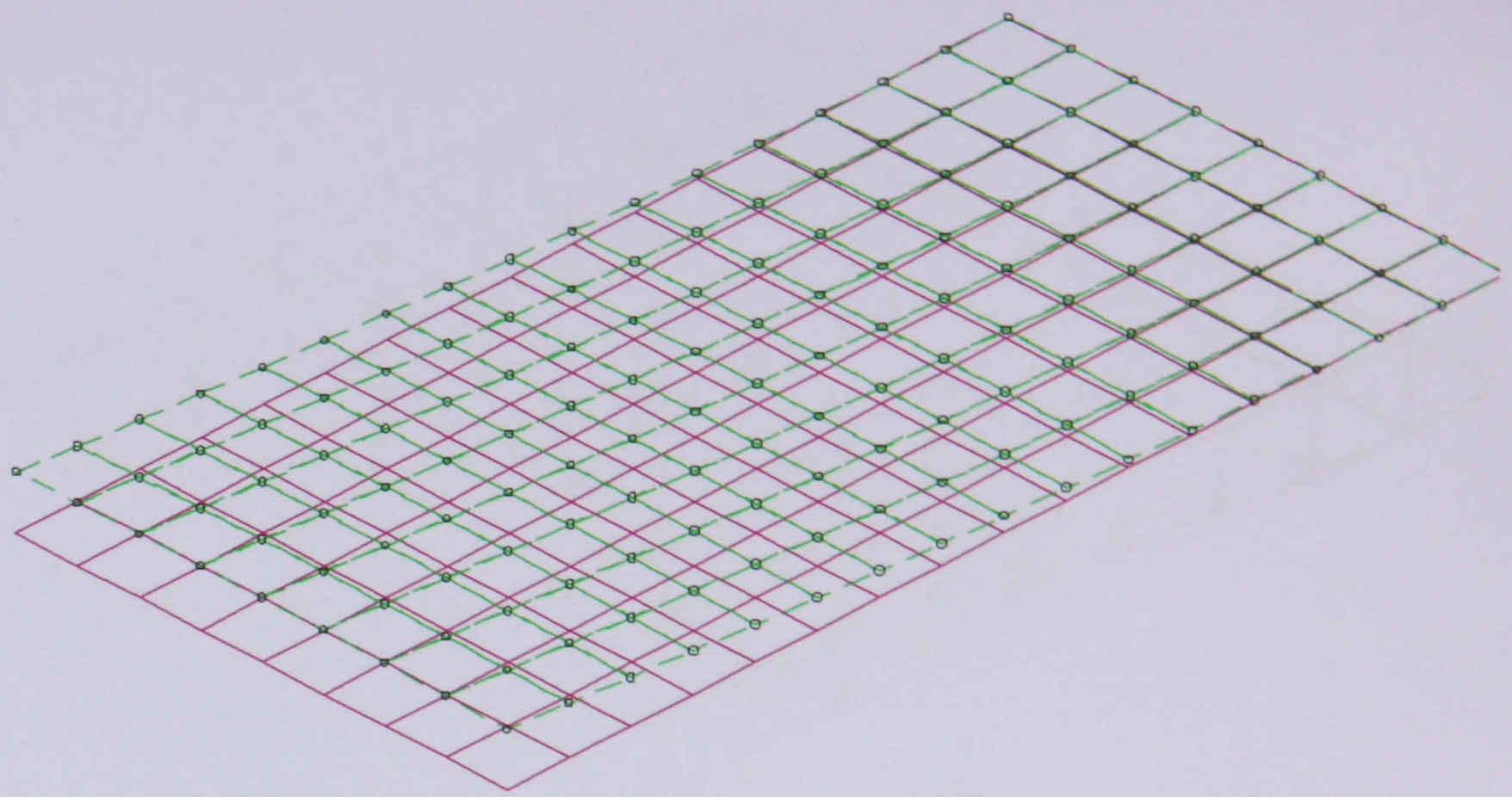

Figure (8.27) First mode shape of 8-layer unstiffened rectangular plate.

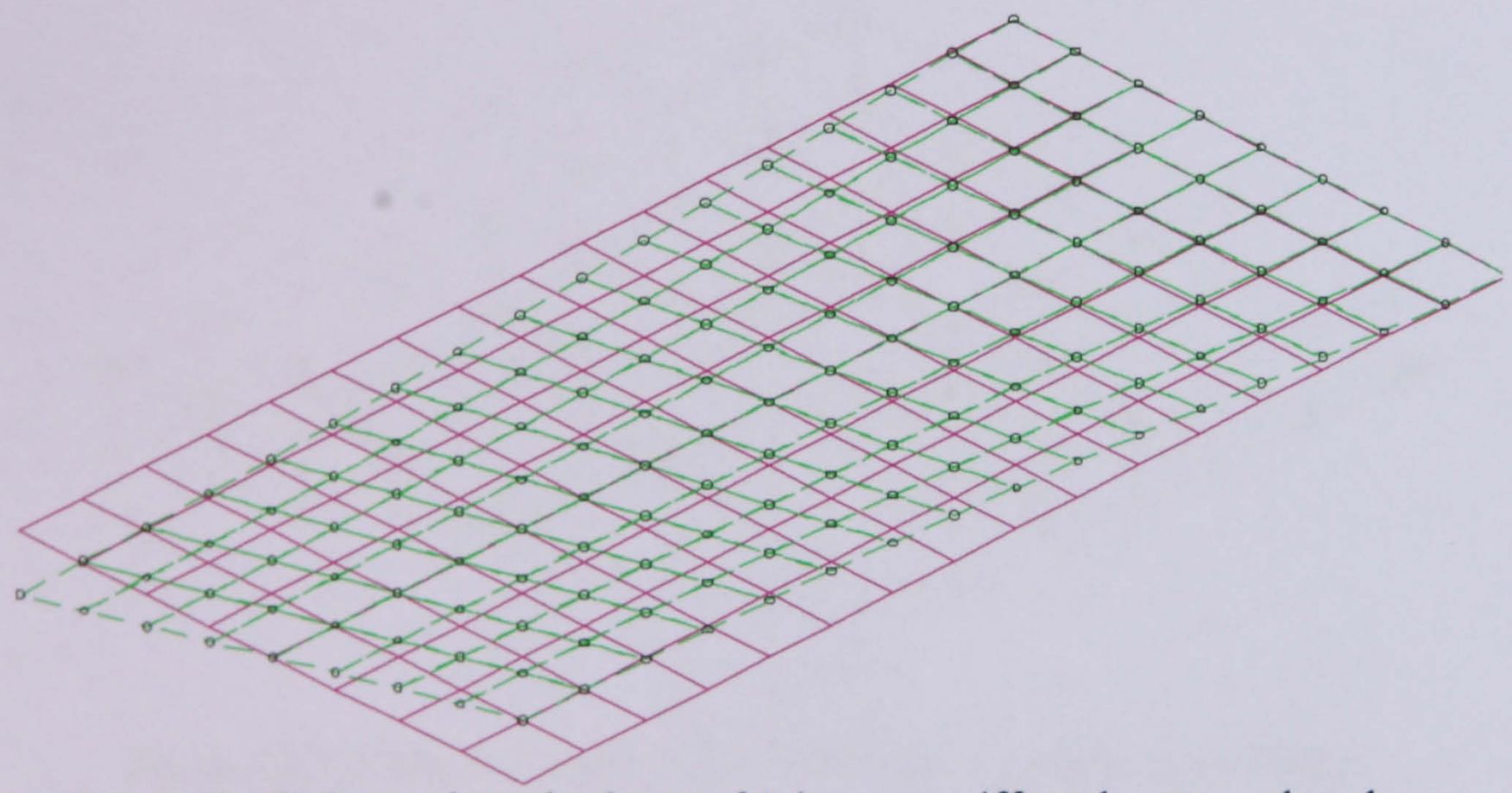

Figure (8.28) Second mode shape of 8-layer unstiffened rectangular plate.

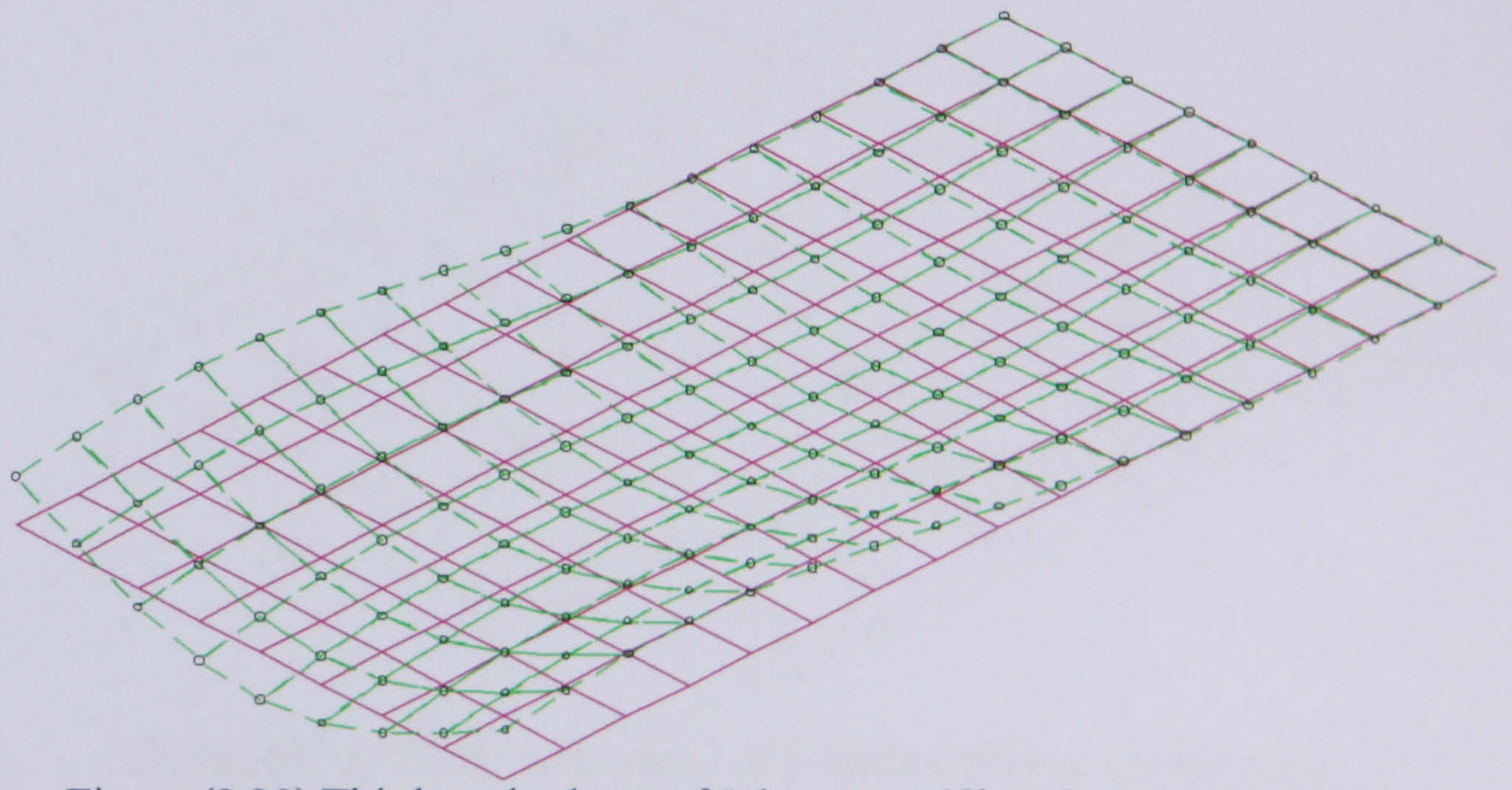

Figure (8.29) Third mode shape of 8-layer unstiffened rectangular plate.

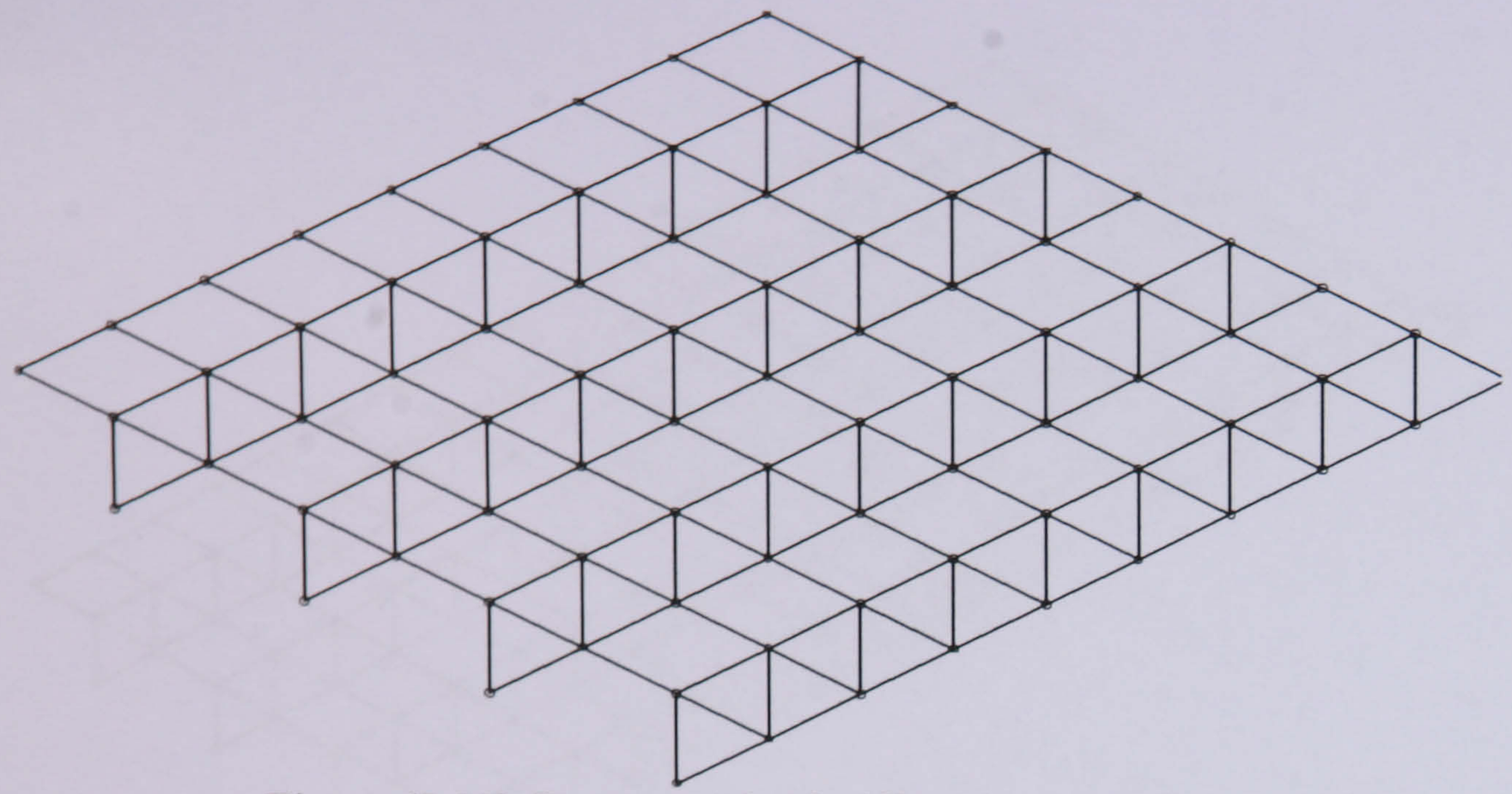

Figure (8.30) Coarse mesh of stiffened square plate.

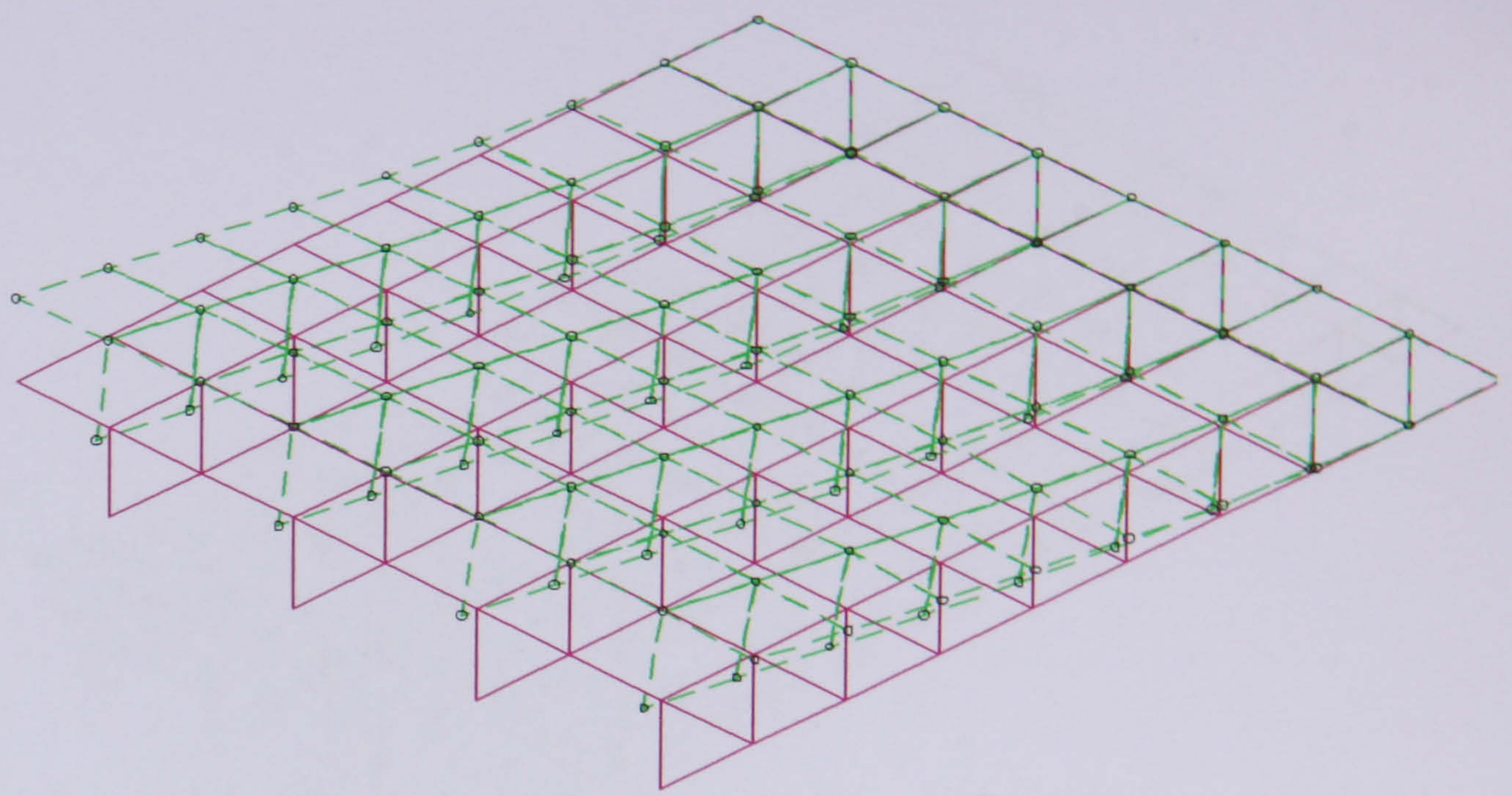

Figure (8.31) First mode shape of 8-layer stiffened square plate.

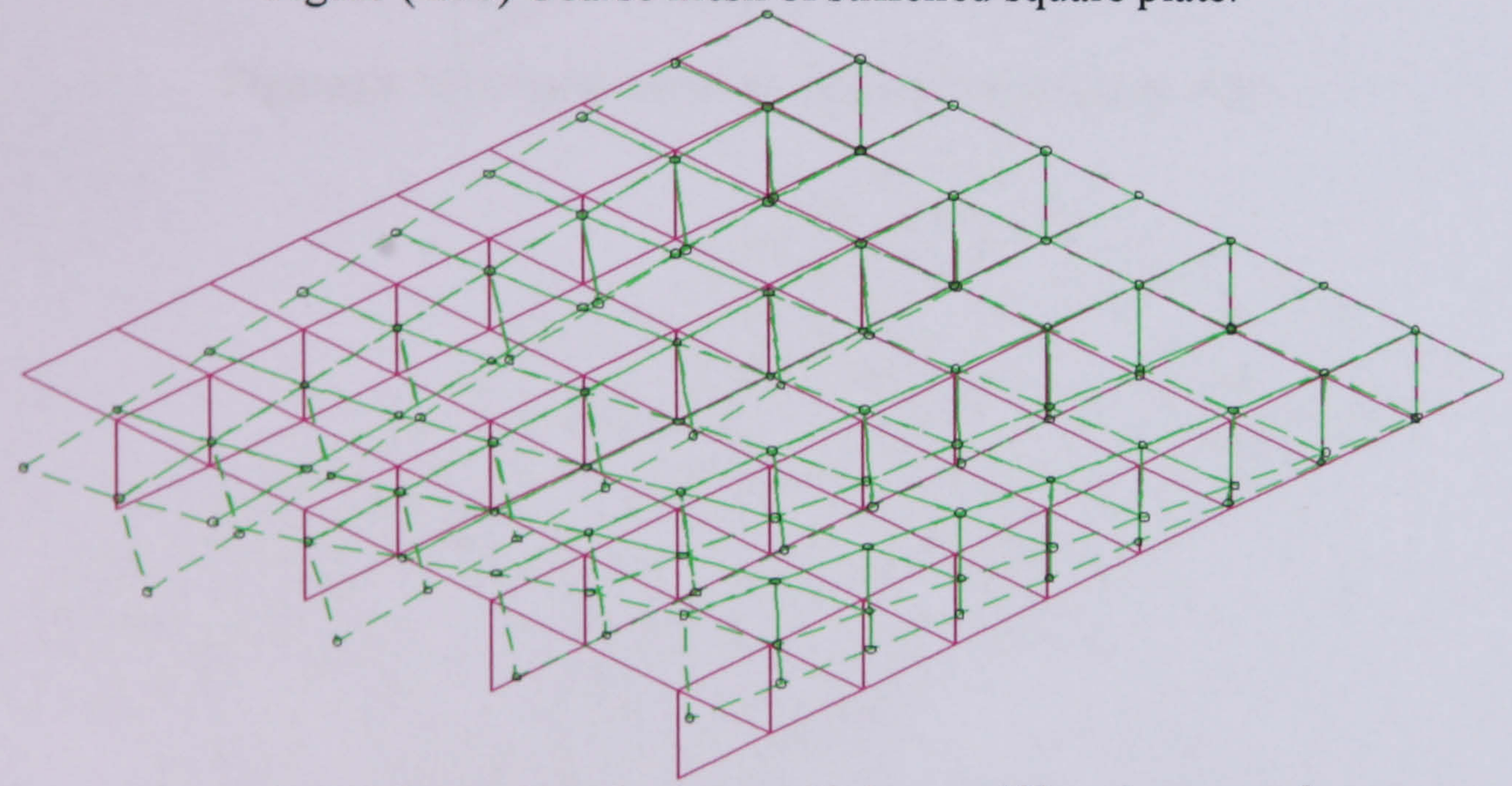

Figure (8.32) Second mode shape of 8-layer stiffened square plate.

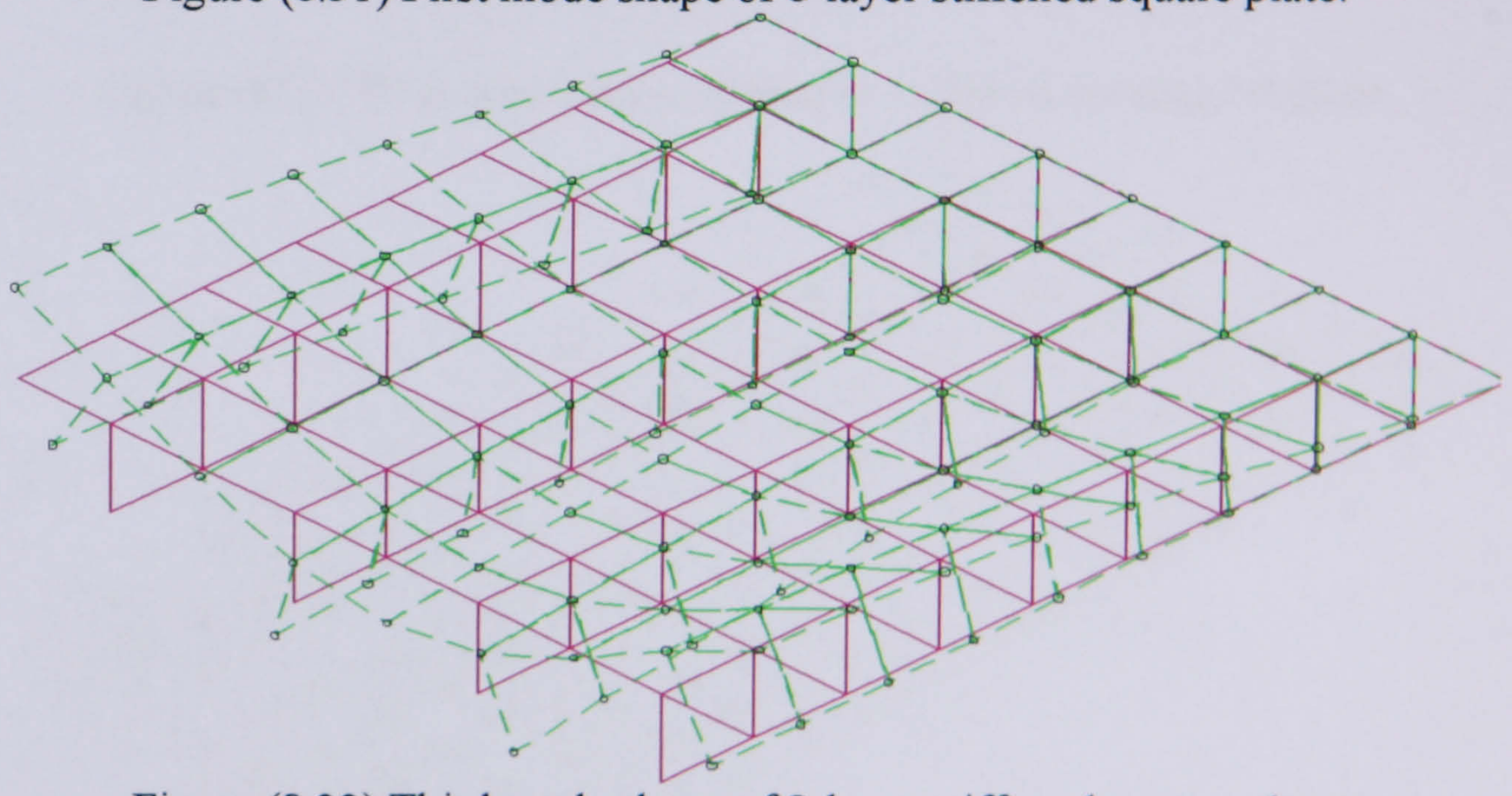

Figure (8.33) Third mode shape of 8-layer stiffened square plate.

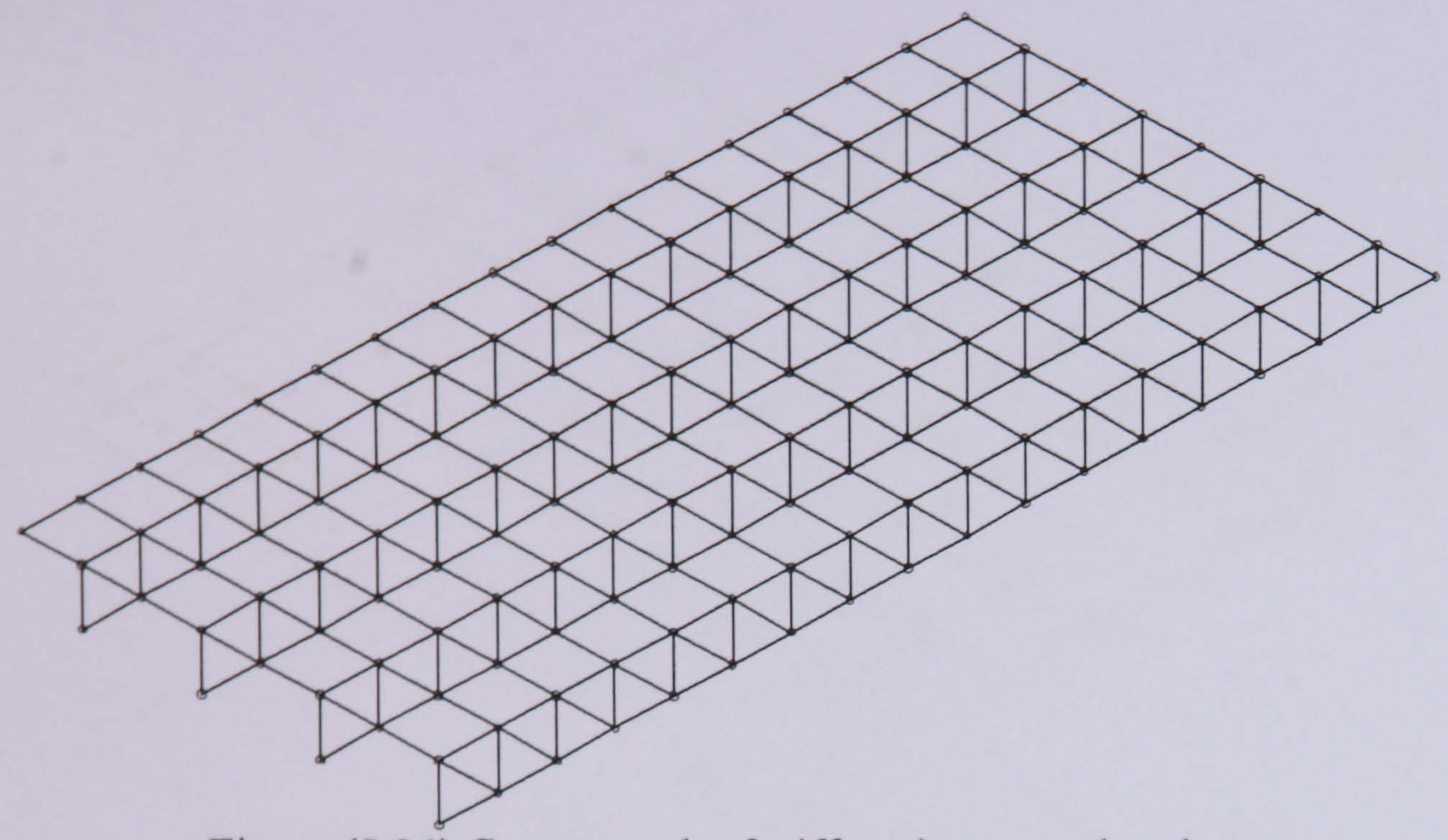

Figure (8.34) Coarse mesh of stiffened rectangular plate.

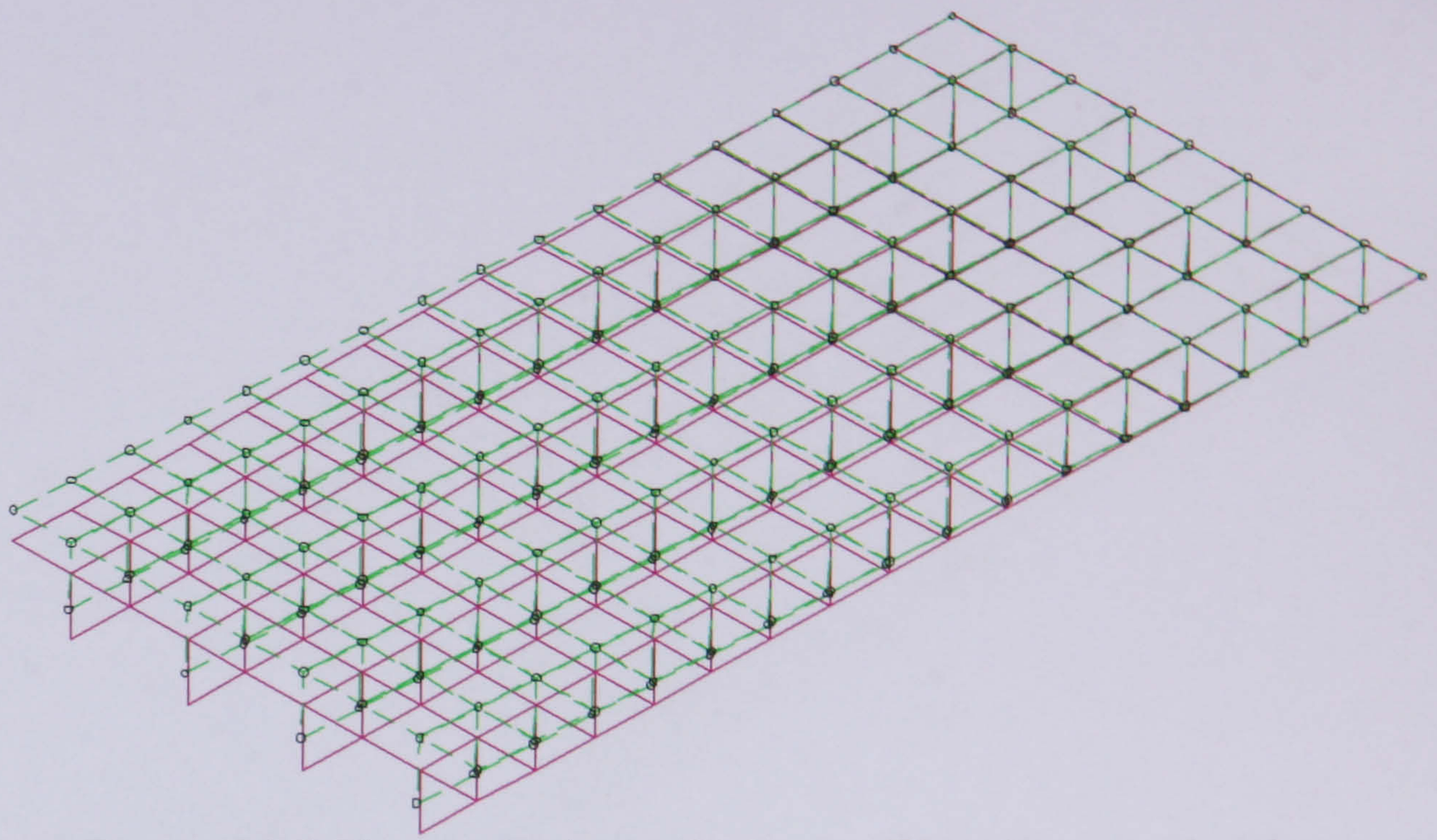

Figure (8.35) First mode shape of 8-layer stiffened rectangular plate.

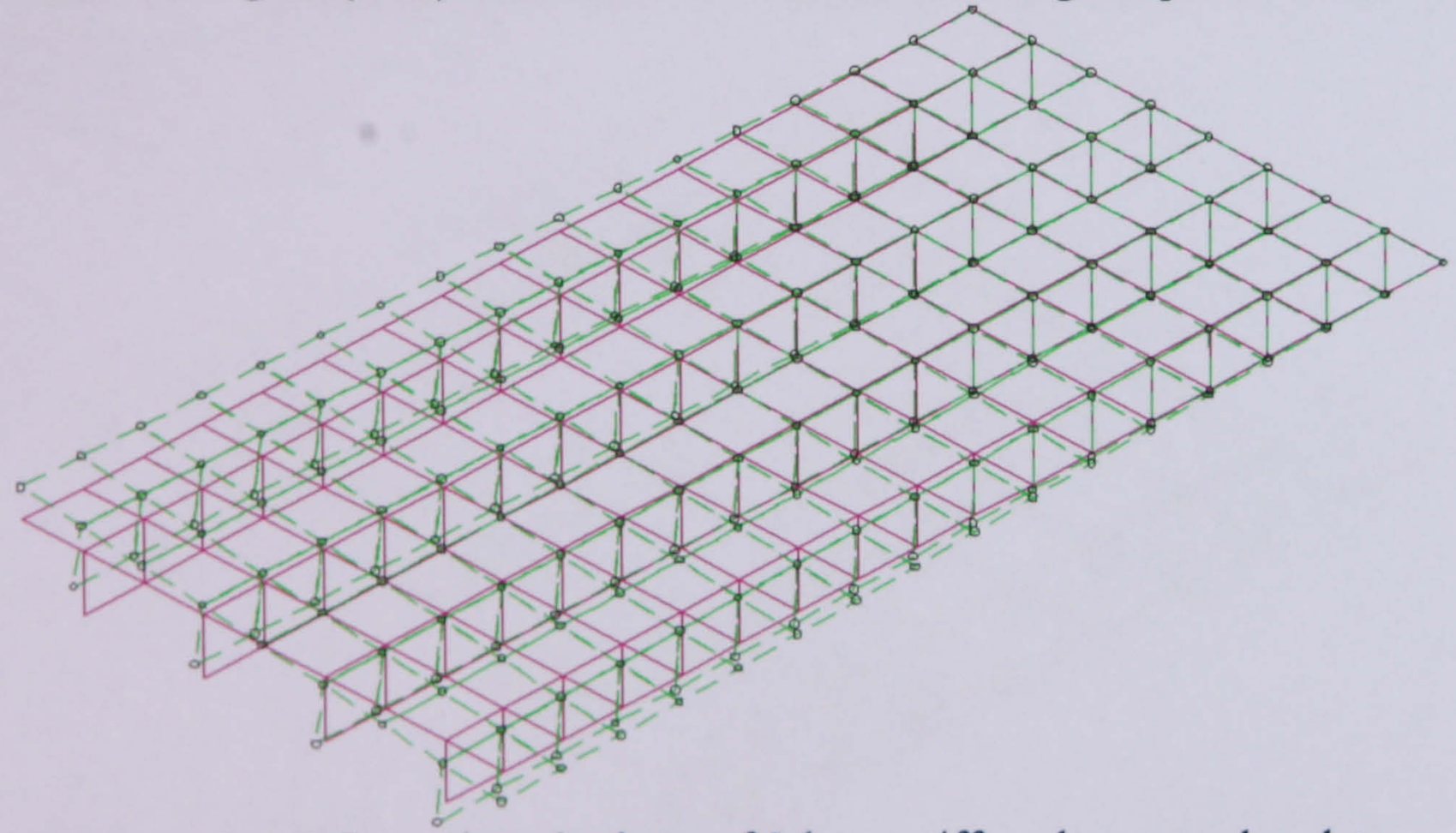

Figure (8.36) Second mode shape of 8-layer stiffened rectangular plate.

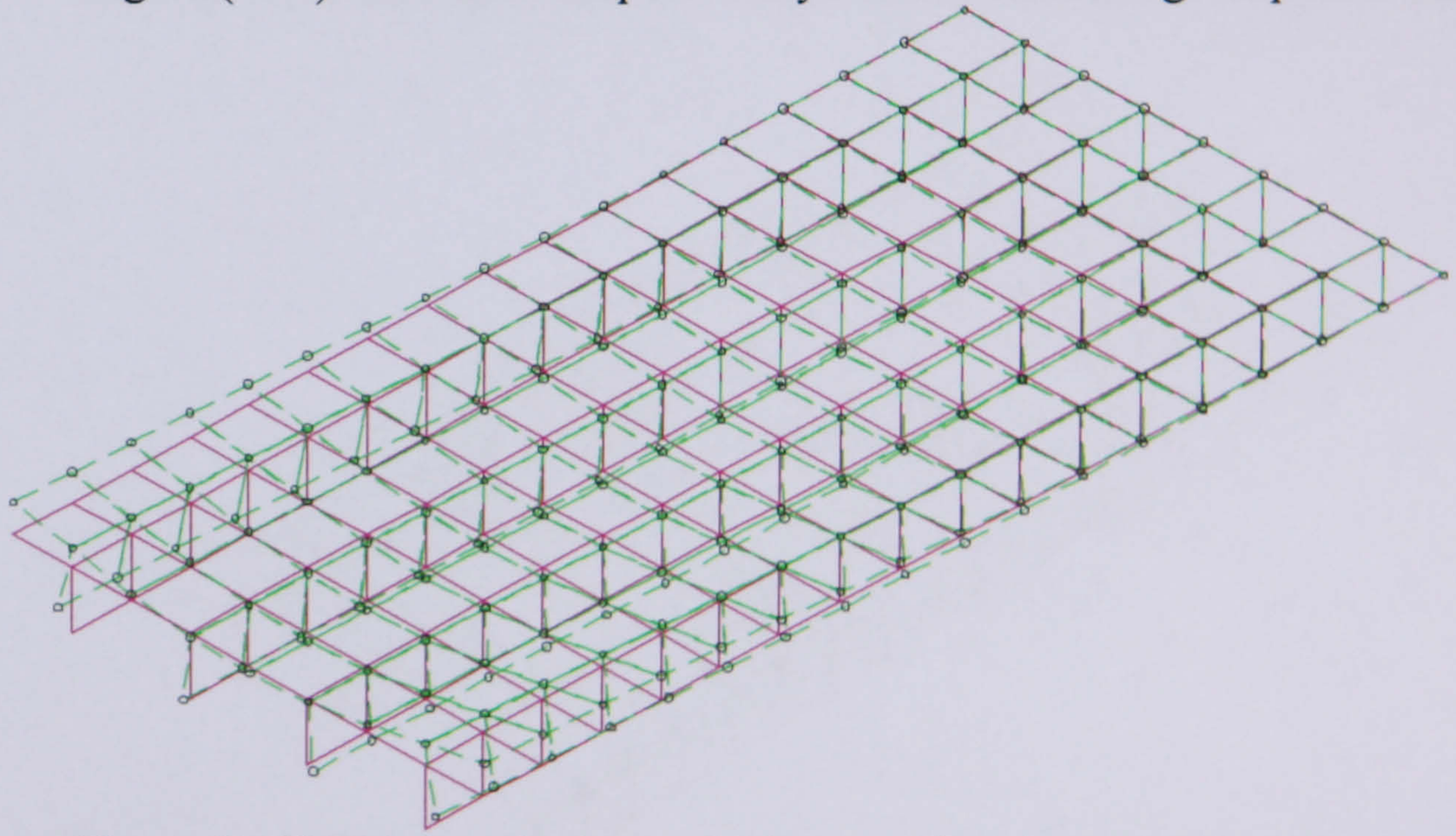

Figure (8.37) Third mode shape of 8-layer stiffened rectangular plate.

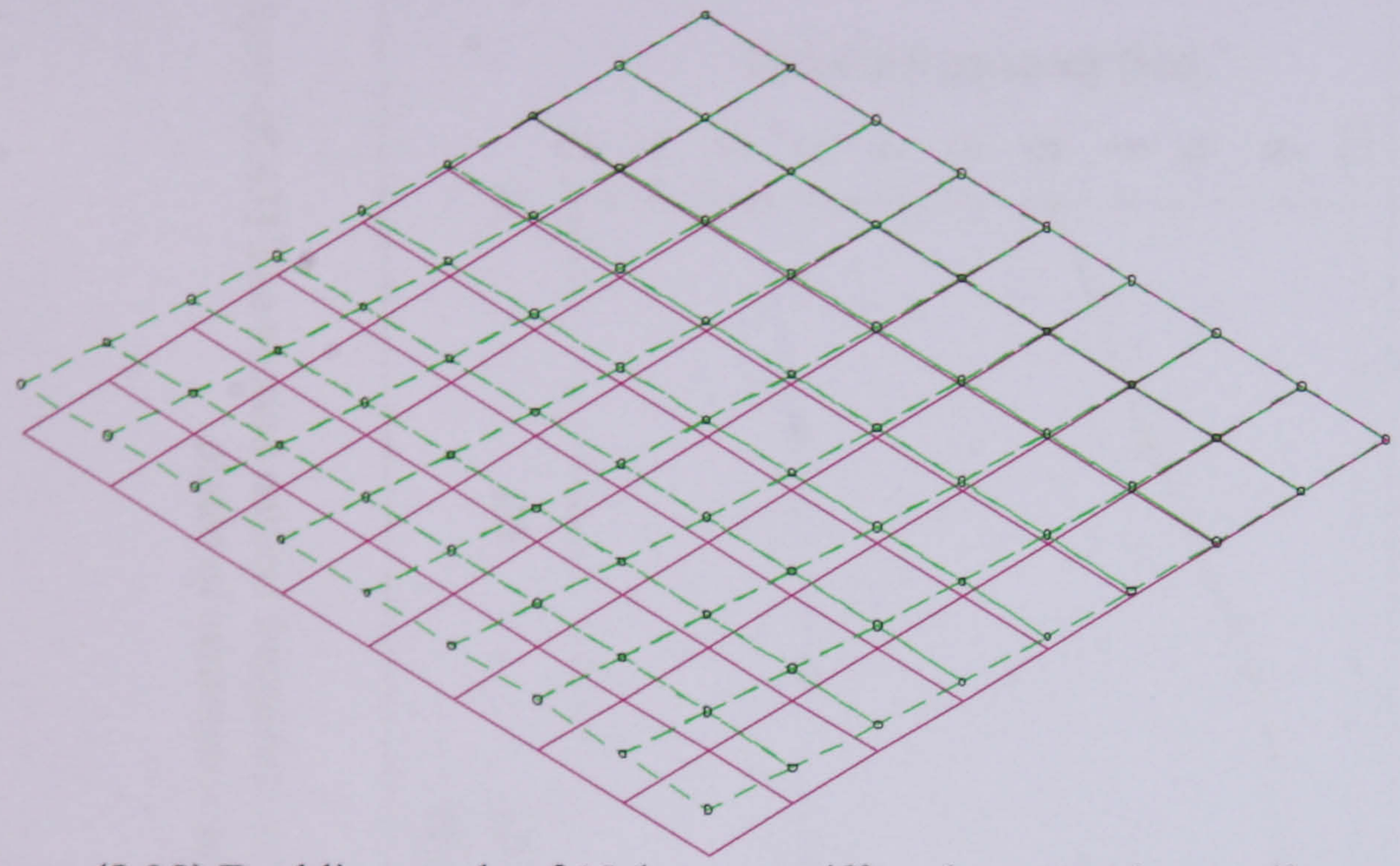

Figure (8.38) Buckling mode of 12-layer unstiffened rectangular cantilever plate.

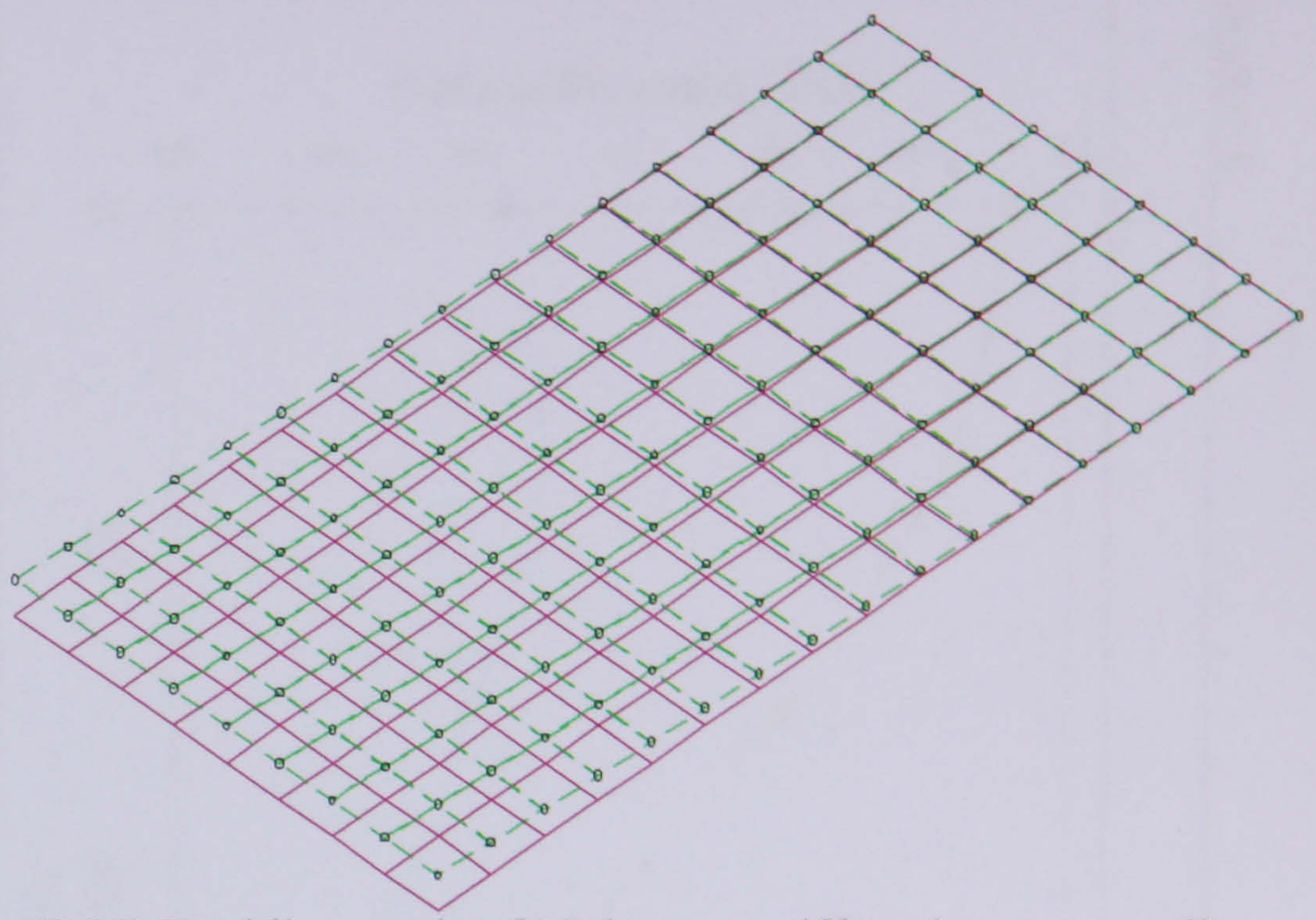

Figure (8.39) Buckling mode of 12-layer unstiffened square cantilever plate.

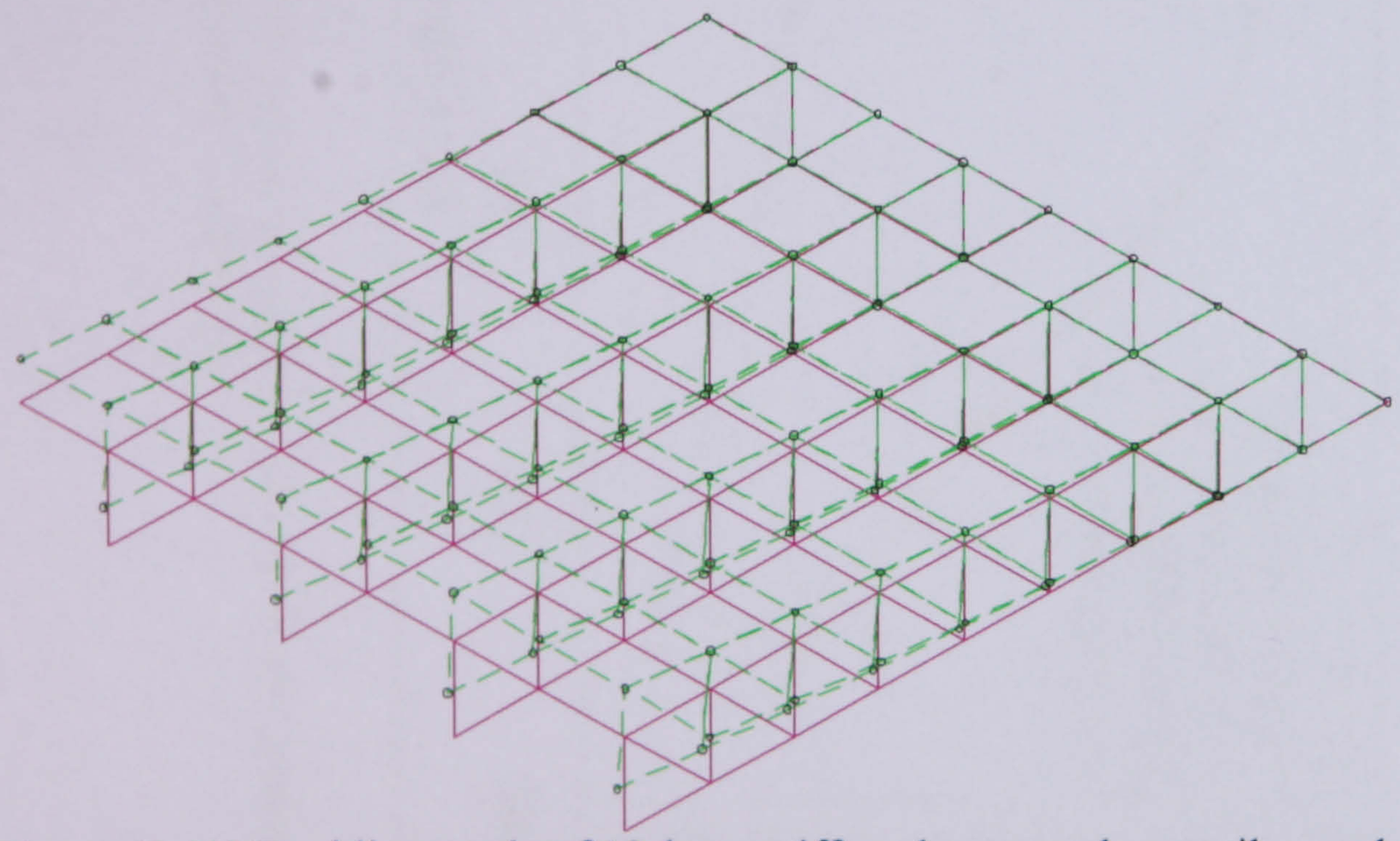

Figure (8.40) Buckling mode of 12-layer stiffened rectangular cantilever plate.

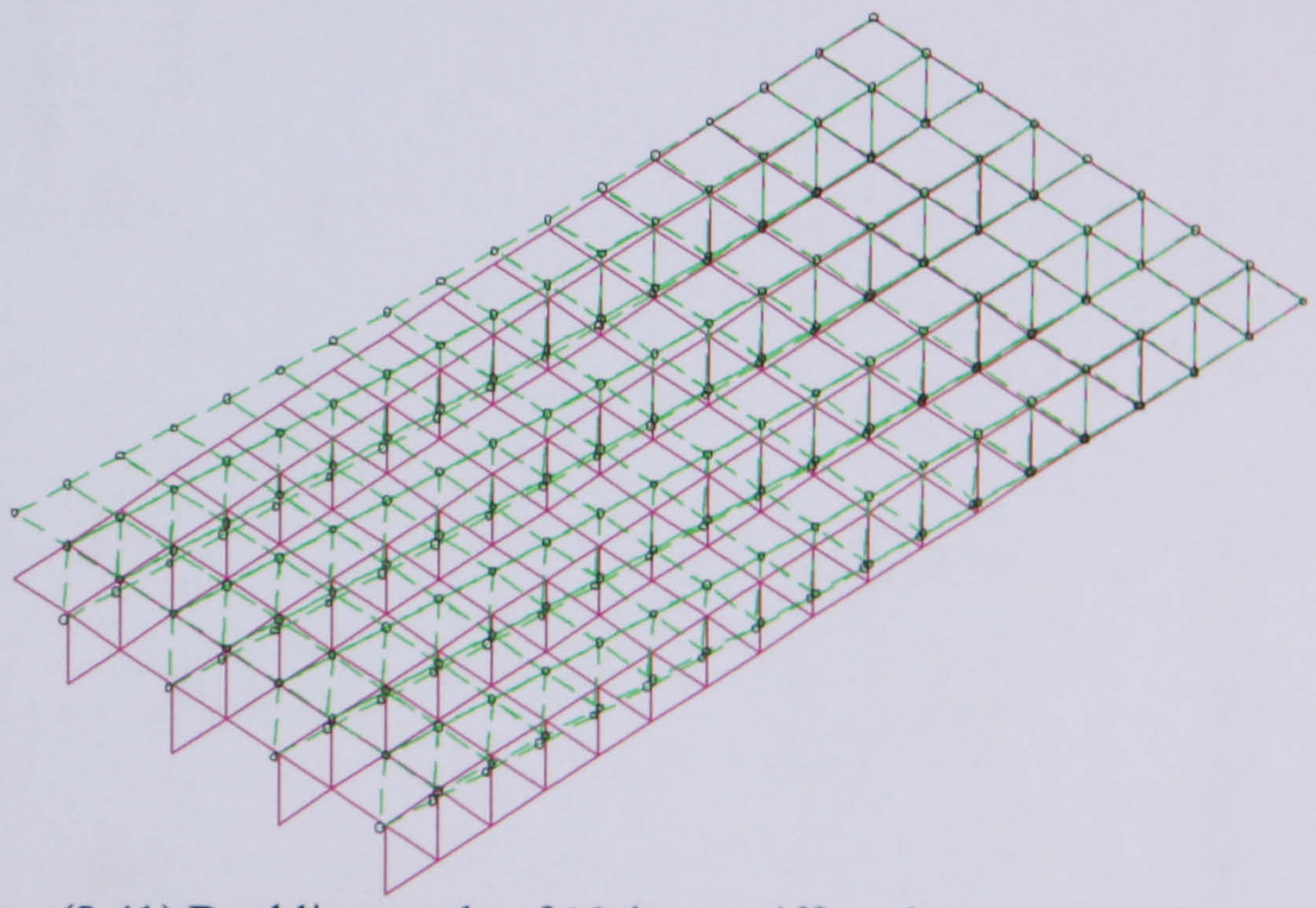

Figure (8.41) Buckling mode of 12-layer stiffened square cantilever plate.

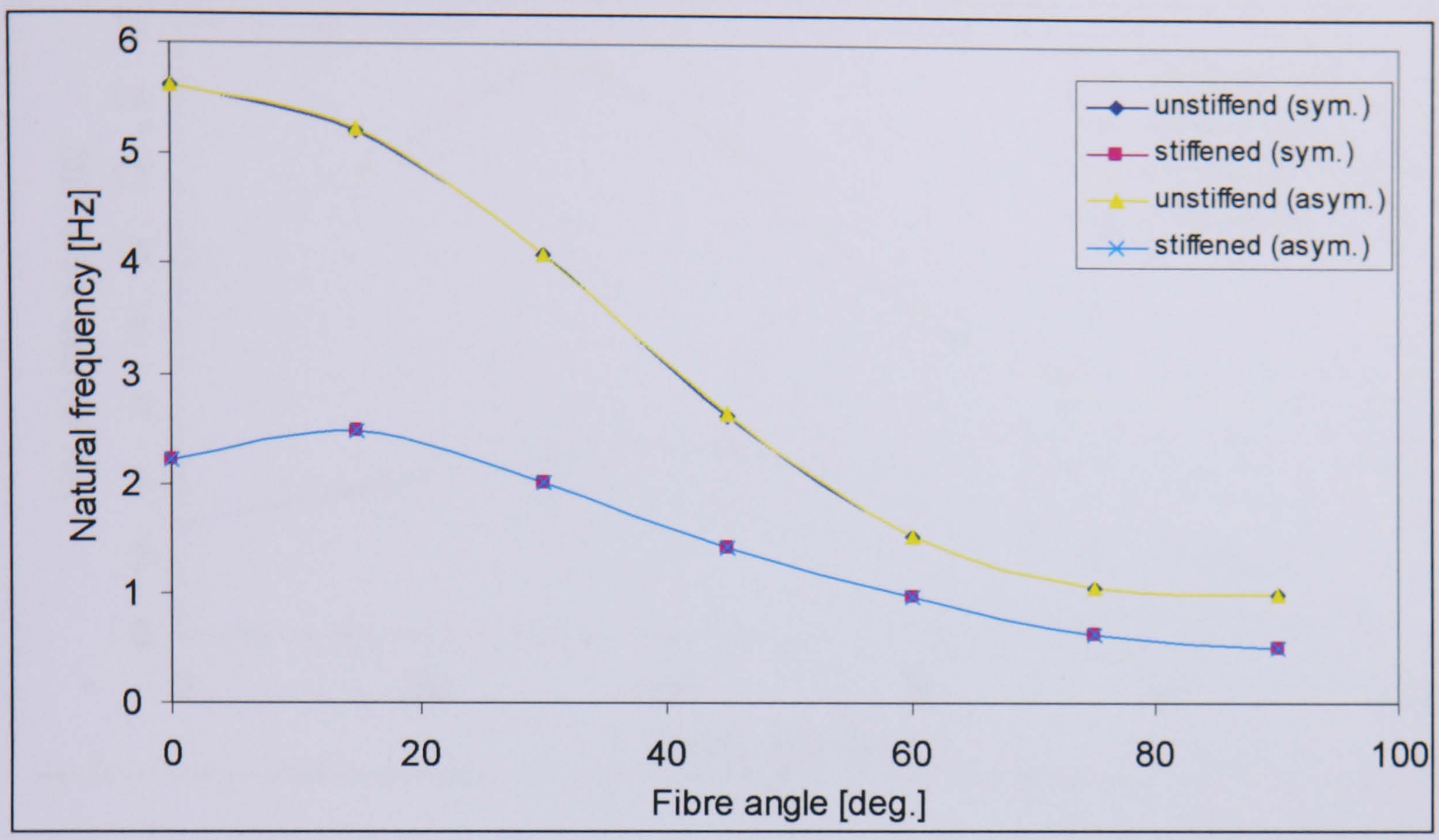

Figure (8.42) The first natural frequency versus fibre angle of stiffened and unstiffened square plates of symmetric and asymmetric composites.

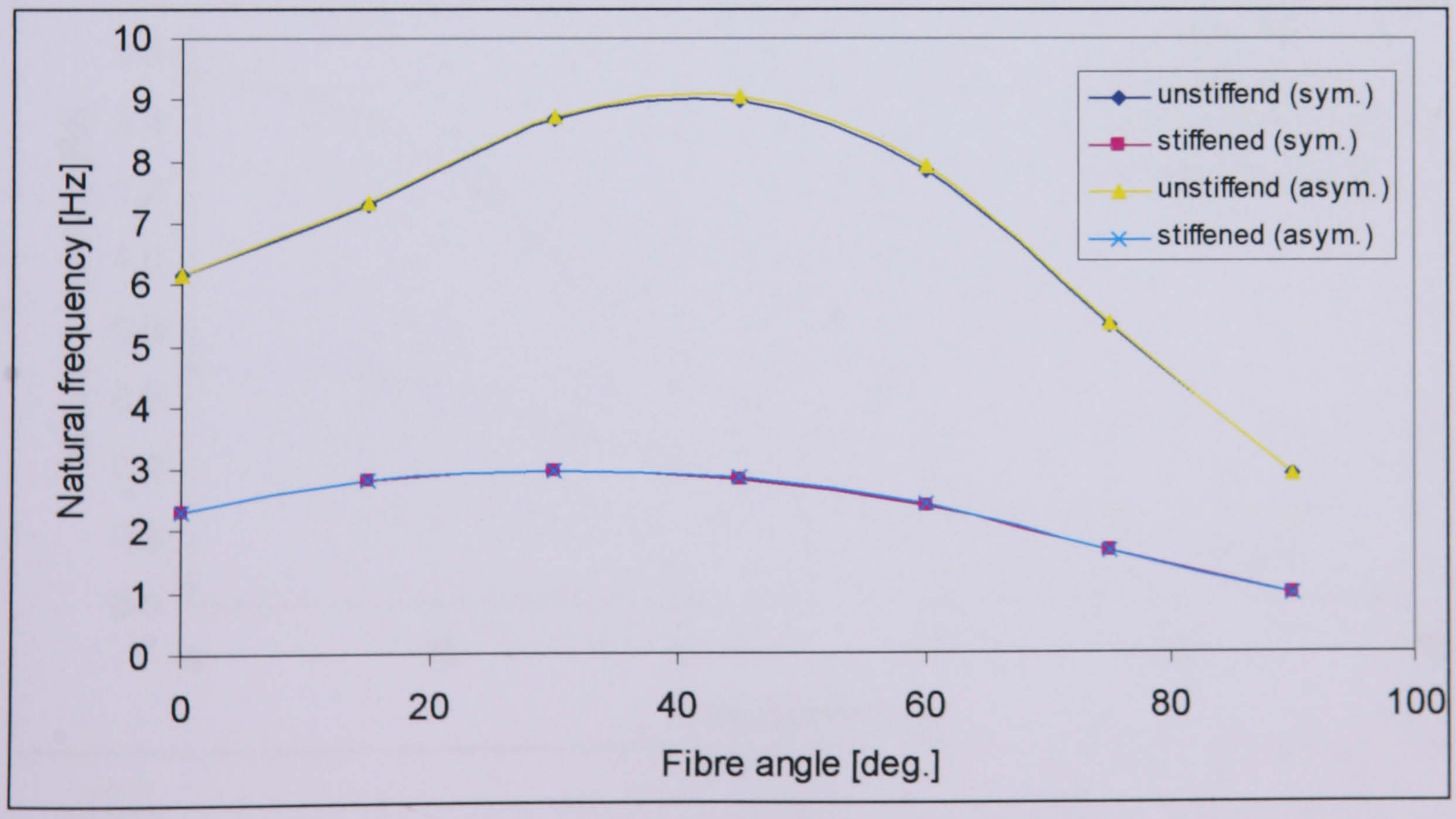

Figure (8.43) The second natural frequency versus fibre angle of stiffened and unstiffened square plates of symmetric and asymmetric composites.

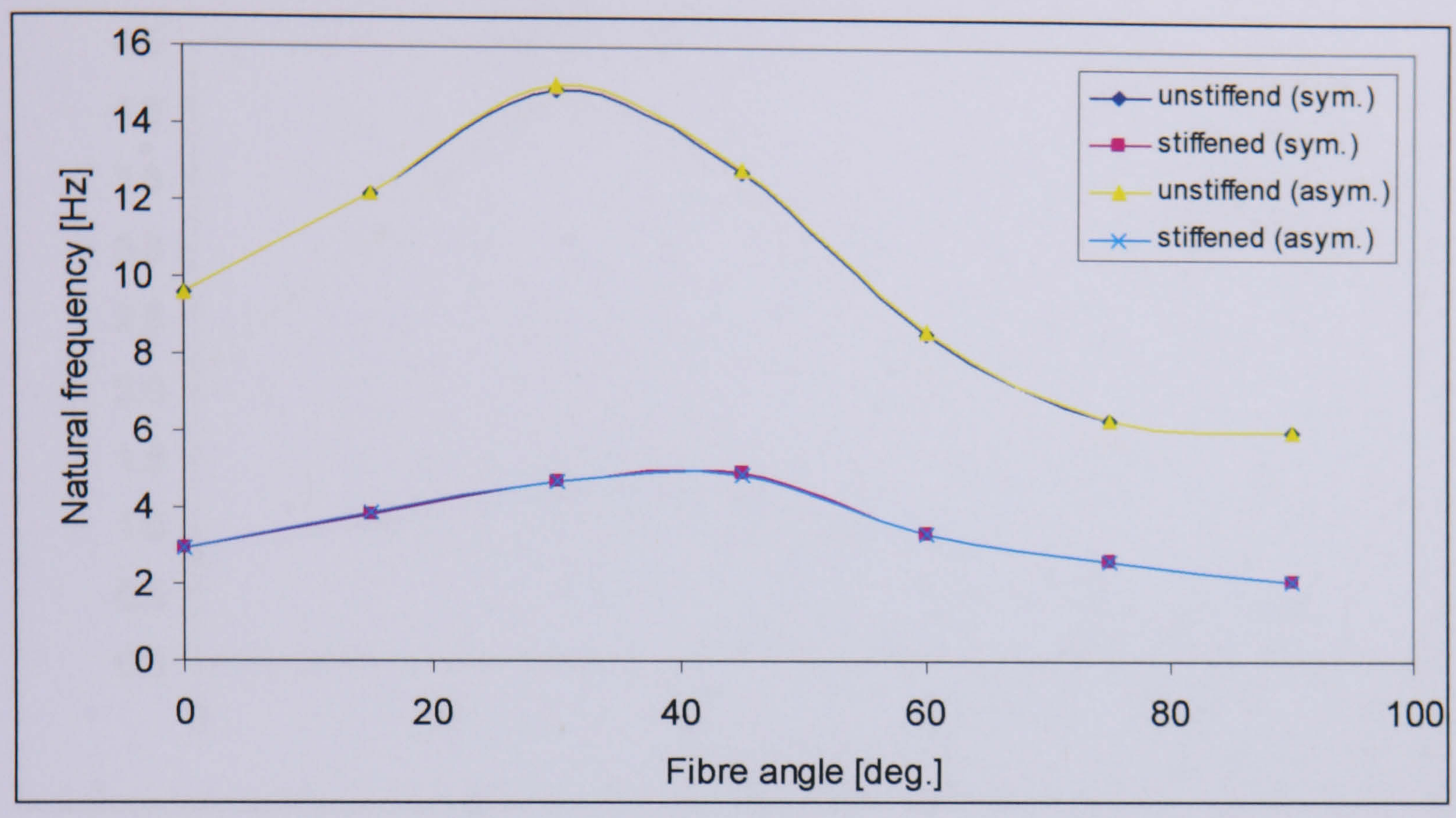

Figure (8.44) The third natural frequency versus fibre angle of stiffened and unstiffened square plates of symmetric and asymmetric composites.

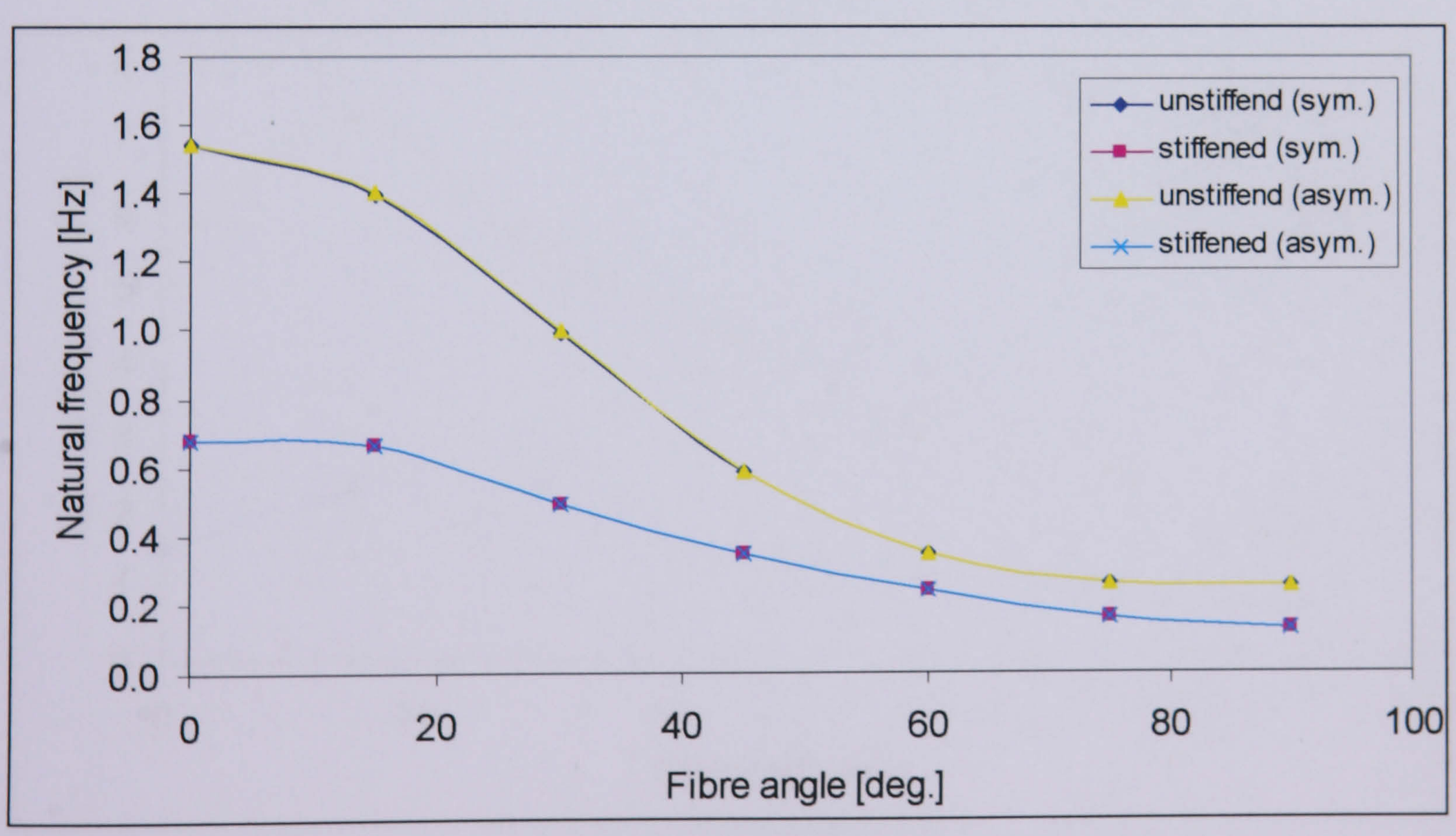

Figure (8.45) The first natural frequency versus fibre angle of stiffened and unstiffened rectangular plates of symmetric and asymmetric composites.

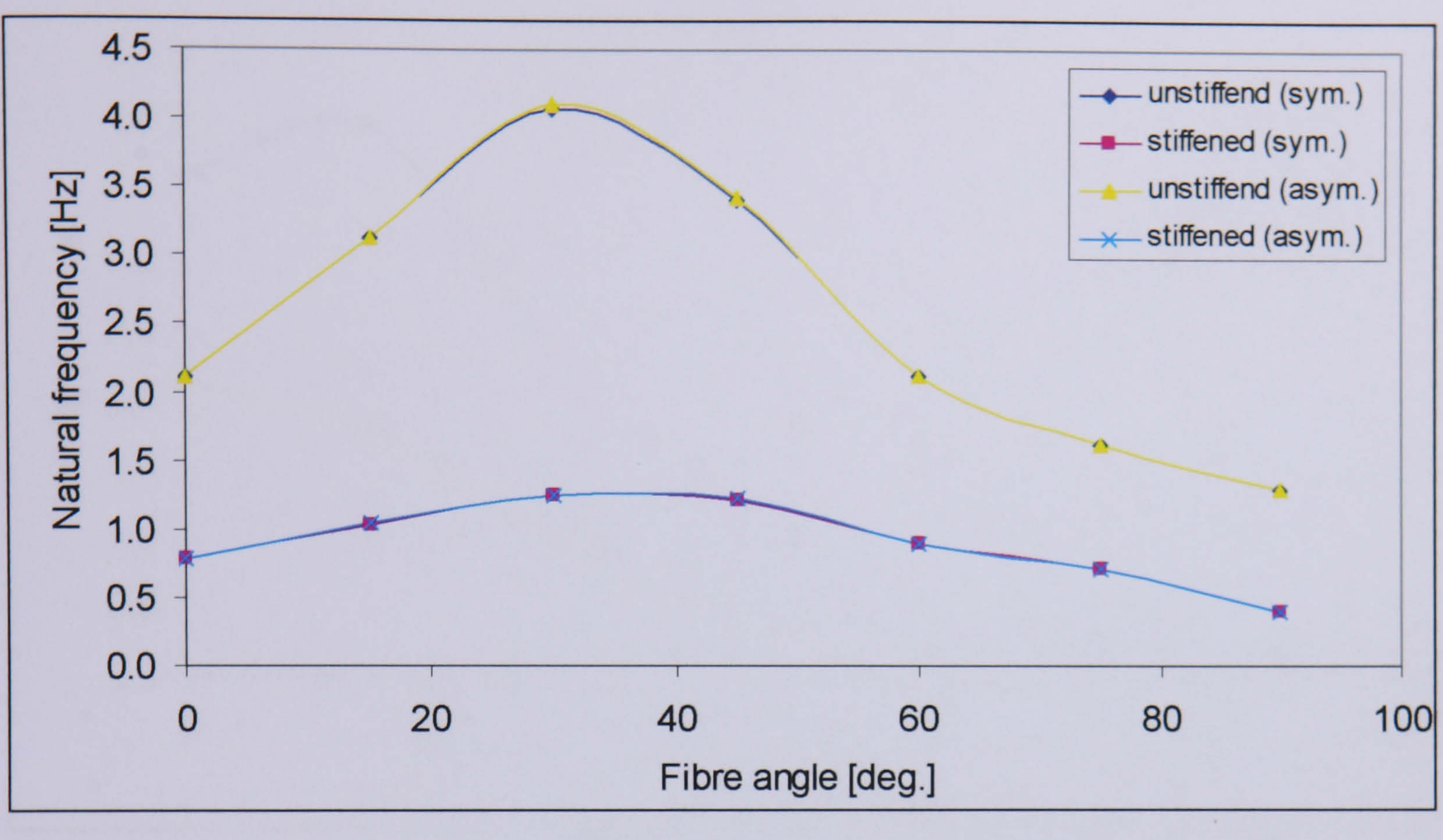

Figure (8.46) The second natural frequency versus fibre angle of stiffened and unstiffened rectangular plates of symmetric and asymmetric composites.

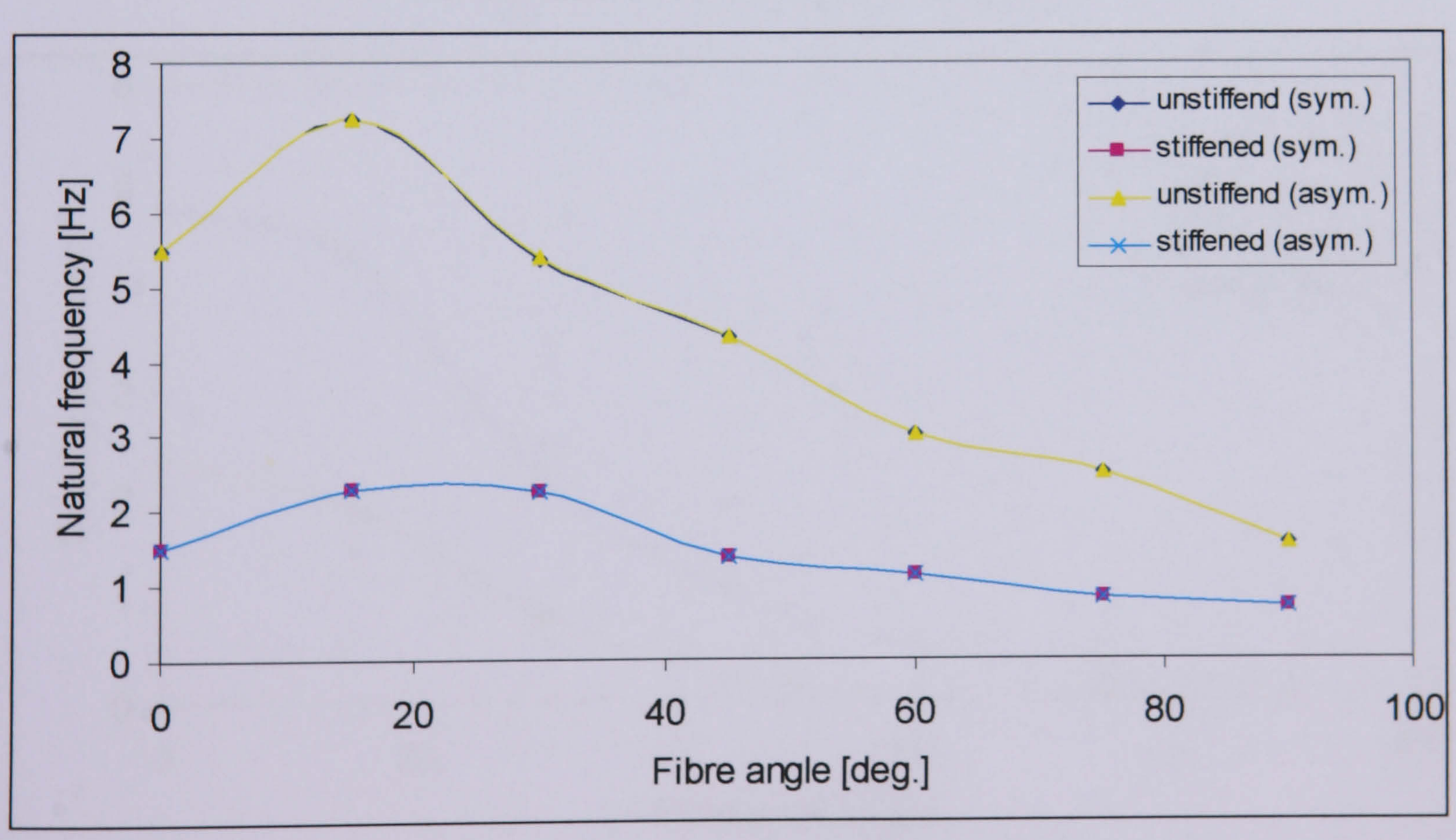

Figure (8.47) The third natural frequency versus fibre angle of stiffened and unstiffened rectangular plates of symmetric and asymmetric composites.

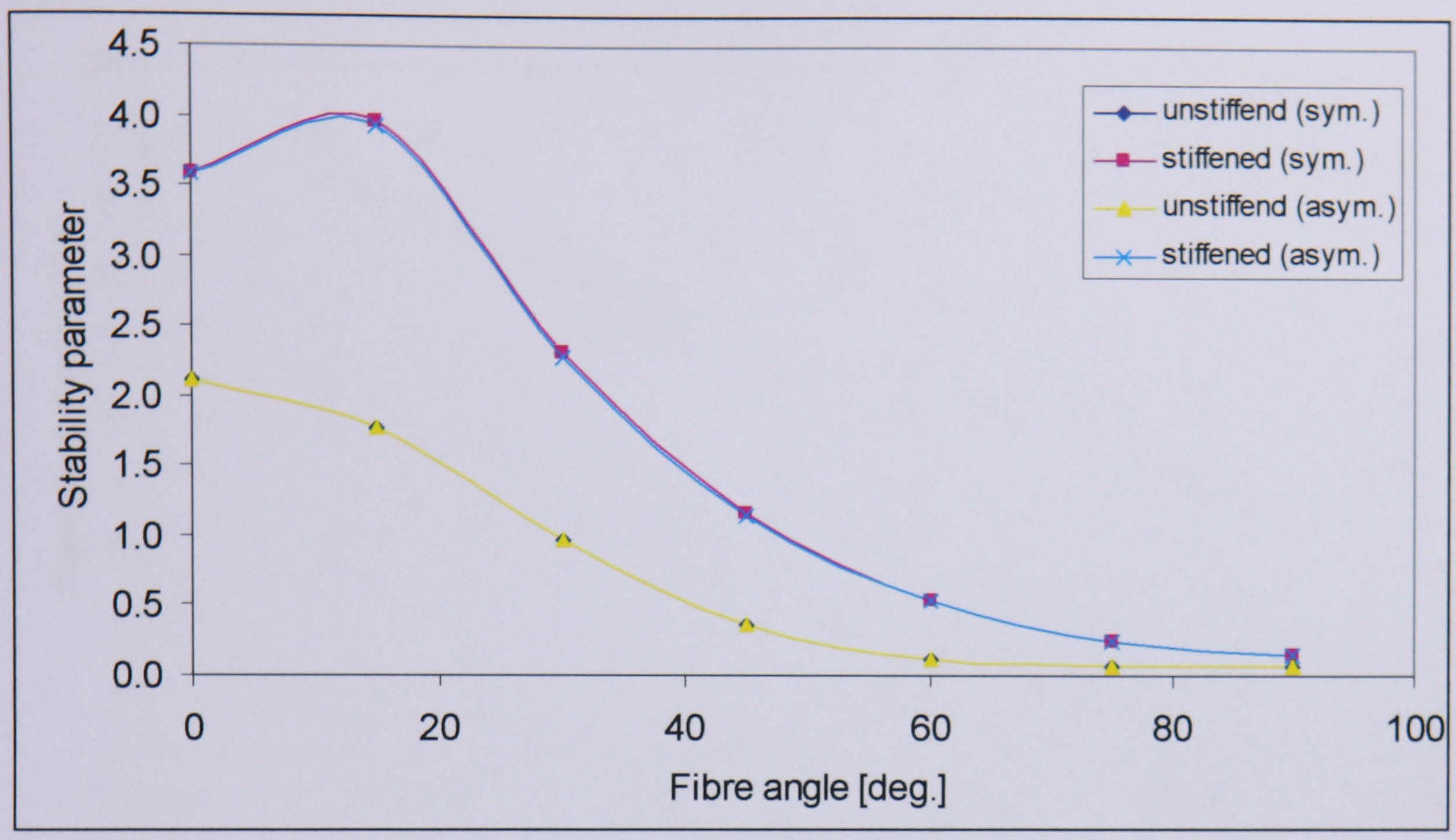

Figure (8.48) The stability parameter versus fibre angle of stiffened and unstiffened square plates of symmetric and asymmetric composites.

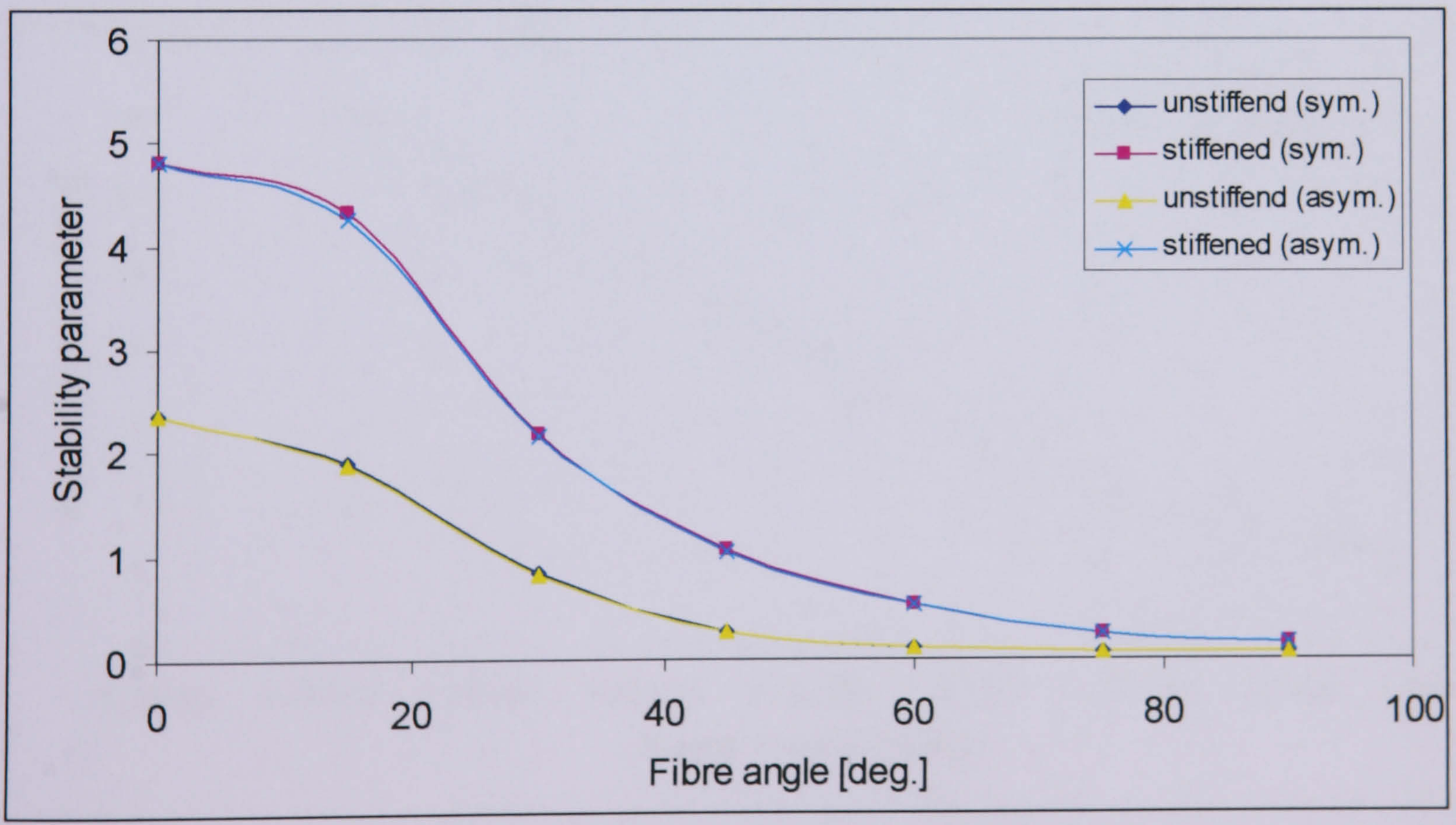

Figure (8.49) The stability parameter versus fibre angle of stiffened and unstiffened rectangular plates of symmetric and asymmetric composites.

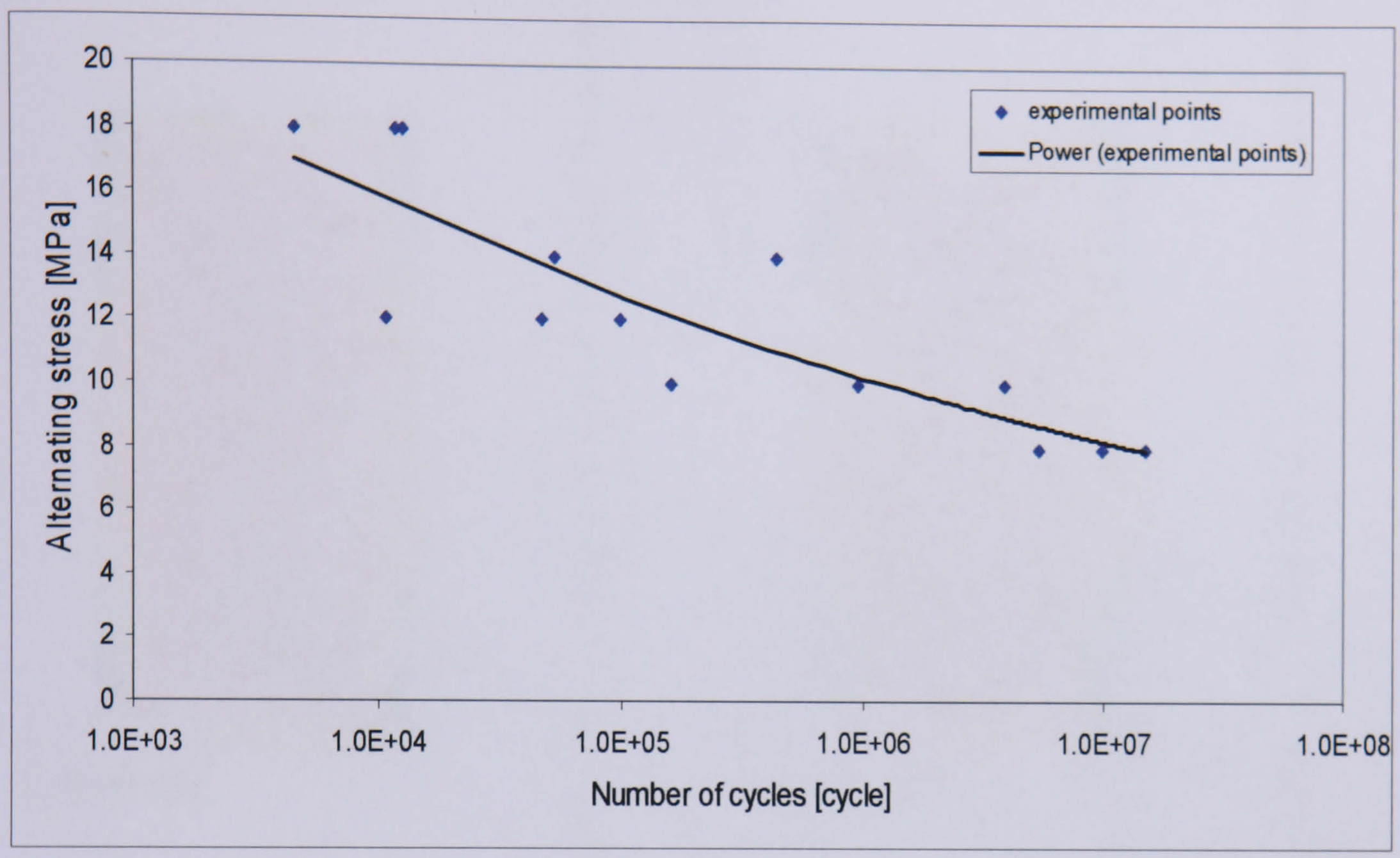

Figure (8.50) S-N diagram for carbon/epoxy under cyclic load with frequency 10 Hz.

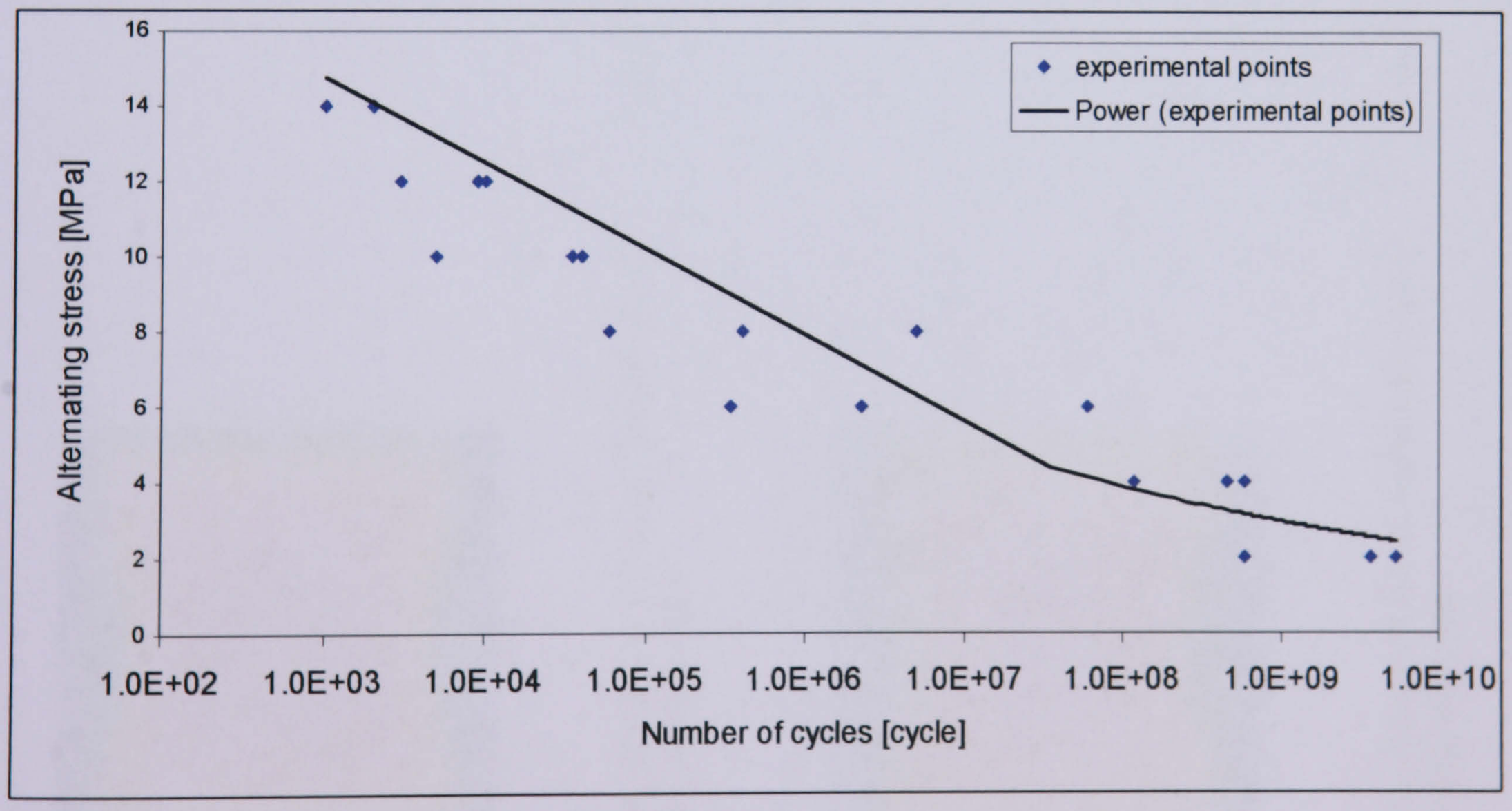

Figure (8.51) S-N diagram for glass/epoxy under cyclic load with frequency 10 Hz.

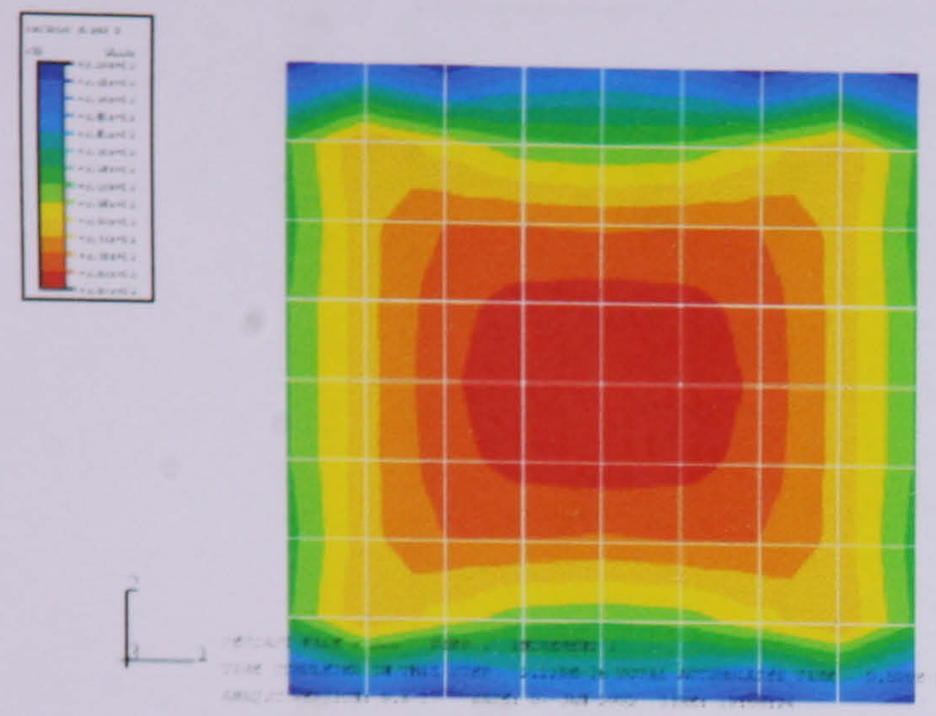

Figures (8.52) The stress σ_x contour at lower surface for square carbon/epoxy case.

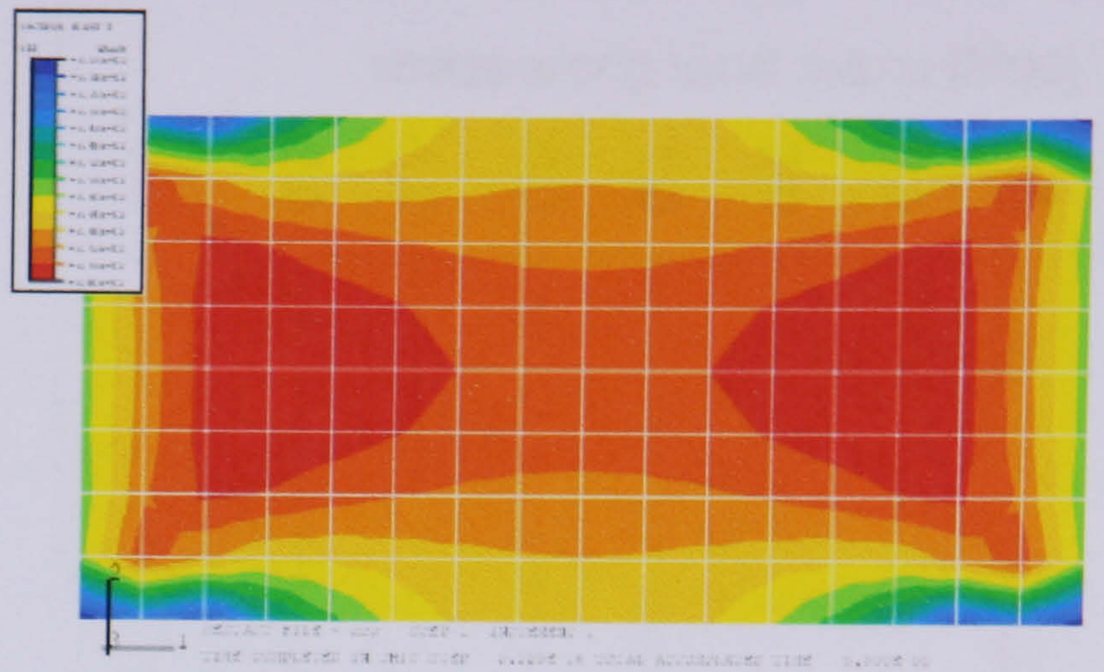

Figures (8.53) The stress σ_x contour at lower surface for rectangular carbon/epoxy case.

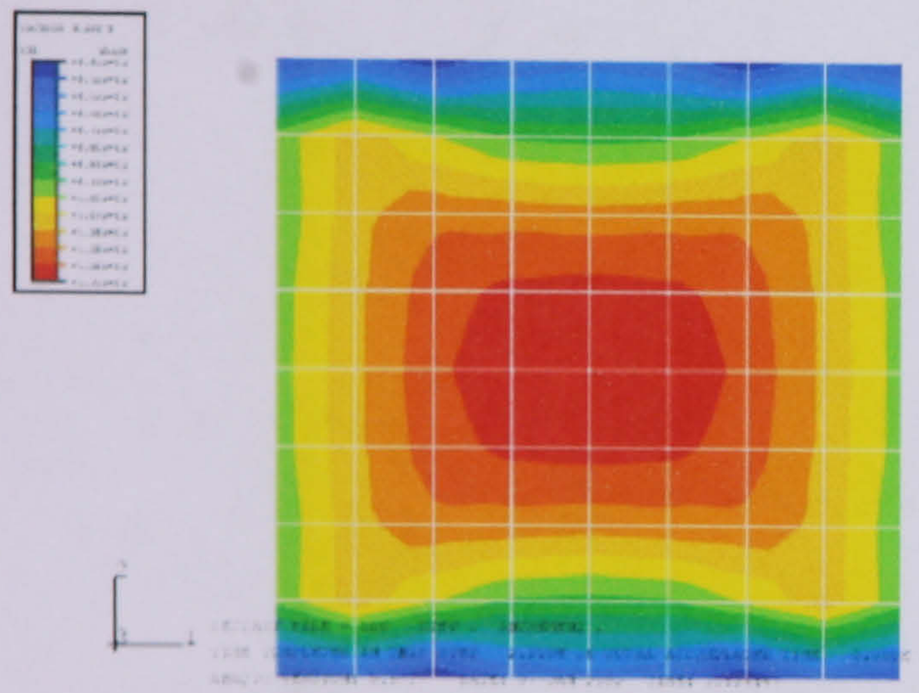

Figures (8.54) The stress σ_x contour at lower surface for square glass/epoxy case.

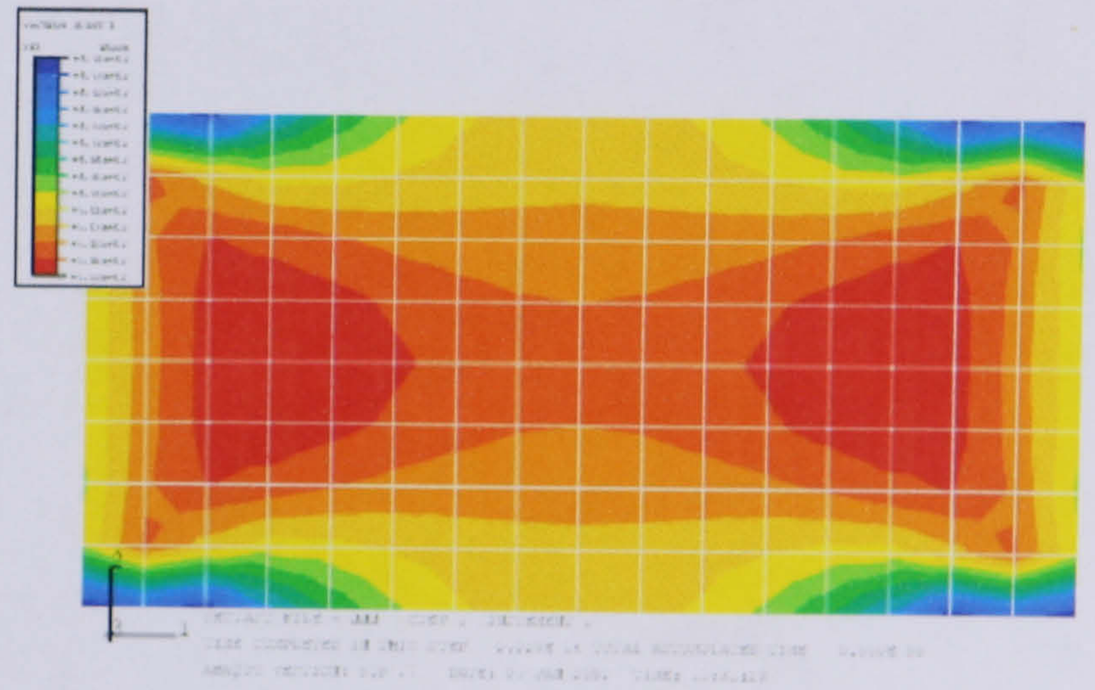

Figures (8.55) The stress σ_x contour at lower surface for rectangular glass/epoxy case.

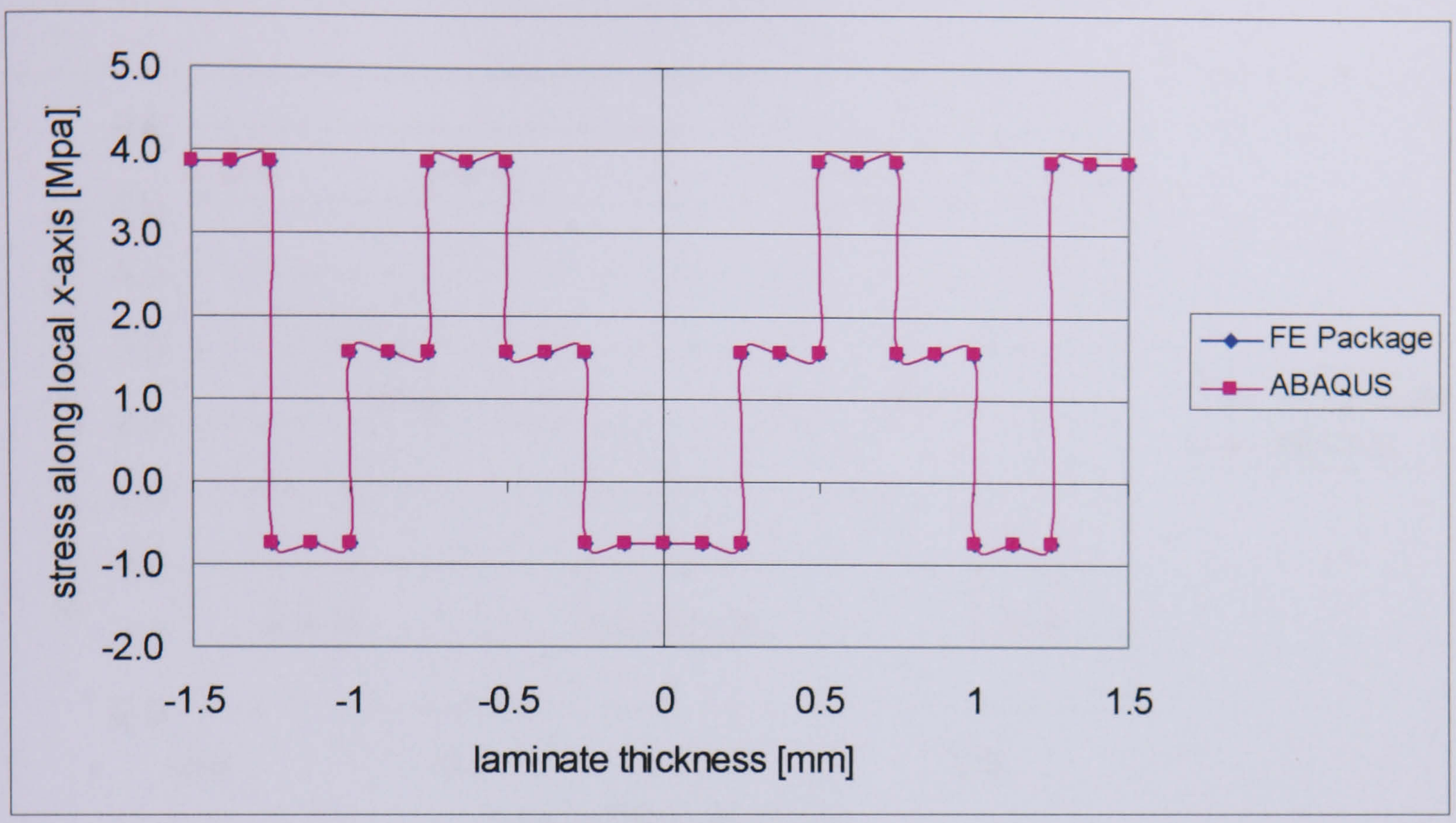

Figure (8.56) Axial stress (σ_x) distribution through the carbon/epoxy square plate thickness at node 41.

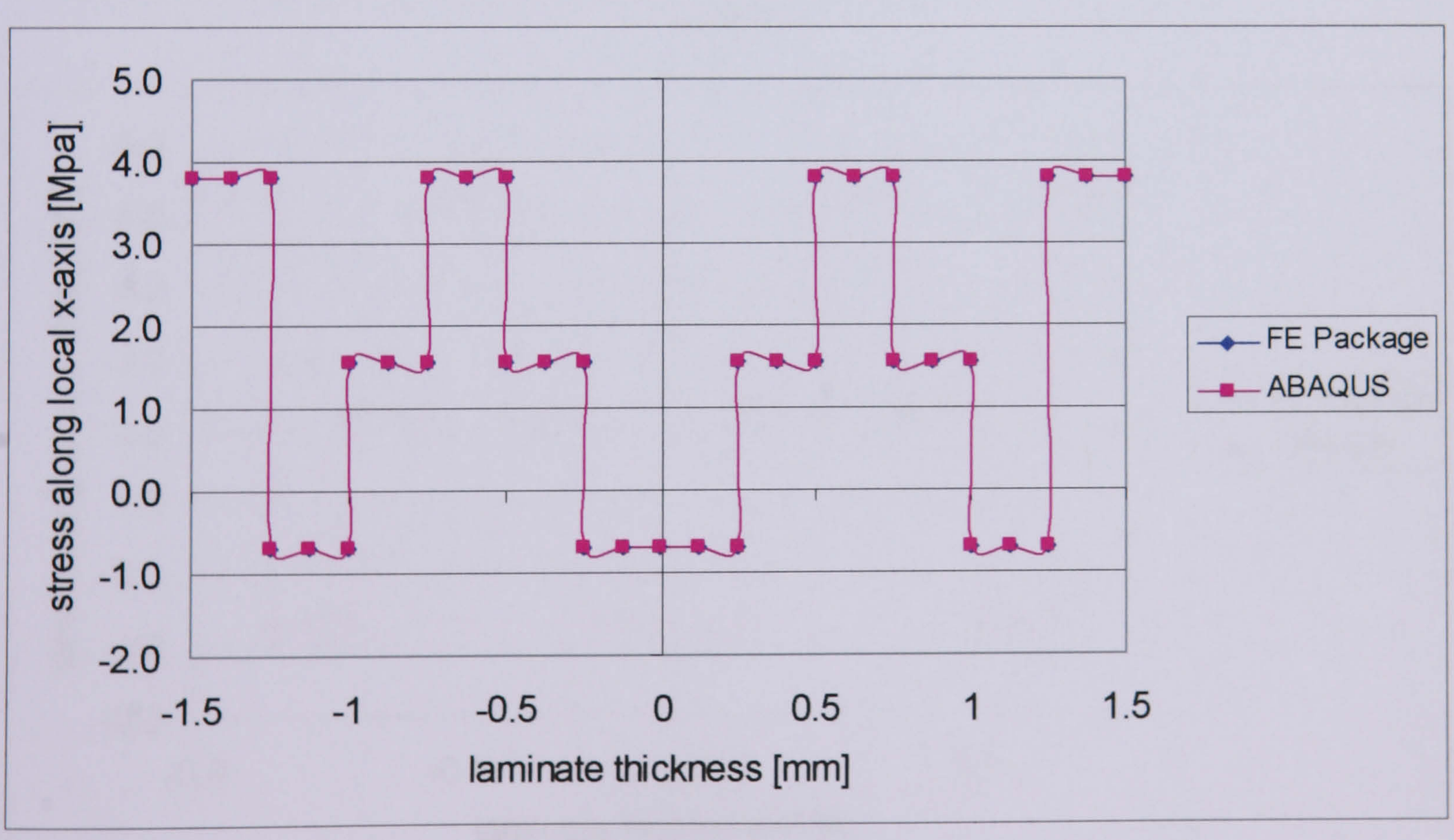

Figure (8.57) Axial stress (σ_x) distribution through the carbon/epoxy rectangular plate thickness at node 82.

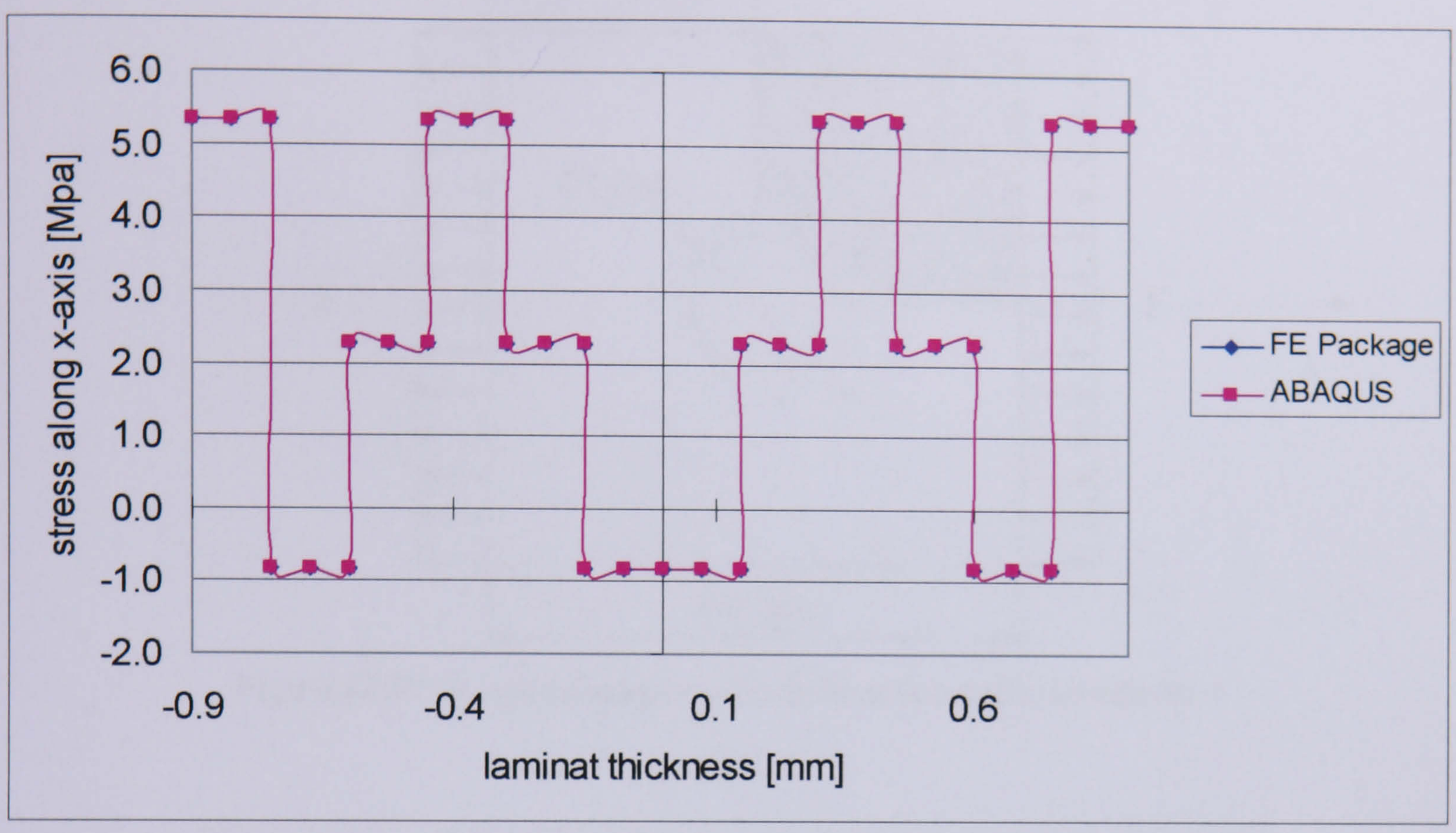

Figure (8.58) Axial stress (σ_x) distribution through the glass/epoxy square plate thickness at node 41.

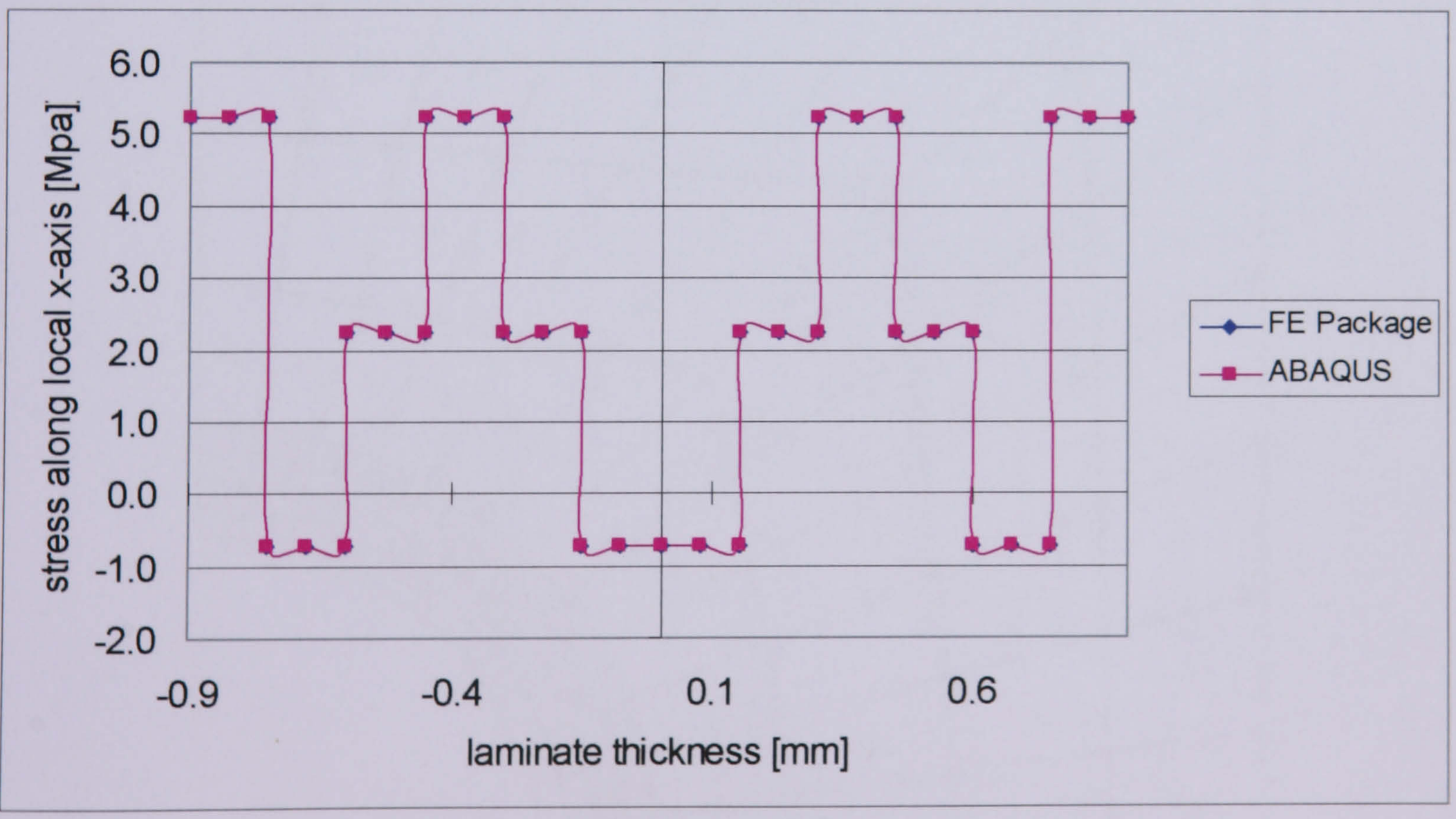

Figure (8.59) Axial stress (σ_x) distribution through the glass/epoxy rectangular plate thickness at node 72.

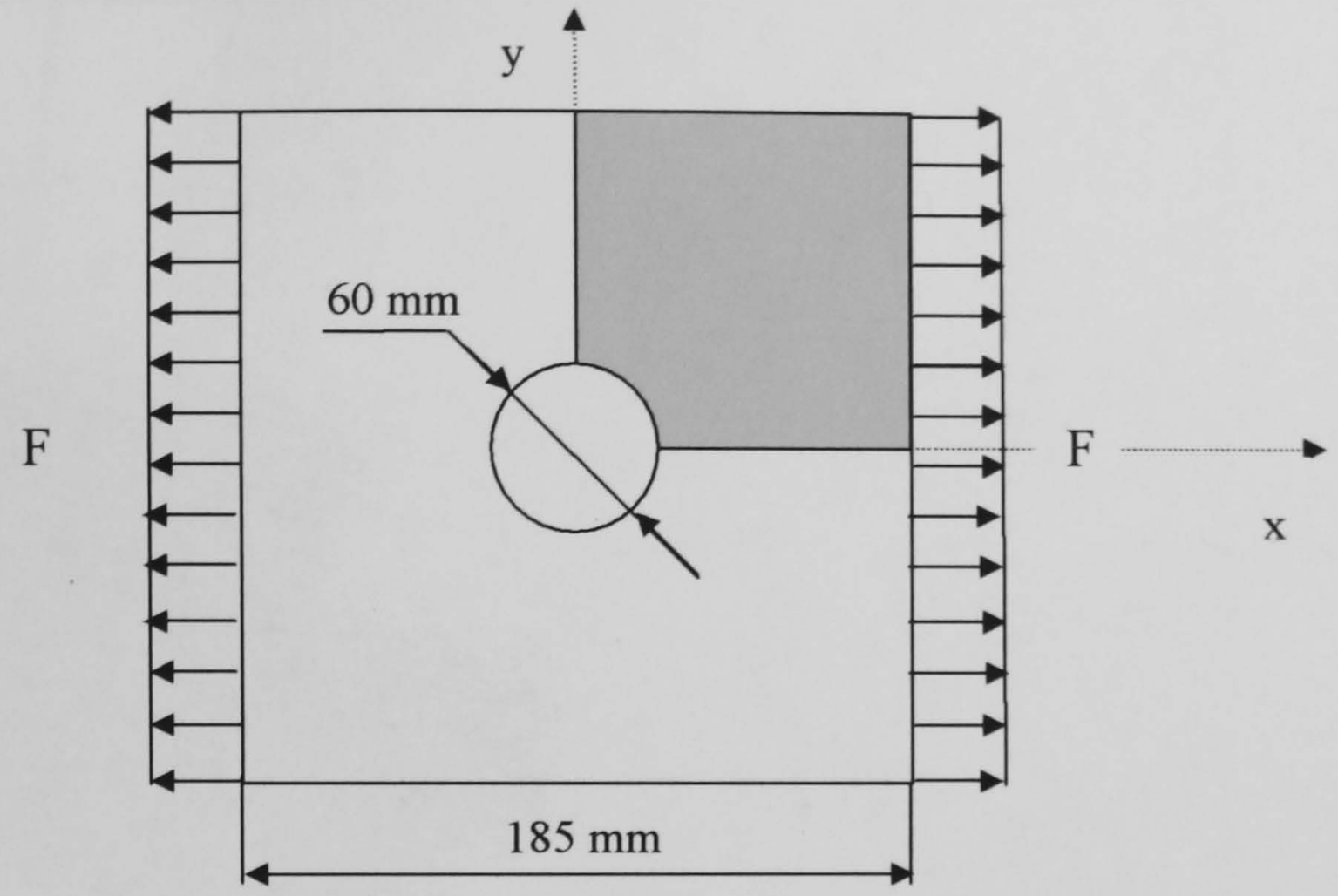

Figure (8.60) A square coupon with hole under cyclic tensile load.

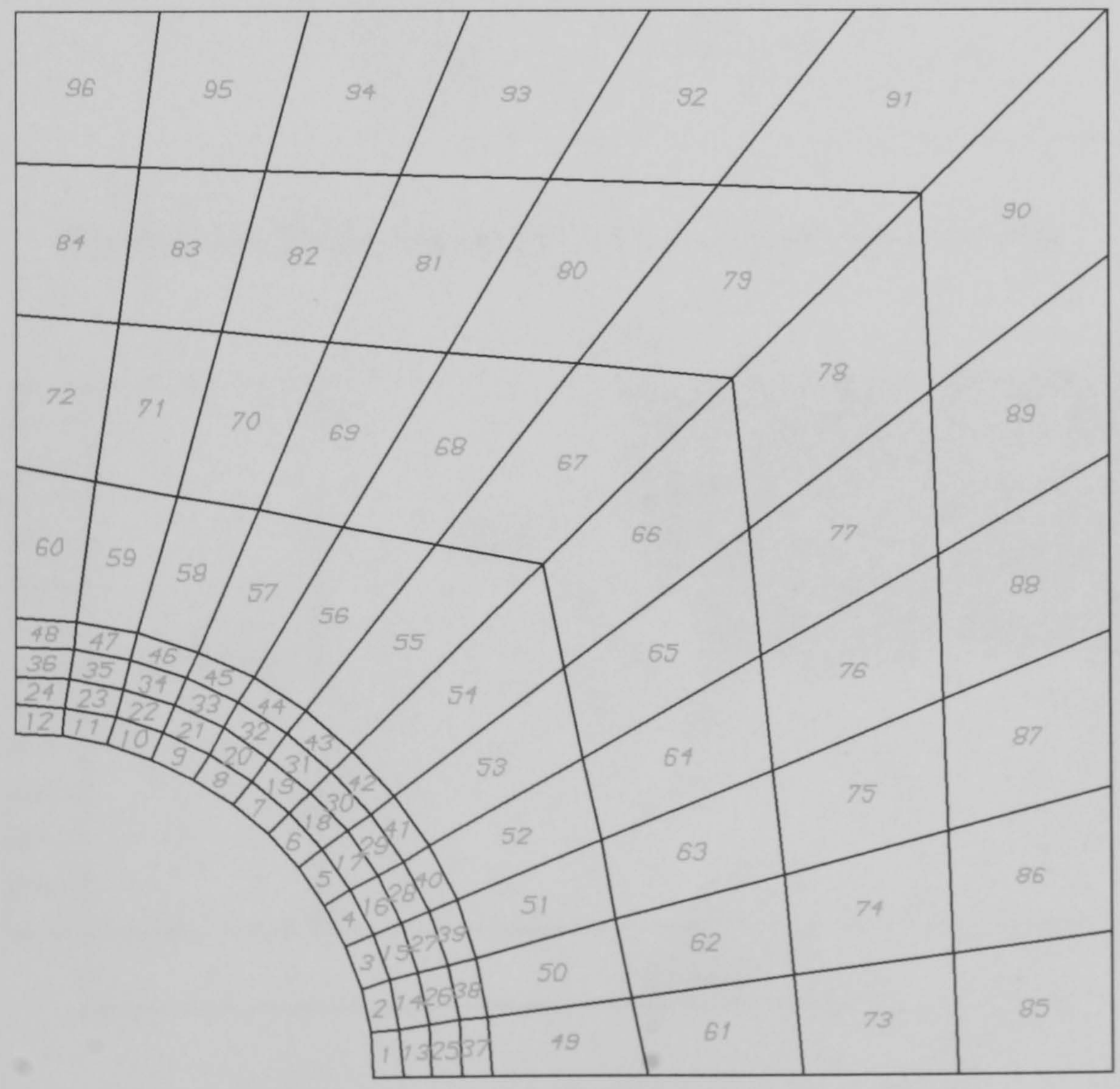

Figure (8.61) Mesh of the square plate with hole.

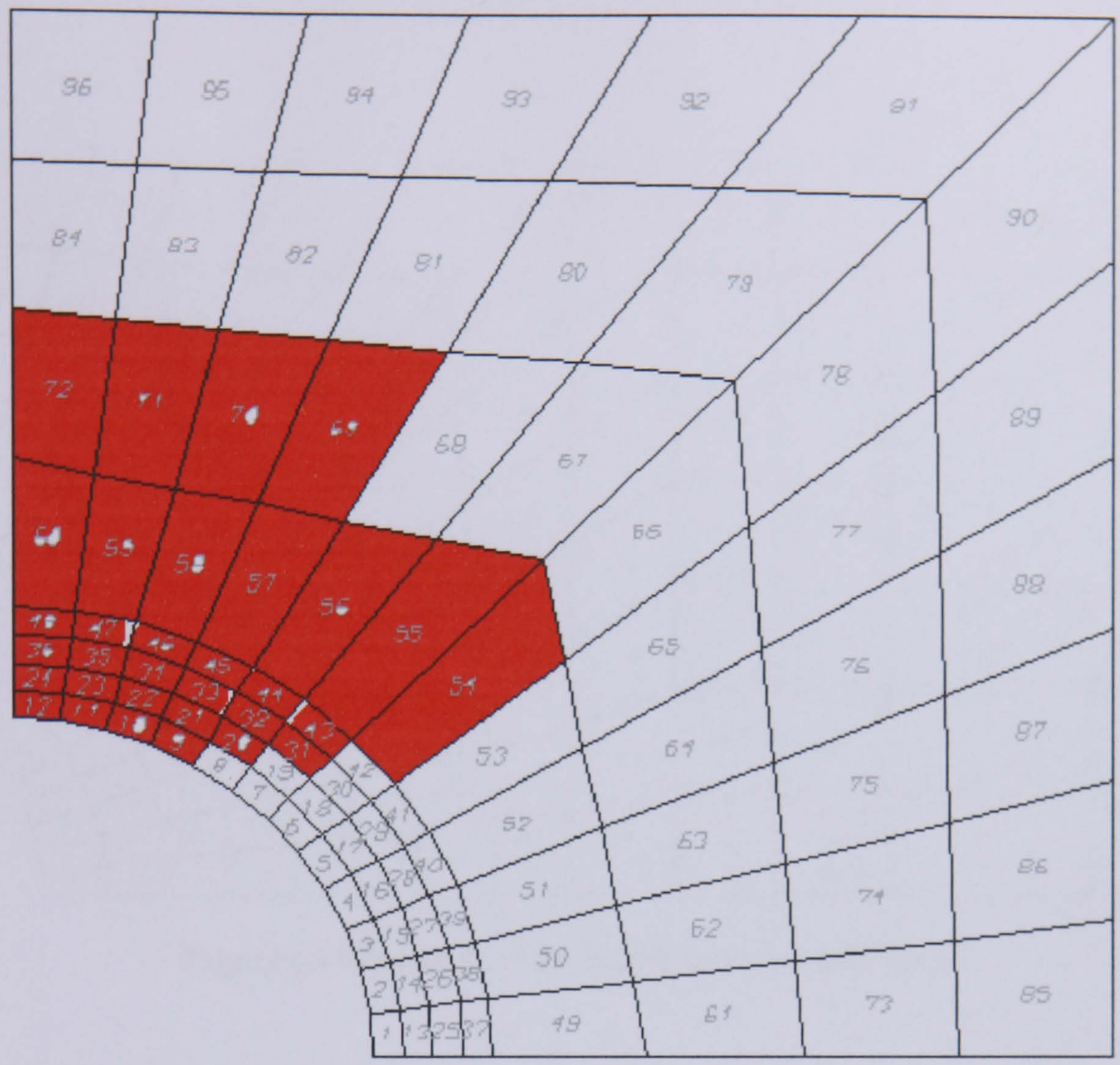

Figure (8.62) Stress concentration zone of square plate with hole.

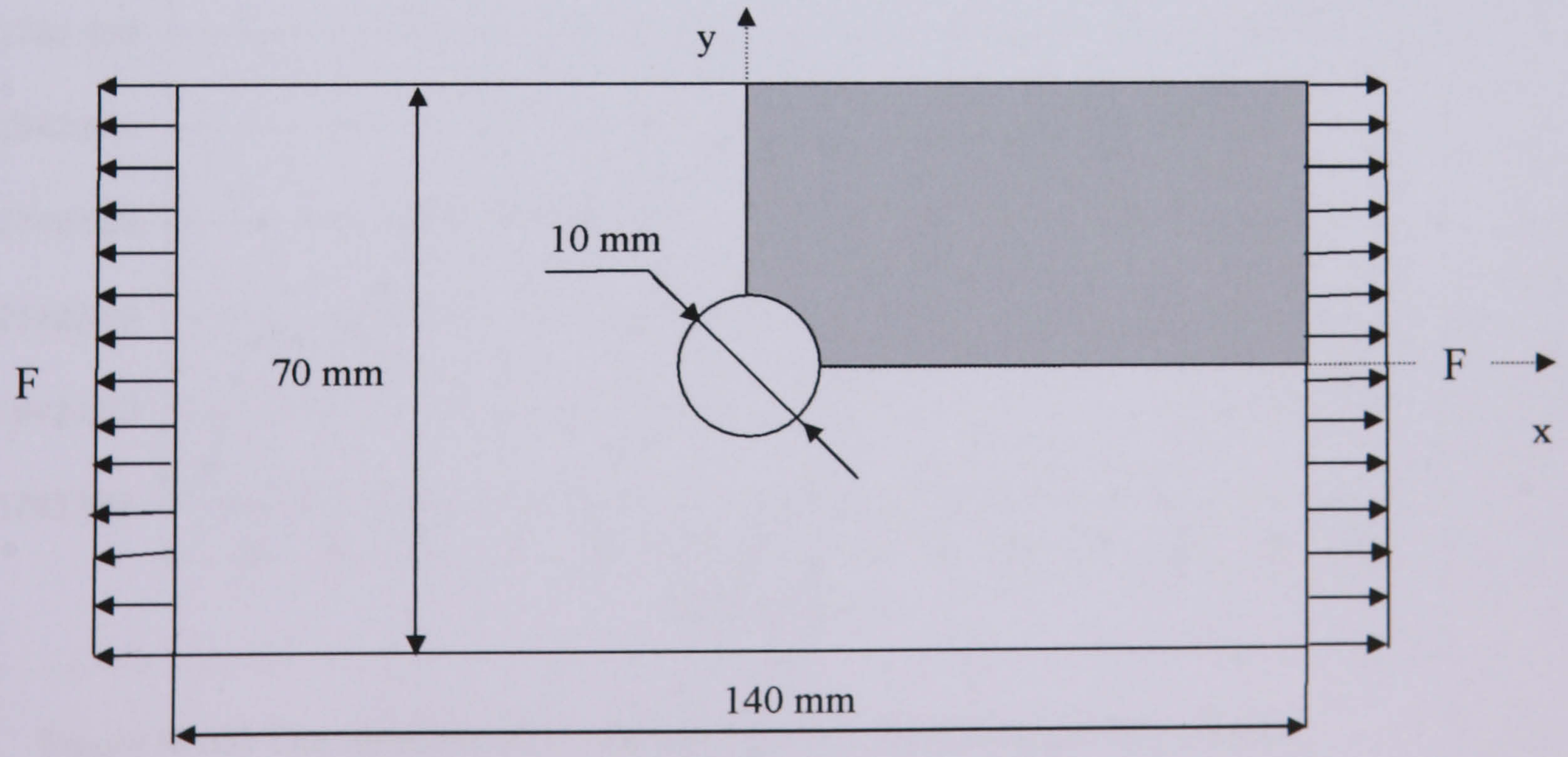

Figure (8.63) A rectangular plate with hole under cyclic tensile load.

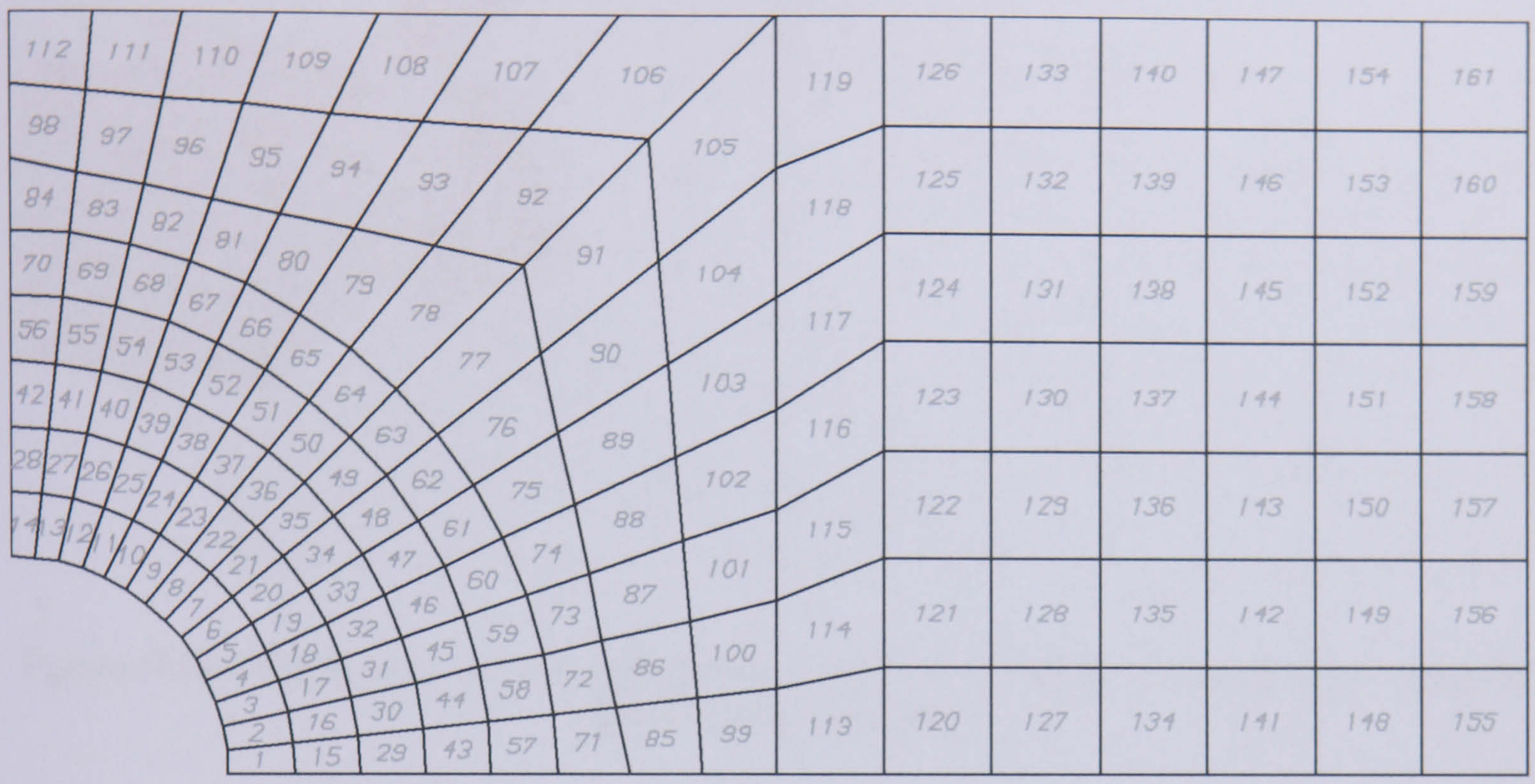

Figure (8.64) Mesh of rectangular plate with hole.

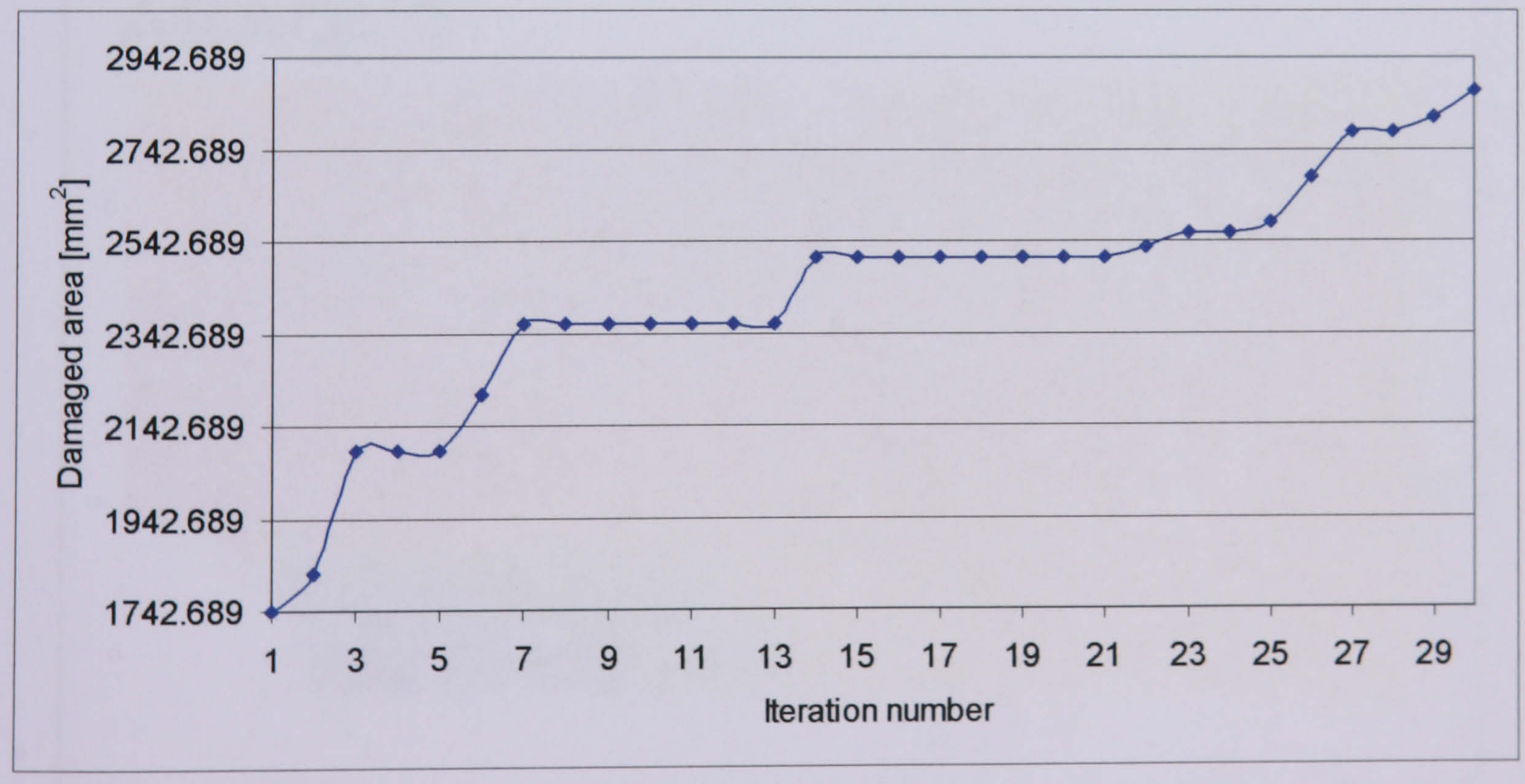

Figure (8.65) The variation of the damaged areas with the number of iterations.

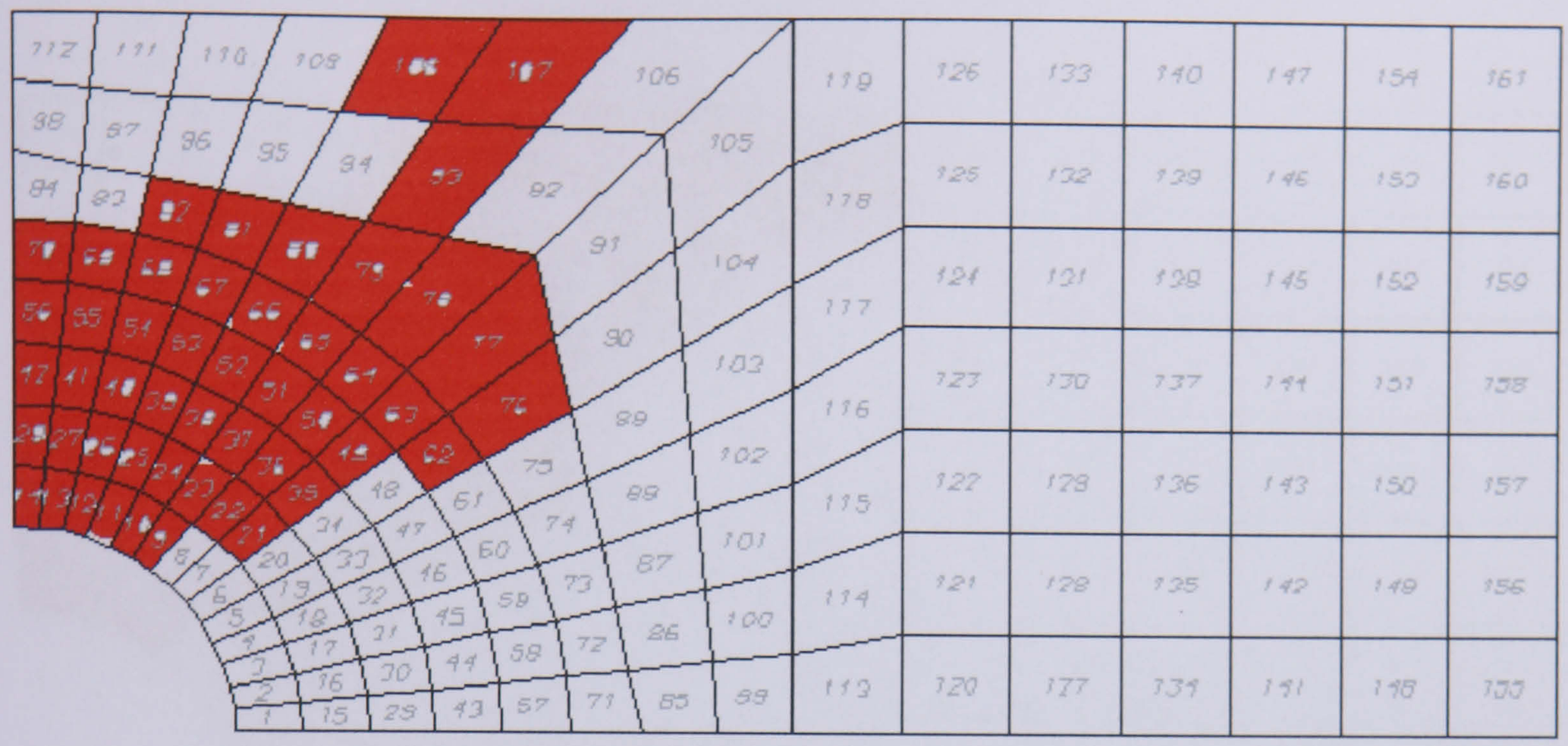

Figure (8.66) The damage zone of layer number two of the plate at the first iteration using the finite element package.

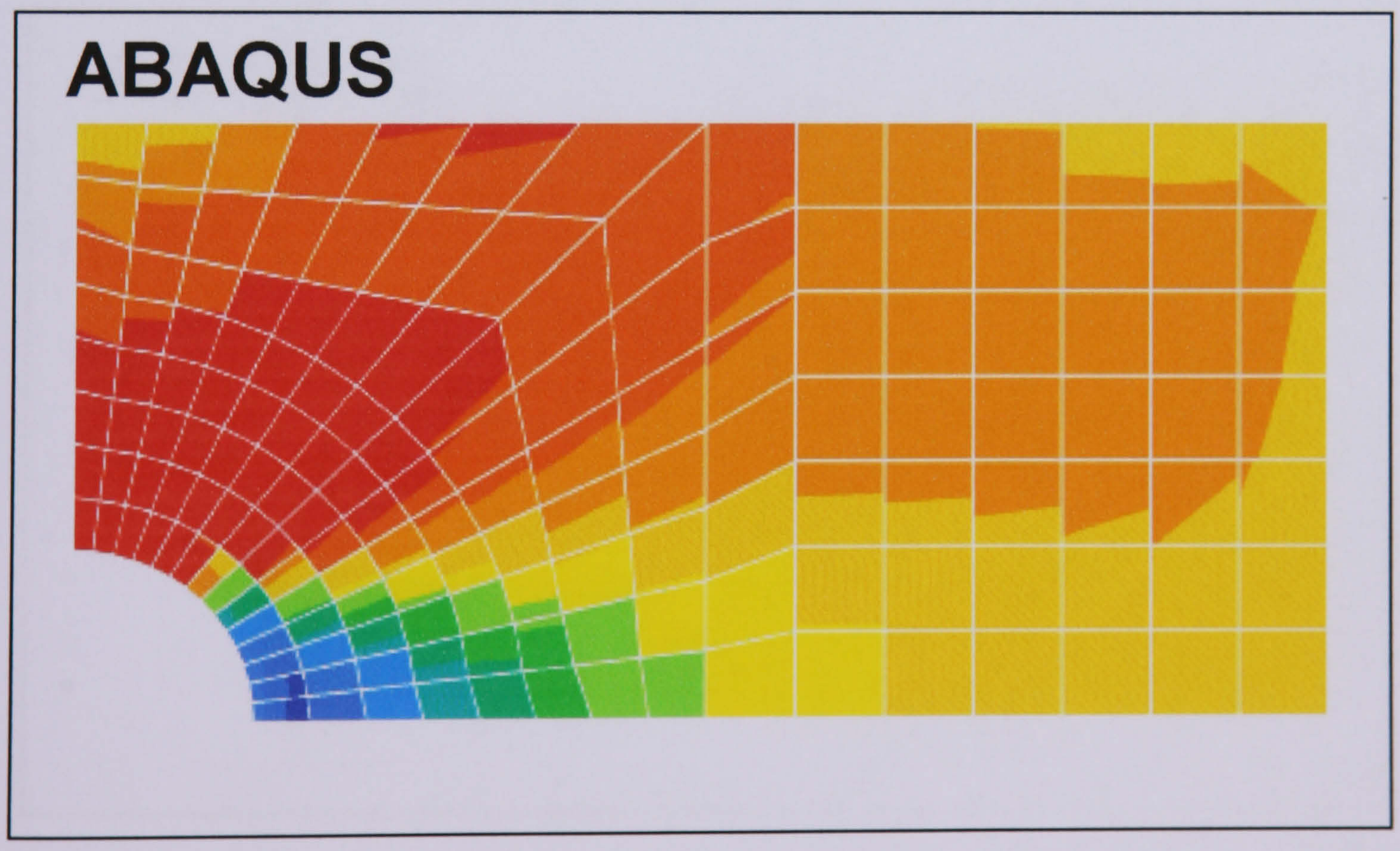

Figure (8.67) The damage zone of layer number two of the plate at the first iteration using ABAQUS package.

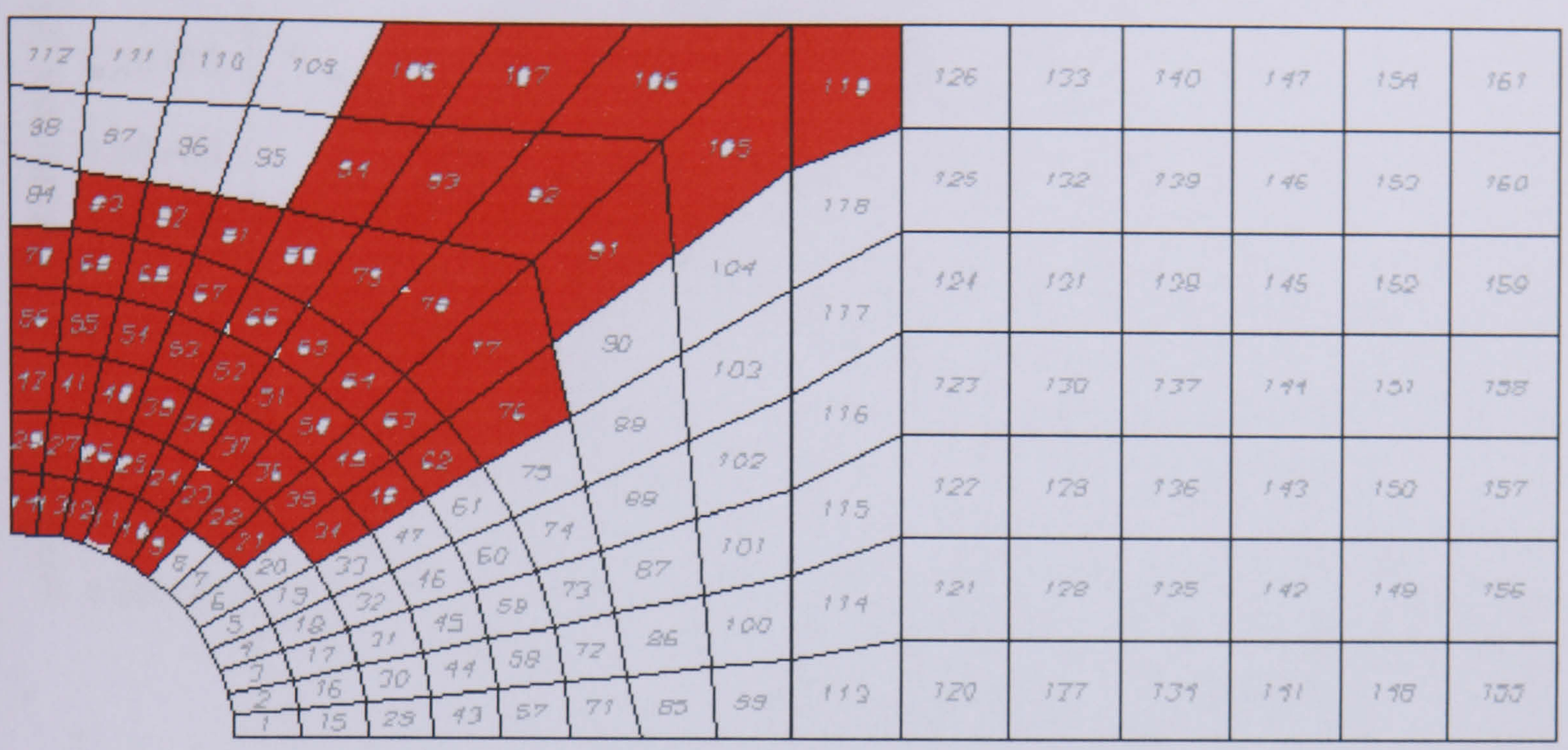

Figure (8.68) The damage zone of layer number two of the plate at the 23rd iteration using the finite element package.

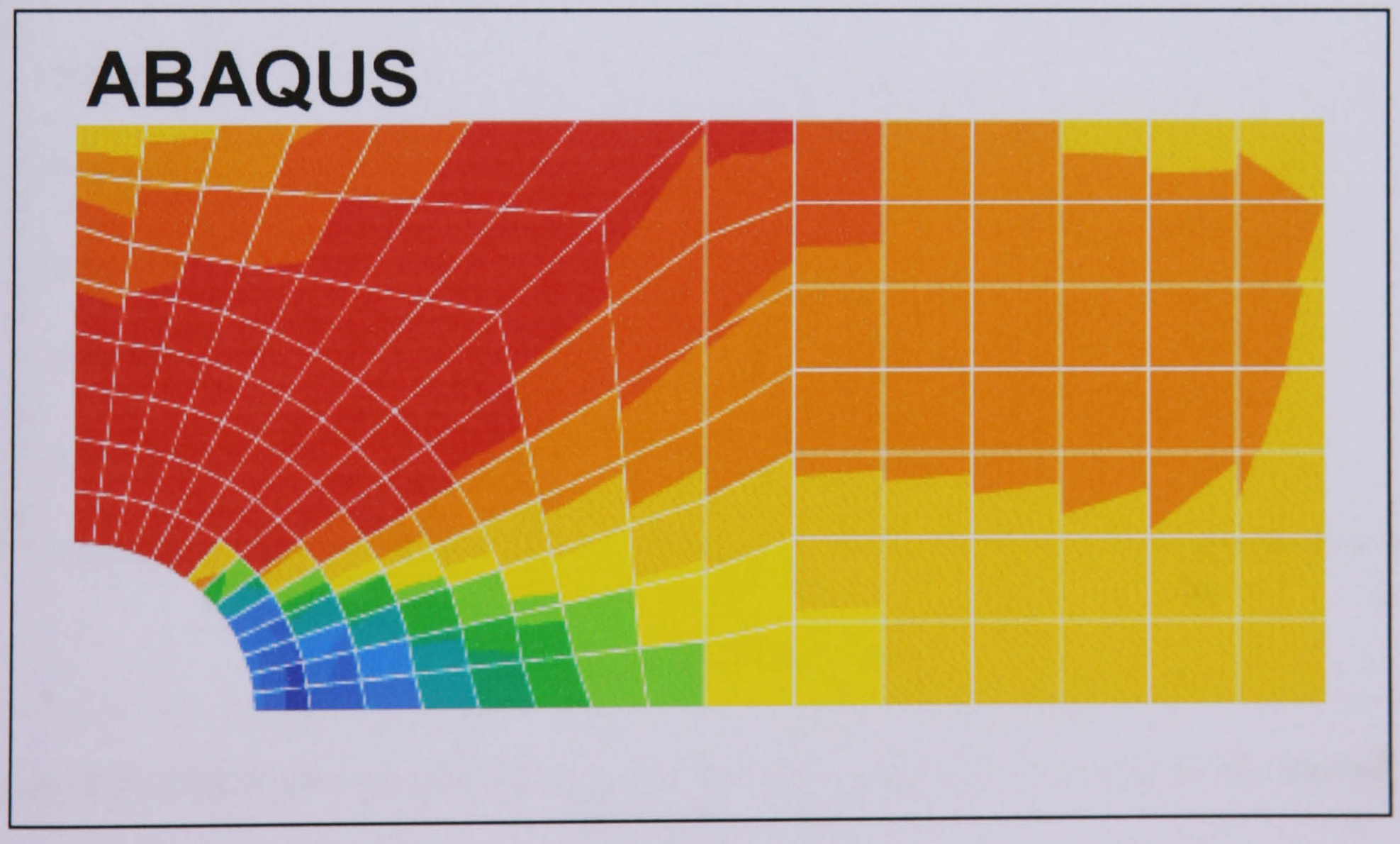

Figure (8.69) The damage zone of layer number two of the plate at the 23rd iteration using the ABAQUS package.

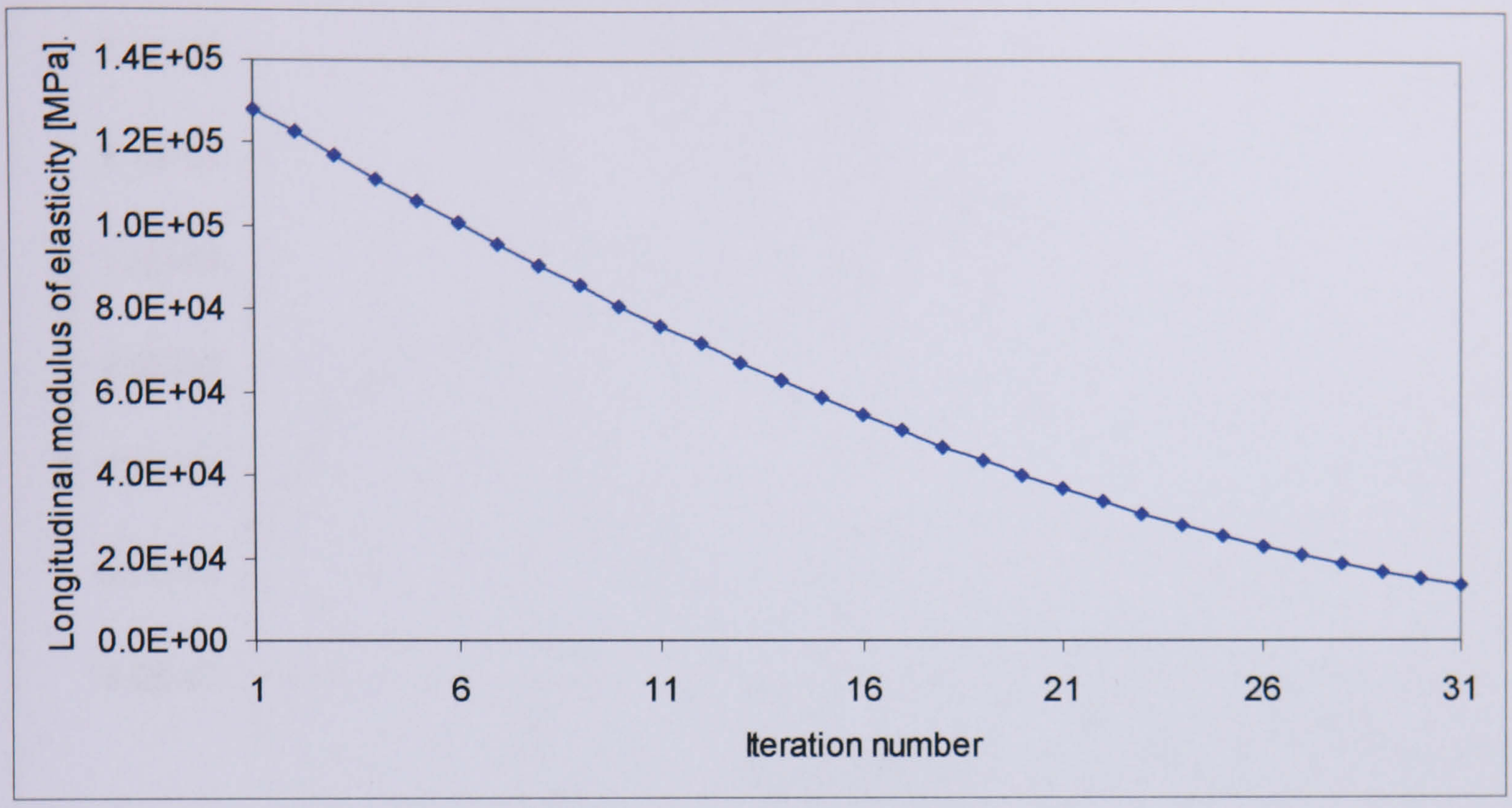

Figure (8.70) Longitudinal modulus of elasticity versus the number of iterations for the element 14 within layer number 2.

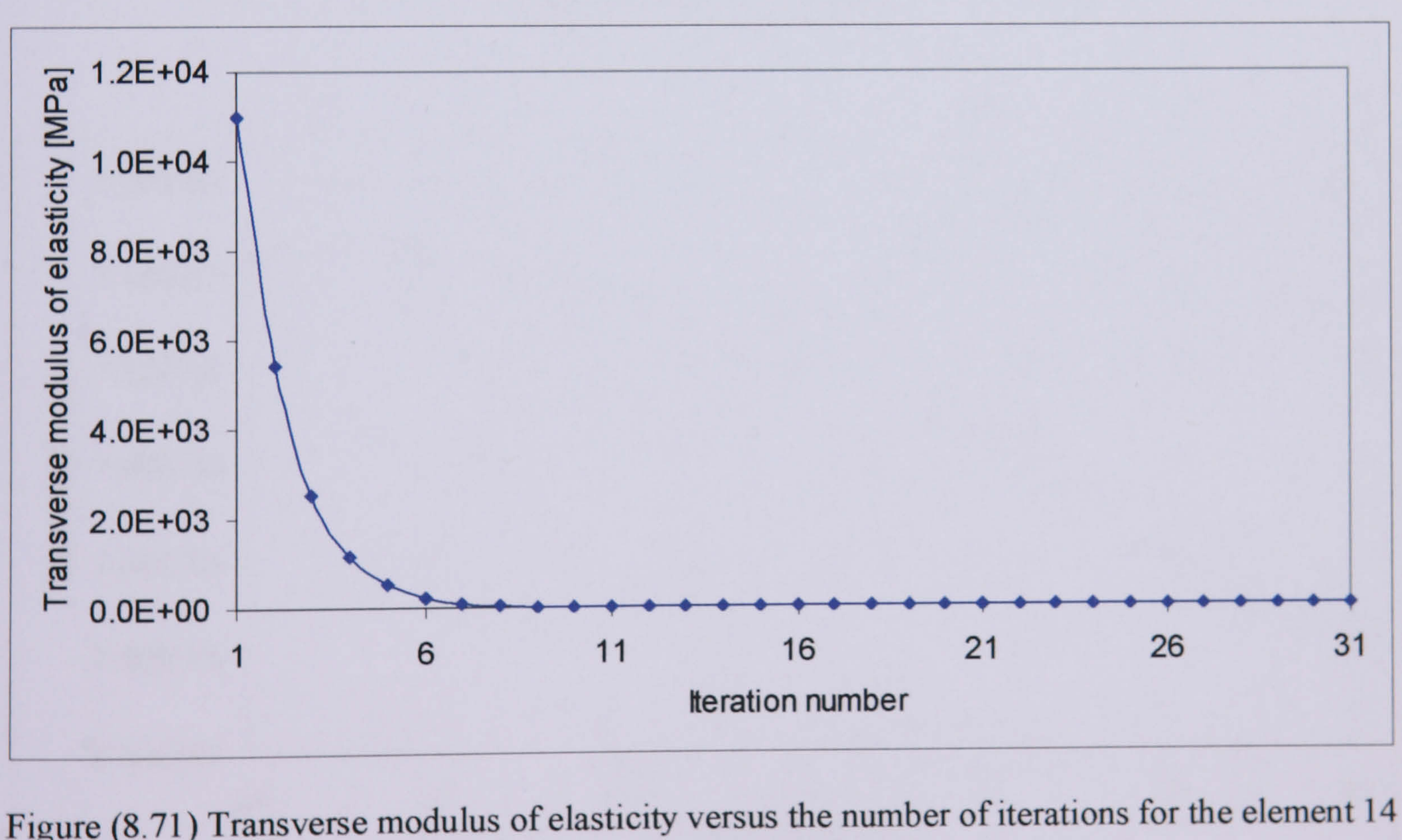

Figure (8.71) Transverse modulus of elasticity versus the number of iterations for the element 14 within layer number 2.

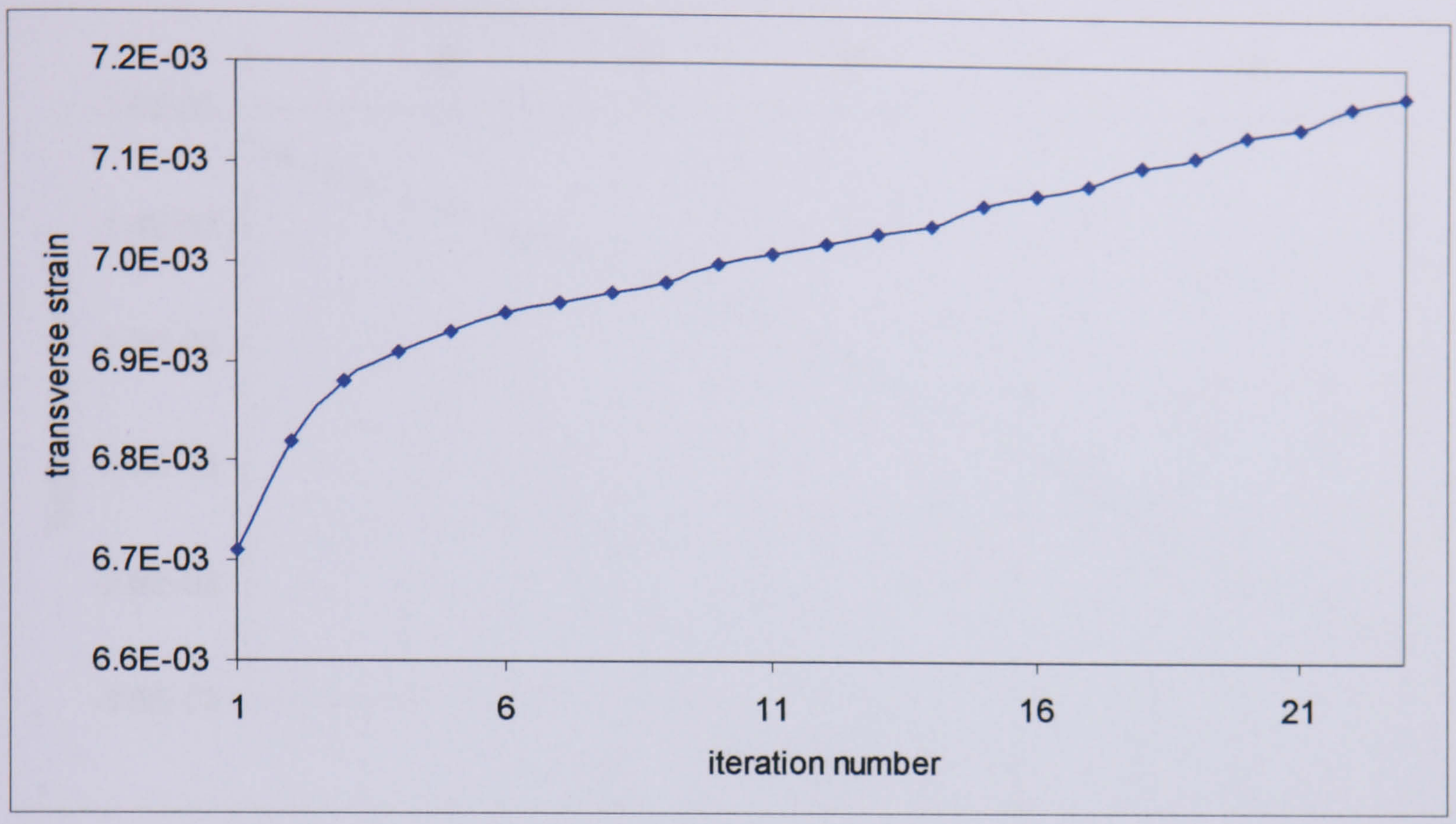

Figure (8.72) The transverse strain (strain in matrix direction) with the first 23 iterations for the element 14 within layer 2.

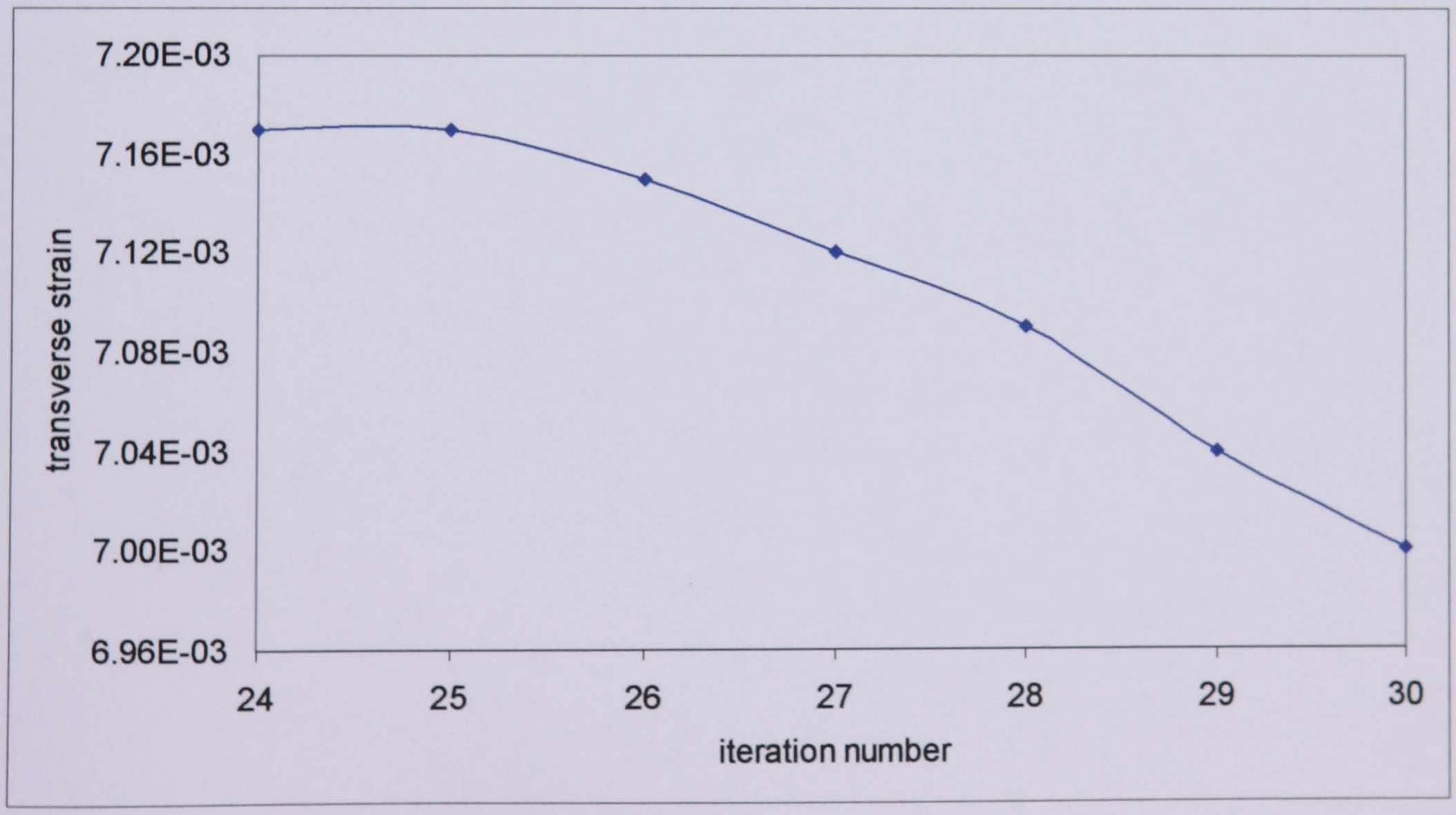

Figure (8.73) The transverse strain (strain in matrix direction) with the rest of iterations for the element 14 within layer 2.

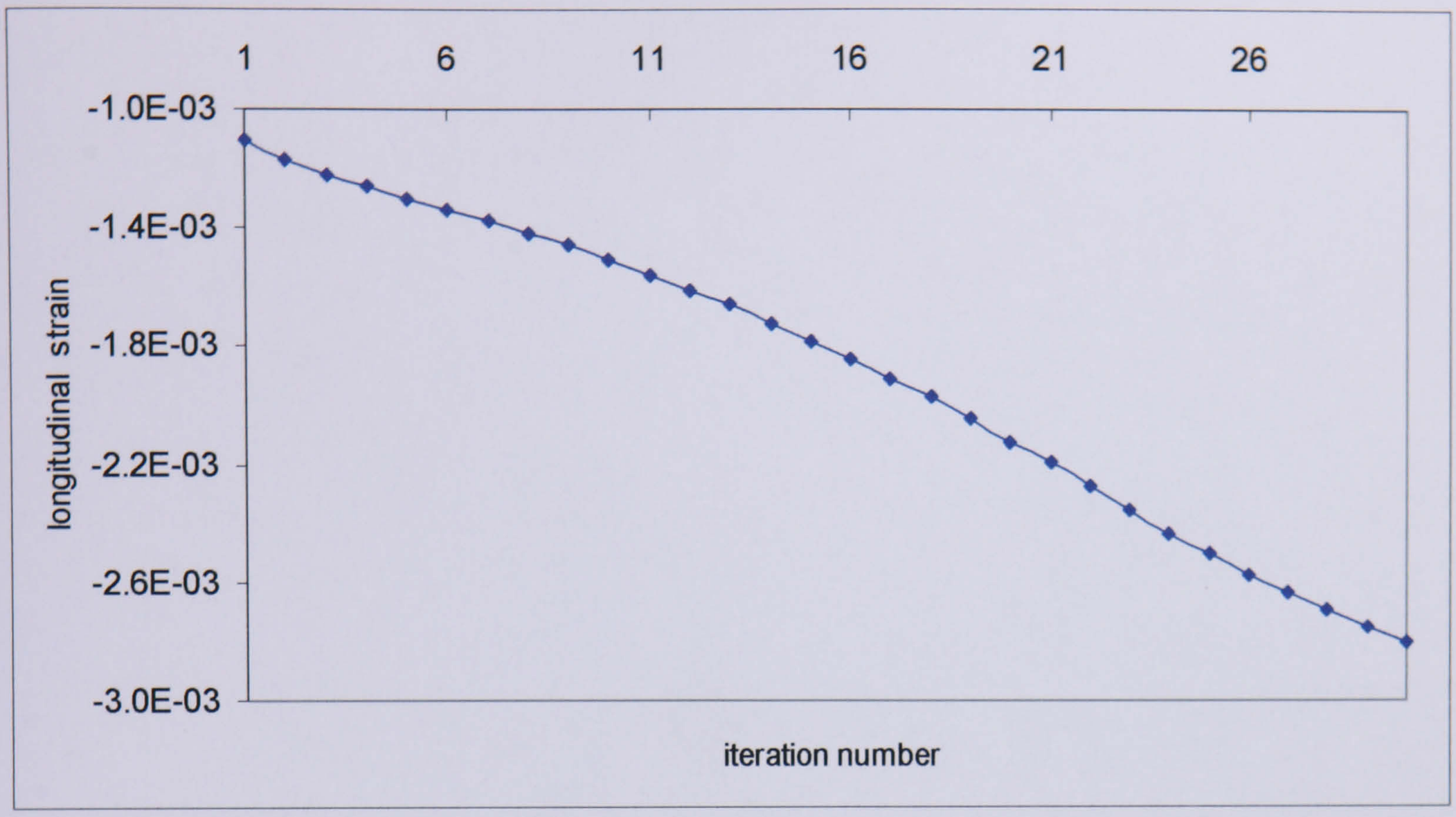

Figure (8.74) Longitudinal strain (strain in fibre direction) with the number of iterations for the element 14 within layer 2.

9

CONCLUSIONS

9.1 CONCLUSIONS

The basic objectives of this research have been successfully achieved, and a powerful versatile finite element package, which is capable of linear and nonlinear static analysis, stability analysis, natural frequency analysis and fatigue damage analysis for thin and thick composite layered plates and shells, has been developed based on advanced theories and efficient algorithms.

New finite element derivation has been presented based on a high-order shear deformation theory, which proves to provide accurate results for different types of analyses for thin and thick composite layered plates and shells.

The coupling between bending and membrane behaviour has been introduced through the study of geometric nonlinearity effect and is represented separately by the equivalent force vector $\underline{F}_L$, and simple expressions for the nonlinear finite element equilibrium equations have been obtained.

The developed finite element package has been successfully validated through comparison of the package results with published and experimental results. The validation results have proved to be accurate for thin and thick composite plates and shells with different types of load, different boundary conditions, different number of layers, and different stacking sequences.

Experimental measurements have been accomplished to validate the stability and natural frequency analyses and to predict the fatigue life diagrams (S/N diagrams), for two different types of composite materials (carbon/epoxy and glass/epoxy).

Parametric study has been carried out on different composite plates. Some conclusions can be summarized from this study as follows:

(i) Conforming and non-conforming elements provide close results to each other. Nevertheless, it was observed that the non-conforming elements are more accurate to be adopted for stiffened plate analysis as the conforming elements are only suitable for plates.

(ii) The natural frequencies decrease by increasing the number of surfaces where it is recognized that the natural frequencies of the unstiffened square plates are higher than the corresponding

ones for the unstiffened rectangular plates, and the natural frequencies of the stiffened square plates are also higher than those of the rectangular stiffened plates.

(iii) In contrast with the natural frequencies, the stability parameter increases by increasing the number of surfaces where it is recognized that the stability parameter of stiffened rectangular plates is higher than that of the stiffened square plates. Similarly, the stability parameter of the unstiffened rectangular plates is higher than that of the square unstiffened plate.

(iv) The natural frequencies of the stiffened plates are lower than those of the unstiffened ones, while the stability parameter of the stiffened plates is higher than that of the unstiffened ones.

(v) The stacking sequence has no effect on the stability and the natural frequency results for unstiffened and stiffened plates at fibre angles 0° and 90° but a small, not effective, difference has been observed with other fibre angles.

Fatigue life assessment by fatigue damage growth for composite plates and shells can be achieved via a single run of the developed package, which automatically considers the damage progress by means of different steps during which material degradation takes place. The energy release rate and the rate of growth of the damaged area are estimated automatically as functions of the damaged area, allowing the number of cycles to failure to be calculated by direct integration. The algorithm adopted in the package leads to enormous saving in user efforts and computer resources, as compared with procedures based on existing finite element packages.

Some original contribution has been achieved through the course of this study, which can be summarized as follows:

(i) The derivation of a new finite element based on the high-order shear deformation theory, which is accurate for a wide range of thickness.

(ii) The formulation of a simple and accurate algorithm for the geometric nonlinear stress analysis.

(iii) The development of a versatile computer package based on the proposed finite element theory to deal with different types of analysis, such as, static analysis, stability analysis, natural frequency analysis and fatigue damage analysis.

(iv) The formulation and implementation of an efficient automatic algorithm for fatigue life assessment of composites by fatigue damage growth, which leads to a considerable saving in user efforts and computer resources.

Some papers based on the developed work have been published (Moutaz et al. 1999, 2001), and others are being prepared for publication.

9.2 FUTURE RESEARCH

The research in the field of fatigue damage of composite materials is very demanding and requires continuous investigation, both theoretically and experimentally. Some recommendations for further work are summarized as follows:

(i) Experimental measurements on fatigue damage growth are required to provide more accurate information on material degradation, and rates of damage growth, as required for the life assessment algorithm.

(ii) The range of applications of the package can be extended to include fatigue damage by delamination and nonlinear dynamic analysis.

(iii) The derivation of high-order quadrilateral and triangular elements with more nodes, so as to deal accurately with different geometrical shapes.

REFERENCES

Attia O. (1996) "Finite element static, dynamic, and flutter analysis of rotating composite layered plates and shells" Ph.D. Thesis, SME, Cranfield University.

Attia O. and El-Zafrany A. (1999) "A high-order shear element for nonlinear vibration analysis of composite layered plates and shells" International Journal of Mechanical Sciences, Vol. 41, 461-486.

Attia O., Kinloch A. J. and Matthews F. L. (2001) "Modelling the fatigue life of polymer-matrix fibre-composite components" Composites Science and Technology, Vol. 61, 2273-2283.

Ashton J. E. and Whitney J. M. (1970) "*Theory of laminated plates*" Progress in material science series, Vol. IV, Technomic Publication, Stanford.

Badaliance R. and dill H. d. (1982) "Damage mechanism and life prediction of graphite/epoxy composites" Damage in composite Materials, ASTM STP 775, K. L. Reifsnider, Ed., American Society for testing and Materials, 229-242.

Barbero E. J. (1998) "*Introduction to composite material design*" PA: Taylor and Francis, Philadelphia.

Bathe K. J. and Edward D. L. (1976) "*Numerical methods in finite element analysis*" Prentice-Hall, Englewod Cliffs, New Jersey.

Boniface L. and Ogin S. L. (1989) "Application of Paris equation to the fatigue growth of transverse ply cracks" Journal of Composite Material, Vol. 1, 735-754.

Carl O. (1982) "*Fatigue design*" A. Wheaton & Co. Ltd., Exeter, UK.

Chang K. and Chang F. (1987a) "A progressive damage model for laminated composites containing stress concentrations" Journal of Composite Materials, Vol. 21, 834-855.

Chang K. and Chang F. (1987b) "Post failure analysis of bolted composite joints in tension or shear-out mode failure" Journal of Composite Materials, Vol. 21, 809-833.

Chang K., Liu S. and Chang F. (1991) "Damage tolerance of laminated composites containing an open hole and subjected to tensile loading" Journal of Composite Materials, Vol. 25, 274-301.

Chattopadhyay B., Sinha P. K. and Mukhopadhyay M. (1995) "Geometrically nonlinear analysis of composite stiffened plates using finite elements" Composite Structures, Vol. 31, 107-118.

Chung-Li L. and Reddy J. N. (1990) "Analysis of anisotropic, stiffened composite laminates using a continuum-based shell element" Computers & Structures, Vol. 34, No. 6, 805-815.

Crawley E. F. (1979) "The natural modes of graphite/epoxy cantilever plates and shells" Journal of Composite Materials, Vol. 13, 195-205.

Daniel I. M. and Ishai O. (1994) "*Engineering mechanics of composite materials*" Oxford university press, Oxford, UK.

Eason T. G. and Ochoa O. O. (1996) "Modeling progressive damage in composites: a shear deformable element for ABAQUS" Composite Structures, Vol. 34, 119-128.

El-Zafrany A. (1995) "*Finite element techniques for engineering analysis*" Ellis Horwood.

El-Zafrany A. and Cookson R. A. (1986a) "Derivation of Lagrangian and Hermitian shape functions for triangular elements" International Journal of Numerical Engineering, Vol. 23, 275-285.

El-Zafrany A. and Cookson, R. A. (1986b) "Derivation of Lagrangian and Hermitian shape functions for quadrilateral elements" International Journal of Numerical Engineering, Vol. 23, 1939-1958.

Enderby C. (1993) "*A fatigue test of notched coupon*" MSc Thesis, Mechanical Department, Imperial college, London.

Ewalds H. L. and Wanhill R. J. H. (1986) "*Fracture Mechanics*" Edward Arnold Ltd., London, UK.

Feng X., Gilchrist M. D., Kinloch A. J. and Matthews F. L. (1997) "Development of a method for predicting the fatigue life of CFRP components" NAFEMS World Congress '97, University of Stuttgart, Germany, Vol. 1.

Ferreira A. J. M. and Barbosa J. T. (2000) "Buckling behavior of composite shells" Composite Structures, Vol. 50, 93-98.

Fuchs H. O. and Stephens S. I. (1980) "*Metal fatigue in engineering*" John Wiley & Sons, Inc., USA.

Gaudenzi P. (1995) "A general formulation of higher-order individual layer theory" Composite Structures, Vol. 20, 103-112.

Gdoutos E. E. (1993) "*Fracture mechanics*" Kluwer Academic Publishers, Netherlands.

Gilchrist M. D., Kinloch A. J. and Matthews F. L. (1996) "Mechanical performance of carbon-fibre- andglass-fibre-reinforced epoxy I=beams: I. Mechanical behaviour" Composite Science and Technology, Vol. 56, 37-53.

Gilchrist M. D., Kinloch A. J. and Matthews F. L. (1996) "Mechanical performance of carbon-fibre- andglass-fibre-reinforced epoxy I=beams: II. Fractographic failure observation" Composite Science and Technology, Vol. 56,1031-1045.

Gilchrist M. D., Kinloch A. J. and Matthews F. L. (1999) "Mechanical performance of carbon-fibre- andglass-fibre-reinforced epoxy I=beams: III. Fatigue performance" Composite Science and Technology, Vol. 59, 179-200.

Hashin Z. (1985) "Analysis of cracked laminates: a variational approach" Mechanics of Materials, Vol. 4, No. 2, 121-136.

Hinton E. and Owen D. R. J. (1979) "*An introduction to finite element computations*" Pineridge Press Limited, Swansea, UK.

Hinton E., Razzaque A., Zienkiewiez O. C. and Davies J. D. (1975) "A simple finite element solution for plates of homogeneous, sandwich and cellular construction" Proc. Inst. Civ. Engs., Vol. 59, 43-65.

Hojo M., Tanaka K., Gustafson C. G. and Hayashi R. (1987) "Effect of stress ratio on near-threshold propagation of delamination fatigue cracks in unidirectional CFRP" Composites science and Technology, Vol. 29, 273-292.

Howard G. H., Gurtin W. A. and Reifsnider K. L. (1996) "Fatigue life of individual composite specimens based on intrinsic fatigue behavior" International Journal of Fatigue, Vol. 19, No. 5, 369-377.

Huang X., Gillespie J. W., Eduljee R. F. and Shen Z. (2000) "Matrix cracking behavior of K3B/IM7 composite laminate subject to static and fatigue loading" Composite Structures, Vol. 49, 435-441.

Istvan A. V. and Laszlo P. K. (2001) "Buckling of rectangular orthotropic plates subjected to biaxial normal forces" Journal of Composite Materials, Vol. 35, No. 7, 625-635.

Jiang W., Bao G. and Roberts J. C. (1997) "Finite element modeling of stiffened and unstiffened orthotropic plates" Computers and Structures, Vol. 63, No. 1, 105-117.

Kam T. Y., Sher H. F., Chao T. N. and Chang R. R. (1996) "Predictions of deflection and first-ply failure load of thin laminated composite plates via the finite element approach" International Journal of solids Structures, Vol. 33, No. 3, 375-398.

Khdeir A. A. (1988) "Free vibration and buckling of symmetric cross-ply laminated plates by an exact method" Journal of Sound and Vibration, Vol. 126, No. 3, 447-461.

Khdeir A. A. and Reddy J. N. (1999) "Free vibrations of laminated composite plates using second-order shear deformation theory" Computers and Structures, Vol. 71, 617-626.

Kim K. D. (1996) "Buckling behavior of composite panels using the finite element method" Composite Structures, Vol. 36, 33-43.

Kreja I., Schmidt R. and Reddy J. N. (1997) "Finite elements based on a first-order shear deformation moderate rotation shell theory with applications to the analysis of composite structures" International Journal of Non-linear Mechanics, Vol. 32, No. 6, 1123-1142.

Lekhnitskii S. G. (1963) "*Theory of elasticity of an anisotropic elastic body*" Holden-Day, San Francisco, USA.

Leung A. Y. T. and Zhou W. E. (1996) "Dynamic stiffness analysis of laminated composite plates" Thin-Walled Structures, Vol. 25, No. 2, 109-133.

Liu S. and Nairn J. A. (1992) "The formation and propagation of matrix microcracks in cross-ply laminates during static loading" Journal of Reinforced Plastics and Composites. Vol. 11, 158-178.

Madhujit M. and Abhijit M. (1990) "Finite element buckling analysis of stiffened plates" Computers and Structures, Vol. 34, No. 6, 795-803.

Mahmood M. S. and Lessard L. B. (1997a) "Multiaxial fatigue behaviour of unidirectional plies based on uniaxial fatigue experiments-I. modelling" International Journal of Fatigue. Vol. 19. No. 3, 201-207.

Mahmood M. S. and Lessard L. B. (1997b) "Multiaxial fatigue behaviour of unidirectional plies based on uniaxial fatigue experiments-II. Experimental evaluation" International Journal of Fatigue, Vol. 19, No. 3, 209-217.

Mahmood M. S. and Lessard L. B. (2000a) "Progressive fatigue damage of composite materials, part I: modeling" Journal of Composite Materials, Vol. 34, No. 13, 1056-1080.

Mahmood M. S. and Lessard L. B. (2000b) "Progressive fatigue damage of composite materials, part II: material characterization and model validation" Journal of Composite Materials, Vol. 34, No. 13, 1081-1116.

Mallikarjuna and Kant T. (1993) "A critical review and some results of recently developed refined theories of fiber-reinforced laminated composites and sandwiches" Composite Structures, Vol. 23, 293-312.

Mark S., Beaumont P. W. R. and Ashby M. F. (1991) "Fatigue damage mechanics of notched graphite-epoxy laminates" Composite Materials: Fatigue and Fracture, ASTM STP 1110, Vol. 3, 617-637.

Matsunaga H. (2000) "Vibration and stability of cross-ply laminated composite plates according to a global higher-order plate theory" Composite Structures, Vol. 48, 231-244.

Meek J. L. and Ristic S. (1997) "Large displacement analysis of thin plates and shells using a flat fact finite element formulation" Computer Methods and Applied Mechanics Engineering, Vol. 145, 285-299.

Mei C. and Prasad C. B. (1987) "Influence of large deflection and transverse shear on random response of rectangular symmetric composite laminates to acoustic loads" NASA Contractor Report, 178313

Mindlin R. D. (1951) "Influence of rotatory inertia and shear in flexural motions of isotropic elastic plates" Journal of Applied Mechanics, Vol. 18, 31-38.

Moita J. S., Soares C. M. and Soares C. A. (1999) "Buckling and dynamic behavior of laminated composite structures using a discrete higher-order displacement model" Computers and Structures, Vol. 73, 407-423.

Moutaz M. H., Kyriacou S., El-Zafrany A. (1999) "The use of hermitian timoshenko finite element for the dynamic analysis of a lightweight manipulator" Proceedings of the 8th ASAT Conference, Cairo, Egypt.

Moutaz M. H., Kyriacou S., El-Zafrany A. (2001) "Large deflection and stability analysis of composite layered plate using a new high-order element" Proceedings of the 9th ASAT Conference, Cairo, Egypt.

Nairn J. A. (1989) "The strain energy release rate of composite microcracking a variational approach" Journal of Composite Materials, Vol. 23, 1106-1124.

Narin J. A. and Hu S. (1994) "Chapter 6. Matrix microcracking, *Damage mechanics of composite materials* (ed. Talreja, R.)" Elsevier Science Publishers, New York.

Narita Y. and Leissa A. W. (1990) "Buckling studies for simply supported symmetrically laminated rectangular plates" International Journal of Mechanics and science, Vol. 32, No. 11, 909-924.

Narita Y. and Leissa A. W. (1992) "Frequencies and mode shapes of cantilevered laminated composite plates" Journal of Sound and Vibration, Vol. 154, No. 1, 161-172.

Noor A. K. and Burton W. S. (1989) "Assessment of shear deformation theories for multilayered composite plates" Applied Mechanics Review, Vol. 42, No. 1, 1-13.

Norman L. and George J. D. (1988) "Progressive transverse cracking in composite laminates" Journal of Composite Materials, Vol. 22, 900-916.

Ogin S. L. and Smith P. A. (1987) "A model for matrix cracking in corssply laminates" ESA Journal, Vol. 11, 45-60.

Ogin S. L., Smith P. A. and Beaumont P. W. R. (1985) "A stress intensity factor approach to the fatigue growth of transverse ply cracks" Composite Science and Technology, Vol. 24, 47-59.

Parhi P.K., Bhattacharyya S. K., and Sinha P. K. (2000) "Finite element dynamic analysis of laminated composite plates with multiple delaminations" Journal of Reinforced Plastics and Composites, Vol. 19, No. 11, 863-882.

Paris P. and Erdogan F. (1963) "A critical analysis of crack propagation laws" Journal of Basic Engineering, Trans. ASME 85, 528-534.

Phan N. D. and Reddy J. N. (1985) "Analysis of laminated composite plates using a higher-order shear deformation theory" International Journal for Numerical Methods in Engineering, Vol. 21, 2201-2219.

Pica A., Wood R. D. and Hinton E. (1980) "Finite element analysis of geometrically nonlinear plate behavior using a Mindlin formulation" Computers and Structures, Vol. 11, 203-215.

Ramkumar R. L. (1982) "Compression fatigue behaviour of composites in the presence of

delaminations" Damage in composite Materials, ASTM STP 775, K. L. Reifsnider, Ed., American Society for testing and Materials, 184-210.

Rakesh K. K. and Andrew E. L. (1996) "Free vibration of thick generally laminated cantilever quadrilateral plates" AIAA Journal, Vol. 34, No. 7, 1474-1486.

Rao S. S. (1982) "*The finite element method in engineering*" A. Wheaton & Co. Ltd. Exeter.

Ratwani M. M. and Kan H. P. (1982) "Effect of stacking sequence on damage propagation and failure modes in composite laminates" Damage in composite Materials, ASTM STP 775, K. L. Reifsnider, Ed., American Society for testing and Materials, 211-228.

Reddy J. N. (1982) "Analysis of layered composite plates accounting for large deflections and transverse shear strains" Recent Advances in Non-Linear computational Mechanics By Hinton et al., University College of Swansea, Swansea, U.K.

Reddy J. N. (1984) "A refined nonlinear theory of plates with transverse shear deformation" International Journal of Solids Structures, Vol. 20, No. 9/10, 881-896.

Reddy Y. S. N. and Reddy J. N. (1992) "Linear and non-linear failure analysis of composite laminates with transverse shear" Composites Science and Technology, Vol. 44, 227-255.

Reifsnider K. L. (1991) "Fatigue of composite materials" Elsevier Science Publishers, New York, USA.

Reissner E. (1945) "The effect of transverse shear deformation on the bending of elastic plates" Journal of Applied Mechanics, Vol. 12, 69-76.

Schmidt R. and Reddy J. N. (1988) "A refined small strain and moderate rotation theory of elastic anisotropic shells" Journal of Applied Mechanics, Vol. 55, 611-617.

Sciuva M. D., Icardi U. and Villani M. (1998) "Failure analysis of composite laminates under large deflection" Composite Structures, Vol. 40, No. 34, 239-255.

Sheela N., Singh G. and Rao G. V. (1996) "Stability of laminated composite plates subjected to various types of in-plane loadings" International Journal of Mechanics and Structure, Vol. 38, No. 2, 191-202.

Shi G., Lam K. Y. and Tay T. E. (1998) "On efficient finite element modeling of composite beams and plates using higher-order theories and an accurate composite beam element" Composite Structures, Vol. 41, 159-165.

Staab G. H. (1999) "*Laminar composite*" Butterworth Heinemann, USA.

Stephen W. T. and Hahn H. T. (1980) "*Introduction to composite materials*" Technomic published Co. Inc., USA.

Stroud W. J., Greene W. H. and Anderson M. S. (1984) "Buckling loads of stiffened panels

subjected to combined longitudinal compression and shear: results obtained with PASCO, EAL and STAGS computer programs" NASA Technical Report, 2215.

Talreja R. (1987) "Fatigue of composite materials" Technomic Publishing Company, Inc., USA.

Tasneem P. and Zabaras N. (1992) "Transient dynamic and damping analysis of laminated anisotropic plates using refined plate theory" International Journal of Numerical Engineering, Vol. 33, 1059-1080.

Tessler A. (1993) "An improved plate theory of {1,2}-order for thick composite laminates" International journal of Solids Structures, Vol. 30, No. 7, 981-1000.

Verijenko V. E., Adali S. and Piskunov V. G. (1995) "Finite elements based on shear and normal deformation theory for the analysis of laminated composite plates" Computer & Structures, Vol. 54, No. 5, 789-807.

Zienkiewicz O. C. (1977) "*The finite element method*" 3rd Ed. McGraw-Hill, London, UK.

Zienkiewicz O. C., Taylor R. L., Papadopoulos P. and Onate E. (1990) "Plate bending elements with discrete constraints: new triangular elements" Computers and Structures, Vol. 35, No. 4, 505-522.

APPENDIX "A"

STIFFNES "D" MATRICES

The D matrix in equation (3.14) can be expanded in the following form:

$$d_{11} = m^4 d_{11}^{\backslash} + n^4 d_{22}^{\backslash} + 2\,m^2 n^2 (d_{12}^{\backslash} + 2\,d_{44}^{\backslash})$$

$$d_{22} = n^4 d_{11}^{\backslash} + m^4 d_{22}^{\backslash} + 2\,m^2 n^2 (d_{12}^{\backslash} + 2\,d_{44}^{\backslash})$$

$$d_{12} = m^2 n^2 (d_{11}^{\backslash} + d_{22}^{\backslash}) + (m^4 + n^4)\, d_{12}^{\backslash} - 4 m^2 n^2\, d_{44}^{\backslash}$$

$$d_{13} = m^2 d_{13}^{\backslash} + n^2 d_{23}^{\backslash}$$

$$d_{23} = n^2 d_{13}^{\backslash} + m^2 d_{23}^{\backslash}$$

$$d_{14} = -m\,n\left[n^2 d_{22}^{\backslash} - m^2 d_{11}^{\backslash} + (m^2 - n^2)(d_{12}^{\backslash} + 2\,d_{44}^{\backslash})\right]$$

$$d_{24} = -m\,n\left[m^2 d_{22}^{\backslash} - n^2 d_{11}^{\backslash} + (n^2 - m^2)(d_{12}^{\backslash} + 2\,d_{44}^{\backslash})\right]$$

$$d_{15} = d_{16} = d_{25} = d_{26} = 0$$

$$d_{33} = d_{33}^{\backslash}$$

$$d_{34} = -mn(d_{23}^{\backslash} - d_{13}^{\backslash})$$

$$d_{44} = m^2 n^2 (d_{11}^{\backslash} + d_{22}^{\backslash} - 2\,d_{12}^{\backslash}) + (m^2 - n^2)\, d_{44}^{\backslash}$$

$$d_{35} = d_{36} = d_{45} = d_{46} = 0$$

$$d_{55} = n^2 d_{55}^{\backslash} + m^2 d_{66}^{\backslash}$$

$$d_{66} = n^2 d_{55}^{\backslash} + m^2 d_{66}^{\backslash}$$

$$d_{56} = -mn(d_{55}^{\backslash} - d_{66}^{\backslash})$$

and $\quad d_{ji} = d_{ij}$

Hence

$$\underline{D} = \begin{bmatrix} d_{11} & d_{12} & d_{13} & d_{14} & 0 & 0 \\ & d_{22} & d_{23} & d_{24} & 0 & 0 \\ & & d_{33} & d_{34} & 0 & 0 \\ & & & d_{44} & 0 & 0 \\ & \text{symm} & & & d_{55} & d_{56} \\ & & & & & d_{66} \end{bmatrix}$$